UNIVERSITY OF STRATHCLYDE

AN INVESTIGATION INTO COMPOSITE DOUBLE LAYER SPACE GRID STRUCTURES

by

ABDUL AZIZ JABER AL-BAZZAZ, M.Sc.

A Thesis presented for the degree of
Doctor of Philosophy
of the University of Strathclyde
in the Department of Civil Engineering

1976

ACKNOWLEDGEMENT

The author wishes to express his sincere gratitude to Professor A. Coull for giving him the opportunity to carry out this research.

Sincere thanks to Dr. J. Marshall for his supervision and guidance throughout this research.

Thanks are also due to Dr. H. Nooshin of the University of Surrey for his supervision during the preliminary stage of this research.

Thanks are due to Mr. D. Logan for the valuable discussions.

Thanks to Mr. W. Leighton for the great care he took in the construction of the experimental models, and also to Mr. J. Morrin for their help during the testing of the models.

The help of the management and the advisory staff in the computer centre in facilitating the running of the very demanding computer programs as well as in programming matters is gratefully acknowledged.

The author also wishes to express his gratitude and appreciation to The Government of the Republic of Iraq for granting him the financial support.

It is the author's sincere desire to express his appreciation and gratitude to his wife Hanaa for her patience and moral encouragement.

Thanks are also due to Mrs. G. Stewart for the great care she took in typing this thesis.

NOMENCLATURE

X, Y, Z	orthogonal axes
d_x, d_y, d_z	orthogonal components of displacements
θ_x, θ_y, θ_z	plate rotation and angle of torsion
P_x, P_y, P_z	orthogonal components of force
m_x, m_y, m_z	moments around the orthogonal axes
∇	stress
E	Young's modulus
μ	Poisson's ratio
G	modulus of rigidity
I	Second moment of area of section
t	plate thickness
A_c	area of concrete section
A_s	" " steel section
h	centre to centre depth of the structure
C.D.L.G	Composite Double Layer Flat Grids
D.L.G	Double Layer Grid
RPM	Double Layer Grid of Rectangular Parallel Mesh configuration
IRM	Double Layer grid of Inclined Rectangular Mesh
d	Total depth of the structure
SDR	Span/Depth Ratio
σ_s	stress in the steel tubes
σ_c	" " " concrete slab
σ_p, σ_b	in-plane and bending stresses in the concrete slab

T	maximum tensile force
C	maximum compressive force
σ_{pm}, σ_{bm}	maximum in-plane and bending stresses in the concrete slab

CONTENTS

ERRATA

Figure 5.11 and page 99 do not exist.

Pages 161, 162, 163, 164 do not exist.

SYNOPSIS

This thesis presents an investigation into the behaviour of 'Composite Double Layer Space Grid Structures'. In this research a reinforced concrete slab was used as the top layer of a thin steel tube space frame. The stiffness matrix method of analysis was used for the theoretical analysis in which the slab was represented by 'Finite Elements'.

Two experimental models were designed and constructed mainly to verify this analysis and to check its convergency and also to study the influence of top joint eccentricity.

The research showed that these structures are more rigid and have better stress distribution patterns than the comparable double layer grids, and hence can be used for larger spans. The critical factor in the design of these structures is the buckling of the diagonal shear members, hence an 'economical depth' has been found.

Plate analogy was found to be of great value, by which it was possible to explain and predict the stress behaviour, also a criterion is found for designing an 'Efficient Section' where no concrete is subjected to tensile action.

Since this type of structure requires large computer facilities, which are neither easily available nor economical even for short spans, approximate methods are suggested, some of which are based on a plate analogy and do not need a computer. Finally a design procedure using these methods

has been outlined by which it is possible to have a quick and approximate idea about the appropriate section properties for any given span within the specified loading and boundary conditions.

CHAPTER 1

INTRODUCTION

This thesis presents an investigation into the behaviour of composite double layer grids. The idea behind these structures is to replace the top layer of the prismatic flat double layer grid by a continuum such as a reinforced concrete slab. Thus the higher in-plane rigidity of the slab can be utilised, especially when a concrete slab has to be used anyway as cladding, such as in car parks, office building, etc.

Very little work has been done on this topic other than that concerning prismatic double layer grids which is undoubtedly of relevance to this topic.

Therefore it was necessary to verify the validity of almost all steps taken in this research.

The stiffness method of analysis was used for the theoretical analysis, which is ideally suited to accommodate the finite element method which is used for the plate analysis. In this analytical solution, a linear elastic superposition of stiffness matrices for prismatic members in space and for finite element plate members was possible.

The experimental models were designed and constructed using steel tubes to represent the prismatic members and perspex plate to represent the concrete slab. The first model is a composite double layer grid based on a 'square parallel mesh' configuration. The second model is a

tubular pyramid module with its apex supporting a rectangular perspex plate at its centre.

A series of laboratory tests were done on these models in order to:

a) verify the theoretical analysis

b) to check the convergency of the solution

c) to find a suitable finite element mesh so as to have reasonable results without an excessive demand on computer storage and time.

d) To study the influence of eccentricity at joints between prismatic members and plate.

A general and versatile suite of computer programs was developed to do the theoretical analysis. This suite uses direct access disc backing files to store numerical data and results during the execution of the whole program suite. The program suite is capable of analysing, in addition to the composite structures, various structural systems such as prismatic double layer grids, and folded plate structures. Data generating programs were developed to prepare the data for the various configurations and cases analysed in this research.

Because of the high efficiency of the inclined square mesh configuration, the theoretical studies are restricted to two configurations both of which are based on the 'Inclined Square Mesh' configuration. The first one is termed the 'Uniform Mesh' while the second one which is a special case of the first one is termed the 'IRM' 'Composite Structure,

These structures are made of a reinforced concrete

slab and steel tubes of identical cross-section.

Despite the considerable store capacity of 256 K available for the ICL 1904S computer in the University of Strathclyde, the largest problem handled was of 10 x 10 bays (pyramids), and this was only possible by the exclusive use of the full computer system for about twenty five minutes.

Accordingly, all computer run cases in this thesis are limited to this rather short span.

Parameter studies were done to investigate the influence of varying the span, depth, slab thickness, and the steel tubes cross-section on selected crucial members and slab locations. Particular attention was focused on the maximum shearing force due to its anticipated importance in the design procedure.

A slab analogy is suggested as an explanation for the behaviour of these structures. Also a method is suggested to find the moment of inertia of the section from which it is possible to predict the relation between the axial stresses in bottom tubes and the in-plane stresses in the top slab. Furthermore a criterion is suggested from which it is possible to find the section where no part of the concrete slab will be under tension, and is termed accordingly "The Efficient Section".

Engineers have always been interested in short simple design procedures or formulae to be used in preliminary design and also as an approximate checking tool. Certainly, this will be no more so than in this complicated field of composite Double Layer Grids.

Therefore, an important aim of this research was to find such approximate methods.

Hence a few approximate methods are introduced for this purpose.

Some of these methods still need a computer, whilst the others do not. Those which do not need a computer are based on the plate analogy

CHAPTER 2

LITERATURE REVIEW

Flat composite Double Layer Grids are an evolution of double layer space grids, therefore, it is imperative and useful to start from this background, and review their relevant literature and methods of analysis as a basis for the methods which are or ought to be developed for analysing and designing flat composite double layer grids.

2.1 Previous Relevant Works

A. Makowski[1] gives an excellent survey of the different types of space structures with their properties, advantages, and the different commercial joint systems used in their construction. It is useful to emphasize from his book the relevant points of interest.

The efficiency of any design is judged by the ability of the structure to distribute as widely as possible any applied load, thus achieving a fairly even stress distribution over the whole structure. Grid space structures are ideally suited for this purpose. Last war experience proved that grid space structures resisted aerial attacks and explosions much better than any other structural system, and local damage rarely, if ever, led to a collapse of the whole structure.

Although the rectangular arrangements for grids (Fig. 2.1) is popular, nevertheless, it is not the best as far as stress distribution is concerned. A much better arrangement is the diagonal grid system (Fig. 2.2)

where members form an oblique angle with the boundaries. This type is becoming more popular owing to its greater bending rigidity. This is because, the shorter corner members with their greater relative stiffness provide in effect intermediate supports for the longer diagonal members. It is also explained by the fact that members of diagonal grids follow roughly the trajectories of principal stresses in simply supported slab under uniformly distributed load. Therefore, the members are placed both in location and orientation where they are mostly needed.

The most remarkable development for the last few years, has been the evolution of various forms of double layer grids. Spans of up to 300 ft. have already been covered by steel double layer grids. The main advantage of these types of structures is that their members are mainly under the action of axial forces, which leads to the full utilization of their strength. Owing to the high indeterminancy of these structures, buckling of any member under a heavy concentrated load rarely leads to a collapse of the whole structure.

Basically, double layer grids are divided into two main types.

a) Lattice grids, consisting of intersecting vertical lattice girders.

b) True space grids, which consist of tetrahedra, octahedra, or inverted pyramids having square (Fig. 2.3,2.4) pentagonal, or hexagonal bases.

In practice, the depth of double layer grid is between $\frac{1}{20}$ to $\frac{1}{25}$ of the span. So there is always an

ample working space for the installation, maintenance, modification, and services even with small spans of say 80 ft. This factor is of special importance in office buildings.

Due to the regular nature of space structures, and the huge number of identical units, they are a typical example of the prefabricated mass produced form of construction. So far, steel has been playing a leading role on account of its relative low cost and great strength.

B. The first noticeable contribution to extend the concept of space structures to reinforced concrete slabs, is attributed to Castillo.(2) The following are the points of relevant interest in his paper.

He calls his system 'Tridilosa' which is a form of reinforced concrete floor slab, in which a relatively thin top slab of concrete combined with a structural steel space frame beneath. Fig. (2.5) shows the Tridilosa assembly. When the system takes the form of a beam it is called 'triditrabe'. It is stated that until the 'Tridilosa' design was introduced to the market, nobody had successfully taken away the unnecessary dead weight of the cracked concrete in tension zones of slabs. No clue was given to the theory used, other than that the calculation of this form of structure can be developed from a theory in his book(3) which allows for the calculation of all elastic three-dimensional structures.*

---

* The author and the University library were unable to get hold of this book which is written in Spanish language.

A loading test was done on a slab made of 10' x 10' x 1' 'Tridilosa' assembly with $\frac{3}{8}$" diameter structural steel spaced at 20 in c.c., with 2 in. low stress concrete slab on the top. The total bearing load was about 615 psf. The same structure, but without concrete on top, was tested and gave a bearing capacity of 41 psf only, with failure occurring by buckling of the compression rods in the top layer.

This small test allowed rough confirmation of his theory.

The system has been used in the floor slabs of multi storey buildings and car parks in Mexico City in Mexico. In one of these buildings, the self weight of 16 'Tridilosa' floors for a fifteen storey building was equal to that of the slabs of an eight storey flat slab building, with the added advantage of longer spans and greater bearing capacity.

It is admitted that in comparison with the traditional type of slabs, there are two distinct disadvantages.

a) The lack of protection of the steel rods against fire and corrosion.

b) The use of a larger amount of steel for shear stresses.

The former is overcome by painting the uncovered steel and covering with concrete all steel under tension.

The latter is advantageously balanced by the savings in tension and compression steel and the volume of concrete beneath the neutral axis, and also the savings in

shutterings, or even the possibility of avoiding completely the use of form work. The problem of temperature cracks in this structure is practically non-existent since the structure is very rigid.

C. A relevant study, but with different outlook was presented by Chambers et al.[4] This study is an investigation into another type of space/plate structure. They proposed a Braced Double Skin structure (Fig. 2.6) in metal as an alternative to welded stiffened plating.

They used space/finite element analysis in their dual theoretical approach to compare with experiments.

a) Panel skins were represented by discrete strips joining the nodes transversely, longitudinally, and diagonally. Since the stresses in the skin were relatively low, the forces in core members were effected only slightly, but not the skin stresses near the joints.

b) Finite element was used to analyse the skin stresses. The results showed better agreement with the test as far as tubes and reaction, but comparison was difficult for skin stresses, because they were very low.

The following relevant conclusions were given:

1. Resistance to local lateral loading on the skin was governed largely by the buckling of the rods under or near the applied load, rather than membrane action of the skin.

2. Shear strength is relatively low, and less than simple theory predicts. The shear meant here is the one due to horizontal forces.

Overall crushing characteristics show that there is

a capacity to absorb energy as the struts buckle, and simple bending theory is adequate for pure bending.

D. Bellamy, J.[5] has carried out an investigation into the effects of attaching roofing sheets to the top of a flat D.L.G. He used an experimental model to assess the accuracy of his computer analysis.

The model was a parallel rectangular mesh (PRM-Grid) (Fig. 2.3) loaded under uniformly distributed loading. He used three cladding distances, $2\frac{1}{2}$", $4\frac{1}{2}$" and 6" from the top grid. Fig. (2.7) shows a top joint in the model. He used plane stress rectangular finite elements to analyse the cladding. Joints deflections and member axial forces compared favourably with test results but not cladding analysis. He attributed the discrepancies to the following:

a - The coarseness of the elements used which itself contributes errors up to 17.5% on deflection, and more than that on stresses.

b - Number of secondary factors, such as initial lack of straightness of the sheeting, the overlapping of sheetings and their overhangs.

His conclusions were:

1. The cladding has had little effect on the behaviour of the roof structure only when it is closest to the roof.

2. The cladding, in general, has had little effect on the behaviour of the steel structure roof.

Therefore, it would appear that if the sheeting is

insufficiently strong to carry sizable portion of the applied load, say 20% across the span on its own, then there is no point in including its effect in the analysis. A conclusion confirmed the standard design office procedure of neglecting the effect of cladding.

E. Theron[6] used finite difference calculus to analyse flat Double Layer Grids. Then he analysed a flat slab of perspex using finite elements method. Then super-imposed the two analyses and termed it composite analysis. In fact the slab was just acting as a cladding material only.

Using a computer, numerical results were calculated for simplified cases of two D.L.G. systems. Namely, (PSM-Grid) (Fig. 2.3) and (ISM-Grid) (Fig. 2.4) made out of short 7" plastic or perspex tubes. Only vertical displacements were measured, and subsequently compared favourably with analytical analysis, where experimental errors did not have a significant effect. Then the thin perspex plate was cemented to the previous two models and retested under U.D.L. The vertical displacements comparison was favourable as before.

No attempt has been made to investigate the influence of the various parameters on the behaviour of the structure, or the influence of cladding on the structure.

2.2 Methods of Analysis

Basically, there are three lines of analysis for double layer grids.

a) Stiffness Method of Analysis[7] which is exact within the limits of the assumptions of linear prismatic bars. It is the most common method, and the most versatile one. This method owes its popularity and success, naturally to the electronic computers. But because of its demand on computers storage capacity and time, designers resort to other methods as a preliminary step.

This method was used by Makowski[1] and Bellamy,[5] Chambers et al.[4] used it even to represent the continuum skin layer. This method is ideal for combination with the Finite Elements Method, which could be used to represent the continuum as in the case of cladding,[5] roofing[6] and skin plates.[4]

b) Analytical Methods

They are mainly means to get approximate design parameters, leaving the final answer to the stiffness method and the electronic computers.

These methods are usually cumbersome mathematically, especially for engineers, and in the end do not give good results for the boundary areas and particularly for the corners. They are mainly based on plate analogy.

Theron[6] used analytical method and found a solution for RPM grid and ISM grid.

Renton[8,9,10] used continuum analogy using mainly the finite difference method. The technique makes use of the regularity of such structures by considering only the

small set of equations governing the behaviour of a typical module of the structure. These take the form of stiffness equations relating the external loads to the module deflections and those of the adjoining ones.

Renton[8] showed the related behaviour of plane grids, space grids and plates. He also succeeded in giving equations for many configurations.[10]

c) Plate Analogy

Plate analogy for flat grid structures has been used extensively in the literature.

Timoshenko[11] suggested it for one layer rectangular grids which is made out of rigid beams (Fig. 2.8), by considering it a special case of orthotropic plate. He took the average values of the bending and torsion stiffnesses.

Plate analogy, in common with other approximate methods has difficulties in boundary areas, particularly in corners which are a highly stressed part in the plate. Renton[10] recognizes the importance of these drawbacks and the difficulty in combating them.

Makowski[12] drew the attention to those points also, and confirmed that plate analogy gives a good approximation for the central part of the structure. However, the difference in shearing forces is much greater than in tension and compression layers, and he specified 'ISM' grids as a case where neither plate analogy nor rigorous analytical methods will hold, because of the influence of boundary conditions.

In certain cases, depending on the type of bracing and configuration of the grid, the influence of boundary conditions could extend right into the centre of the structure.

Heki[13] confirms the same observations, and adds, that, in general, this is due to the effects of anisotropy, effective rigidity, shear deformation and finiteness of mesh length. He suggested that the width of boundary area in the case of Double Layer Lattice Grids, is of the order $\sqrt{hl}$, where h is the depth of the structure and l is the span width. This suggested width is much larger than that of solid plates which has been shown by Reisner[18] to be of the order t, where t is the slab thickness.

It is clear from the above review, the extent of the difficulties facing the stress analyst and the designer in the relatively simple cases of ordinary one material, pin jointed double layer grids, due to the rather excessive computer requirements.

Understandably, the difficulties are much more in the case of composite double layer grids, where the designer and the analyst have to face the added complexity of the plate as a shell element, and hence, having in hand a structure with six degrees of freedom.

Therefore, for large span structures, even the large modern computers will have difficulty in accommodating them in their rather limited storage capacity and time consideration.

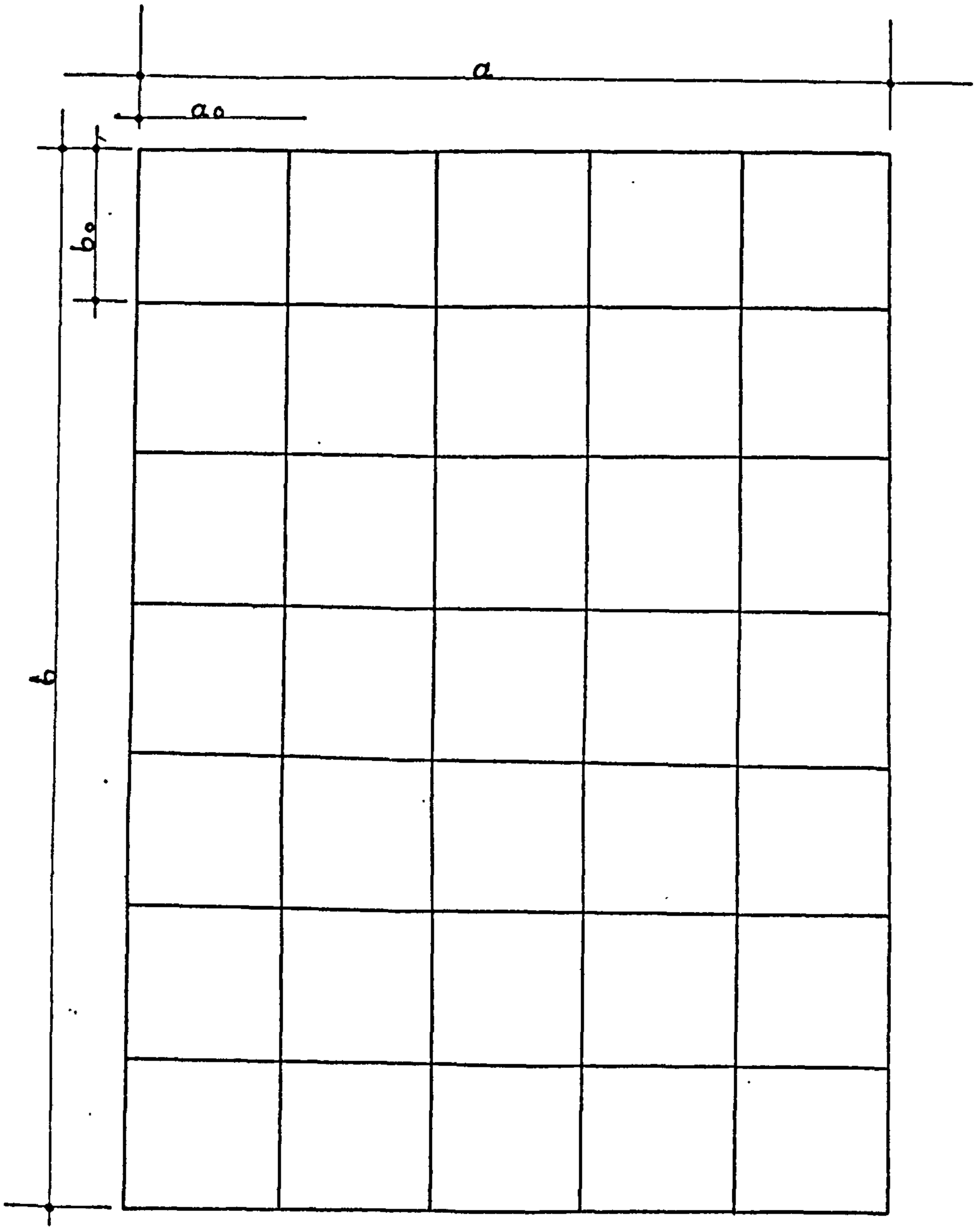

Fig. 2.1 Rectangular Mesh Grid

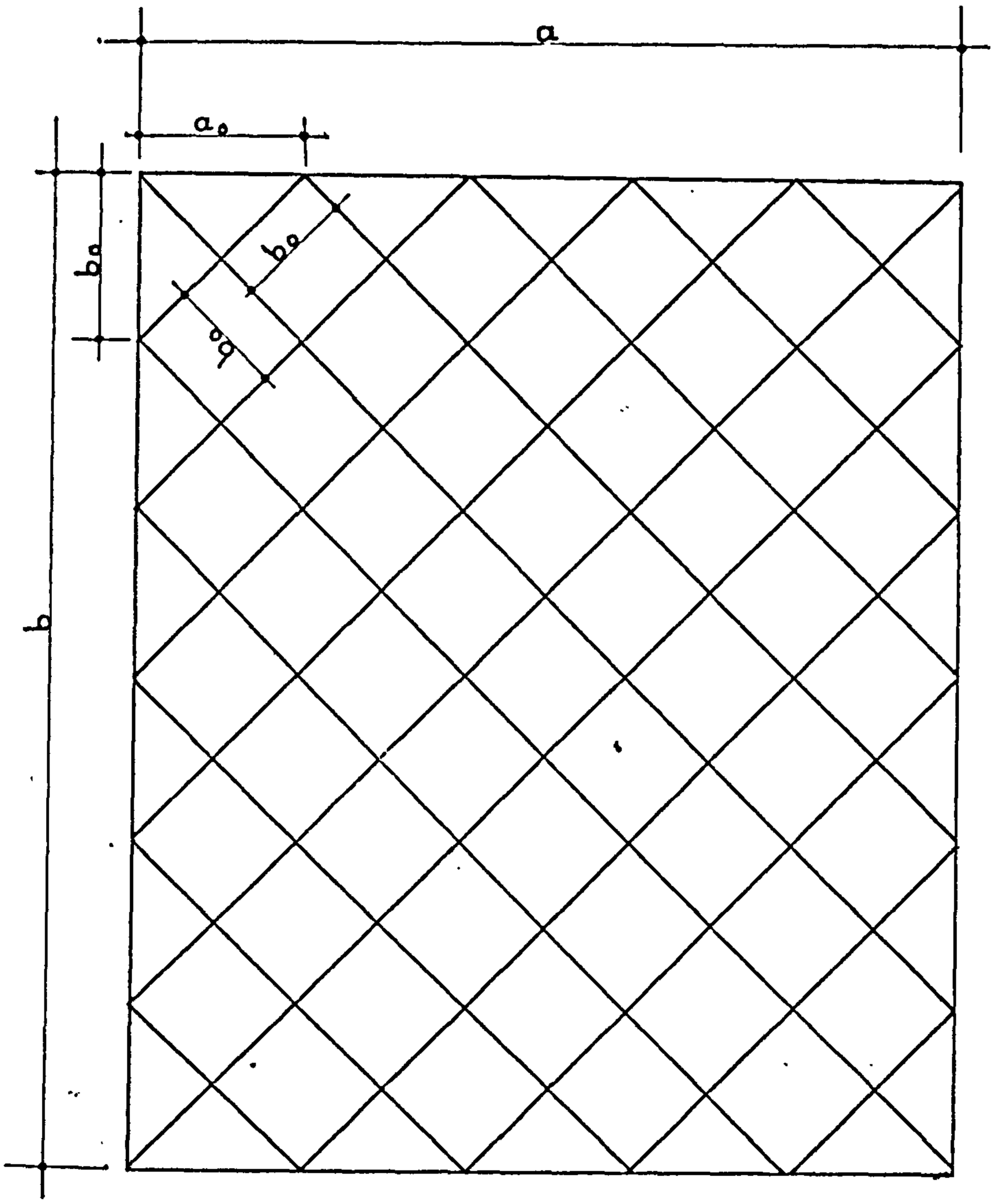

Fig. 2.2 Inclined Rectangular Grid

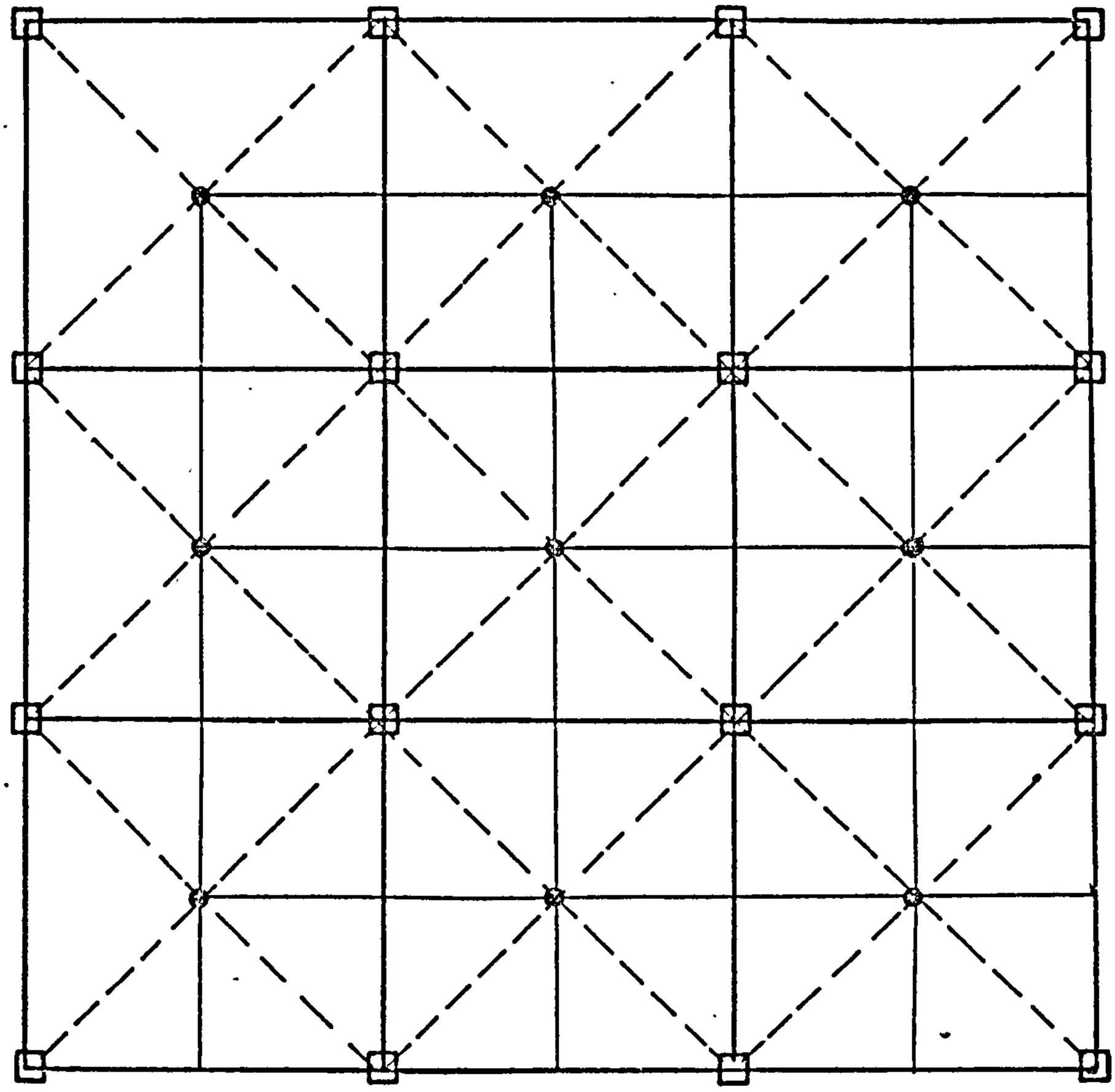

Fig. 2.3 Plan of a part of a double layer grid with parallel rectangular mesh (PRM)

——— Top layer members

——— Bottom layer members

———·— Diagonal shear members

□ Top joints

● Bottom joints

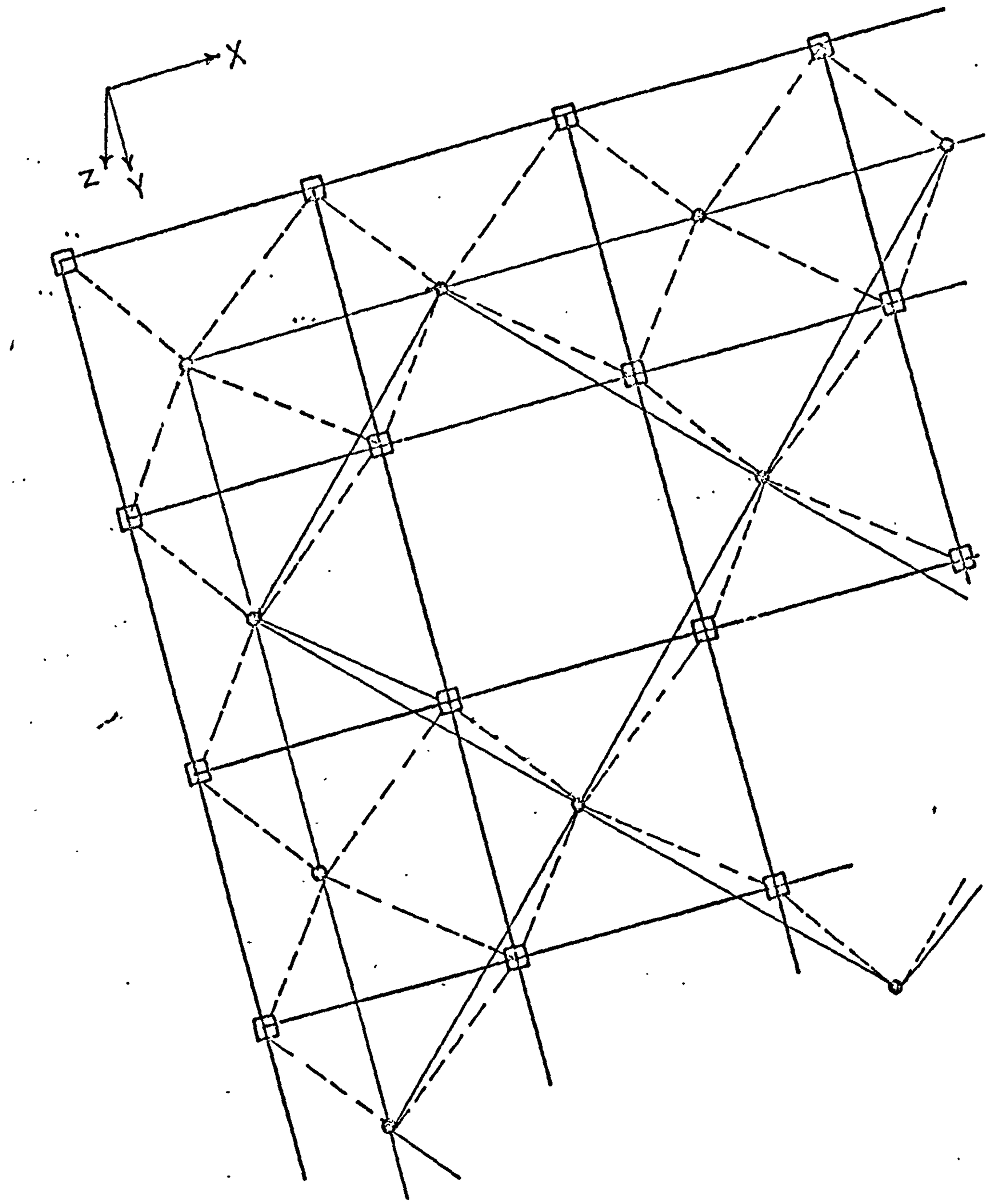

——— Top members

——— Bottom members

— — — Pyramids sides members

□ Top joints

○ Bottom joints

Fig. 2.4 3 Dimensional view of a double layer grid with inclined rectangular meshes figuration (IRM)

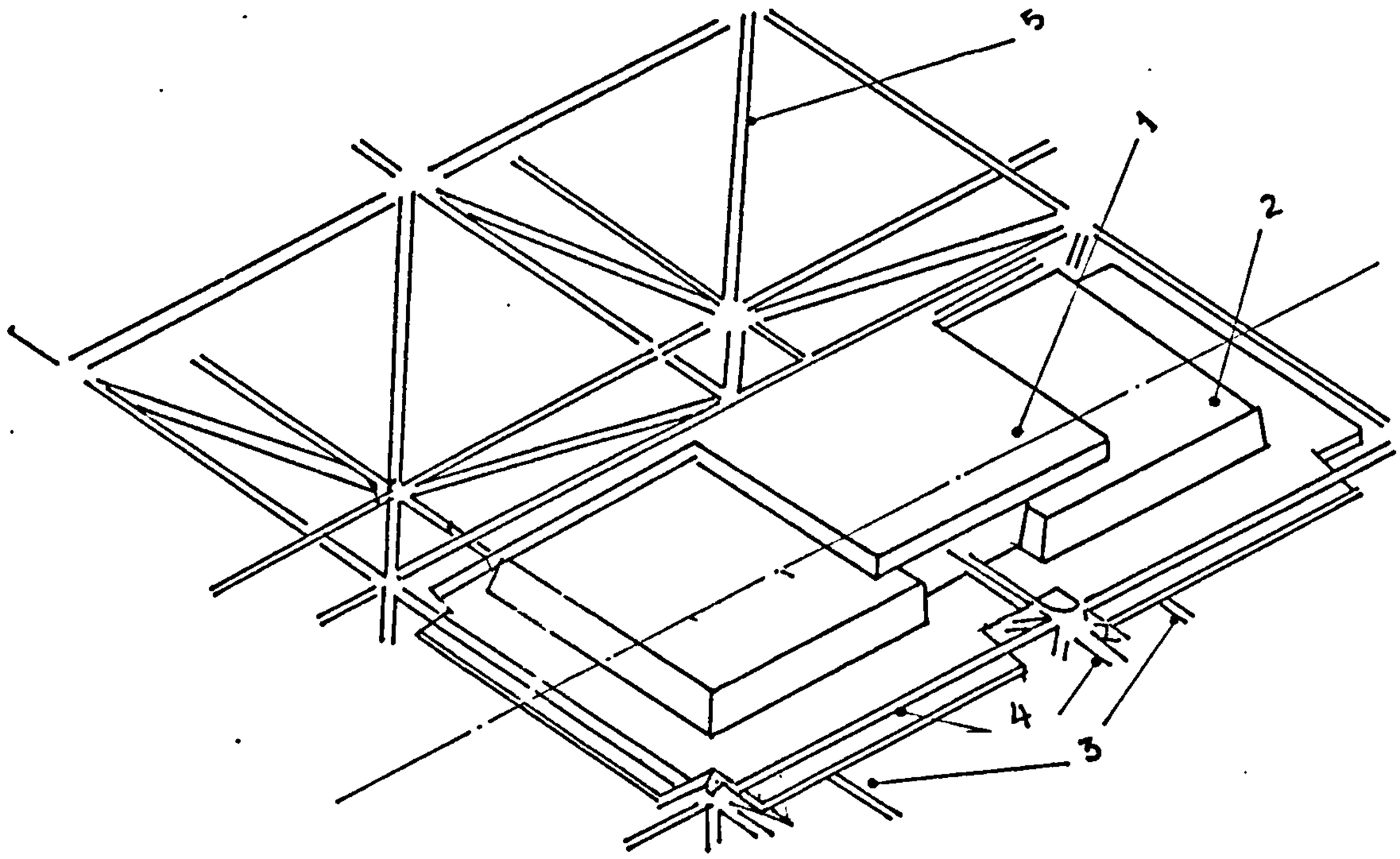

1. In-situ concrete
2. Precast light weight concrete
3. Tension steel in lower part of grid
4. Compression steel in upper part of grid
5. Bracing members.

Fig. 2.5 Tridilosa System

after Castillo[2]

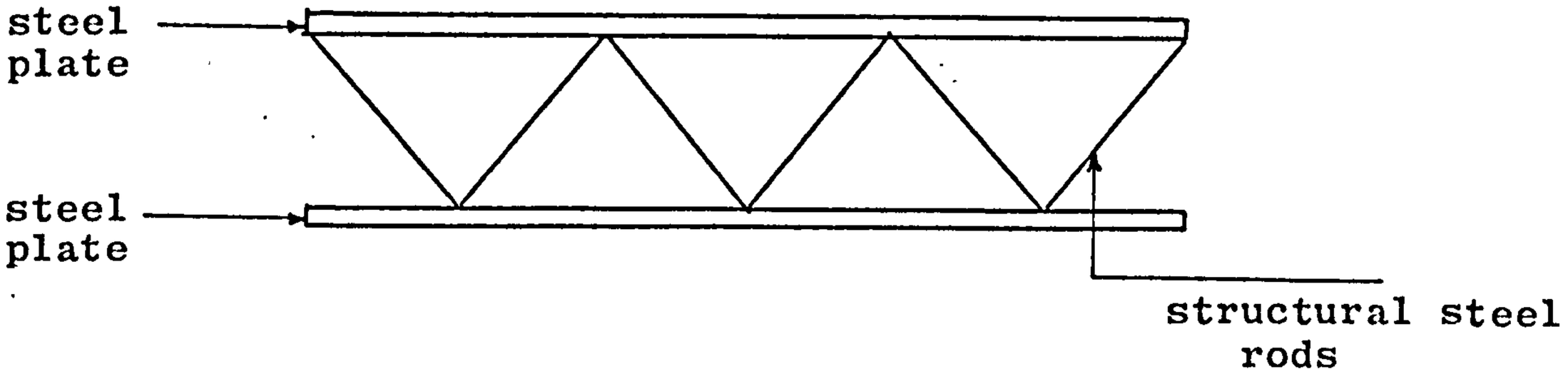

a) Section

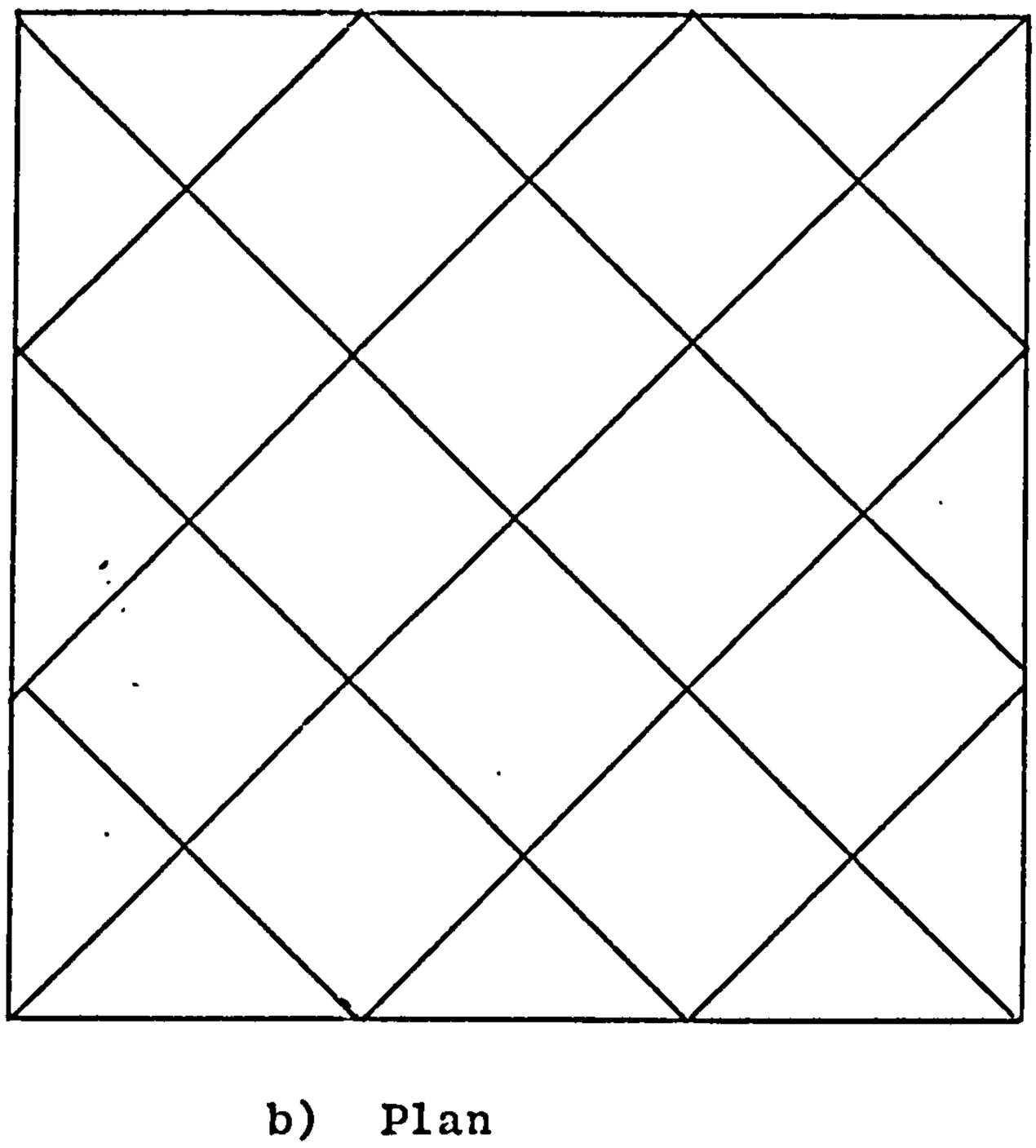

b) Plan

Fig. 2.6 Braced Double Skin Structure

after Chambers et al.[4]

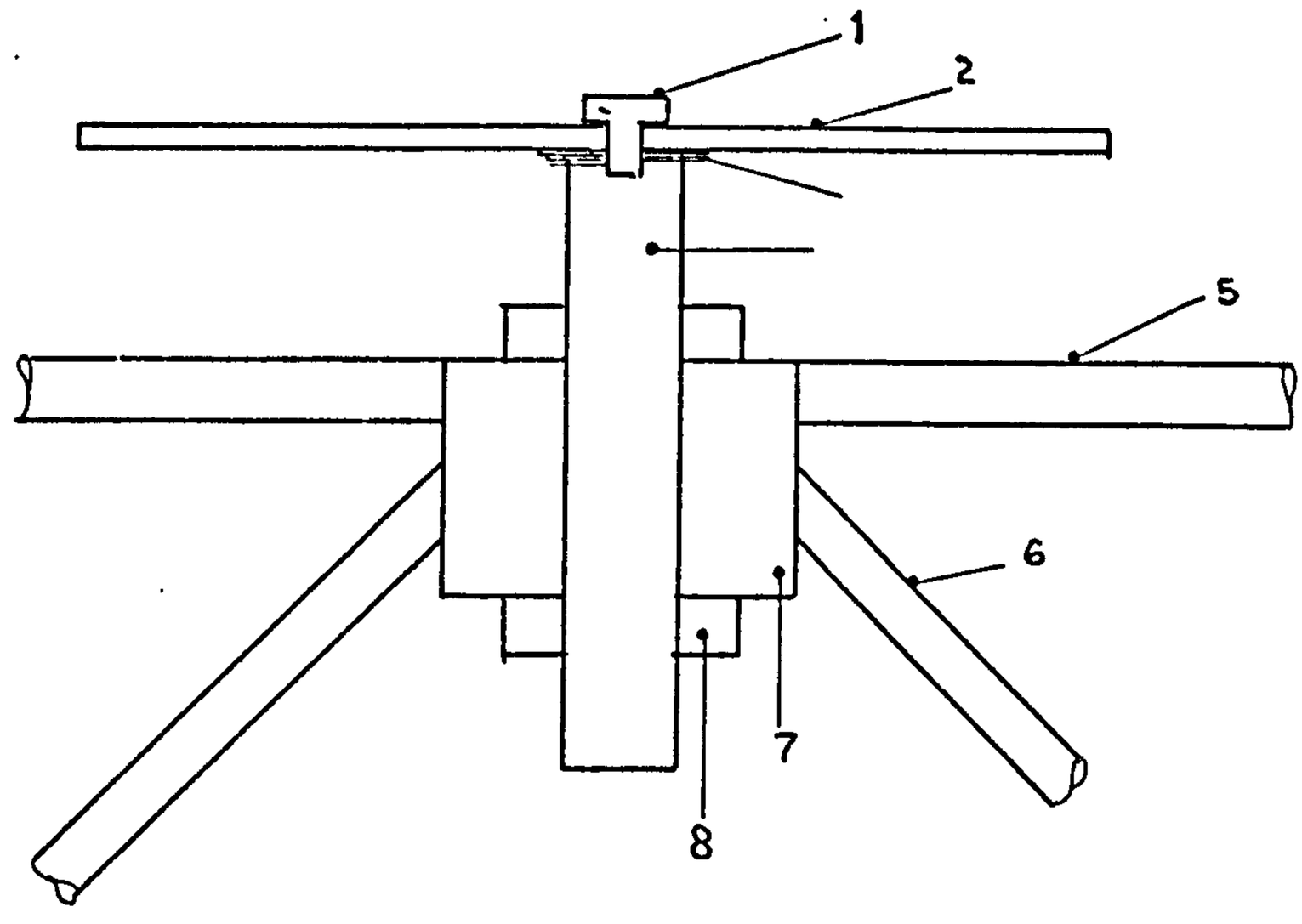

1. Securing bolt
2. Preform cladding
3. Washers
4. Screwed rod
5. Top Grid member
6. Diagonal member
7. Joint Boss
8. Lock nut

Fig. 2.7

after Bellamy[5]

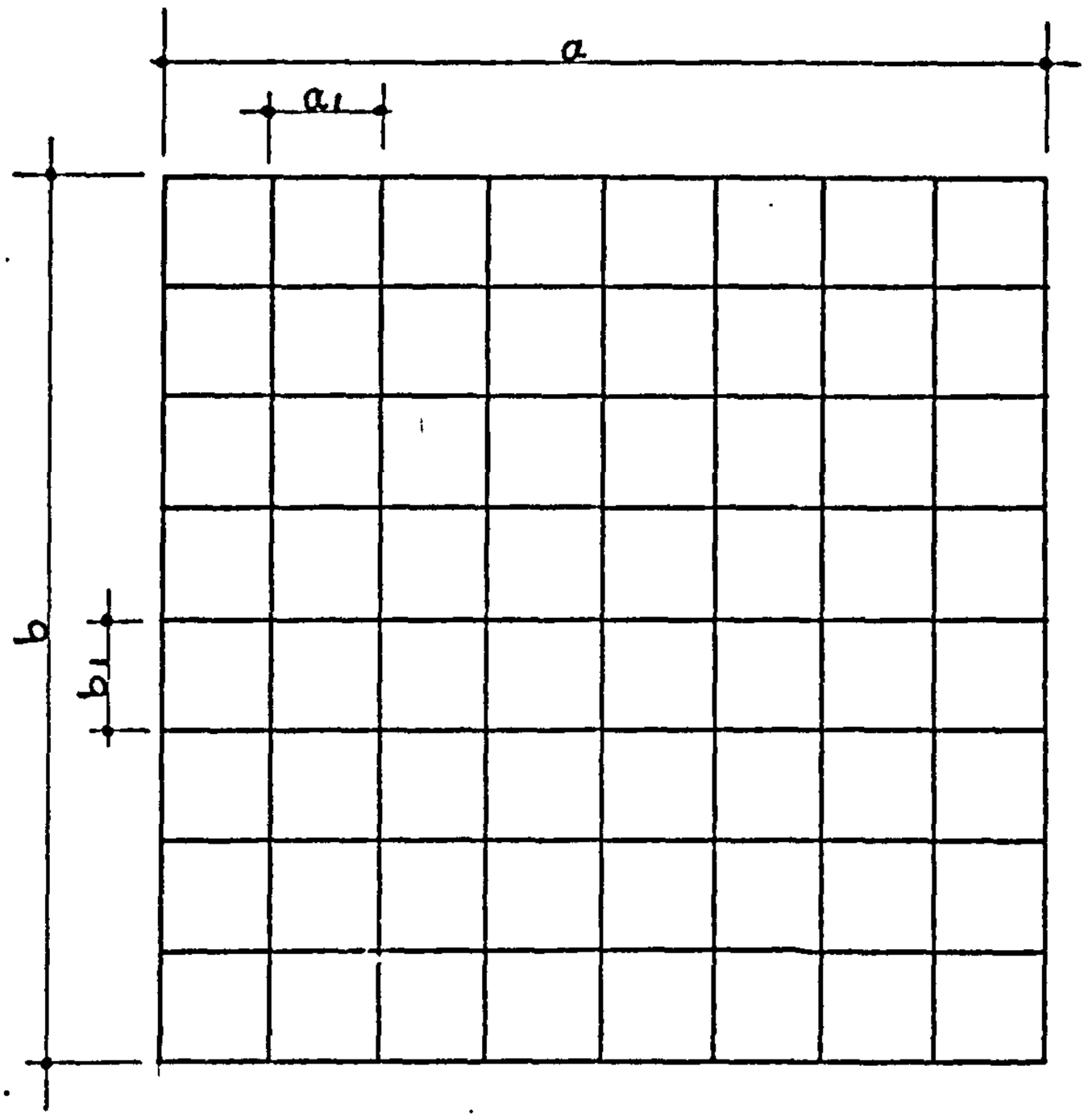

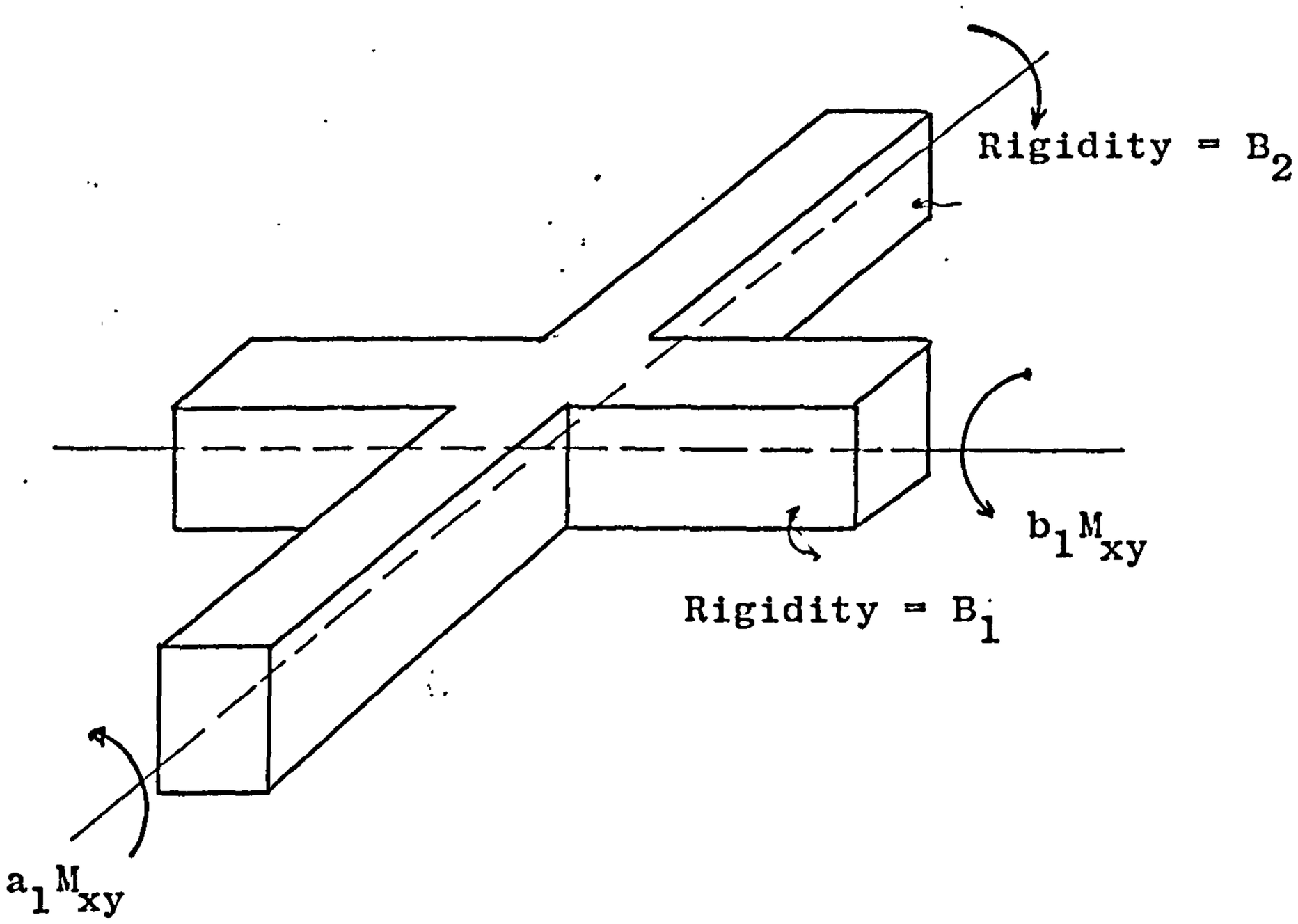

Fig. 2.8 Grid System

CHAPTER 3

LABORATORY EXPERIMENTS

Laboratory experiments were necessary to verify the theoretical analysis. Since the idea behind this research project was to replace the top layer in double layer grids by concrete in the construction field, it was decided to use perspex sheet as a laboratory substitute for concrete, because it has the advantages of being a linear elastic material, and commercially available in different sizes and thicknesses, in addition to the ability to produce appreciable strains due to its low modulus of elasticity.

Two models were made

1. Composite Double layer grid model, and will be referred to as Model I.
2. Single pyramid cantilever model; and will be referred to as Model II.

3.1 Composite Double Layer Grid Model (MODEL I)

It was expected that this type of structure would be very rigid, therefore the following steps were taken to make the model less rigid.

a) Contrary to common practice in ordinary D.L.G. where structures have a top layer of larger area than the bottom, in this model the top layer was made smaller than the bottom one.

b) Simply supported boundary conditions were simulated.

c) The tubes were chosen to have a small cross sectional area with thin walls in order to have appreciable axial strains.

Because it was intended to study the influence of the thickness of the top layer, and top joints eccentricity on the strains in the structure, the model was so designed, that it was easy to vary the top layer thickness and its eccentricity without changing other parameters.

The overall dimensions of the model were governed by practical considerations, in particular the standard sizes of perspex sheets available and cost. Since there was no additional advantage in having a rectangular model, it was decided to make a square model with a perspex area of 48" x 48".

The dimensions of the tubes were chosen after taking into consideration the perspex sheet dimensions, and the desire to have all tubes of the same length and diameter. In addition, the tube member should be long enough to have the

middle third of it unaffected by the end stress conditions and with enough circumference to cement three single strain gauges longitudinally around it. Therefore annealed cold drawn seamless steel tubes were chosen with $\frac{1}{2}$" diameter and 0.036 in. wall thickness. These are thick enough to withstand a jointing process and have the added advantage of not losing strength due to the welding heat. All tubes were chosen to be of 15" length.

Taking all the above factors into consideration in addition to the boundary conditions and loading requirements, the model was finally designed and made as shown in Plate Nos. (3.1, 3.2) and Fig. 3.1 from the following

a) Bottom flat layer made of a 60" x 60" tubular square grid, each side having four 16" c.c. bays. All tubes are of 15" x $\frac{1}{2}$" x 0.036 inch dimensions (Gauge 20).

b) Top flat layer of 48" x 48" acrylic perspex sheet.

c) 64 Tubes grouped in fours. Those tubes connect the top layer to the bottom layer.

Four tubes were made of Gauge 16 (t = .054 in.) because they were located at the corners of the structure so they can transmit the high concentrated reactions to the supports.

Basically, the tubes part of the structure is made out of identical pyramid units, each one of them is made out of eight identical tubes as seen in Fig. 3.2.

3.1.1 Boundary Conditions

Since the structure was internally highly indeterminant, it was useful for practical purposes to make it externally determinant. This was done by supporting the model at the four corner joints only, and also by having only one vertical component at each corner.

Three different support arrangements were used to impose the following restrictions.

1. Support A restricted in the X and Z directions as seen in Fig. 3.3, and Plate No. 3.3.

2. Support B restricted in the Z direction only, as seen in Fig. 3.4.

3. Support C restricted in the X, Y and Z directions, as seen in Fig. 3.5.

All four joints resting on the supports were free to rotate.

3.1.2 Loading Conditions

Because it was intended to have as accurate results as possible, it was decided to apply a single central load only, rather than uniformly distributed loading, to avoid any eccentricity errors or creating undesired bending or torsional strains during loading. Therefore, the model was so made as to have a joint at the centre of the bottom layer. This joint was drilled vertically through its central axis, hence it was possible to apply a single load by using wire steel cable which was pulled by a hydraulic jack. This arrangement has the additional advantage of being able to predict almost exactly the strains at the

tubes directly connected to this joint, as is the case at reaction joints without resort to any computer programming or complicated calculations. Fig. (3.6) shows the central joint.

3.1.3 Joints Systems

Two types of joints were used.

a) The top layer joints. Each of these joints as shown in Fig. (3.7) is made of two metal pieces of 2" x 2" x 0.048 in. The bottom piece is made of mild steel, while the top one is of aluminium. The pieces were connected together by five bolts and nuts. The aluminium was used to lessen the possibility of creating stress concentrations in the perspex sheet. Naturally, it would have been preferable to have both pieces made of aluminium, but because the steel tubes were brazed to the bottom piece, it was not possible to have a bottom aluminium piece too. This joint arrangement makes it easy to change perspex sheets according to the required thicknesses, and also to raise the perspex middle plane at will.

b) The bottom layer joints. Fig. 3.8 shows this type of joint which is a solid $1\frac{1}{4}$" diameter steel ball. Since there were no mild steel balls available at the time of model making, ordinary $1\frac{1}{4}$ in. ball bearings were used, after being annealed and sand blasted.

Spherical joints were chosen because tubes cross-sections can fit perfectly on spherical surfaces with any orientation desired.

3.1.4 Assembly of the Model

The model was quantitatively made out of the following

a) 40 horizontal tubes.

b) 64 space oriented tubes.

c) 25 steel ball joints.

d) 16 plate joints.

e) 1 acrylic perspex sheet of 48" x 48" x t, where t is either $\frac{1}{2}$ in., or $\frac{1}{4}$ in. or $\frac{1}{8}$ in., according to the thickness required for the test.

Since it is more practical to assume joints to be fully fixed, than to assume them pin-jointed, it was decided to fix the tubes rigidly to the joints. A technical problem was faced here and had to be overcome, since the tubes and balls were rather small in dimension and having in some joints eight tubes, it was a rather difficult and delicate job.

The tube wall was very thin in comparison with the $1\frac{1}{4}$" solid steel ball. Therefore, ordinary welding was ruled out for fear of burning out the tube's wall, besides the difficulty in controlling the soldering material. Brazing with silver solder was used instead, because it needs less heat and is more controllable.

Due to the regular nature of the model and the desire to have identical orientation in all modules, two jigs were made.

Plate No. 3.4a shows the first jig which was made from a 4 in. steel cube trimmed into 26 faces. Eight

square ones each making an angle of 90^{o} with the horizontal plane. Eight trapezoidal faces each making an angle of 45^{o} with the horizontal plane, and another eight trapezoidal faces each making an angle of 225^{o} with the horizontal plane. Finally, two parallel octagonal horizontal faces, with $1\frac{1}{4}$ in. diameter hole drilled through one of them to a depth of $2\frac{5}{8}$ in. The ball was secured in the hole in an exact central position; with each face representing certain tube orientation.

The second jig which is shown in Plate No. 3.4b. was made to maintain the proper orientation for the pyramid tubes during brazing.

Finally a large flat asbestos sheet was used to keep the whole model flat and in position when brazing the odd connecting tubes.

3.1.5 Strain and Deflection Measurements

The model has the useful property of being symmetrical about three axes, therefore strain gauging and analysis of one eighth ($\frac{1}{8}$) of the problem is sufficient. Nevertheless, it was useful to utilize this property by taking the strains of symmetrical points of expected appreciable strains and taking their average, thus eliminating the built in eccentricities of jointing and assembly. This arrangement gives also a check on the accuracy of readings and loading.

Dial gauges were used to measure vertical deflections, and two arrangements of strain gauges were used as shown in Fig. 3.11.

a) Single resistance strain gauges type PL-3 (gauge factor 1.96) were used for the steel tubes. Each three of these were located as shown in Fig. 3.9 in order to measure axial and flexural strains at the middle cross section of the tube.

b) 45^{o} rosette arrangements of resistance strain gauges type PR-10 (gauge factor 2.07), were used to measure in plane and flexural strains over the perspex surface. Fig. 3.10 shows this arrangement.

In total, eleven tubes and six perspex points were strain gauged, together with eight dial gauges used to measure vertical displacements.

3.2 Single Pyramid Cantilever Model (MODEL II)

Because, it was expected that the composite double layer grid model may not give appreciable flexural strains in the perspex plate, and because it was difficult for storage and computer time consideration to check for convergency of the solution, and in order to investigate joint behaviour in isolation, it was decided to have this small model which is shown in Plate No. 3.5.

This model was made of a typical eight-membered pyramid unit which was fixed to a rigid support, then a rectangular acrylic perspex sheet of 18" x 12" x $\frac{1}{2}$" was fixed at its centre to the apex of the pyramid using the same top joint type used in the previous model.

The tubes, and perspex sheet were strain gauged. The vertical deflections at three symmetrical points on the perspex surface were measured by dial gauges. The arrangement and location of strain measuring devices is shown in Fig. 3.12.

Two single symmetrical loadings were applied using terylene strings, hence introducing flexural strains at the strain gauged points.

This loading arrangement is seen also in Fig. 3.12. Application of symmetrical loading made it possible to analyse one quarter of the model instead of analysing the full model, and to check strain measurement accuracy and to avoid eccentricity errors. Needless to say, that joints and strain measuring devices and arrangements

followed the same principles as their counterparts in the main model.

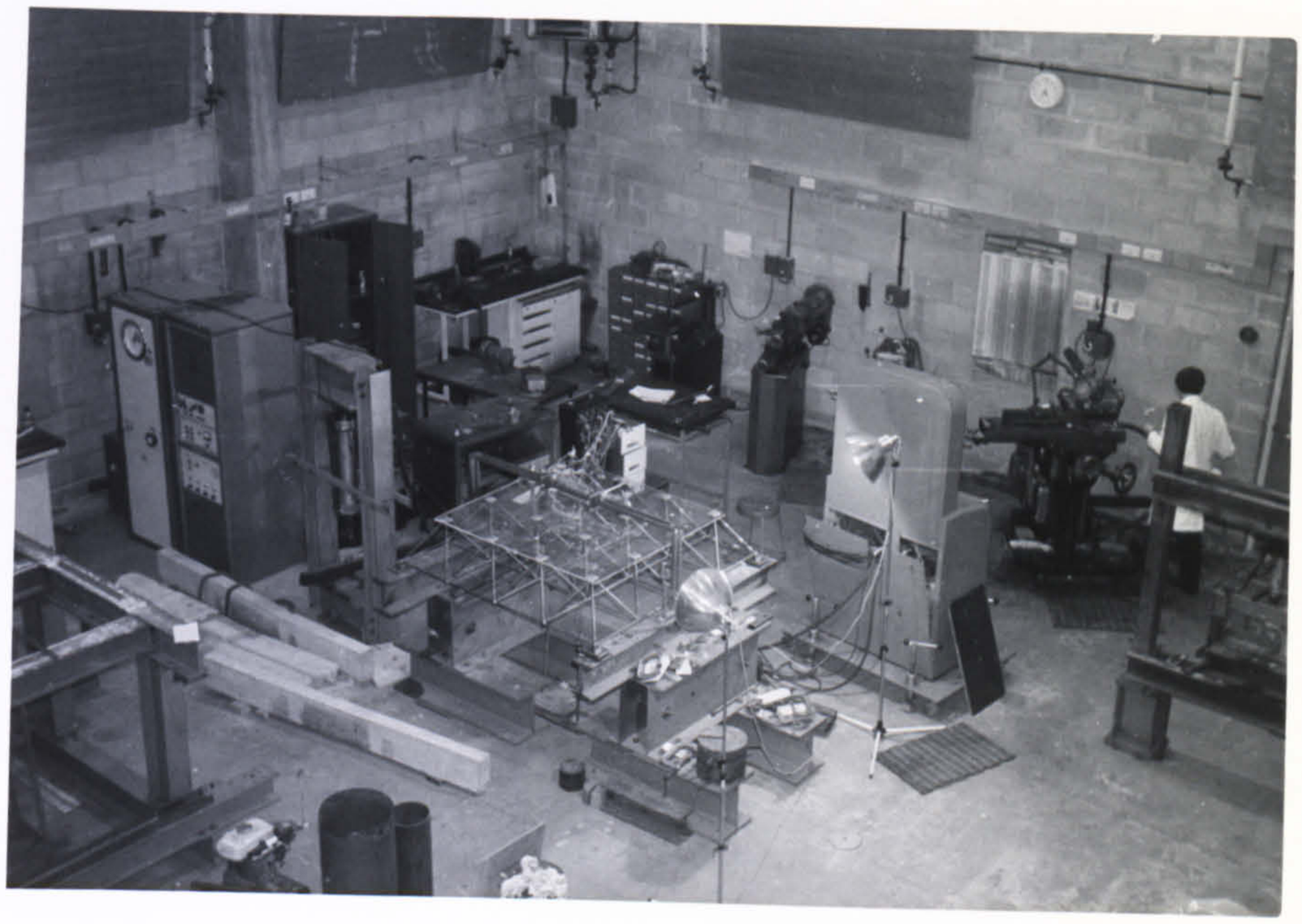

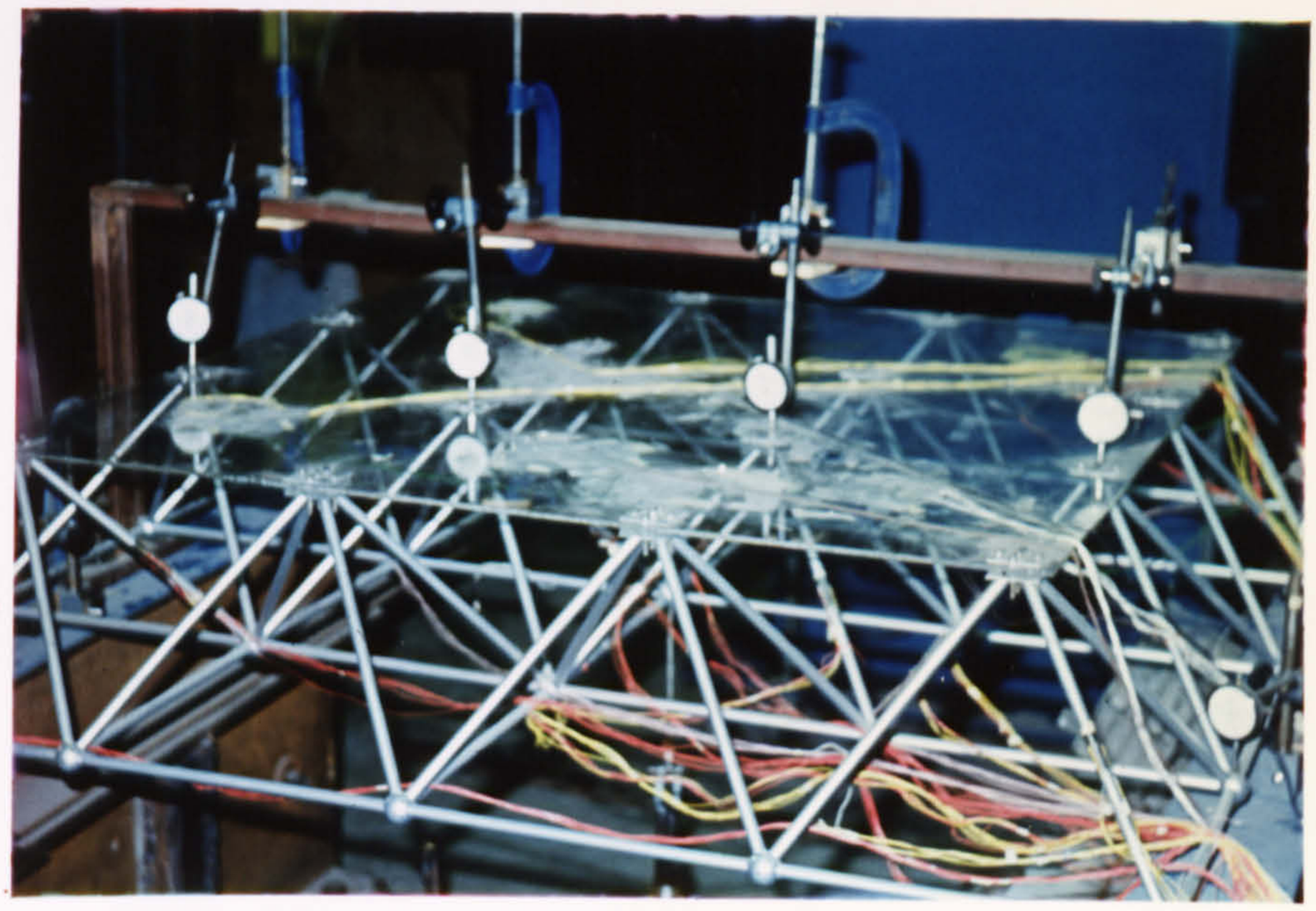

Plate 3.1: Model I, the composite double layer model, general and close up views.

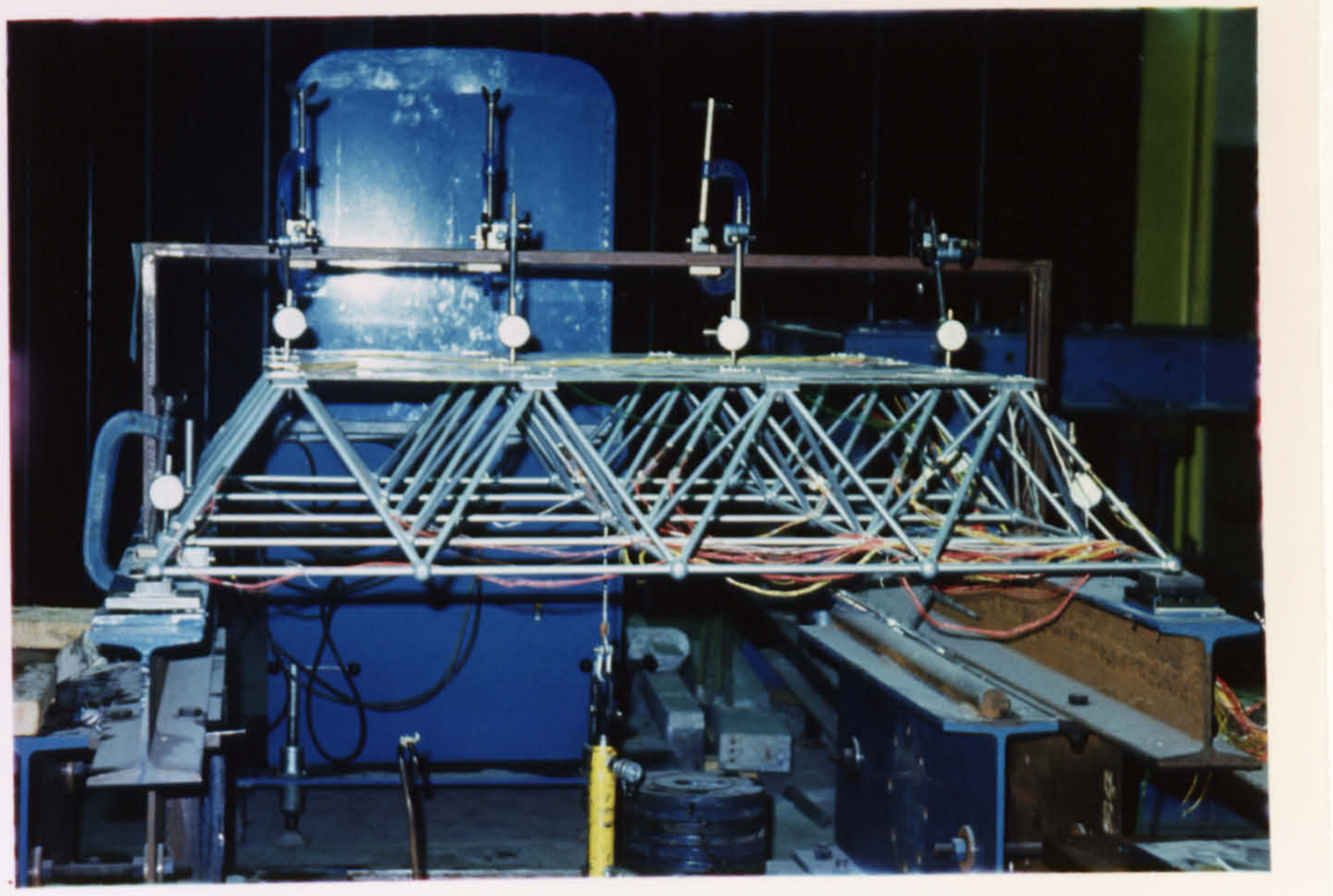

Plate 3.2: The composite double layer grid model, and its loading and support arrangement.

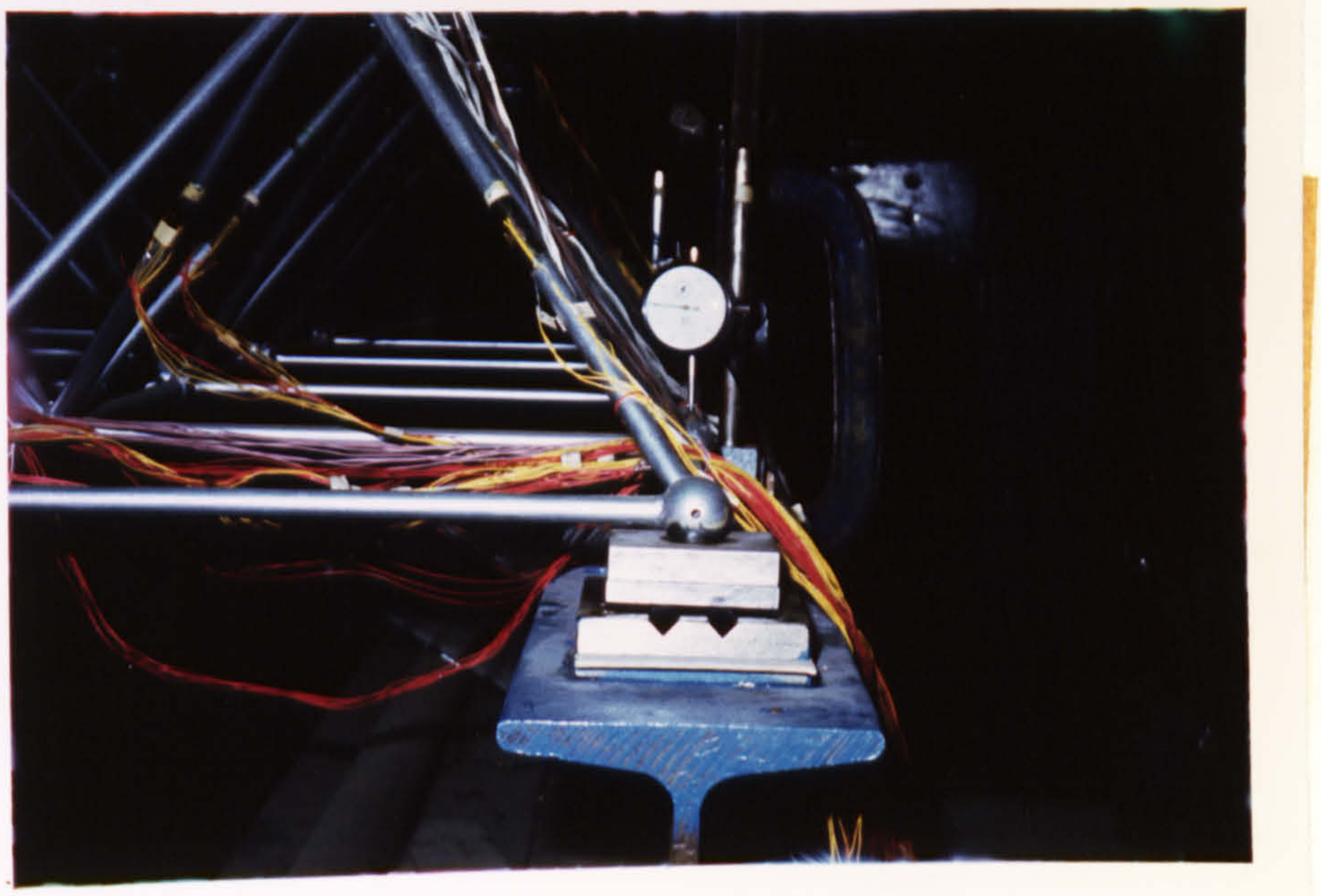

Plate 3.3: Support A, which is restricted in the X and Z-directions only

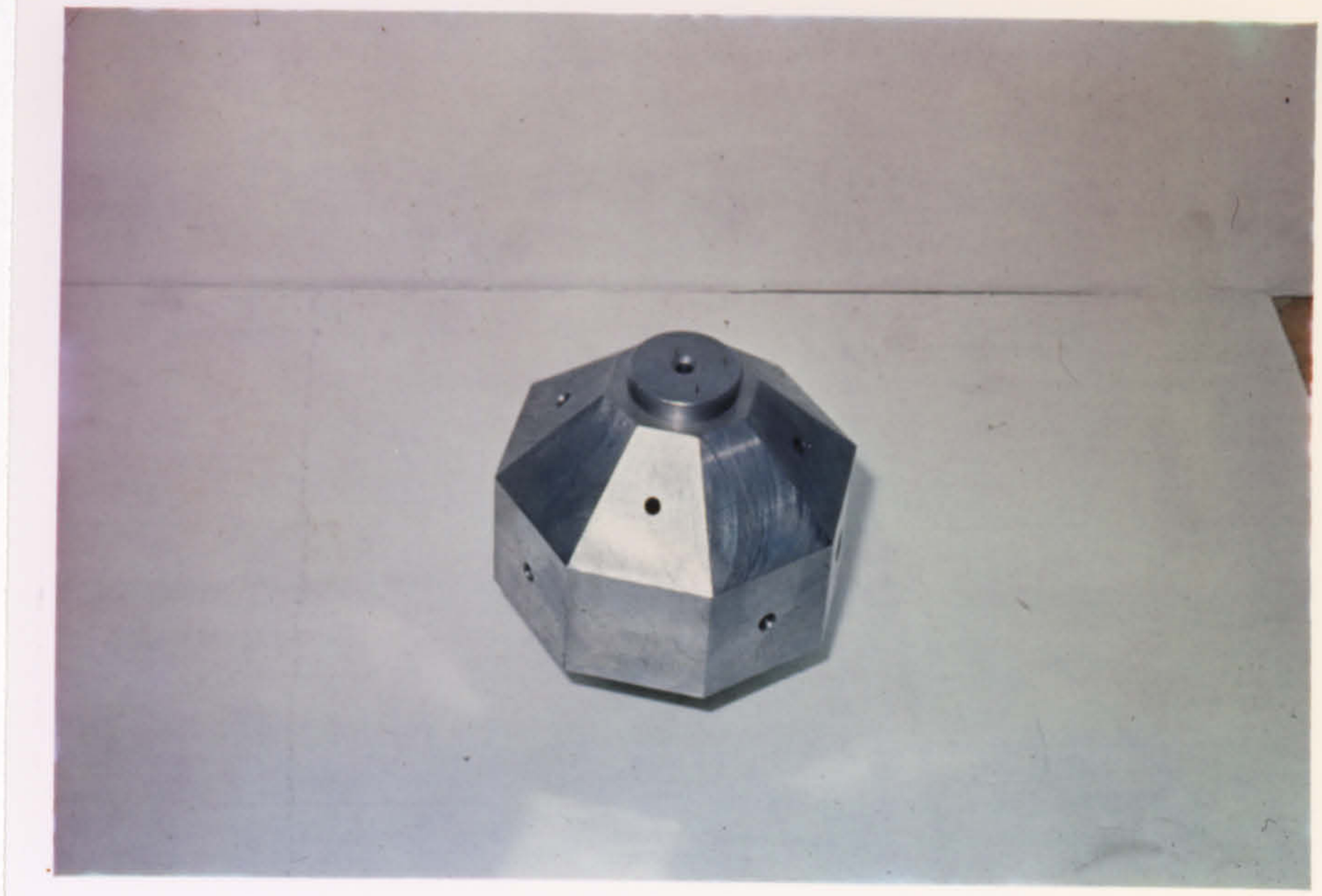

Plate 3.4a: A jig to ensure the proper orientation for the tubes in the ball joint.

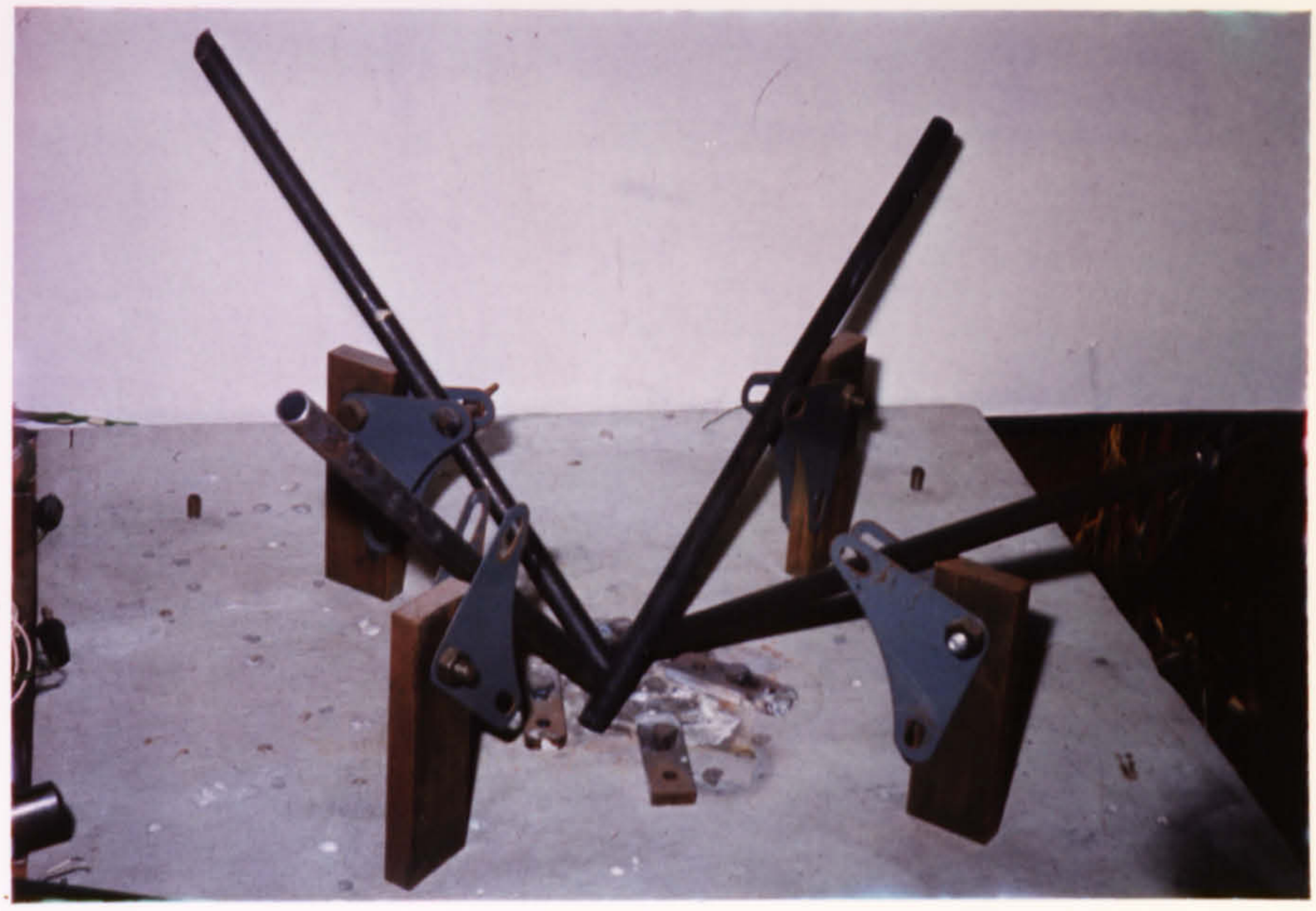

Plate 3.4b: A jig made to ensure the proper orientation for the pyramid tubes during jointing to the ball and plate joints.

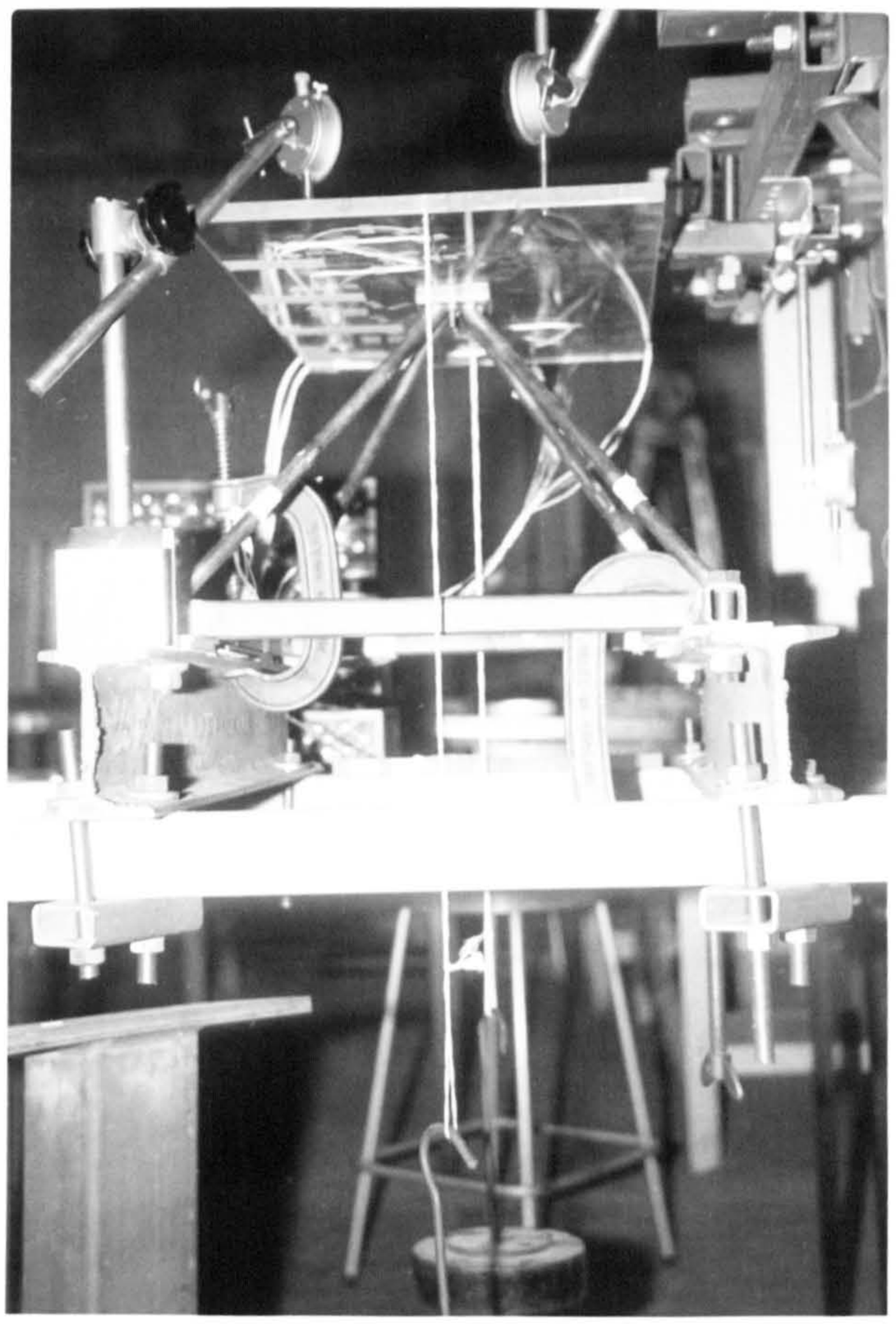

Plate 3.5: Model II, The single pyramid cantilever model, its loading and strain measurement arrangements.

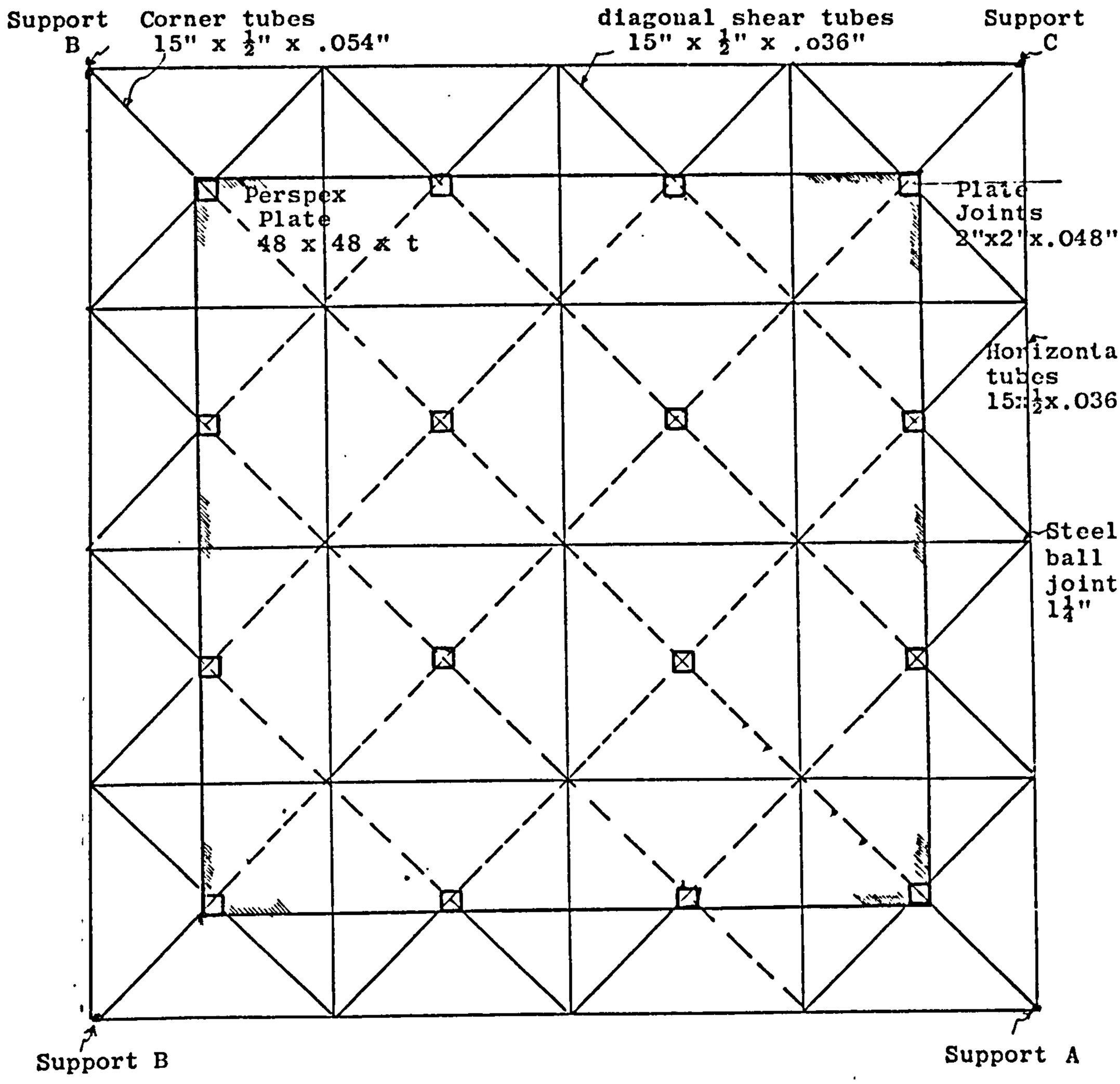

a) Plan

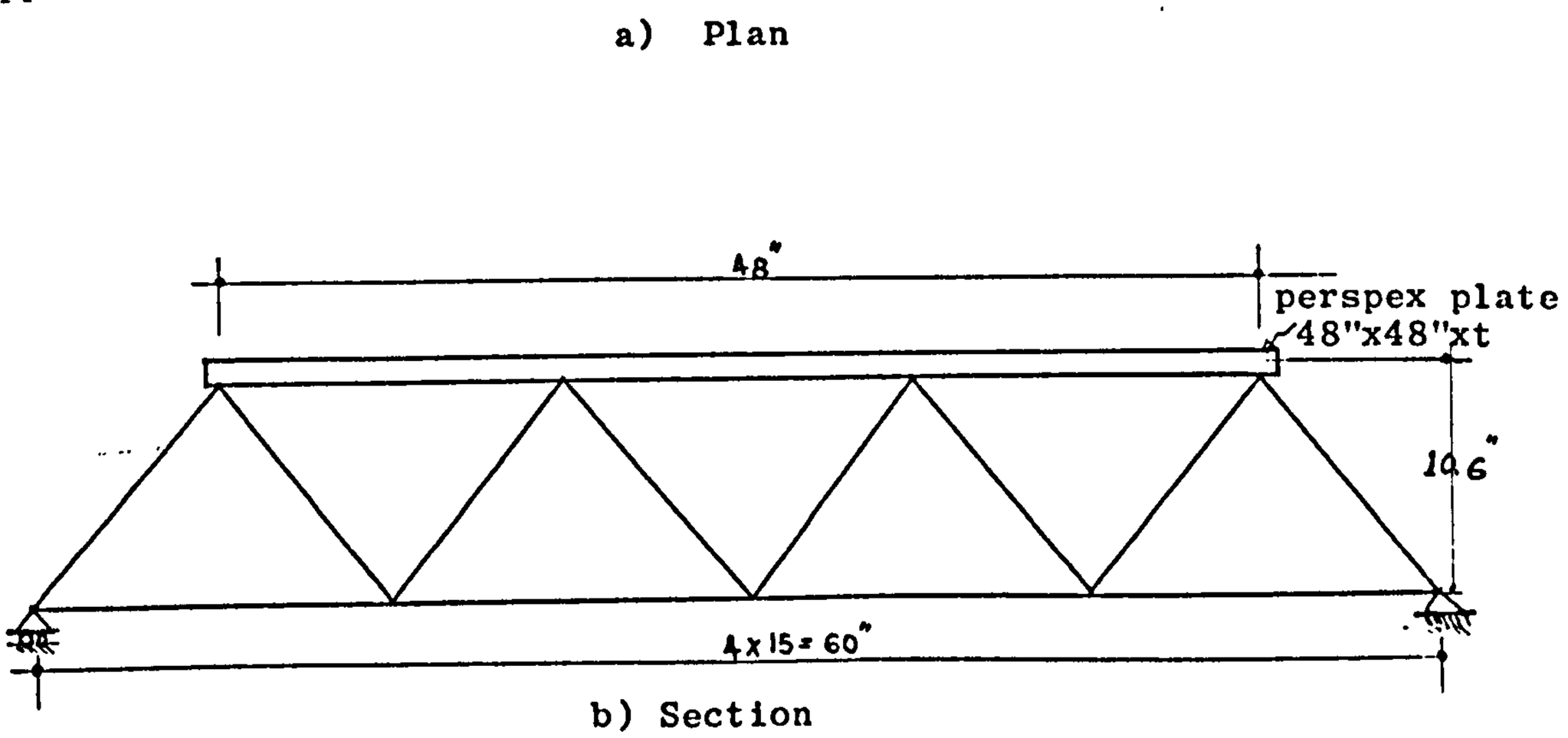

b) Section

Fig. 3.1 The composite double layer grid.

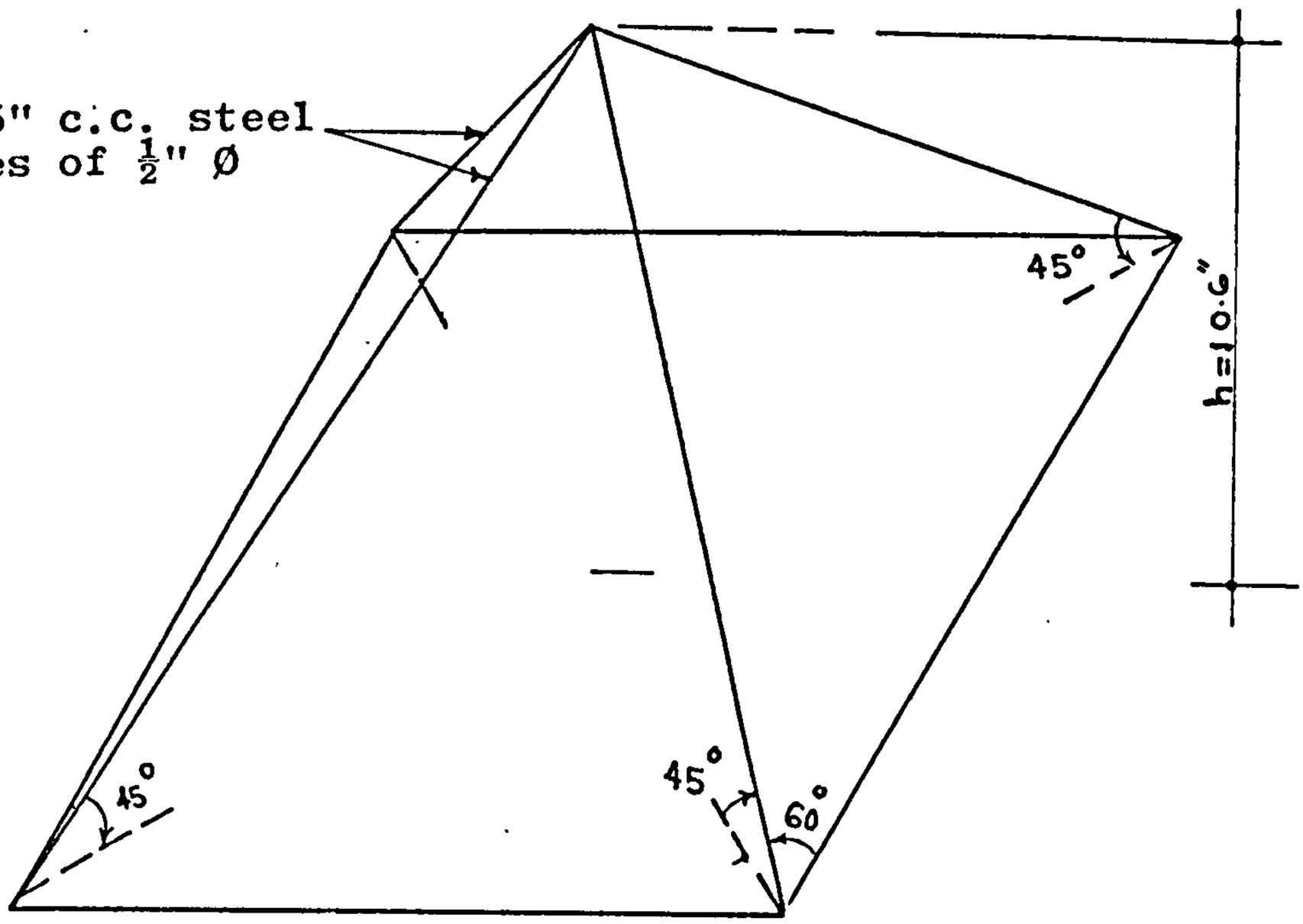

Fig. 3.2 A Typical Pyramid Scale 1/5

40

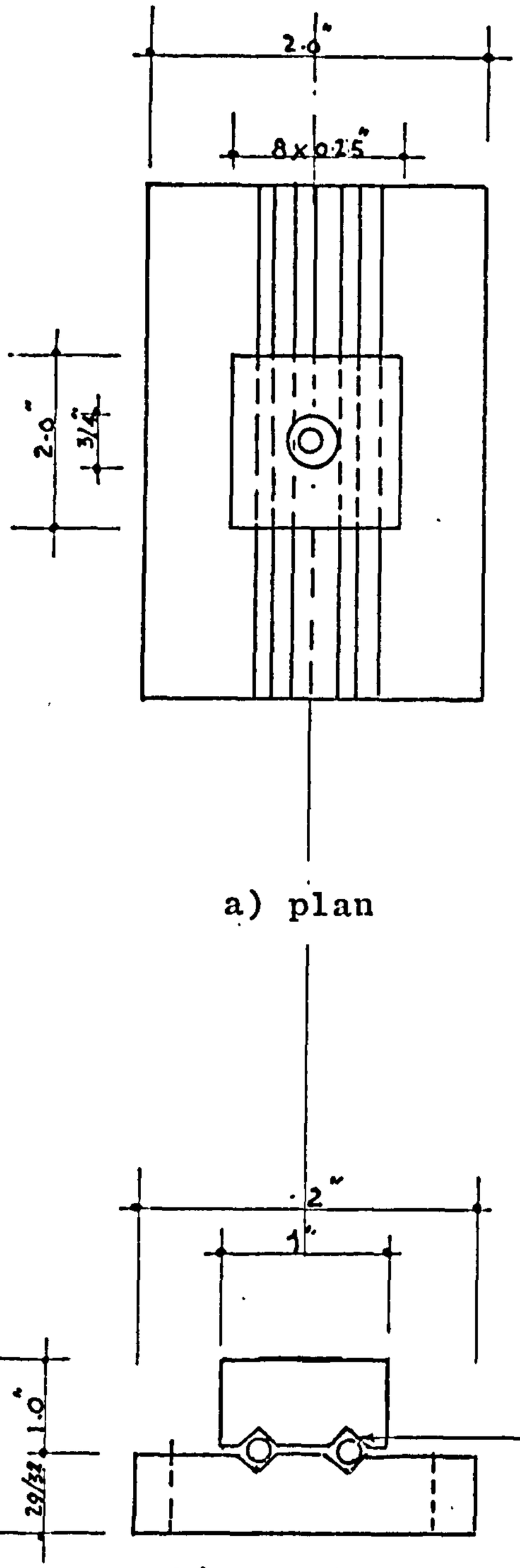

Support A

Fig. 3.3

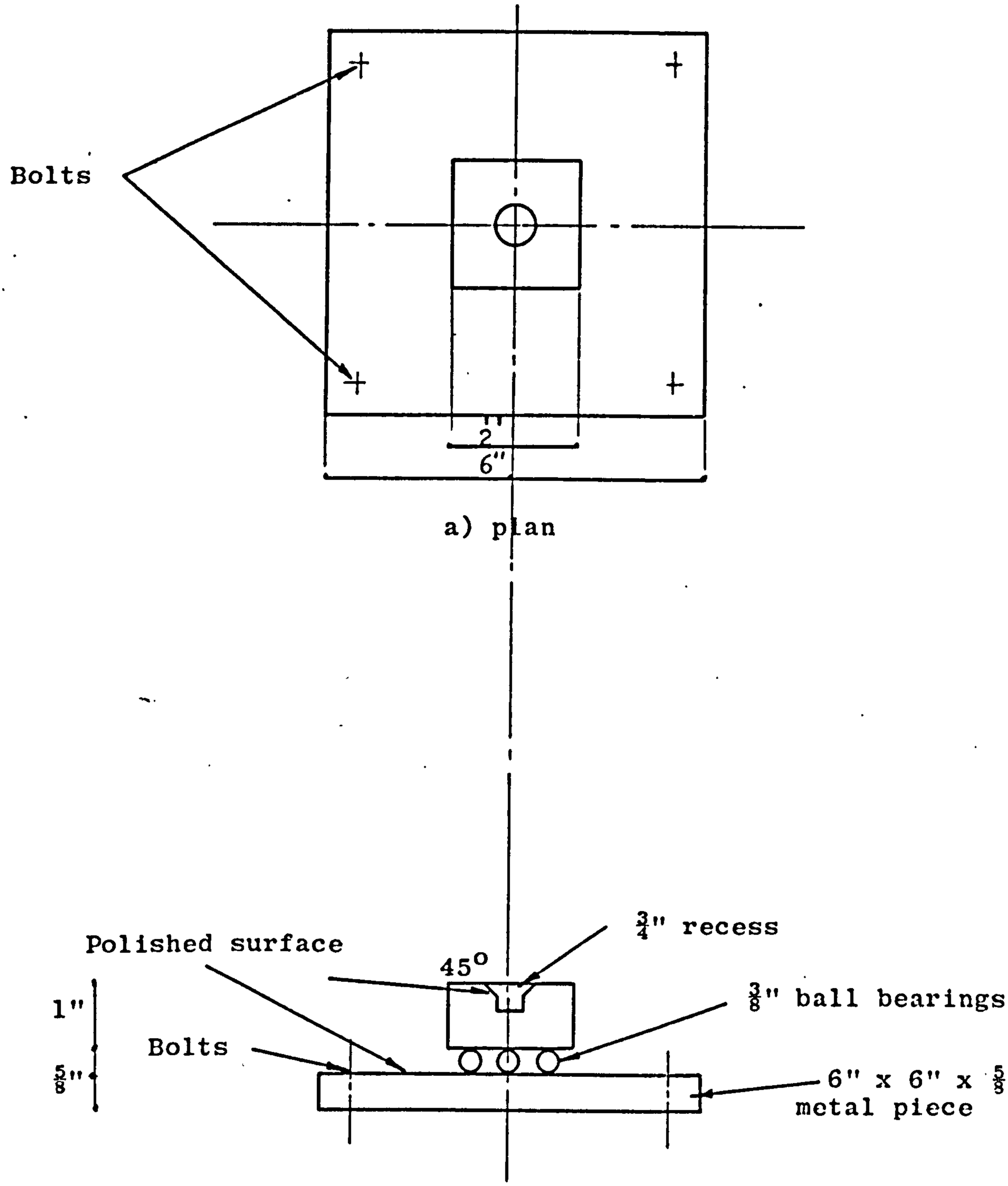

Support B

Fig. 3.4

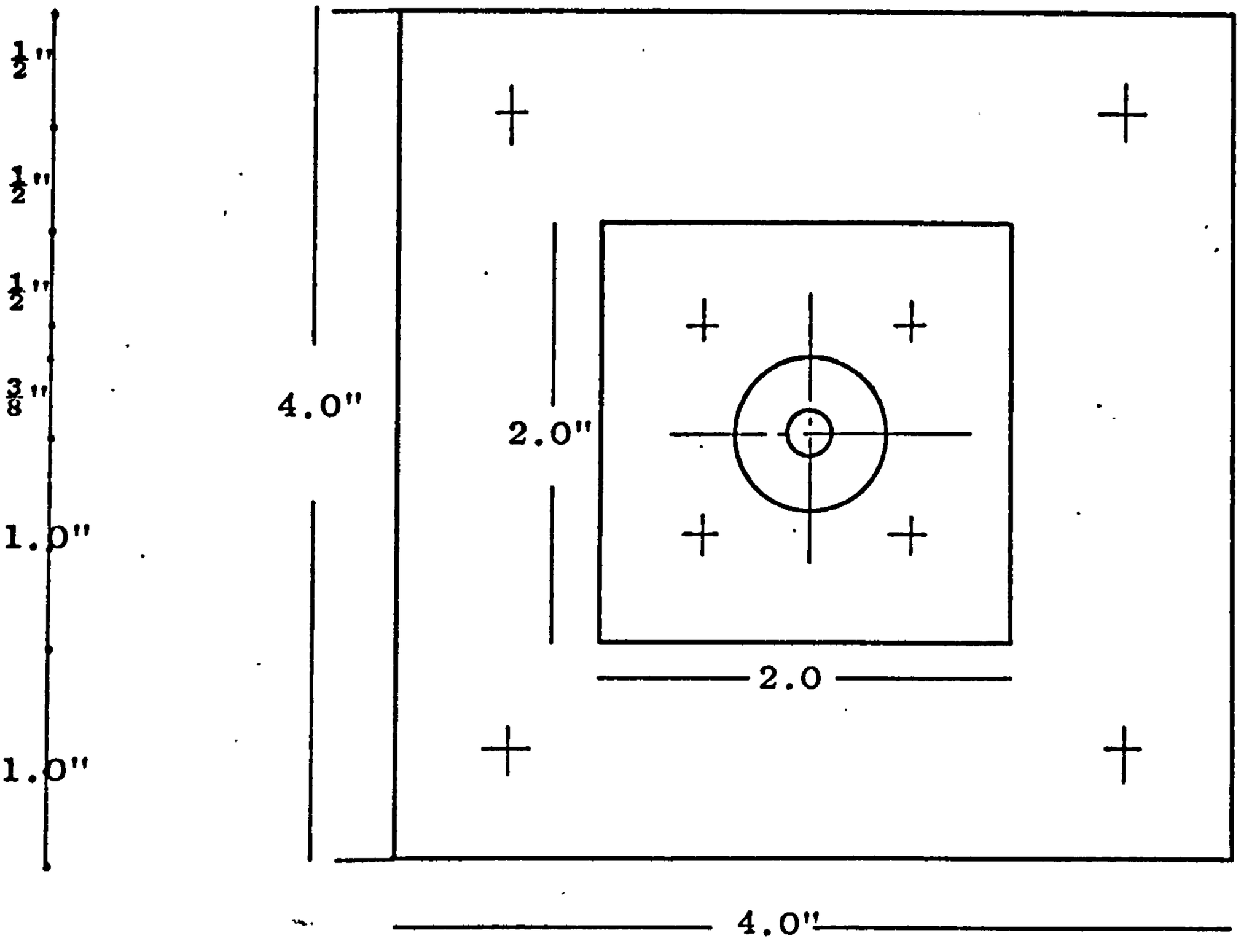

a) Plan

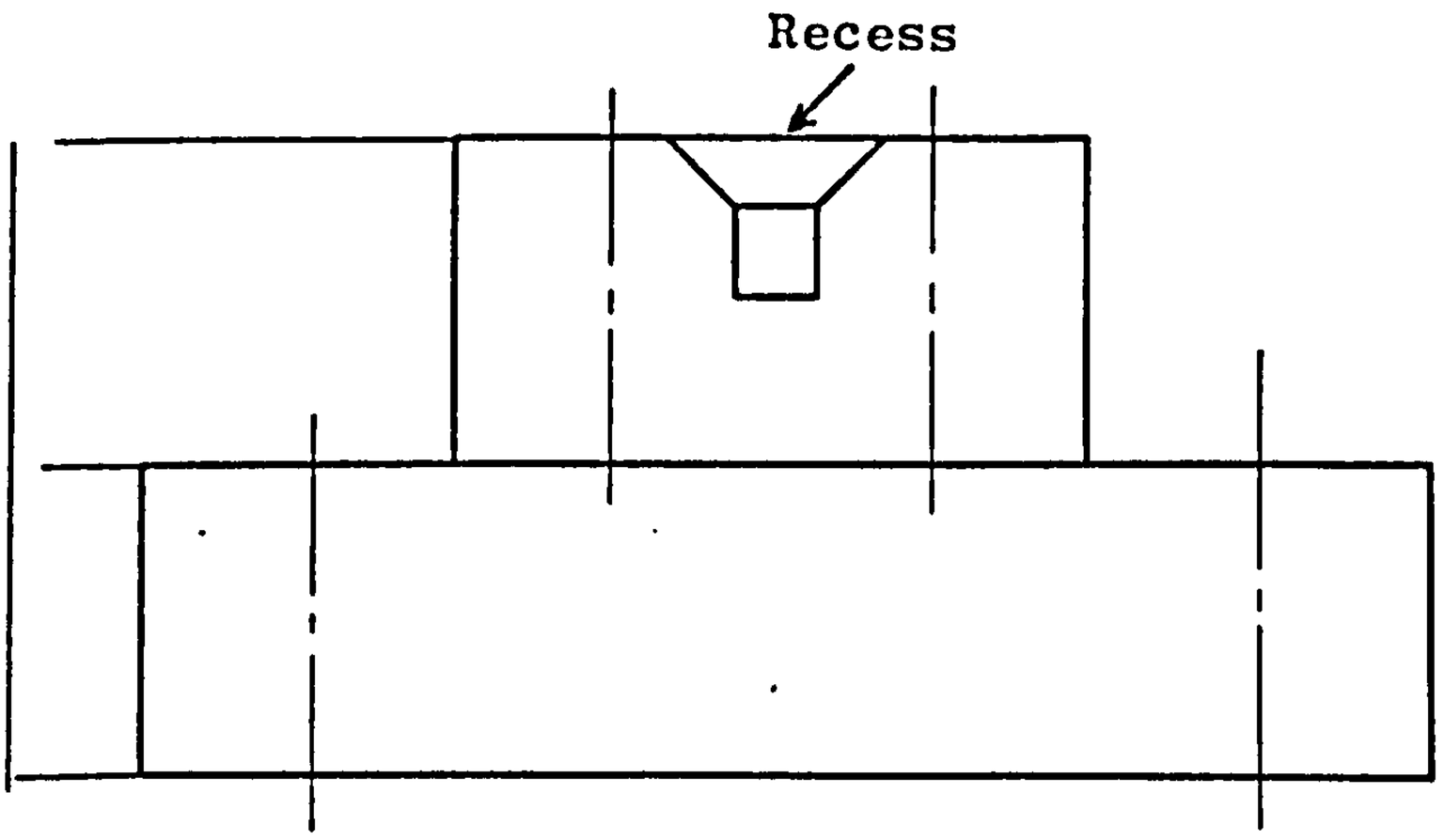

b) Section

Scale 1/1

Fig. 3.5 Support C

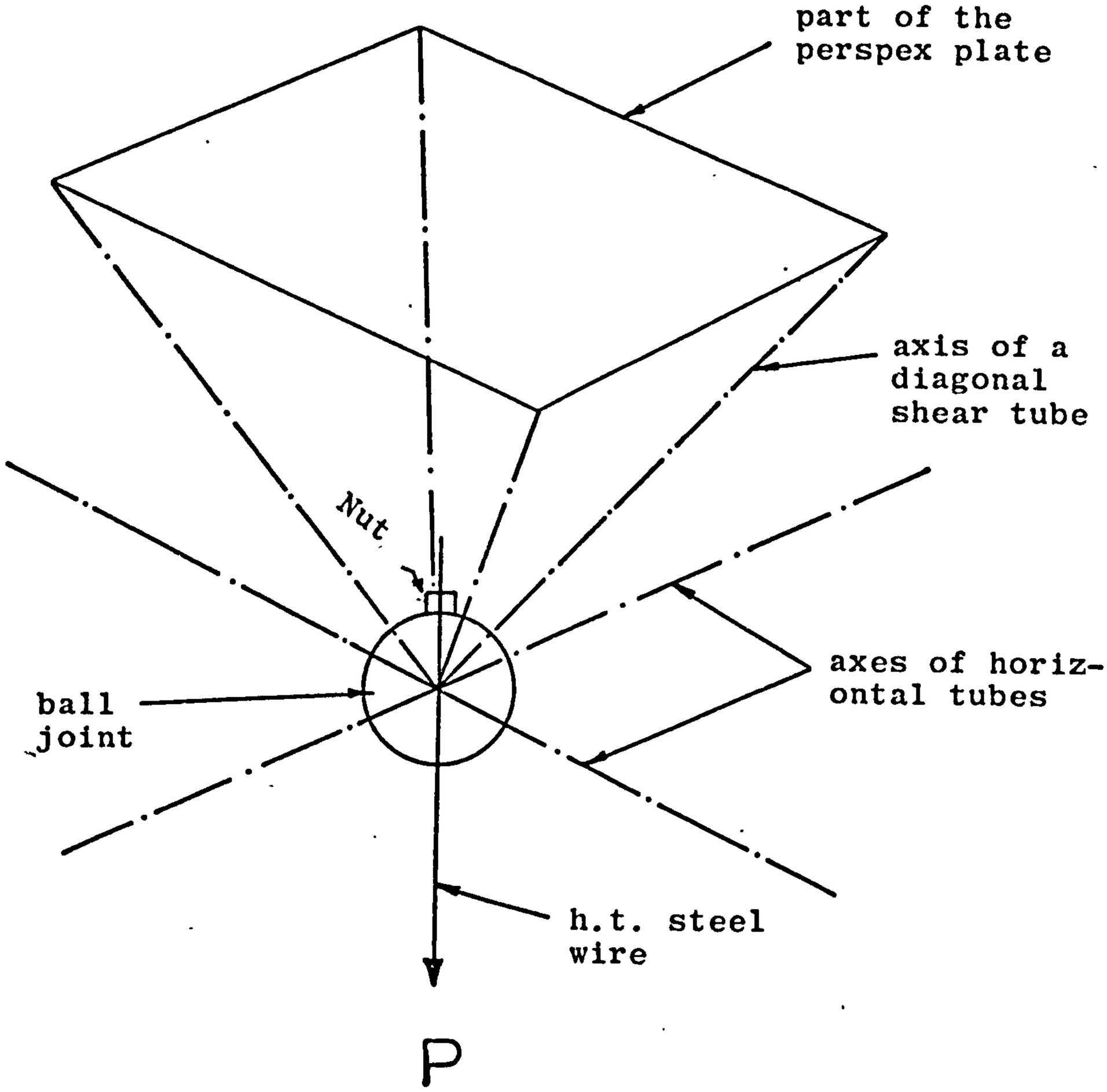

Fig. 3.6 Load application through the centre ball joint

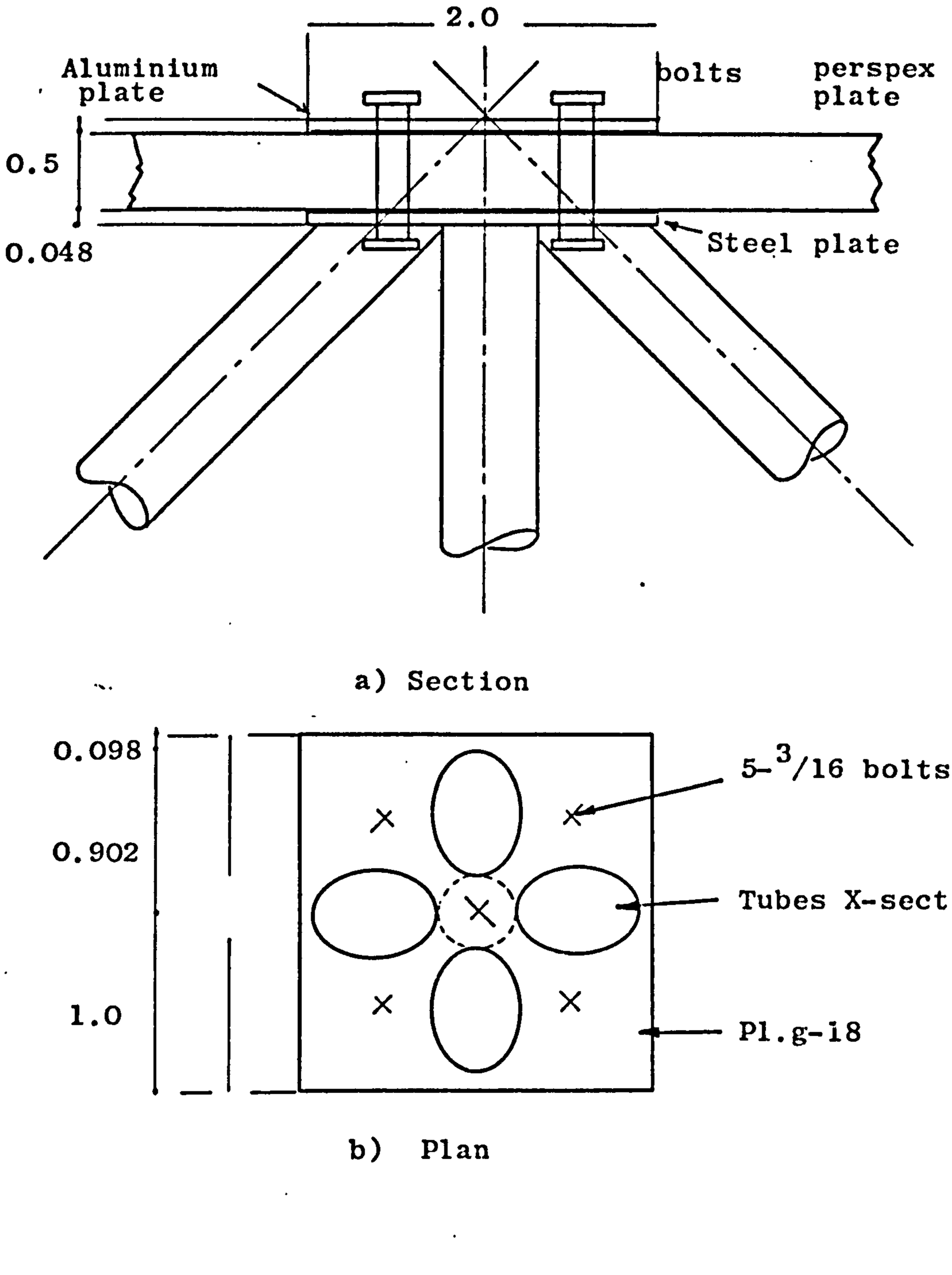

a) Section

b) Plan

Fig. 3.7 Top Joint

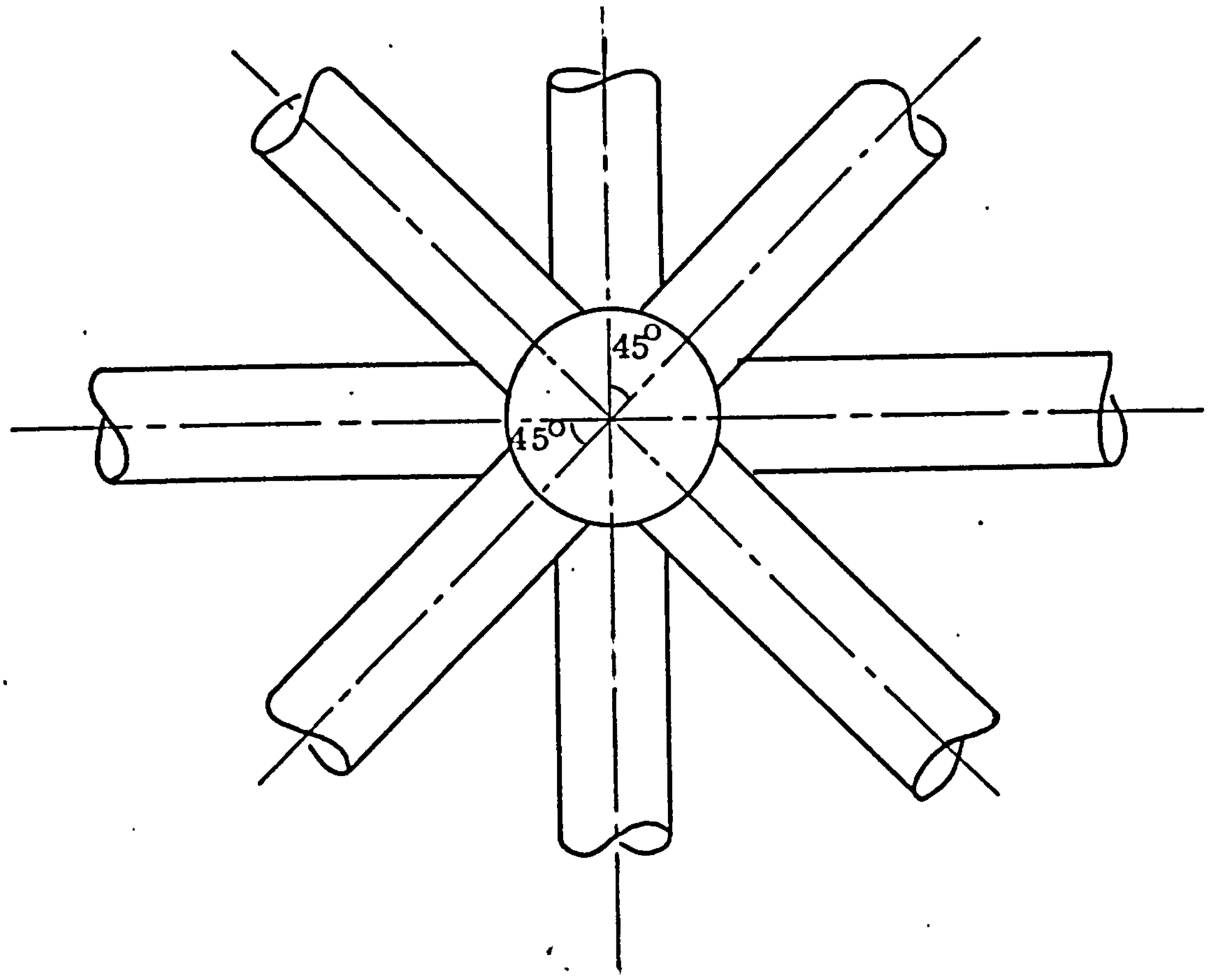

a) Plan

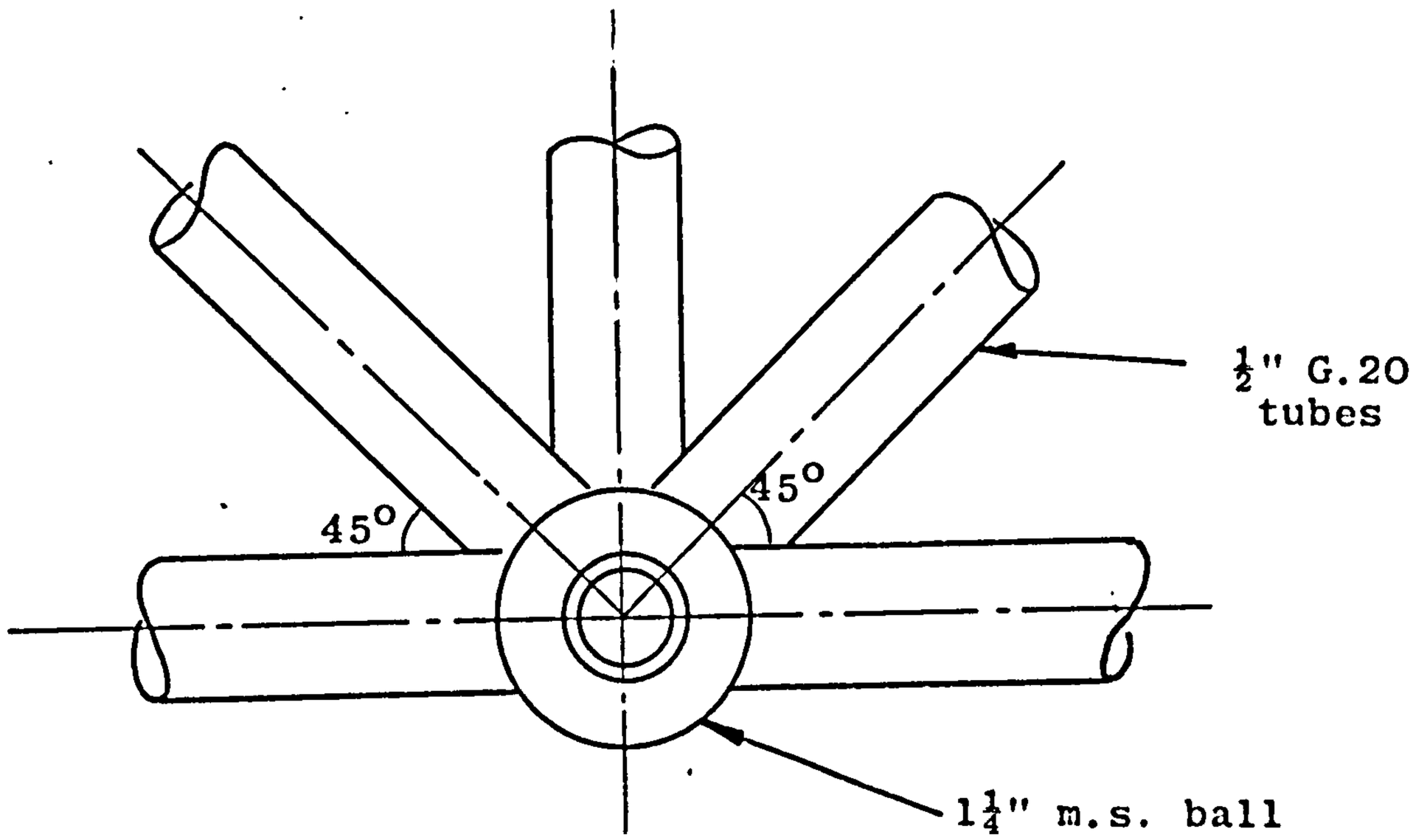

b) Section

Fig. 3.8 Ball Joints

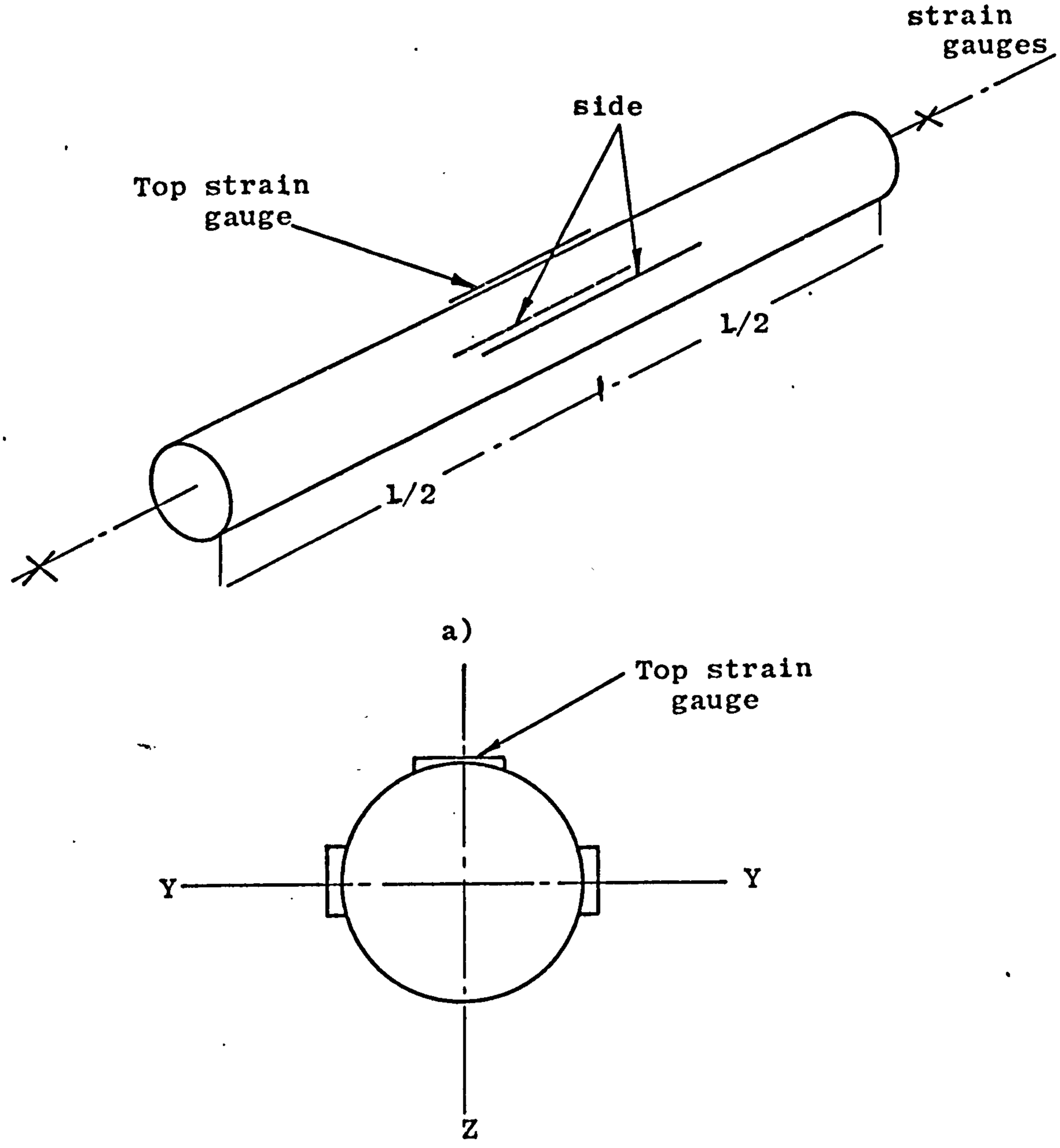

Fig. 3.9 Location and orientations of Resistance Strain Gauges on Tubes

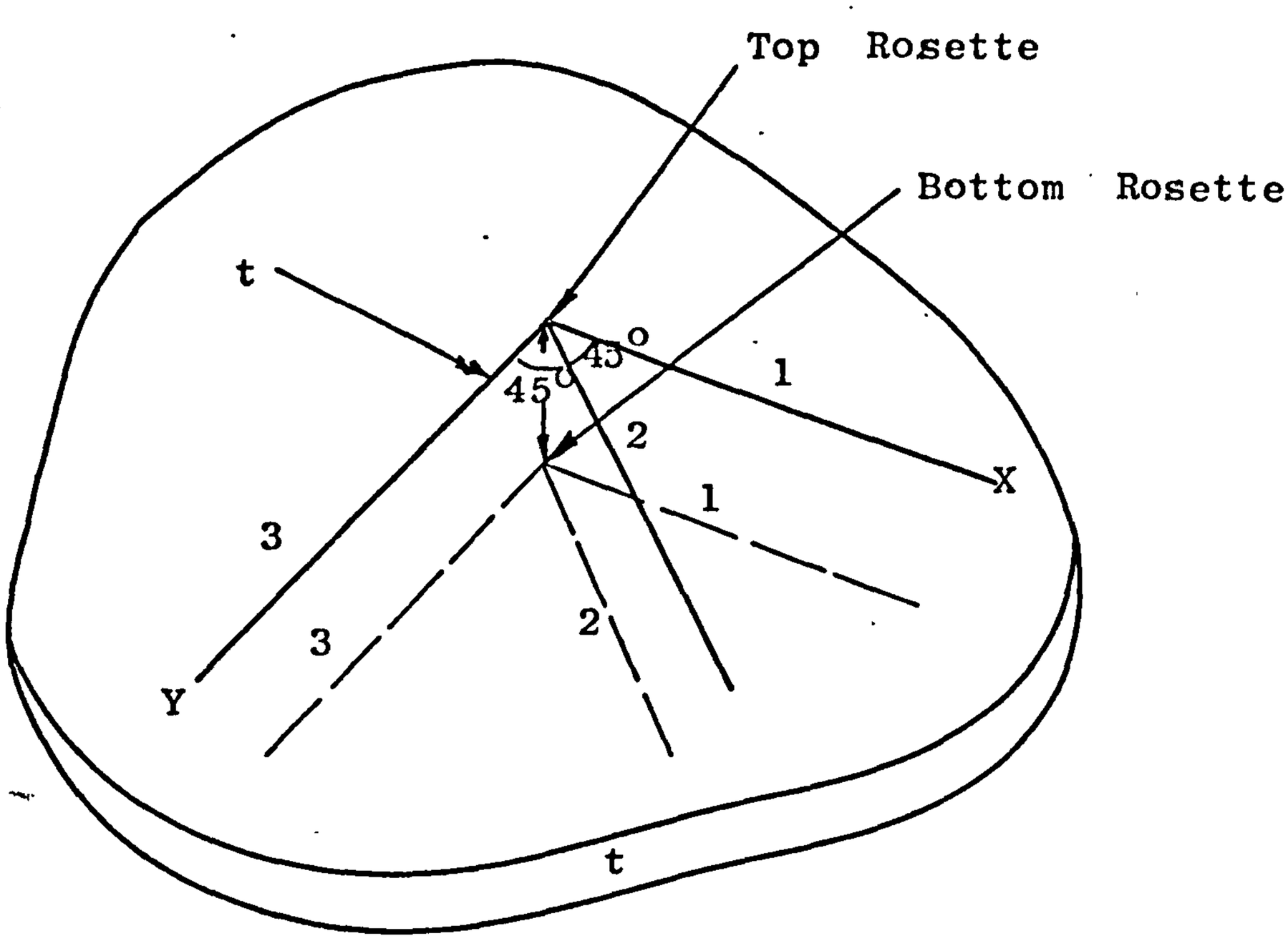

Fig. 3.10 Arrangement of Rosette pairs on perspex sheet

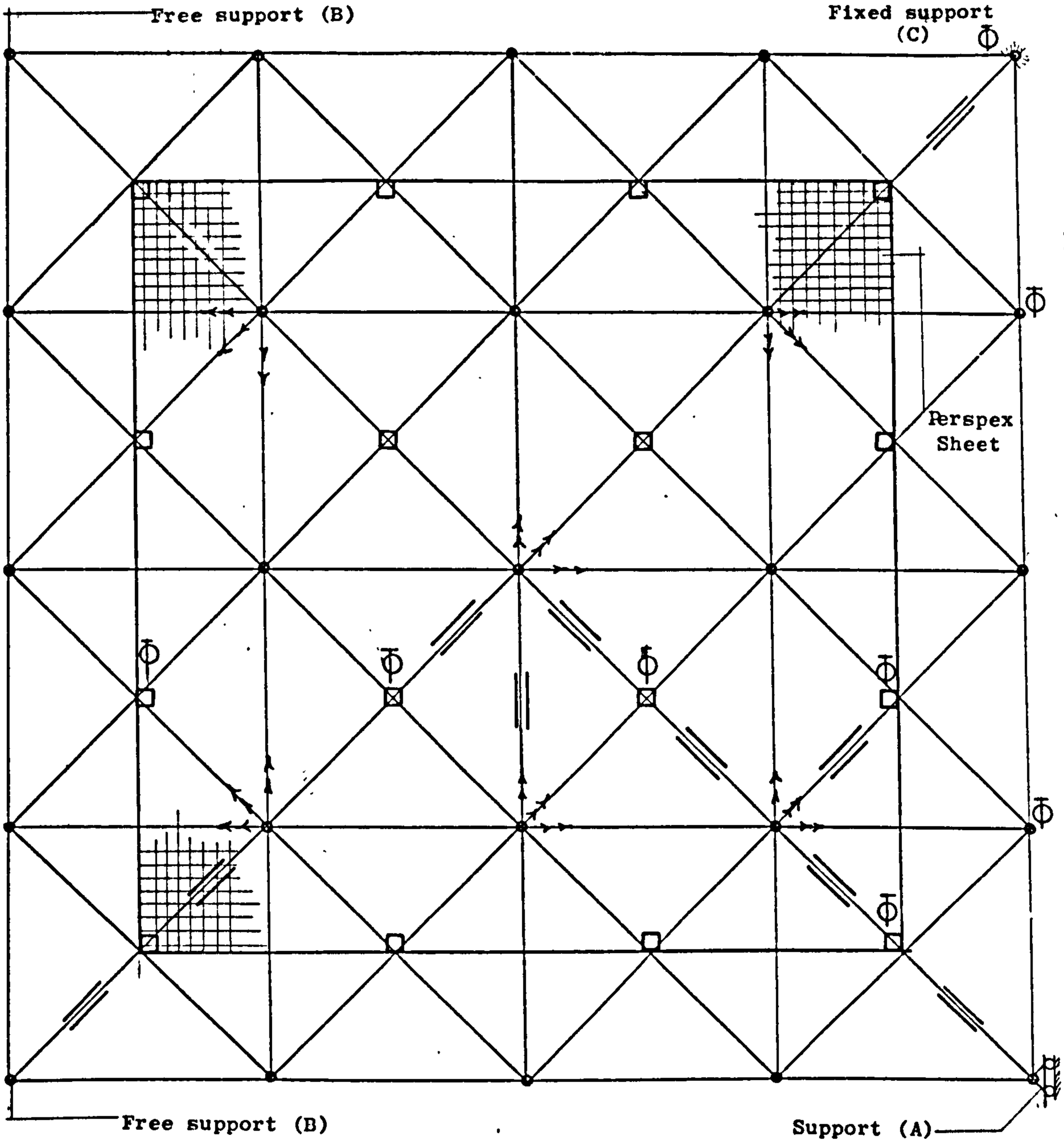

- Top layer joints
- Bottom layer joint
- Location & direction of strain gauges
- Location of dial gauges
- Location & direction of Rosettes gauges

Fig. 3.11 The Location of Strain Measuring Devices for Model I.

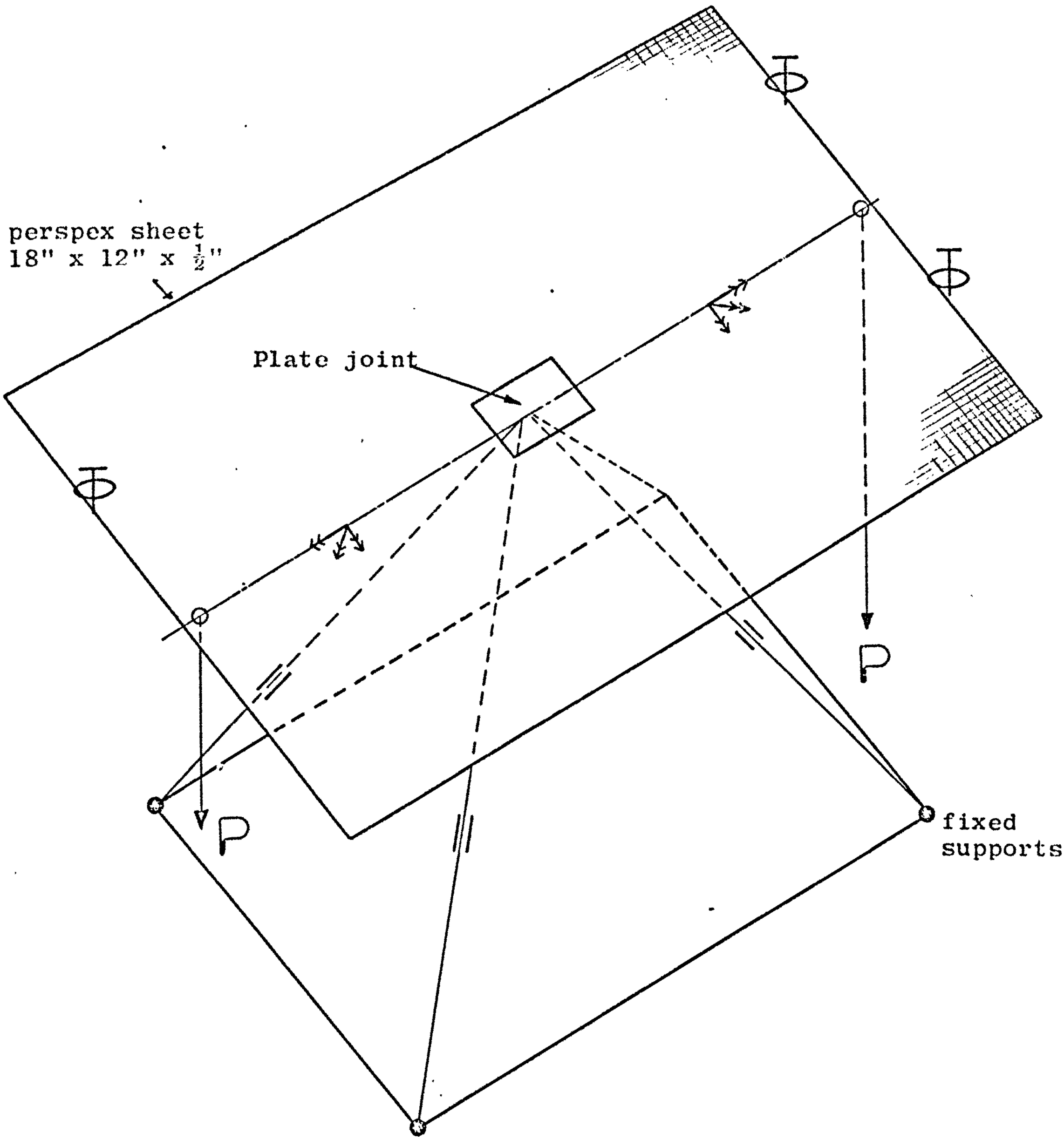

Fig. 3.12 Strain Measurement arrangements, supports conditions, one pyramid unit model

Dial gauge location

Single strain gauges

Pair of rosette strain gauges

Fixed ball joints

CHAPTER 4

THE THEORETICAL ANALYSIS

4.1 Introduction

Since composite double layer grids are a combination of space oriented members and plate members, a composite stiffness matrix analysis was used which is a linear elastic superposition of stiffness matrices for prismatic members in space and for finite plate elements.

Since the stiffness method of analysis is well established and can be found in many text books,[7] no attempt is made to describe it. No attempt is made either to describe the finite elements method for the same reason.[15,16]

Thus, it is implicitly assumed that the structure will behave elastically and that all the assumptions of small deflection theory upon which the theory of thin plates[11] and the finite element analysis[15] are based, are also valid in this analysis.

All structures which have been considered are composed of either thin steel tubes and perspex sheets, as in the practical part of the research, or of thin steel tubes and reinforced concrete slab as in the theoretical part.

Because of the practicality of the square based configuration, as was seen in the literature review, all structures analysed have been based on a square configuration.

Since it was intended to use the finite element method as a suitable tool only, hence a simple rectangular

element was used.[15] The plane stress part of this element is due to Marshall[21] whilst the plate bending part of it is due to Zienkiewicz and Cheug.[15,22] Knowing that the plate bending element is based on a non-conforming displacement function which violates the slope compatibility conditions, it was necessary to verify the convergence of the solution by experiment.[15]

The stiffness matrix for the tubes was that given by Livesley[7] with the exception of changing the signs of the terms relating to the deflection in the Z direction and the rotation about the same axis in order to be compatible with the sign convention used in the finite element analysis. The sign convention followed is shown in Fig. (4.1).

4.2 Elements Stiffness Matrices and the Overall Assembly

The equations connecting the nodal loads and the nodal displacements of a structural member can be written in many ways. In the equilibrium method which is used in this research project the appropriate form is:

$$p_1 = k_{11}d_1 + k_{12}d_2 + k_{13}d_3 + \ldots$$
$$p_2 = k_{21}d_1 + k_{22}d_2 + k_{23}d_3 + \ldots$$
$$p_3 = k_{31}d_1 + k_{32}d_2 + k_{33}d_3 + \ldots \qquad (4.1)$$

where p_1, p_2 ... etc. are nodal forces;

d_1, d_2 ... etc. are nodal displacements

k_{11}, k_{12} ... etc. are stiffness submatrices, the size of which depends on the number of components in the force and displacement vectors.

Equation (4.1) may be rewritten in this form

$$[p]^e = [k]\ [d]^e \qquad (4.2)$$

where

$$[p]^e = \begin{bmatrix} p_i \\ p_j \\ p_k \\ p_l \end{bmatrix} \quad \text{and} \quad [d]^e = \begin{bmatrix} d_i \\ d_j \\ d_k \\ d_l \end{bmatrix} \qquad (4.3)$$

and $[k]$ is the member stiffness matrix.

For a general member in space p_i, p_j etc., and d_i, d_j could be expressed as

$$P_i = \begin{bmatrix} p_x \\ p_y \\ p_z \\ m_x \\ m_y \\ m_z \end{bmatrix} \quad \text{and} \quad d_i = \begin{bmatrix} d_x \\ d_y \\ d_z \\ \theta_x \\ \theta_y \\ \theta_z \end{bmatrix} \tag{4.4}$$

As far as a tube element is concerned, it does have six degrees of freedom, while the shell element has five degrees of freedom only, namely

$$\begin{bmatrix} p_x \\ p_y \\ p_z \\ m_x \\ m_y \end{bmatrix} \quad \text{and} \quad \begin{bmatrix} d_x \\ d_y \\ d_z \\ \theta_x \\ \theta_y \end{bmatrix} \tag{4.5}$$

Fig. (4.2) shows a layout of a typical k_{11} 6 x 6 stiffness submatrix for a shell element and for a prismatic member.

The set of load-displacement equations for a complete structure may be written in the form

$$[p] = [k]\,[d] \tag{4.6}$$

where $[p]$ indicates the complete set of applied joint loads and $[d]$ indicates the corresponding set of unknown joint displacement, and $[k]$ is the stiffness matrix of the structure.

The non-existence of the sixth degree of freedom (θ_z) in eq. (4.5) means that the plate element does not have a component corresponding to in-plane torsional rigidity.

This will have two consequences.

1. At nodes where both tubes and plate meet, which will physically mean that the tubes pyramid apex will be free to rotate without any resisting moment (M_z) from the plate.

i.e. $\sum M_{z(\text{tubes})} = 0$ while $\theta_{z(\text{tubes})} \neq 0$

Although this is intuitively appealing, nevertheless, it is necessary to investigate the other extreme alternative which treats this parameter as a constraint and hence in effect assumes that

$$\sum M_{z(\text{tubes})} \neq 0 \quad \text{whilst} \quad \theta_{z(\text{tubes})} = 0$$

2. At joints where plate members only meet, the non-existence of θ_z here physically means that $\sum M_{z(\text{plate})} = 0$. In this context, this assumption presents no problem as far as individual joints are concerned. But when dealing with the whole structure according to eq. (4.6), then equilibrium equations will not be solved because the structure stiffness matrix $[k]$ becomes singular as long as there are co-planar plates which meet alone in one joint. Knowing that, in the structures concerned, all plate elements are co-planar and parallel to the global coordinates, and most of the nodes are without tube members, the singularity problem has to be faced and be overcome.

The following are the possible ways to overcome singularity

a) To assemble the equations at points where elements are co-planar, in local coordinates, and then to delete the unwanted columns and rows (which are related to $\theta_{z(plate)}$) with their corresponding elements in load vector. The disadvantage in this method is that it needs a lot of computer work and time to reorganize the structural stiffness matrix.

b) By inserting an arbitrary in-plane stiffness coefficient k'_{θ_z} at such points only. This has been suggested by Zienkiewicz.[16] It leads to replacing $0 = 0$ by $k'_{\theta_z} \times \theta_z = 0$. This on transformation leads to a perfectly well behaved set of equations from which all displacements including θ_z are obtained. As θ_z does not affect the stresses and is uncoupled from all equilibrium equations an arbitrary value of k'_{θ_z} can be inserted as an external stiffness without affecting the result.

For a triangular element these were defined by a matrix such that in local coordinates equilibrium is not disturbed. The matrix is

$$\begin{bmatrix} M_{zi} \\ M_{zj} \\ M_{zk} \end{bmatrix} = \propto Et\triangle \begin{bmatrix} 1 & -.5 & -.5 \\ & 1 & -.5 \\ \text{sym.} & & 1 \end{bmatrix} \begin{bmatrix} \theta_{zi} \\ \theta_{zj} \\ \theta_{zk} \end{bmatrix} \tag{4.7}$$

where E is modulus of Elasticity, t is plate thickness, $\triangle$ is element area; and $\propto$ is some coefficient to be specified later. This additional stiffness affects the

results because it occurs at nodes which are not co-planar. However, Zienkiewicz showed that the effect of varying α between 1 and zero is quite small. For practical purposes, he recommends $\alpha = 0.03$ or less. Following the same procedure, for a rectangular element, one can presumably use

$$\begin{bmatrix} M_{zi} \\ M_{zj} \\ M_{zk} \\ M_{zl} \end{bmatrix} = \alpha \, EtA \begin{bmatrix} 0.99 & -.33 & -.33 & -.33 \\ & .99 & -.33 & -.33 \\ & & .99 & -.33 \\ \text{sym.} & & & .99 \end{bmatrix} \begin{bmatrix} \theta_{zi} \\ \theta_{zj} \\ \theta_{zk} \\ \theta_{zl} \end{bmatrix} \tag{4.8}$$

where A is the area of the rectangle and α will subsequently be chosen to be less than 1 and preferably very small and upon trial and error. This method also involves some extra programming and introduces a new approximation factor.

c) By inserting a very large number say (10^{74}) at the diagonal elements relating to such nodes. This in effect means

$$M_z = k'\theta_z \times \theta_z = 0$$

$$= 10^{74} \times 0 = 0$$

The advantage of this method is it does not involve any extra computer work, because it deals with such nodes as it deals with constraints. The disadvantage is that it needs more storage than method (a). Method (c) was used by the author.

Because the structures considered are flat and because the local coordinates are parallel to the global ones, therefore the assembly of finite element stiffnesses was made in local coordinates.

4.3 The Computer Program

A complete computer program was developed to do the analysis. The Algol programming language was used. Since the problems tackled are very demanding both on computer time and storage, it was convenient to split the analysis into separate programs, each executing a certain stage using direct access disc backing files to store the numerical data and results during the execution of the whole program suite. The suite was composed of the following subprograms.

I. Program 1 which reads data from a file.

Members were indexed according to their nature, properties, and orientations.

II. Program 2 which forms the individual stiffness matrices for representative samples, also it forms the individual transformation submatrices for representative orientations.

III. Program 3 which plants the individual stiffness matrices for all members into their proper locations in the structural stiffness matrix. Then it does the following steps.

a) Checking for any diagonal stiffness element of zero value and substitute it by a large number (10^{74}), thus avoiding singularity during the later solution stage.

b) Implementing the prescribed displacements (boundary conditions) by multiplying the displacement and substituting their corresponding diagonal elements by 10^{74}.

c) Implementing the spring conditions if any by adding the spring stiffness to its corresponding diagonal

element.

d) Then the whole stiffness matrix is stored in a half-band width form on the disc backing file.

This program was modified slightly to suit the composite problem from an existing departmental program which only handled elements with equal numbers of nodes. The modification was to make it capable of handling elements with varying number of nodes.

IV. Program 4

This is the only program written in the Fortran programming language. It is also a departmental program which takes the matrix from the disc backing file store. The only modification done was to improve the execution time by skipping the division of off-diagonal elements by the relevant diagonal element whenever the value of this element is very large (10^{74}). This is physically related to an imposed boundary condition or node with finite elements members only. It meant an improvement of up to 25% in some problems. Naturally, this would have been more if a finer finite element subdivision was used.

V. Program 5

This program produces the output results according to the requirement and class of the structure analysed. It prints out the following:

1. Nodal displacements in global coordinates.

2. In relation to tubes, it prints out forces and stresses in local coordinates at the end and middle sections.

3. In relation to Finite Element Members, it

produces the following in local coordinates.

a) Nodal forces and stresses for each element.

b) Forces and stresses at the centre of each element, by taking the average of related nodal forces and stresses.

c) Average principal forces and stresses at the centre of each element.

d) Average nodal forces and stresses for each node in the slab. This is done by dividing the total forces and stresses at the node by the number of contributing elements.

e) Average principal forces and stresses for each node in the slab.

4. Reaction forces in global coordinates.

5. Inter-joint forces which are acting on the slab nodes as a result of tubes displacements.

4.4 The Capabilities of the Computer Program

The developed computer program is capable of analysing the following cases as individual or combined problems.

1. Pin-jointed space skeletal structure.
2. Rigid jointed space skeletal structure.
3. Plate under plane stress conditions only.
4. Plate under bending conditions only.
5. Composite analysis in which plate elements can take any orientation, such as folded plate structures.
6. Spring analogy analysis (see Chapter 10).

It is needless to say that although tubes are the only prismatic members considered in this research, this by no means limits the generality of the computer program in this sense as long as the physical and geometrical properties of the members are known.

4.5 Data Generating Programs

It is obvious that this type of program needs a relatively massive input data especially in large problems. Hence it was necessary to generate the data by computer also. Since the program is general for any configuration and with any finite element subdivision, it was not practical to include such data generating programs in the suite. Thus for each type of configuration covered in this research a special generating program was made assuming 4 Finite Element subdivisions per single pyramid base. Each program needs only the number of pyramids along each side and the loading per node as an input.

4.6 Size of the Structures Analysed

Since all structures analysed in this research are symmetrical about three axes, which is indeed the characteristic of double layer grids in practice, it was theoretically permissible to analyse one eighth of the structure only. But this would have meant the use of triangularly shaped finite elements which are inferior to the rectangular ones, and also would have meant having to deal with partially constrained joints. Therefore one quarter of the structure was always analysed to represent the whole structure.(19)

Despite this great advantage, and the rather considerable store capacity of 256 k available for the ICL 1904S computer system in Strathclyde University yet the number of bays (pyramids)/side used which determines the band width and hence the minimum storage requirements ($= (\frac{BW}{2})^2 + \frac{BW}{2}$) during matrix inversion procedure, was still hampered by the limited storage and time capacities of the computer facilities available. The largest problem handled was of 5 x 5 bays (per quarter). When 130 k storage facility was allocated to the inversion procedure for this problem, a total of 75 minutes of execution time was required. But when the same problem was granted 230k which meant the exclusive use of the machine, the execution time was reduced drastically to 25.41 minutes only, i.e. an improvement of about 300%. This was the result of the reduction in the number of transfers between the disc backing file and the core storage from about 500,000 to

15,663. The size of the half banded structural matrix of the above problem was 1230 x 216, and the span-depth ratios were 40, 29, 22 according to depth classification as shallow, moderate or deep respectively. Nevertheless, this structure is by no means a large span structure especially to the extent envisaged for this type of structure. This clearly demonstrates the limitation of this method of analysis, and highlights the importance of finding an approximate method (or methods) which dispense with the need for such excessive store and time requirements or better still to completely dispense with the use of the computer, at least for the preliminary design steps.

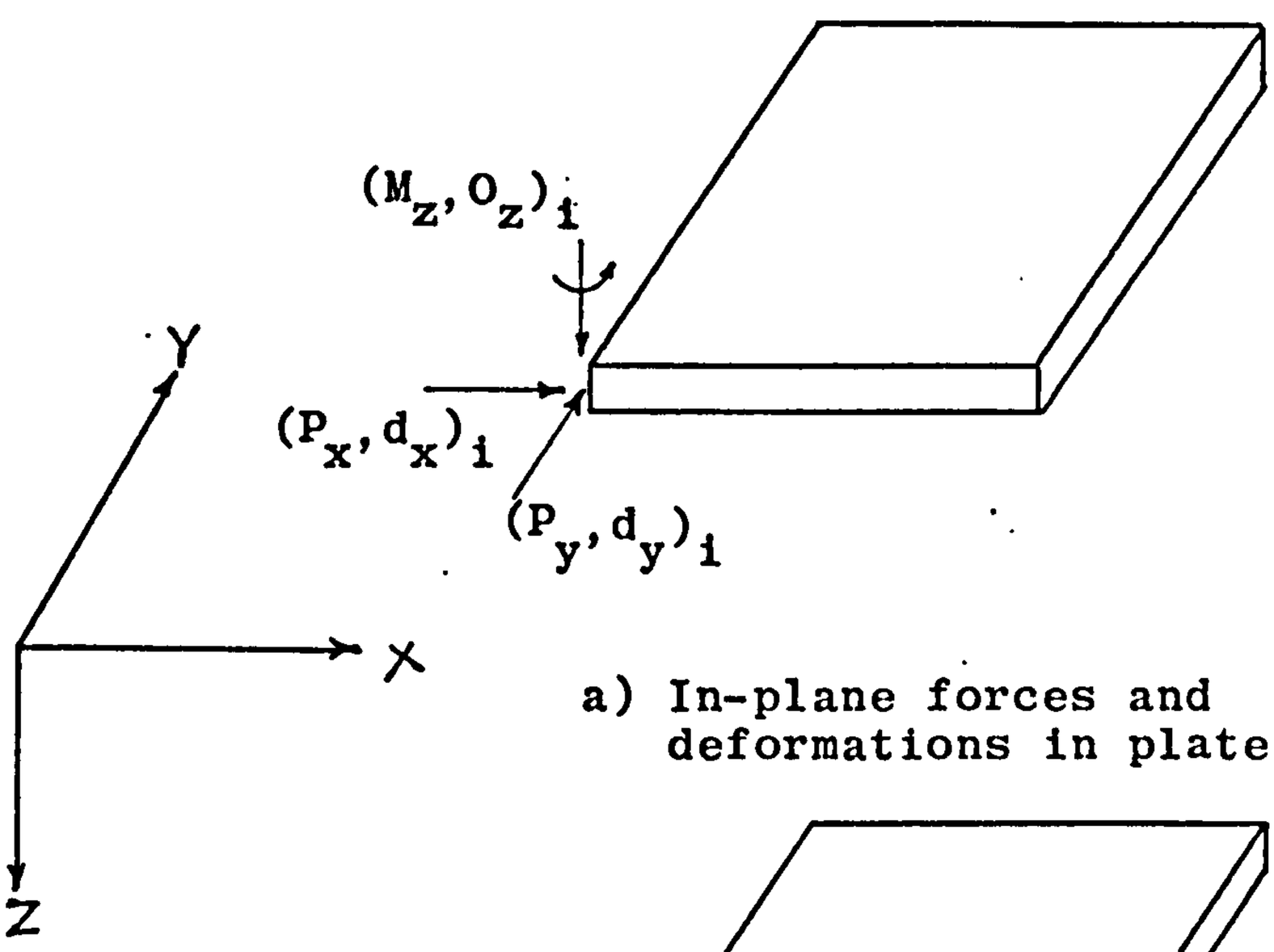

a) In-plane forces and deformations in plate

b) Bending forces and deformation in plate

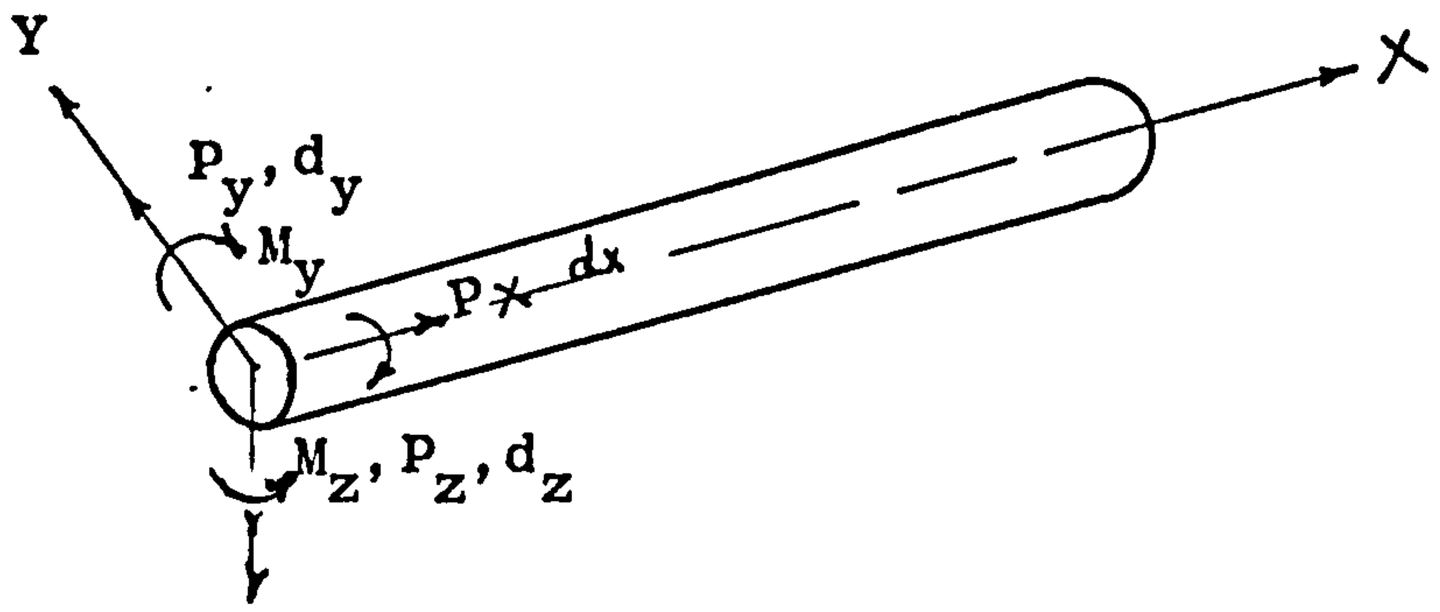

c) Forces and deformation in tube.

Fig. 4.1 Sign Convention

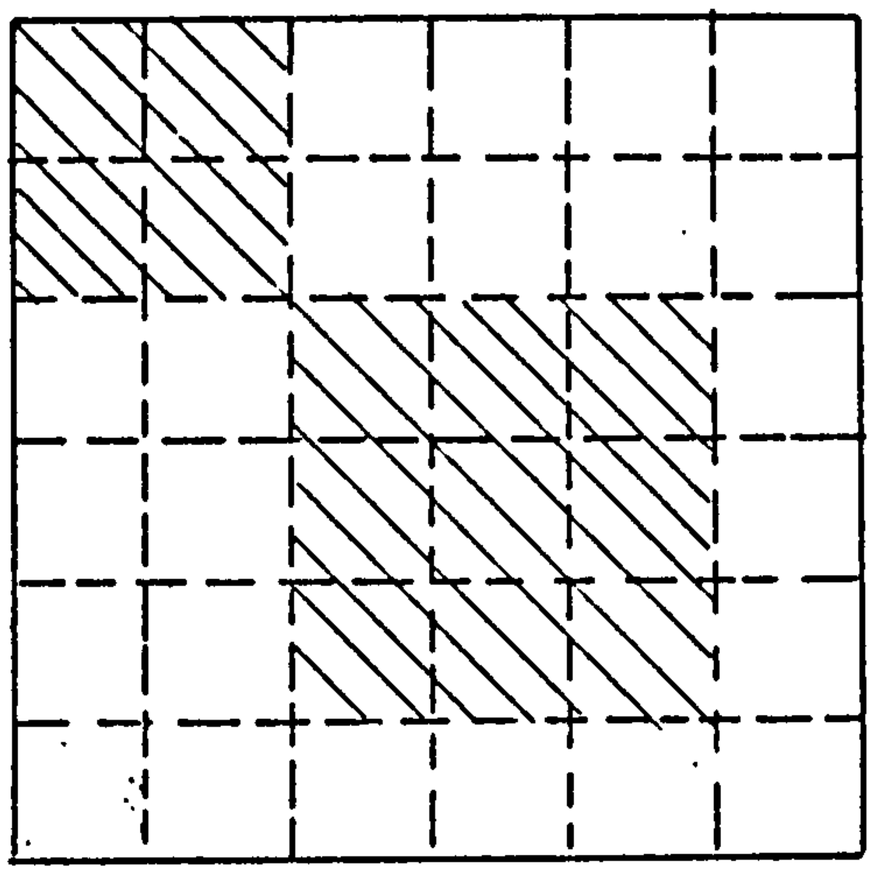

a) K_{11} for the shell element

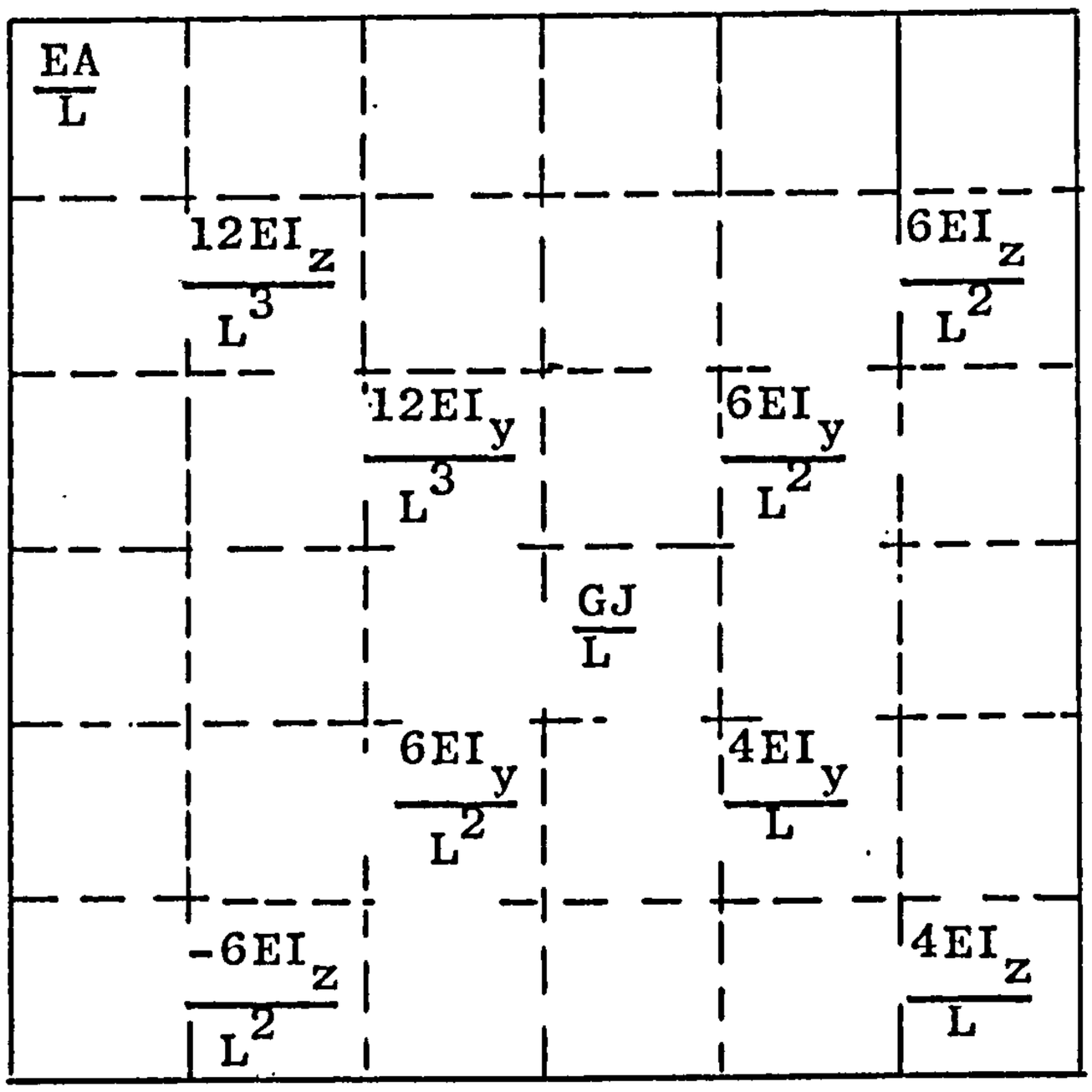

b) K_{11} for the tube element

Fig. 4.2 Stiffness submatrices layouts

CHAPTER 5

THE EXPERIMENTS

5.1 Introduction

Many experiments were done the purpose of which were:

1. Mainly to verify the theoretical analysis.

2. To gain information about the effects of eccentricity in top joints. This has an important practical implication since it is not practical always to keep the top joint without eccentricity, because it means limiting the cross-sections used.

Fig. 5.1 shows top joint conditions for $\frac{1}{2}$ in. and $\frac{1}{4}$ in. plates with and without eccentricity. Control of eccentricity was managed by inserting perspex packings between the perspex slab and the bottom piece of the top joint. A side interest was to investigate the influence of the in-plane rotations in plate.

As it was mentioned in Chapter 3, two types of models were made. Many tests were done on both of them, each test was repeated several times to be sure of the consistency of the results. Strain and deflection readings were taken twenty minutes after applying loads in order to lessen the creep effects in the perspex. Naturally, symmetry was taken into consideration by averaging the results of symmetrical members and locations.

5.2 Elastic Constants

Although both steel and perspex are standard test materials, but because they are combined in one structure, and because perspex is sensitive to creep, temperature, and even to thickness, it was thought better to determine experimentally the elastic constants of both of them.

5.2.a Mild Steel Tubes

Three random samples of the steel tubes were tested under tension conditions. Average elastic constants were found to be

$$E = 31,110,000 \text{ psi and } \mu = 0.2877$$

which are not far from the standard constants of 30×10^6 and 0.3 respectively.

5.2.b Perspex Sheets

Because three different thicknesses were used in Model I, which nominally were $\frac{1}{2}$ in, $\frac{1}{4}$ in, and $\frac{1}{8}$ in. Two beam samples for each thickness were cut from the same model sheets. The length and breadth of the beams were 12" and 2" respectively. Each sample underwent two pure bending tests (not to destruction). Fig. 5.2 shows a sketch of a beam sample with the location of strain and dial gauges.

Fig. 5.3 shows a load/deformation (strain) curve of one test only, because the results of the various tests were consistent. Table 5.1 shows the average elastic constants for two thicknesses only, because the $\frac{1}{8}$" beams were not tested due to the buckling failure of the $\frac{1}{8}$ in

model. E_s is the Modulus of Elasticity found from strain gauge readings, while E_d in Table 5.1 was found from the formula

$$d = \frac{p.a}{24EI}(3l^2 - 4a^2)$$

where d is the deflection at the centre of the beam, and p, a and l are as shown in Fig. 5.2. The discrepancies between E_s, E_d and E might well be due to thickness variations in addition to the fact that strain gauges are sensitive to temperature variations, and even the cementing of strain gauges in itself might induce some local strains, also the dial gauges readings are not as sensitive as electric resistance variations.

5.3 Testing of Joints Effectiveness

It was thought necessary to check that the jointing process did not weaken the tubes' strength and also that the joints themselves are strong enough to stand the expected strains of the tests and to know how far one can go in loading. Therefore, three sample tubes with their ball joints were tested under tension, and two under torsion conditions until failure. The load was applied by using clamping grips.

It was found that the tubes with their joints could safely stand more than 19000 psi in tension and 200 lbs. in torque force. Tubes failed in tension by necking near the joint end inserts (Fig. 5.4) whilst brazing failed in torsion.

5.4 Testing of Composite Double Layer Grid Model (MODEL I)

This model was described in para. 3.1. Three different plate thicknesses used at different times, namely $\frac{1}{2}$ in., $\frac{1}{4}$ in. and $\frac{1}{8}$ inches. For the first two thicknesses, tests were done under two different conditions.

a) No eccentricity in top joints.

b) Eccentricity in top joints.

These models and test conditions will be termed as follows

1. Model IA is Model I with $\frac{1}{2}$ in. plate.
2. Model IAe is as Model IA but with eccentricity.
3. Model IB is Model I with $\frac{1}{4}$ in. plate.
4. Model IBe is as Model IB but with eccentricity.
5. Model IC is Model I with $\frac{1}{8}$ in. plate.

Locations of the strain measuring devices were shown in Fig. (3.11), while Fig. 5.5 shows the numbering of tubes and perspex locations to be compared with the theoretical analysis. Kelvin strain measuring boxes were used for monitoring strains for the $\frac{1}{2}$ in. plate, and the $\frac{1}{8}$ in. plate tests, whilst a data logger (Solartron Schlumberger) was used for the $\frac{1}{4}$ in. plate cases. A single hydraulic retraction jack was used to apply the central load as was shown in Plate No. 3.2.

The jack reaction was taken by the basement roof as is shown in Fig. 5.6 which shows a sketch of the loading arrangements.

Table 5.2 shows the experimental strain results

for the heavily loaded tubes and perspex locations only for Models IA, IAe, IB, and IBe, in which it is clear that not only axial strains dominate the tube's strain whilst in-plane strains dominate the perspex plate strains, but also that bending strains in both tubes and perspex plate are negligible.

Although a jack of 3 tons was used to apply a total load of 827 lbs. for the $\frac{1}{2}$ in. plate tests and a 2 tons jack was used to apply a total load of 760.45 lbs. for the $\frac{1}{4}$ in. plate tests, nevertheless, it was thought better to convert strains into stresses for a projected 1000 lbs. load in order to have a better grasp for them and to have a base for direct comparison between the various tests.

These converted stress results are shown in Tables 5.3, 5.4a, 5.4b, 5.5a and 5.5b. These tables also show the % ratio between the experimental with eccentricity results, and the theoretical results to the normal experimental results. Upon investigation of these tables it is clear that

a) Deflection predictions are good.

b) Tube axial forces predictions are good also, especially in the case of the central and corner tubes (Nos. 7 and 1 respectively) which are the most heavily loaded tubes in the structure for the type of loading used. But bending stresses were not so good, probably, because they are very low as was shown in table 5.2 and consequently are misleading, in addition, strain gauge readings are

sensitive to wall thickness, and to the gauge location and orientation.

c) In-plane stresses in plates are relatively good, whilst bending stresses predictions were not so good or consistent. This is probably due to the nature of the finite element used, the relative coarseness of their subdivision, the impossibility of giving the exact thickness of the plate which is of paramount importance in plate flexural stresses and finally for being very low as was shown in Table 5.2 and hence misleading. In fact, upon measurement of thickness around the plate edges, it was found that plates do not have constant thickness and consequently the average thickness for the $\frac{1}{2}$ in. and $\frac{1}{4}$ in. plates was found to be 0.457 in. and 0.248 in. respectively.

A uniformly distributed loading test on the $\frac{1}{2}$ in. plate model was tried. Using all the static loads available in the laboratory which were grouped in four sets of 140 lbs. each, i.e. 0.276 psi. As expected, the strain developed in the model were very low especially in the plate. Therefore no more tests of this sort were done.

The $\frac{1}{8}$ in. plate test (Model Ic) was done despite the knowledge that the plate might be too thin, but it was intended to go to the extreme. In the event, the model failed in the first test under non-eccentric joint conditions. As can be seen from Fig. 5.7 that there is relatively great variation of thickness all over the area

down to 0.107 in. i.e. 15% less than the nominal thickness in some places. So apparently, due to the extreme thinness of the plate, it was difficult to control the jacking system and suddenly, at a loading of 257.5 lbs. the jack dial indicator began swinging violently to the extent that the whole structure was experiencing load oscillation. Therefore, the test was stopped immediately. When another test was done later, buckling of the plate happened in areas with the least thickness. Several tests were done afterwards and with each test the plate buckled at a lesser load than the previous one. In fact a load of 180 lbs. was enough to buckle the plate in the fourth run. Naturally there was no point in proceeding further and test the model under eccentric conditions. When the model was dissembled, a crack was found in the welding at one of the ball joints which was away from the buckled area.

Table 5.6 shows the strain results of the first test above, and Tables 5.7a and 5.7b show the results converted into stresses for a projected load of 1000 lbs. It is interesting to notice from these Tables the following:

a) In-plane stresses in the buckled area are less than theory predicts, and almost half the amount expected from the experience of the other model tests, while in-plane stress in other areas of the perspex were higher than expected. This is probably due to the high deflection of the buckled area, so the plate was no more plane in this area.

b) Bending stresses in the plate were much higher than expected, this is for the same above mentioned reason.

c) Stress distributions were altered in the tubes also, so while it is noticed that the central tubes on average gave almost the expected stresses, it is clear the corner tubes gave almost half the stresses expected presumably due to the loss of symmetry. This is almost opposite what happened to the perspex plate. Check of symmetry was not possible, because there were no strain gauges at the time in the other corners of the model.

d) Deflections were affected very much and they gave a clearer picture of the loss of symmetry and the amount of buckling experienced in the centre part of the plate at locations F and G.

It is interesting to report that when Model IC was dissembled and examined thoroughly a crack in a joint brazing far from the centre was found. The cracked joint was repaired, and Model IB was assembled and tested without mishaps.

Hence it is clear that the stress distribution has been changed completely due to this failure. Thus one may conclude with relief, that this test proves what was said by Makowski[1] in para 2.1, that buckling of any member in a grid structure, rarely, if ever leads to a collapse of the whole structure.

Since all model test results for the $\frac{1}{2}$ in. and $\frac{1}{4}$ in. plates were linear, hence it suffices to present figs. (5.8, 5.9 and 5.10) only which show the linear relation of load against deflection, tube strains and perspex strains respectively.

5.5 Testing of the Single Pyramid Cantilever Model (MODEL II)

This model and its purpose was described in para 3.2. Locations of the strain measurement devices were shown in Fig. 3.12. Only a plate of $\frac{1}{2}$ in. thickness was used in this test.

Two types of tests were done.

1. Flexural Test in which a single load normal to the perspex plate surface was applied as was shown in Plate No. 3.5 and Fig. 3.12. The load was a 30 lbs. dead load applied in increments of 5 lbs. The model was tested under eccentric and non-eccentric conditions. The actual strain results are shown in Table 5.8, from which it is seen that axial strains in tubes are not so many folds higher than bending strains, whilst naturally flexural strains in the plate are the dominant. These test results will be discussed in para 6.1.

2. Torsion tests: This test was done as an attempt to study the plate in-plane rotation and also to see the effectiveness of the joint systems, used in the model. It was done by applying an in-plane load as seen in Fig. 5.12. But because the perspex plate warped under load, the perspex strain gauges readings were non-linear, but dial gauges results and most tube strain results were linear as shown in Fig. 5.13. This test will be discussed further in para 6.3.

From the above tests it was concluded, among other things that the joint systems used are good and the analytical idealization approach gives good consistent results.

TABLE 5.1

ELASTICITY CONSTANTS FOR PERSPEX PLATES

Method	Thickness	Poisson ratio	E		$\%(\frac{E_s}{E_d} - 1) \times 100$
			by strain gauges E_s	by dial gauges E_d	
Test	0.489	0.38	421000	395000	6.6%
	0.244	0.38	474000	444000	6.6%
Manufacturers Catalogue		0.38	E = 420000		

TABLE 5.2 MODEL I SHOWS EXPERIMENTAL RESULTS IN STRAINS (IN MACROS) FOR THE DIFFERENT TESTS

No.	Case	Plate thick-ness ins	Experi-ment max. load lb.	Deflections in inches		
				Joint A	Joint C	Joint D
1	Model IA	$\frac{1}{2}$	827			
	a) without eccentricity			0.012496	0.0189	0.0276
	b) with eccen-tricity (IAe)			0.012496	0.0207	0.0264
2.	Model IB	$\frac{1}{4}$	760.5			
	a) without eccentricity			-	0.0193	0.0261
	b) with eccen-tricity (IBe)			-	0.0191	0.0259

TABLE 5.2 (Contd)

No.	Case	Strain in tubes				Strains in perspex			
		Corner tube (1)		Central tube (7)		Point I		Point III	
		Axial	Bending (y)	Axial	Bending (y)	Plane stress	flexure	Plane stress	flexure
1	Model IA								
	a) without eccentricity	-110	∓7	202	∓21	-54	∓1	-101	∓3
	b) with eccentricity(IAe)	-104	∓44	199	∓45	-48.5	∓5.5	- 94	∓24
2	Model IB								
	a) without eccentricity	-98.1	∓4.95	163.3	∓21.4	-70.2	∓3.35	-139	∓18.7
	b) with eccentricity (IBe)	-98.1	∓17.7	∓171.7	∓45	-53.1	∓1.36	-115	∓58

N.B Numbers of tubes and points are indicated in Fig. 5.5.

TABLE 5.3

MODEL I

EXPERIMENTAL AND THEORETICAL RESULTS

"DEFLECTIONS"

Joint No.	½ in. plate			¼ in. plate		
	Model IA	Model IAe	Theor-etical	Model IB	Model IBe	Theor-etical
A	0.01511	0.01511	0.01437	-	-	-
%		100	95.1			
B	-	-	-	0.0183	0.0183	0.0204
%					100	111
C	0.02285	0.02503	0.02312	0.0254	0.0251	0.0285
%		110	101		99	112
D	0.0333	0.0319	0.0299	0.0343	0.0341	0.0369
%		96	90		99	108
E	0.020314	0.02031	0.02173	-	-	-
%		100	107			

NB: The % comparisons are with Model IA, and Model IB results

TABLE 5.4a MODEL I EXPERIMENTAL AND THEORETICAL RESULTS
"STRESSES IN TUBES" t = ½ in.

Tube No. %	MODEL IA			MODEL IAe			THEORETICAL		
	Axial Stresses	Bending Stresses		Axial Stresses	Bending Stresses		Axial Stresses	Bending Stresses	
	∇x psi	∇by psi	∇bz psi	∇x psi	∇by psi	∇bz psi	σ_x psi	σ_{by} psi	σ_{bz} psi
1	-4145	-257	-257	-3912	-1657	-148	-4017	-277	-0.0
%				94	645	57	97	108	0
2	0.0	0.0	0.0	0.0	0.0	0.0	23.4	14	26
%				100	100	100	∞	∞	∞
3	3671	0.0	0.0	3573	114	36	2443	195	~0.0
%				97.3	∞	∞	66.5	∞	100
4	555	-48	-26	188	226	-509	394	-26	-75
%				34	-246	1926	71	54	286
5	-3856	132	132	-3649	-638	75	-3231	67	~0.0
%				95	483	57	84	51	0
6	-1938	-395	60	-2238	-394	-394	-1736	178	40
%				116	99.6	656	90	45	67
7	7591	-809	-373	7482	-1696	-482	6707	-235	~0.0
%				98.6	210	129	88.4	29	0.0
8	4609	207	207	4589	302	264	3484	252	~0.0
%				99.6	146	128	76	128	0

TABLE 5.4b MODEL I EXPERIMENTAL THEORETICAL RESULTS
STRESSES IN PERSPEX

Location	Method/Model	Stresses					
		σ_x	σ_y	σ_{xy}	M_x	M_y	M_{xy}
I	Model IA	-44.3	-44.3	0.0	0.815	0.815	0.0
	Model IAe	-39.8	-39.8	0.0	-4.52	-4.52	0.0
	%	90	90		-555	-555	
	Theoretical (16F.E/PR)	-29.7	-29.7	19.24	0.08	0.08	0.016
	%	67	67	∞	10	10	∞
II	Model IA	-63.2	-37.7	~0.0	-5.15	-8.02	~0.0
	Model IAe	-60.8	-38.9	~0.0	-11.1	-1.67	~0.0
	%	96	103		215	21	
	Theoretical	-53.3	-27.4	10.05	0.172	0.0835	-0.00013
	%	84	73	∞	3.3	1	∞
III	Model IA	-822	-81.6	0.0	-1.11	-3.5	0.0
	Model IAe	-77	-76	0.0	-19.7	-21.2	0.0
	%	94	94		177	61	
	Theoretical	-59	-59	15.1	0.825	0.225	0.003
	%	72	72	∞	20	0	∞

TABLE 5.5a MODEL I EXPERIMENTAL AND THEORETICAL RESULTS
"STRESSES IN TUBES" t = $\frac{1}{4}$ in.

Tube No. and %	MODEL IA			MODEL IAe			THEORETICAL		
	Axial Stresses	Bending Stresses		Axial Stresses	Bending Stresses		Axial Stresses	Bending Stresses	
	σ_x psi	σ_{by} psi	σ_{bz} psi	σ_x psi	σ_{by} psi	σ_{bz} psi	σ_x psi	σ_{by} psi	σ_{bz} psi
1	-4013	-1.72	0.0	-4000	-6.17	0.0	-4014.3	-300	~ 0.0
				98	358	100	100	174	100
2	-903.7	0.8	-5.13	-3344	14.9	-4.74	26.4	-30.5	-21.6
%				370	1862	92	-3	-3815	421
3	2335	79.3	-89	-89	1657	-533.5	1881	264	~ 0.0
%				- 4	2089	601	81	333	0.0
4	-302	-355	302	-1532	-2263	2148	-642	-36.3	95.2
%				508	635	712	213	10	32
5	-3587	523	-302	-1621	616	245.5	-3169	78.2	~0.0
%				45	118	813	88	15	0
6	-2078	-171	380	-350	-1485.5	-1324	-1775	-223	-61
%				17	868	349	85	130	16
7	6684	-879	-5	7031	1835	0.0	6702	-309	0.0
%				105	209	0	100	35	0
8	3640	632	632	-4237	1456	-277	3556	315	0.0
%				116	231	- 44	92	50	0

TABLE 5.5b

EXPERIMENTAL AND THEORETICAL RESULTS
'STRESSES IN PERSPEX' t = 0.25 in.

Location	Type of Results	STRESSES					
		σ_x	σ_y	τ_{xy}	M_x	M_y	M_{xy}
I	a	-71.5	-71.5	0.0	-3.4	-3.4	0.0
	b	-52.7	-57	0.0	-0.75	-1.94	0.0
	%	74	75	100	22	57	100
	c	-53.4	-53.4	30.0	0.02	0.02	0.0036
	%	75	75	∞	5	5	∞
II	a	-109	-102	$\sim$0.0	7.3	-30	$\sim$0.0
	b	-117.5	-102	$\sim$0.0	-8.07	4.6	$\sim$0.0
	%	107	100	100	-110	-15	100
	c	-97.4	-51.8	19.2	0.04	0.02	$\sim$0.0
	%	89	51	∞	1	$\sim$0	100
III	a	-140	-140	0.0	-19	-19	0.0
	b	-115.4	-115.4	0.0	-58.1	-58.1	0.0
	%	82	82	100	311	311	100
	c	-109.7	-109.7	77.42	0.051	0.051	0.0
	%	78	78	∞	$\sim$ 0	$\sim$0	100

Results type a is Experimental results of Model IB
" " b " " " " Model IBe
" " c " Theoretical results (16F.E/Pyramid)

TABLE 5.6 MODEL IC 'STRAIN RESULTS OF THE FAILED TEST'
t = 0.125 in., load = 257.5 lb.

Deformation in inches			Strain in tubes nos.				Strain in perspex at location			
Joints			1		7		I		III	
D	F	G	Axial ϵ_x	Bending ϵ_{bx}	Axial ϵ_x	Bending ϵ_{bx}	In-plane ϵ_x	flexural ϵ_{bx}	in-plane ϵ_x	flexural ϵ_{bx}
0.00915	0.157	0.21733	-15.7	$\pm$2	46.2	$\mp$0.8	-85.4	$\mp$9.7	-58.7	300

TABLE 5.7

MODEL IC SHOWS VARIOUS EXPERIMENTAL RESULTS AND THEIR COMPARISON WITH (16 x 16 F.E. MESH) THEORETICAL RESULTS (t = 0.125 in., load = 1000 lbs)

a - Deflections

Method	Deflection at points Nos.					
	A	D	C	F	G	H
1. Experiment (1)	.016059	.03553	.020876	.611	0.844	0.020
2. Experiment (2)	.037	.107	.050	.75	1.07	.247
3. Experiment (3)	.070	.123	.055	.465	.835	.085
4. Theoretical (16 F.E./Sq.)	.0268	.0575	.04379	.04621	0.0623	.04621
% 4/1	72	162	88	8	8	231

TABLE 5.7

MODEL IC

b-- Axial forces in tubes, and stresses in plate

Nos.	Descriptions	Locations and types of strains			
1	Experiment (1) axial forces results in tubes	Tubes			
		Corner		Centre	
		1	1a	7	7a
	i) experiment (1)	-180	-165	293.24	402.23
	ii) theoretical	-351.4	-351.4	351	351
	iii) % Theory / experiment	195	213	120	87
2	Experiment (1) moments, stresses in perspex	Perspex plate			
		In-plane stress		Moments	
		σx	σy	M_x	M_y
a)	Point I				
	i) experimental results	-232.33	-218	-0.06	-0.074
	ii) theoretical results	-100.9	-100.9	0.003	0.003
	iii) % theory / experiment	43	46	5	4
b)	Point II				
	i) experimental results	-341	-214.5	-1.06	-3.9
	ii) theoretical results	-189.8	-107.6	0.0074	0.0034
	iii) % theory / experiment	56	50	-0.6	-0.08
c)	Point III				
	i) experimental results	-155.4	-155.4	-2.06	-2.06
	ii) theoretical results	-220.5	-220.5	0.010	0.010
	iii) % theory / experiment	142	142	-0.5	-0.5

TABLE 5.8 ACTUAL STRAIN IN MODEL II

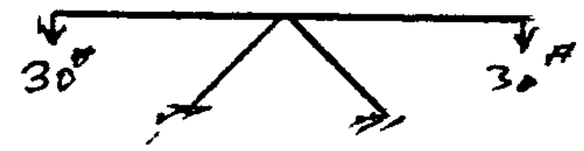

No.	Case	Load lb.	Plate thick-ness in.	Deflection in.	Tube		Perspex	
					Axial Strain μ	Bending Strain (Y) μ	In-plane strain μ	Flexural strain μ
1	Model 2a (without ecc.)	30	$\frac{1}{2}$"	0.1405	-12.2	-6	-29.3	$\pm$ 111
2	Model 2b (with ecc.)	30	$\frac{1}{2}$"	0.1405	-14.2	-5.7	-20.2	$\pm$ 119.8

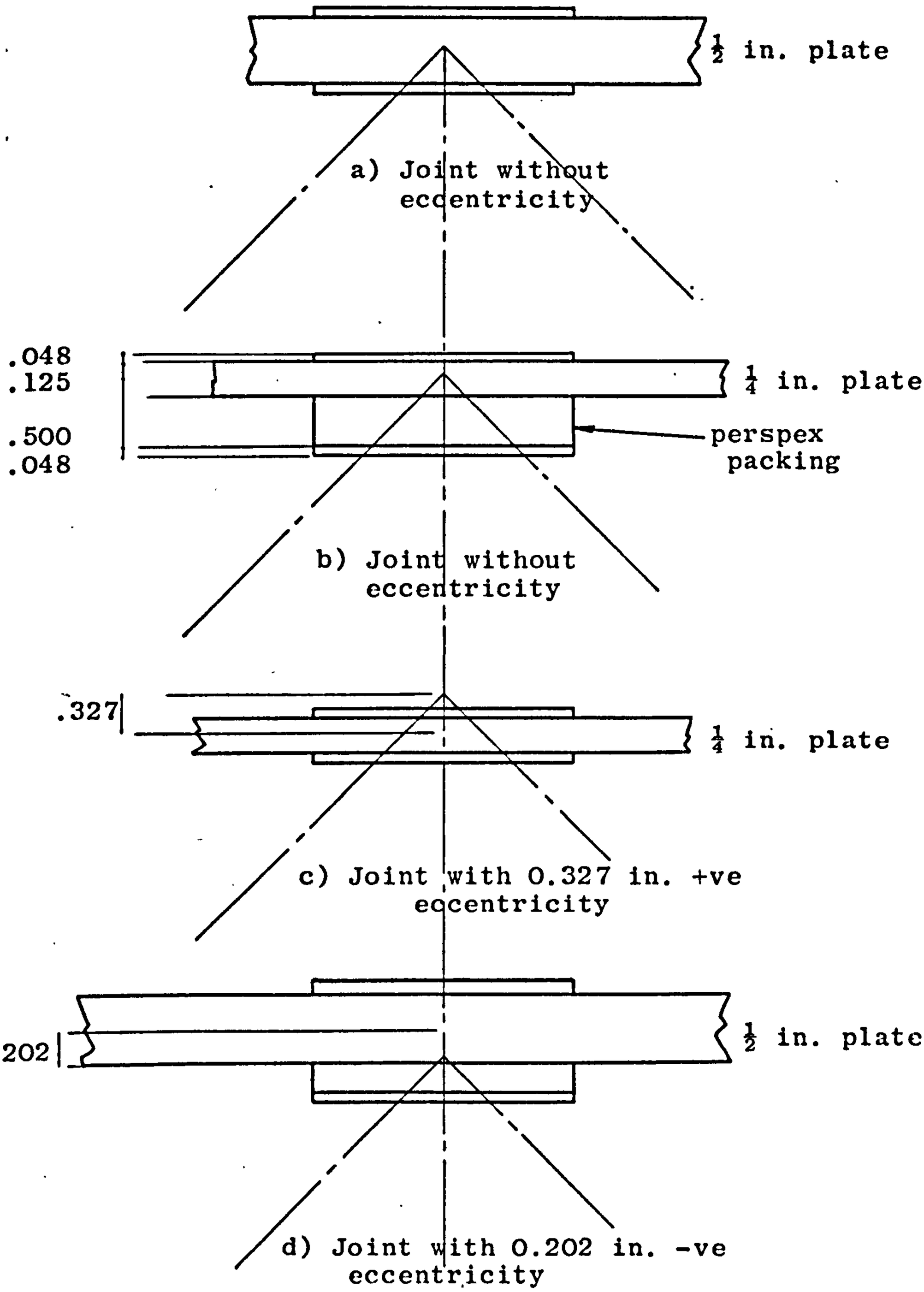

Fig. 5.1 Top Joint Conditions

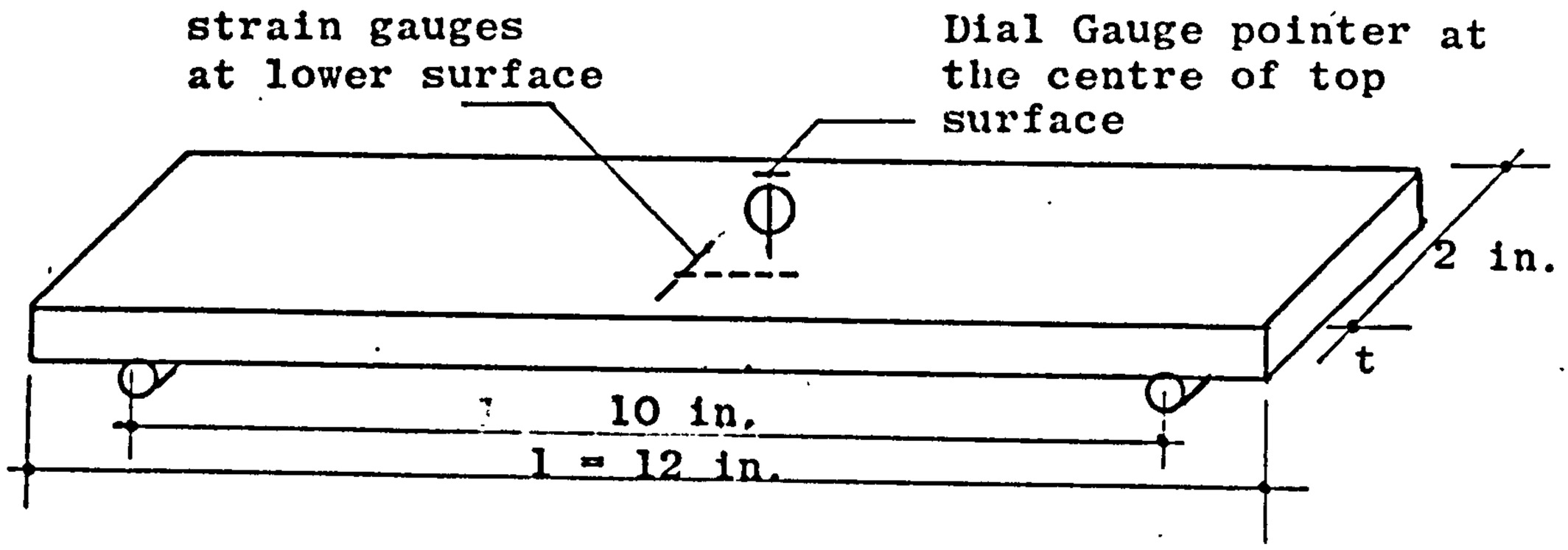

a) beam sample

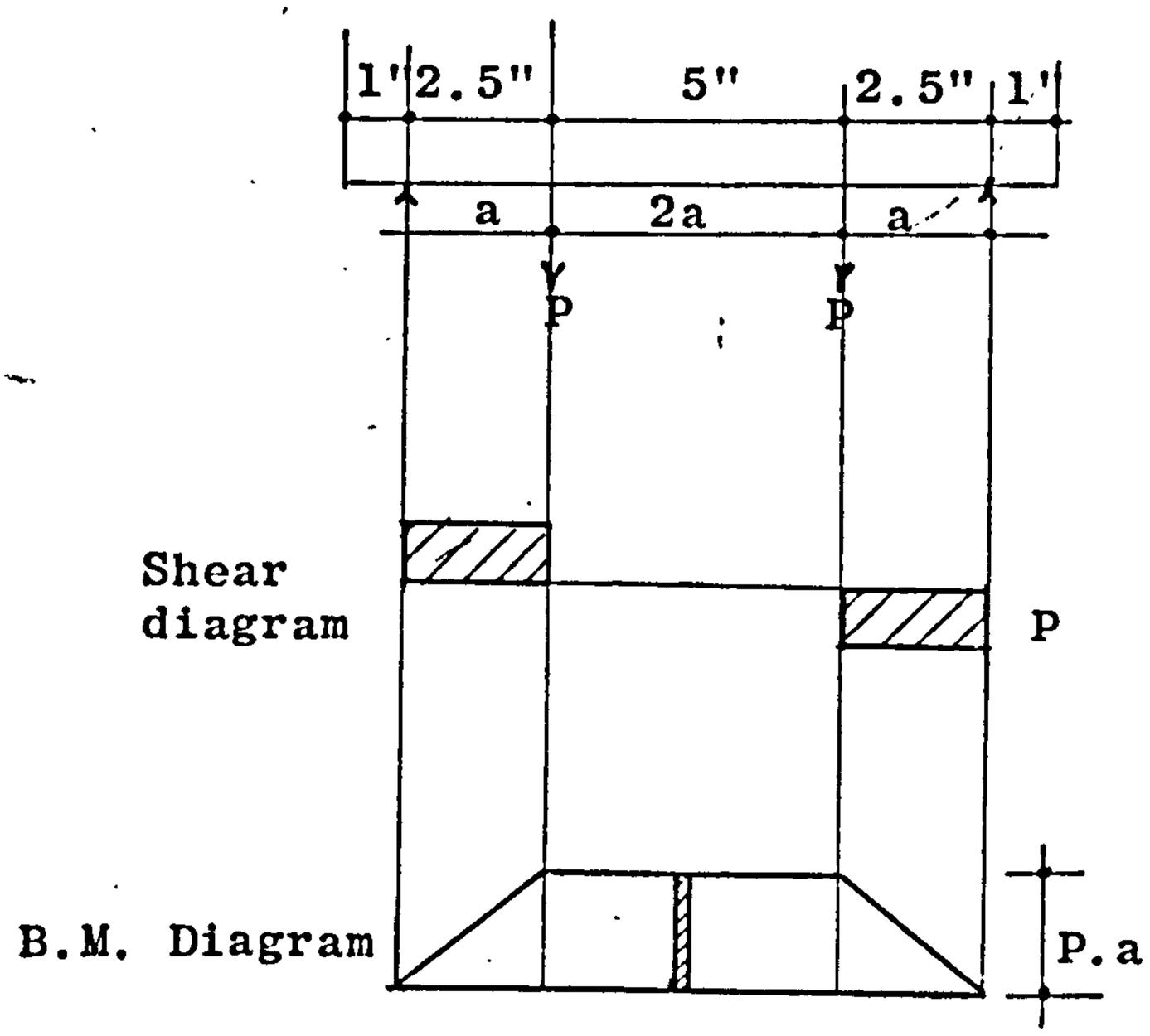

b) Shear and bending diagrams

Fig. 5.2

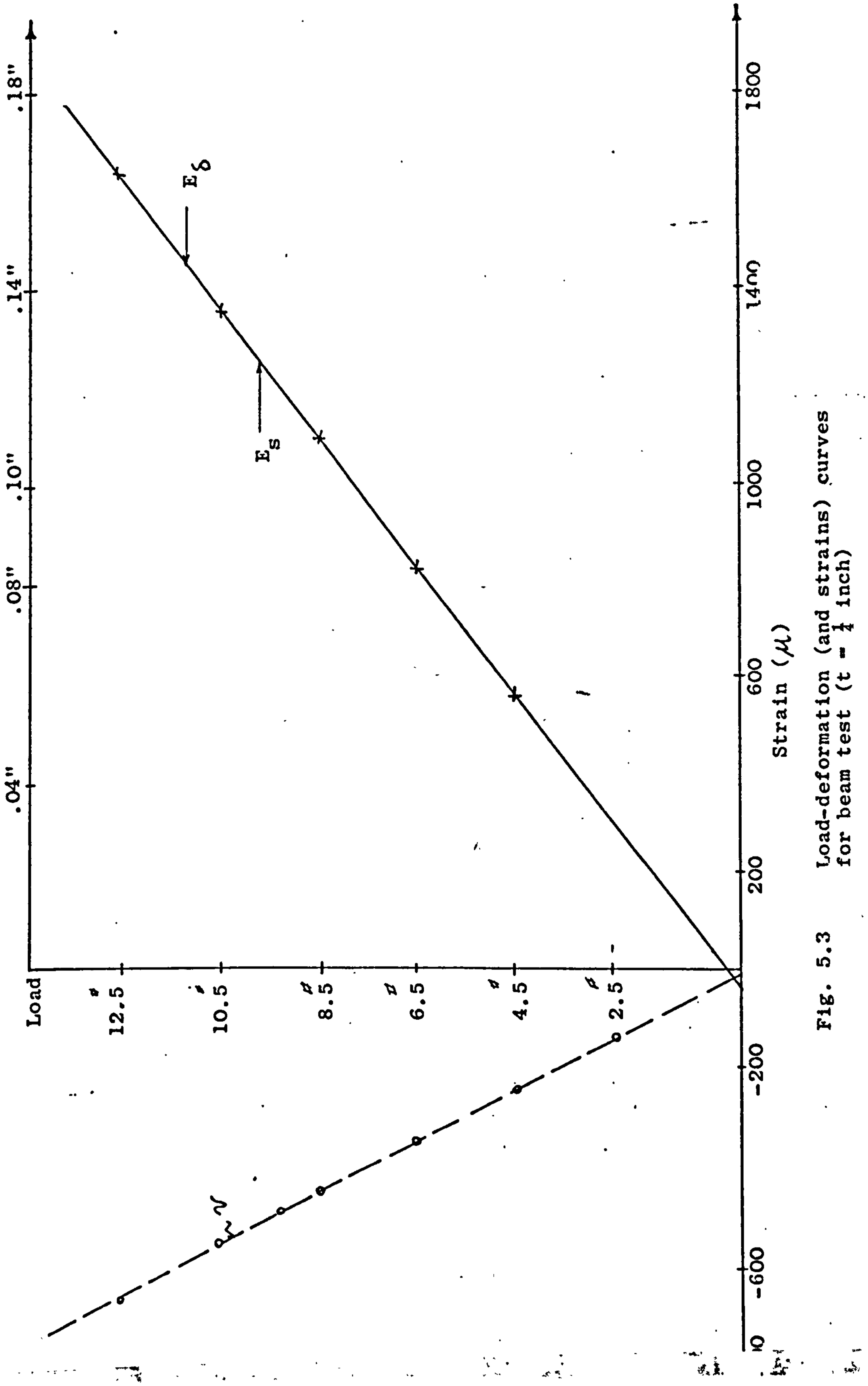

Fig. 5.3 Load-deformation (and strains) curves for beam test ($t = \frac{1}{4}$ inch)

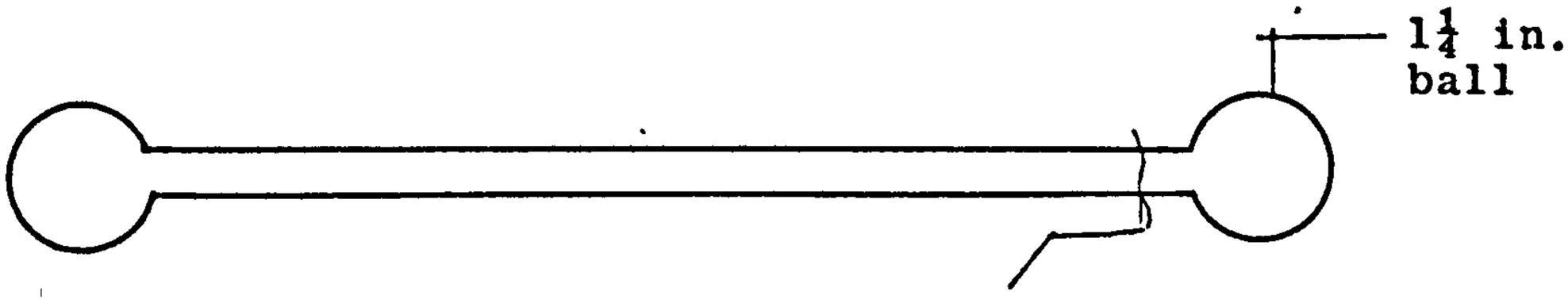

a) Test tube sample

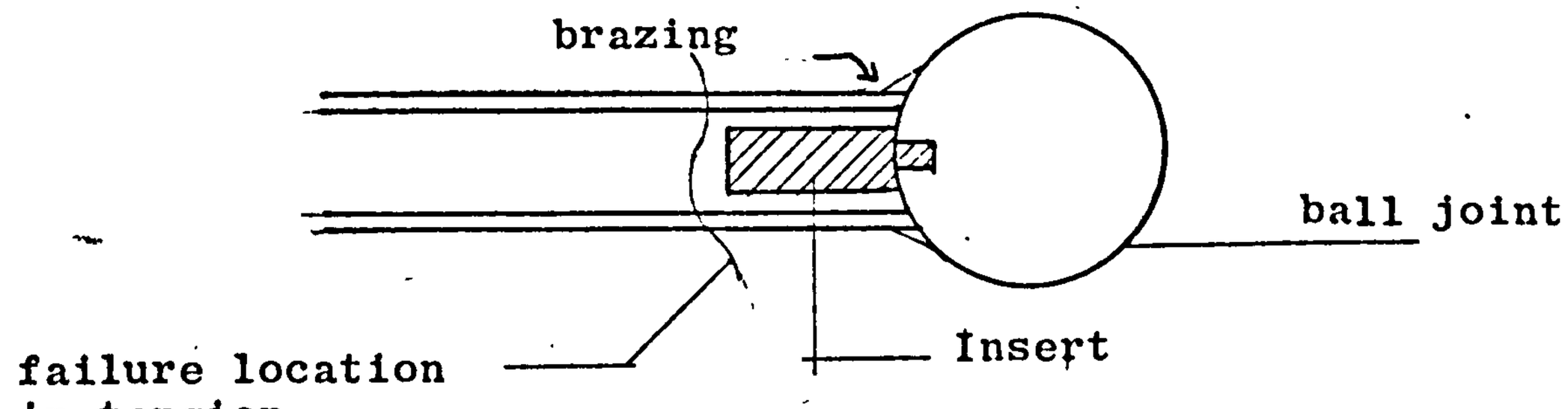

b) Ball Joints details and
failure tendency

Fig. 5.4

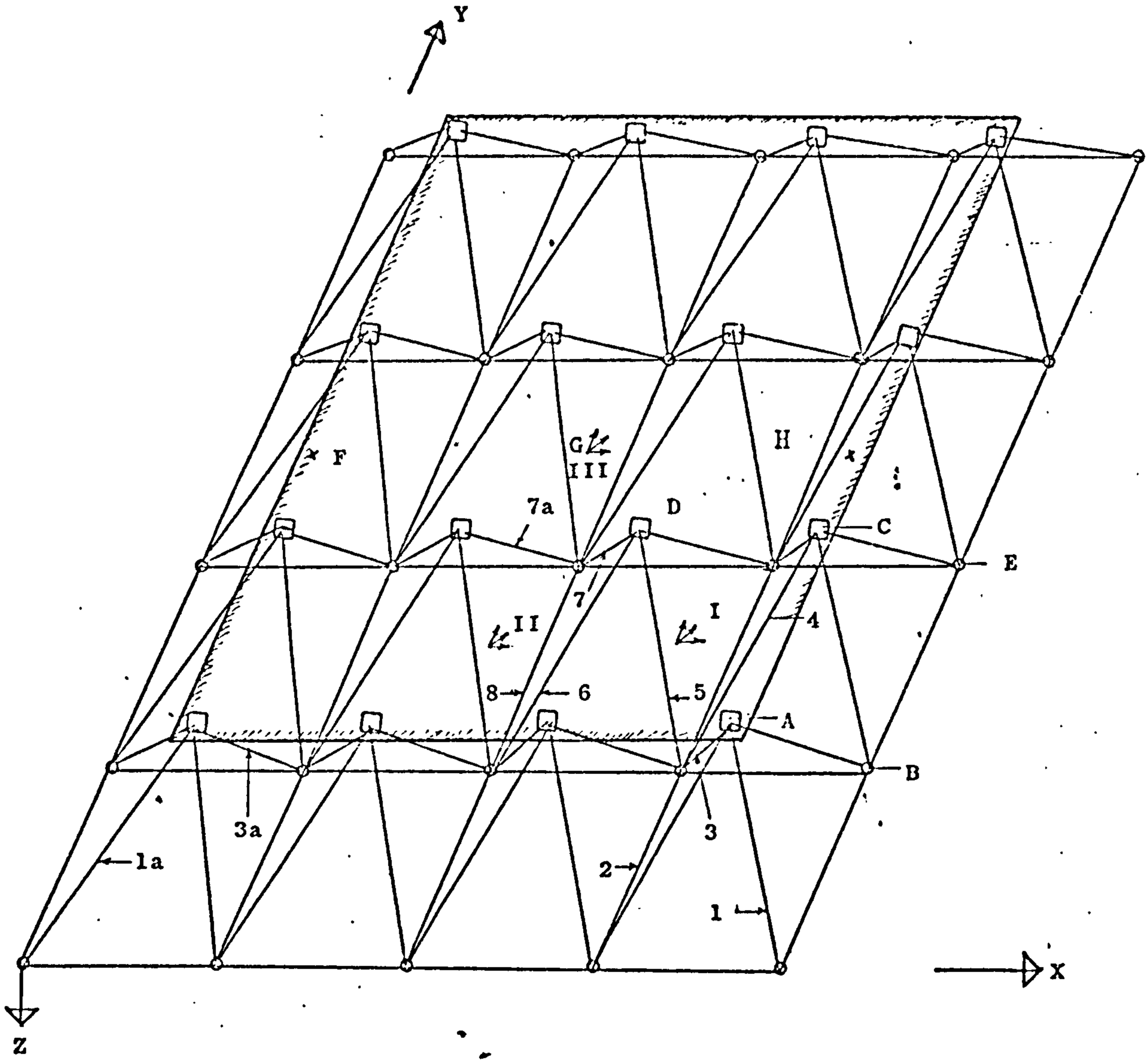

Fig. 5.5 3-Dimension view of Model I showing reference numbers for tubes, joints and perspex ros.ette locations.

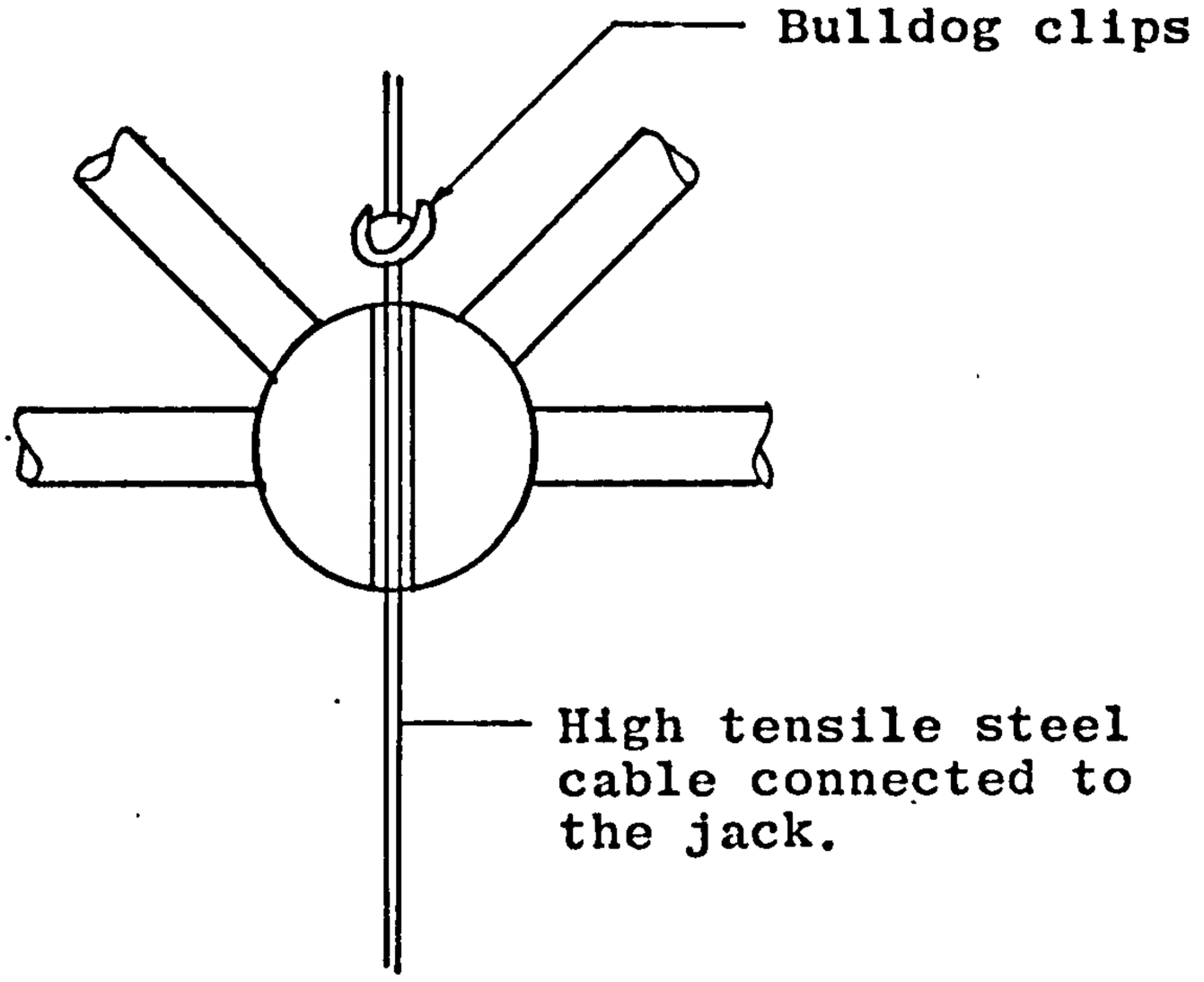

a) Load application arrangement

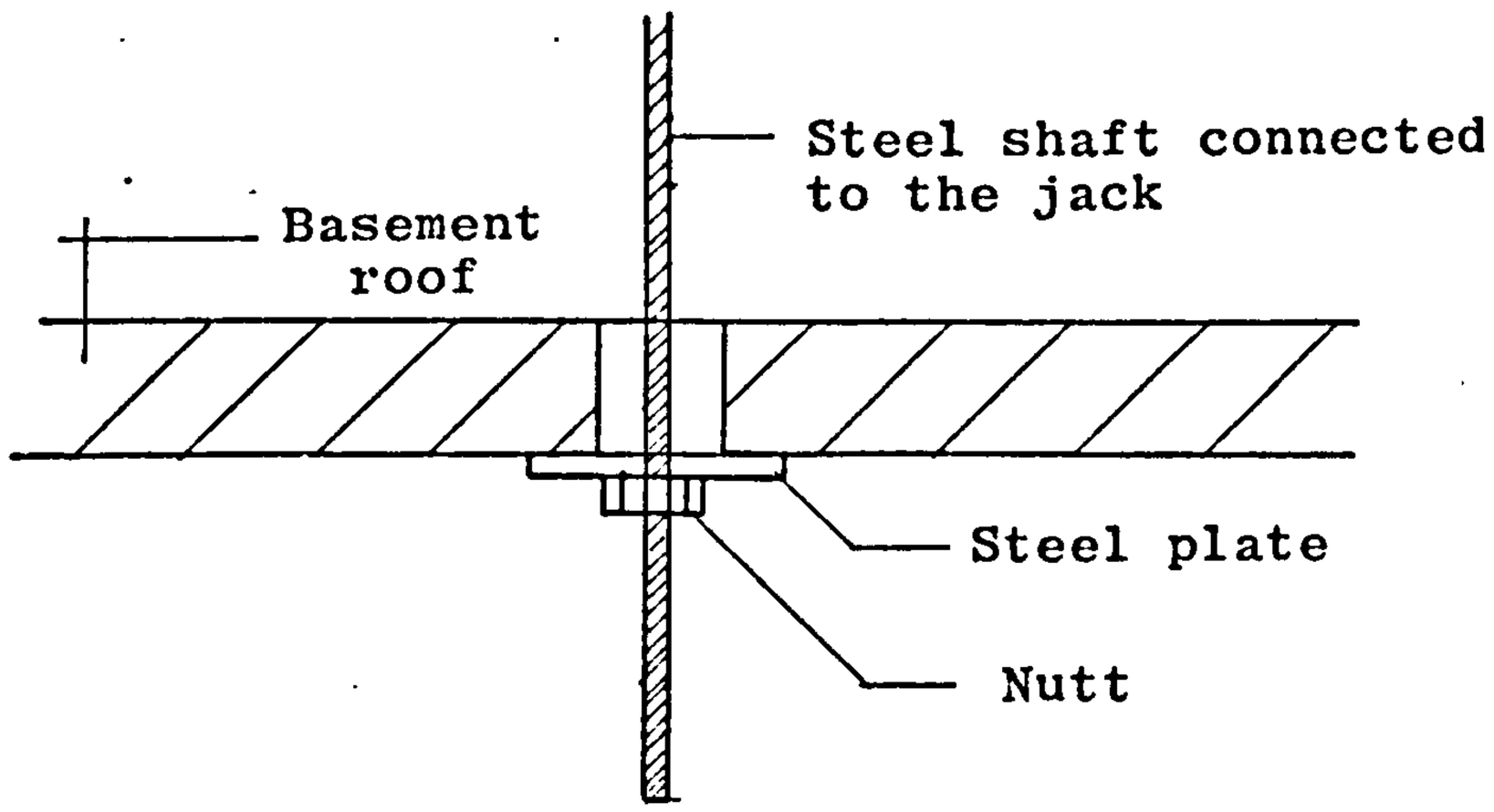

b) The Jack Support

Fig. 5.6

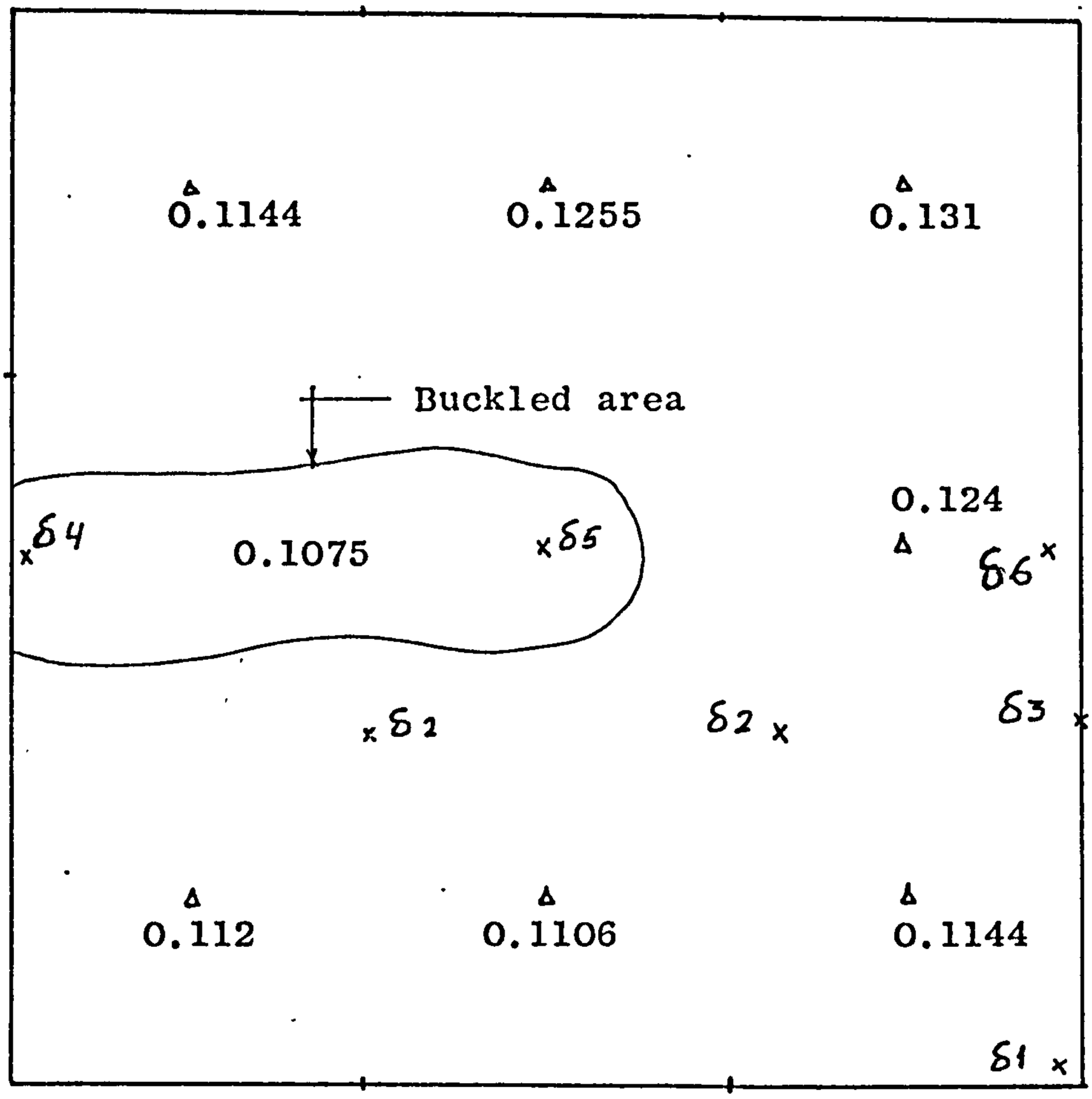

Fig. 5.7 Variation of thickness over the $\frac{1}{8}$ in. plate, and the buckled areas and location of dial gauges (δ)

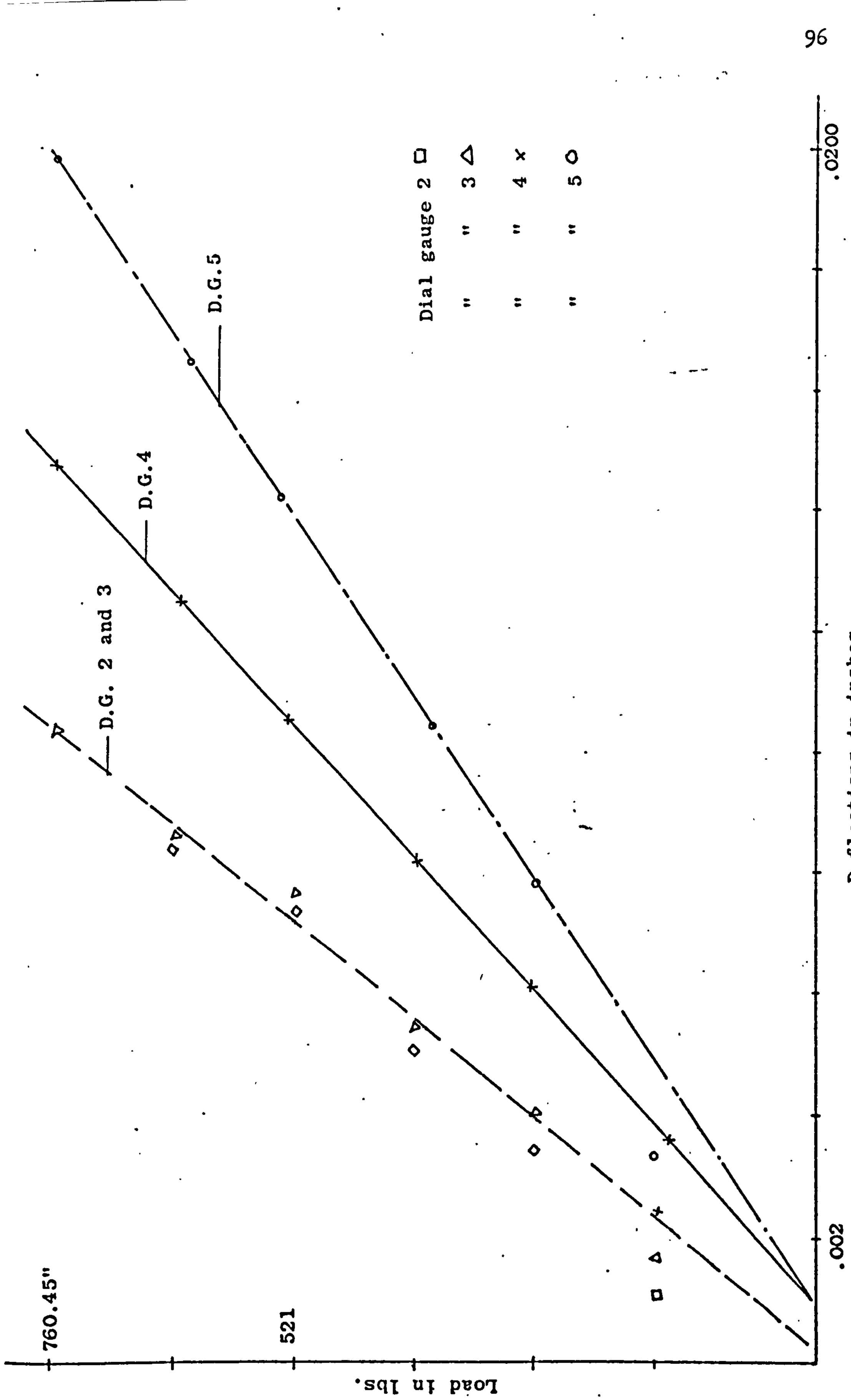

Fig. 5.8 Load-deflection curves for the test of Model IBe

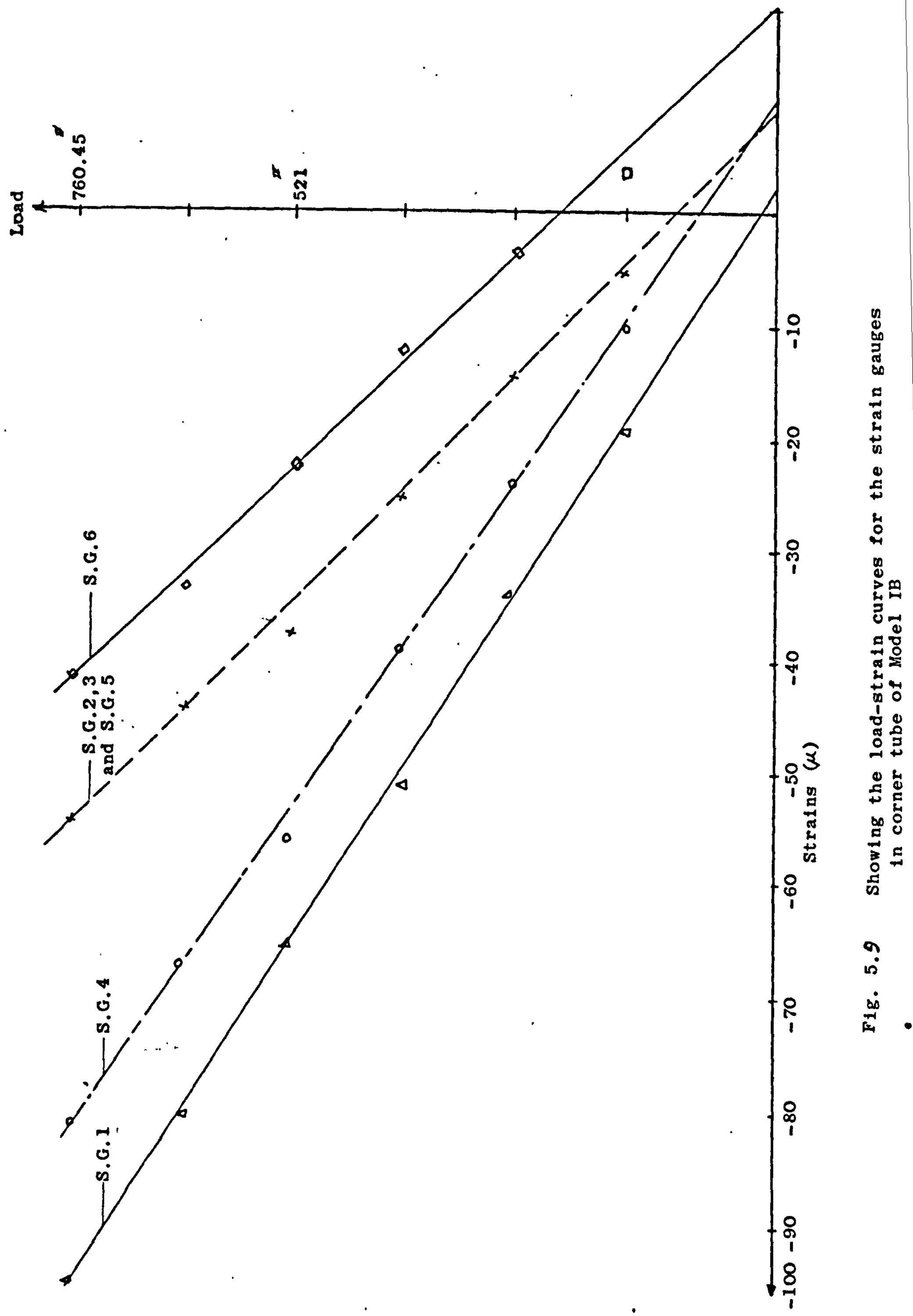

Fig. 5.9 Showing the load-strain curves for the strain gauges in corner tube of Model IB

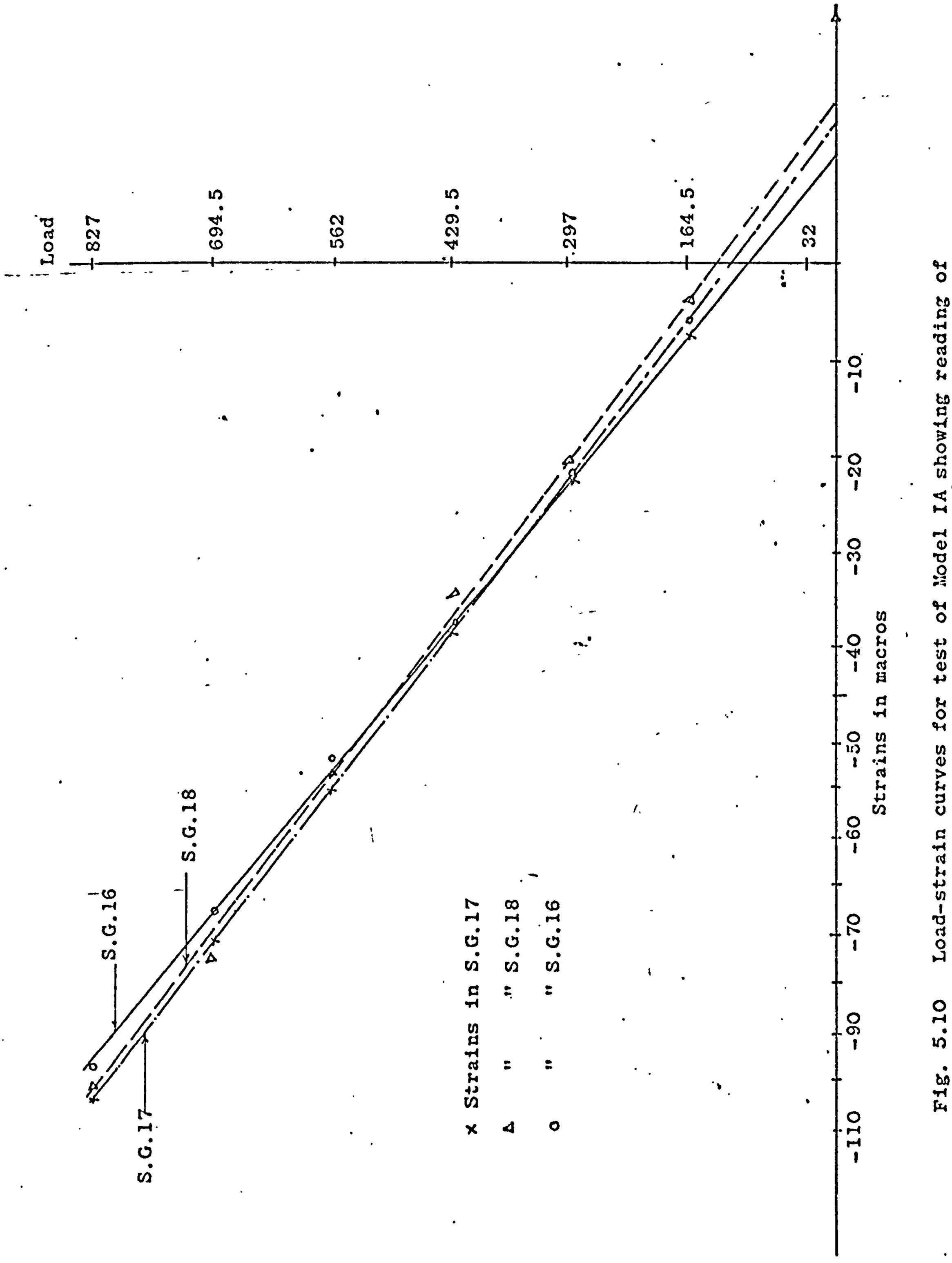

Load-strain curves for test of Model IA showing reading of strain gauges at point III at perspex plate

Fig. 5.10

PAGES
MISSING
IN
ORIGINAL

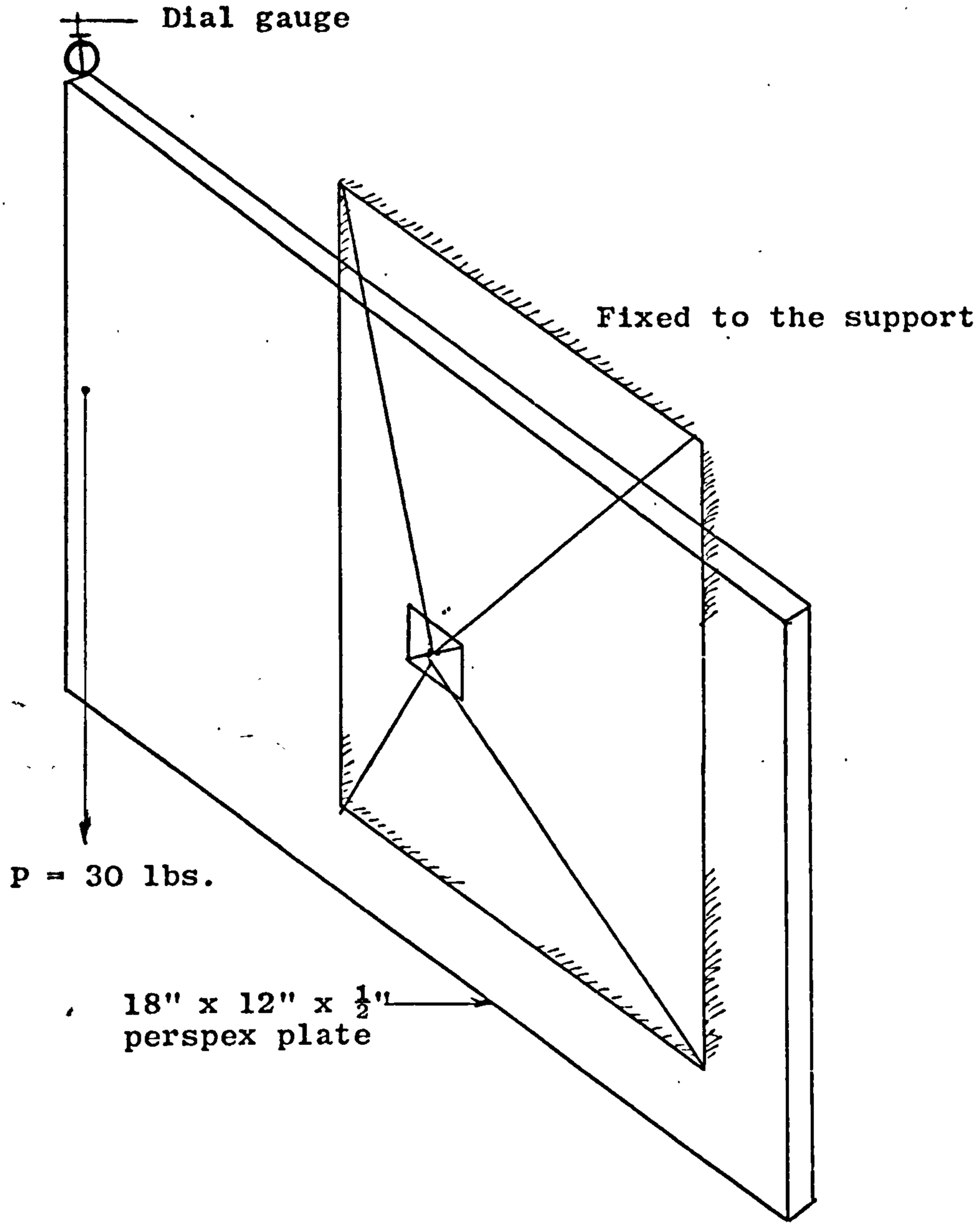

Fig. 5.12 Torsion Test

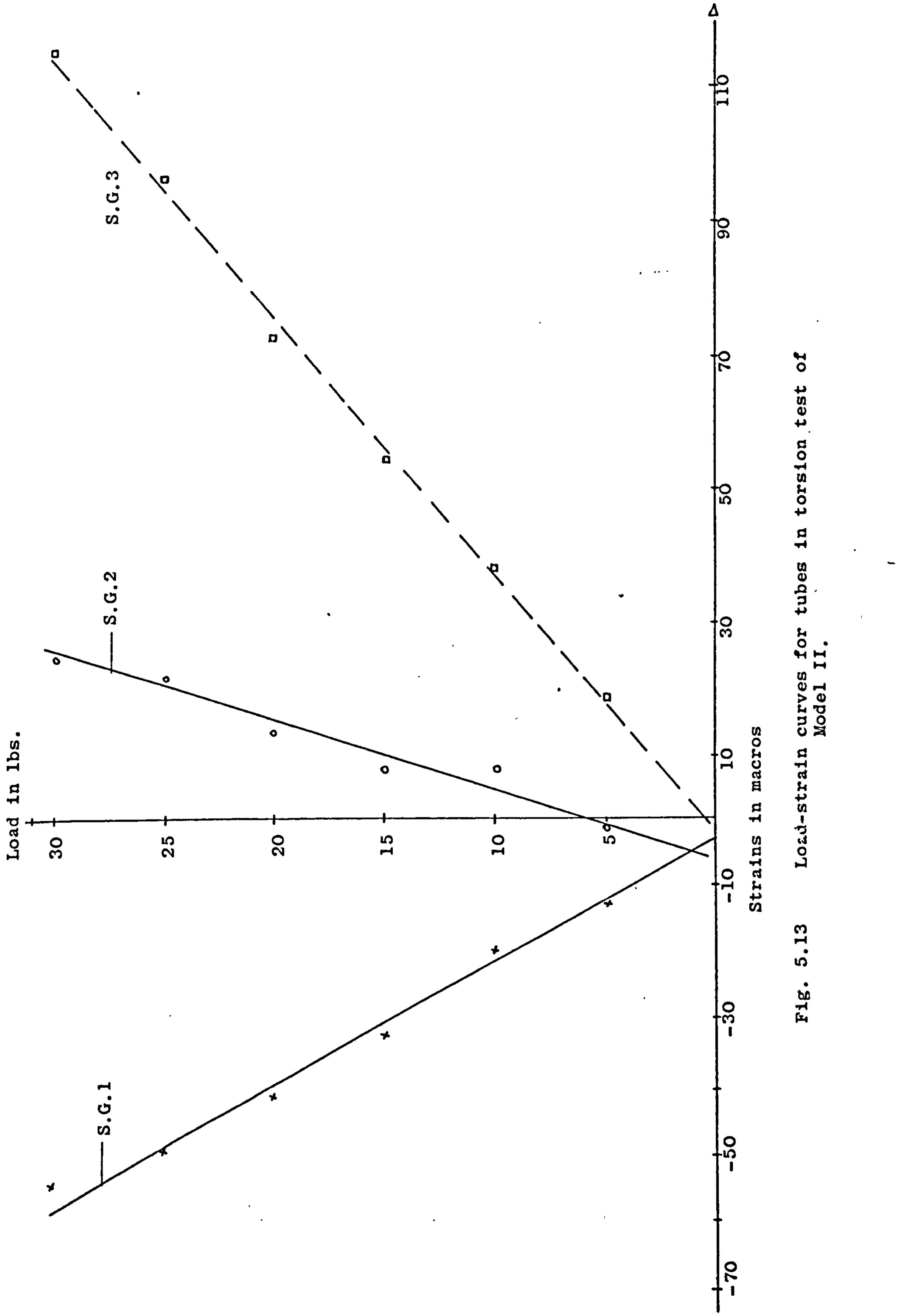

Fig. 5.13 Load-strain curves for tubes in torsion test of Model II.

CHAPTER 6

SOME THEORETICAL AND EXPERIMENTAL ASPECTS OF THE TESTS

6.1 Checking Convergency of the Solution

As it was mentioned in para 4.1, it was necessary to verify the convergency of the theoretical solution, and also to choose the suitable finite element mesh size. Model IA was used to check the convergency of the axial force in tubes and the in-plane stress in the perspex plate, whilst Model II was used to check the convergency of the flexural stresses in the perspex plate.

Three square finite element meshes were used in Model IA convergency analysis which were 1 x 1, 2 x 2 and 4 x 4 square elements, while four square finite element meshes were used in Model II convergency analysis, namely 2 x 2, 4 x 4, 8 x 8 and 16 x 16 square elements.

Tables 6.1 and 6.2 and Figs. 6.1 and 6.2 show the good convergency of the theoretical results towards the experimental results of the significant forces, stresses and deflections. Bending stresses in tubes for both models, and plate bending stresses in Model I were not shown because they were negligible, hence the comparison would have been misleading. Naturally, in-plane stresses do not exist theoretically in Model II.

A point worth mentioning is that using 1 x 1 finite element mesh in Model I was good enough as far as stresses in tubes are concerned, but not so for deflections, whilst

the results were misleading for plate stresses. This is because the locations on the plate where stresses are measured, are located in the middle of the element, where stress variation is very high and not linear.

It is clear from the above tables and Figures that axial forces in tubes invariably compare well with the experimental results. In fact, one can get the axial stresses in tubes to a good degree of accuracy using very coarse F.E. mesh without resort to fine meshes at all.

It is further noticed from Table 6.1 that the use of 16 x 16 F.E. mesh in Model II, which is a very fine mesh made differences in the results of only 7% in deflection and 20% in flexural stresses in plate and none in axial stresses in the tubes to those of a 2 x 2 F.E. mesh. This shows that a moderate mesh size say 4 x 4 is good enough even for moments. Therefore a mesh of 4 x 4 square Finite Elements was used for the theoretical analysis of Model I and a mesh of 8 x 8 was used in Model II analysis.

6.2 Effects of Eccentricity of Top Joints

Fig. 6.3 shows the effects of eccentricity on axial stresses in tubes, deflection of joints and plane stresses in plate expressed as % ratios which are taken from Tables 5.3, 5.4a, 5.4b, 5.5a and 5.5b in Chapter 5. It is seen from this figure and these tables that top joint eccentricity has a significant effect on the stress conditions in the structure. In fact the strain results during test of Models IAe and IBe were not always linear, hence it was not easy to draw a straight line through them sometimes.

Studying the above mentioned tables and Fig. 6.3 shows that:

1. Deflections of joints nearest to the point of load application were decreased in the case of -ve eccentricity.

2. Tubes were very much effected, the extent and sense of these effects could be related to the plate thickness, in other words, to the degree and direction of eccentricity.

a) In Model IAe, the axial stresses have been relatively decreased in the far located tube, while no apparent change in the tubes located near the centre of the structure, with the exception of tube No. 6 in Fig. 5.5 which has increased. Bending stresses have increased substantially.

b) In Model IBe the effect is more pronounced and all members are effected tremendously with the exception of Tube No. 1 which is a reaction member.

So the axial stresses in the tubes near the centre of the structure have increased while they decreased drastically in the far tubes and even some changed signs. Almost all bending stresses have increased.

3. Perspex plate stresses were affected also, especially in the $\frac{1}{4}$ in. plate case (Model IBe).

In-plane stresses in general have decreased while bending stresses have increased. These effects might be explained by the sketch as shown in Fig. 6.4. This explanation is based upon the fact that

a) The structure is sustained mainly by a couple produced by axial forces in the bottom layer and in-plane forces in the top one. The lever arm of this couple is equivalent to the distance between the centres of the two layers, i.e. the depth of the structure. But since the eccentricity in the $\frac{1}{2}$ in. plate case (Model IAe), makes a negligible difference to this depth, then its effects are negligible on the axial forces in the tubes (except tube No. 4 which has negligible strains, therefore, the comparison might be misleading). Nevertheless, the eccentricity itself still has a more apparent effect on the bending stresses in the tubes by increasing them. In the case of Model IBe which has a $\frac{1}{4}$ in. plate, the eccentricity has more effect on the axial forces because of its larger lever arm which in effect increased the depth of the structure, and also because of the high eccentricity in comparison to the plate thickness, therefore its effect is more pronounced on both axial and

bending stresses.

b) Fig. 6.4 might also explain the tendency towards getting lower in-plane stresses and greater bending stresses in the plate. This explanation is based upon the fact that eccentricity is bound to change the deflection of the centre part of the plate elements where the rosette gauges are located, and therefore in-plane stresses and flexural stresses decrease or increase according to the equation.

$$p_1 \times e_1 = p \times e$$

so if $e_1 > e$ then p_1 is $< p$ and vice versa. The same explanation is valid for the change in value and sign of the flexural stresses.

In conclusion, it may be said that

1. Positive eccentricity effects are:

a) Increasing the axial strains in the tubes nearest to the point of load application while decreasing the axial strains in the far located tubes.

b) To increase the bending strains in almost all tubes.

c) To decrease plane strains while increasing flexural strains in the plate.

2. Negative eccentricity effects are less significant in this study case due to having a relatively small lever arm in these tests. Nevertheless, it may be said that both types of eccentricity tend to have the same effects on both tubes and plate elements.

Although the tests were done under unfavourable

conditions as far as eccentricity is concerned in comparison to the more practical double layer grids of having the top layer larger in area than the bottom one, and of being under uniformly distributed loading rather than under single loading, one may still conclude that eccentricity in top joints should be avoided, and most probably will have more pronounced effects on the plate in the normal conditions.

6.3 The Plate In-plane Rotation

As was mentioned in para. 4.2, the 'θ_z' parameter and its counterpart 'M_z' do not exist as far as the thin theory of plates is concerned, unlike the case with the tubes. Therefore, it is worthwhile to go to the other extreme and assume infinite torsional rigidity and to see if this makes any remarkable differences, and if so, in what direction? This was done by treating 'θ_z' at joints which have both plate elements and tube members, as a constraint, and assuming it to be equal to zero. This theoretical test was done on Model I and the results showed no significant difference. Some examples can be seen in Tables 6.3. This indifference might well be due to the nature of the structure and the type of loading. Therefore another theoretical test was done for the case of horizontal loading as is shown in Fig. 6.5. The comparison of the results is shown in Table 6.4, where no significant difference is noticed except for the 'M_z' parameter for the tubes in the central area. But 'M_z' for tubes is not a crucial factor because it is low in comparison with other moments.

In-plane rotation was further investigated by the cantilever torsion test mentioned in para. 5.5. A sketch of the test orientation was shown in Fig. 5.12. Because test arrangements were not sophisticated enough, the plate warped and consequently rosettes results were completely non-linear or consistent. The test was redone but with the same mishap. Nevertheless vertical dial

gauge readings and most tube's strain readings were more linear as was shown in Fig. 5.13. Naturally theoretical solution for this test is impossible because it is a mechanism. The experimental results of this torsion test is shown in Table 6.5.

This discrepancy between theory and test might well be due to not simulating the plate joint correctly. In fact, this joint is not a single point joint, but a 5 points joint as can be seen in Fig. (3.7). Thus, there are in fact in-plane forces which create a couple to counter-balance the in-plane torsional moment created by the in-plane external load, and hence preventing the development of mechanism.

Therefore, it may be concluded that it is correct to assume that the plate element has only five degrees of freedom, at least for the types of structures considered in this thesis.

6.4 Effects of changing perspex plate thickness

There is not sufficient data to give definite conclusions about the effects of varying plate thickness. This is because of the failure of the $\frac{1}{8}$ in. plate test (Model IC) so that there are only results for two thicknesses.

Comparison of the results of the tests on Models IA and IB as were shown in Tables 5.3, 5.4a, 5.4b, 5.5a and 5.5b show that

1. The bending stresses in the tubes have increased with the decrease in the plate thickness. This coincides with the theoretical prediction.

2. The in-plane and flexural stresses in the plate have also increased with the decrease in plate thickness which is also as predicted by the theoretical analysis.

3. An unexpected feature is the decrease in axial stresses in tubes 1 and 7 which should not have changed and also the decrease in tube 8 instead of increasing according to theory. This discrepancy might well be due to experimental errors.

TABLE 6.1

THE CONVERGENCY OF THE THEORETICAL SOLUTION
MODEL II
USING $\frac{1}{2}$ in. PLATE AND 1000 lb. LOAD

Method	Deflection in.	Tubes axial force lb.	Moments in perspex plate lb.in.
1. Experiment without eccentricity	0.1405	-19.875	-10.77
2. Experiment with eccentricity	0.1405	-23.171	-10.644
%R	100	117	99
3. Theoretical analysis			
a) 2 x 2 F.E. mesh	0.1424	-21.189	-10.8
%R	101.3	106.7	100.3
b) 4 x 4 F.E. mesh	0.14196	-21.189	-11.42
%R	101	106.7	106
c) 8 x 8 F.E. mesh	0.14172	-21.189	-11.58
%R	100.8	106.7	107.5
d) 16 x 16 F.E. mesh	0.1328	-21.189	-13.02
%R	95	106.7	121
e) Ratio of results of 16 x 16 mesh/2 x 2 mesh	93	100	120

N.B. $\% R = \frac{\text{Results (x)}}{\text{Results (1)}} \times 100$

TABLE 6.2 THE CONVERGENCY OF THE THEORETICAL SOLUTION MODEL IA USING $\frac{1}{2}$ in. PLATE AND 1000 lb. LOAD.

	Deflections at Joints Nos.			Axial forces in tubes No.		In-plane stresses in points Nos.		
	A	C	D	1	7	1	2	3
1. Test without eccentricity (IA)	0.01511	0.02285	0.0333	363.35	-398.3	-44.3	-63.2	-82.2
2. Test with eccentricity (IAe)	0.01511	0.02503	0.0319	342.9	-392.6	-40	-60.8	-77
$\%\ ^{2}/_{1}$	100	110	96	94.4	98.6	90.3	96	93.67
3. Theoretical analysis								
a) 1x1 F.E.mesh	0.01034	0.01667	0.02153	352.28	-352.18	-39.96*	-50.6	-83.61
$\%\ ^{3.a}/_{1}$	68.4	72.4	64.6	96.9	88.4	90.2	80	101.7
b) 2 x 2 F.E. mesh	0.01348	0.02171	0.02818	352.2	-352.06	-22.9	-48.4	-38.2
$\%\ ^{3.b}/_{1}$	89.2	95	84.6	96.9	88.4	51.7	77	46.5
c) 4 x 4 F.E.mesh	0.01438	0.02314	0.02999	352.17	352.03	-29.8	-53.3	-589.6
$\%\ ^{3.c}/_{1}$	95	101	90	96.9	88.4	67.3	84	71.7

* These points are located at centre of finite elements, therefore results are the average of nodal forces for these elements.

TABLE 6.3a THE EFFECTS OF ASSUMING CONSTRAINED TOP JOINTS
MODEL I 'TUBES'

(See Figure 5.5 for Tube Nos.)

Method of Analysis	Plate thickness	TUBES NOS.											
		1			2			7			8		
		Axial str.	Bending stresses		Axial str.	Bending stresses		Axial stresses	Bending str.		Axial str.	Bending stresses	
		σ_x	σ_{by}	σ_{bz}	σ_x	σ_{by}	σ_{bz}	σ_x	σ_{by}	σ_{bz}	σ_x	σ_{by}	σ_{bz}
1. Normal analysis	$\frac{1}{2}$"	-4017	- 277	0.0	23.4	14	25.9	6707	-235	~0.0	3483	252.3	~0.0
2. Top joint constrained %		-4017	-276.7	0.0	23.44	14.14	25.68	6707	-235	~0.0	3483.8	252.7	~0.0
1. Normal Analysis	$\frac{1}{4}$"	-4014.3	-300	0.0	26.4	-30.52	-21.6	6702	-308.5	0.0	3556	315	-0.0
2. Top joint constrained %		-4014.3	-299.5	0.0	26.5	-30.8	-21.3	6702.1	-308.6	0.0	3555	315.3	~0.0

TABLE 6.3b THE EFFECTS OF ASSUMING CONSTRAINED TOP JOINTS
MODEL I 'PERSPEX PLATE'

Method of Analysis	Thickness	LOCATION NOS.											
		I						III					
		In-plane stresses			Moments			In-plane stresses			Moments		
		σ_x	σ_y	τ_{xy}	M_x	M_y	M_{xy}	σ_x	σ_y	τ_{xy}	M_x	M_y	M_{xy}
1. Normal analysis	$\frac{1}{2}$"	-29.685	-29.681	19.24	0.0798	0.0798	0.01609	- 59	- 59	15.1	0.225	0.225	0.003
2. Top joint constrained		-29.68	-29.68	19.24	0.0798	0.0798	0.01608	- 59	- 59	15.1	0.225	0.225	0.003
%		99.99	99.99	100	100	100	100.06	100	100	100	100	100	100
1. Normal analysis	$\frac{1}{4}$"	-53.39	-53.39	30.67	0.017699	0.017699	0.0036	-109.7	-109.7	27.42	0.051	0.051	~ 0.0
2. Top joint constrained		-53.395	-53.395	30.67	0.017691	0.017691	0.00362	-109.7	-109.7	27.42	0.051	0.051	~0.0
%		100	100	100	99.95	99.95	100.55	100	100	100	100	100	100

TABLE 6.4 THE EFFECTS OF ASSUMING CONSTRAINED TOP JOINTS MODEL I WITH HORIZONTAL LOADING (See fig. 6.5)

Method of Analysis	TUBES							
	1-2		1-6		16-21		12-21	
	Axial force lb.	M_z lb.in.	Axial force lb.	M_z	Axial force lb.	M_z	Axial force lb.	M_z
1. Normal analysis	-767.49	-9.789	-211.335	-0.52297	31.3309	0.32525	45.7572	-1.03310
2. Top joint constrained	-766.786	-9.80034	-211.030	-0.524348	31.3844	-1.4323	45.7718	-0.835145
%	99.87	100.116	99.9	100.26	100.1707	-440.36	100.0319	80.839

	PERSPEX						θ_z at point	
	Point 6		Point 16		Centre point		factor = 10^{-4}	
	σ_x	M_x	σ_x	M_x	σ_x	M_x	16	20
1. Normal analysis	-224.486	0.5698	-22.0130	0.07958	-22.3189	0.0248515	2.1937	2.5263
2. Top joint Constrained	-224.466	0.574605	-22.0054	0.07893	-22.3166	0.0249856	0.0	2.7139
%	99.99	100.8	99.96	99.19	99.99	100.136	0.0	107.4

TABLE 6.5 TORSION TEST USING A LOAD OF 30 lb.

δ in.	TUBES					
	2		3		4	
	Axial force lb.	M_z lb.in.	Axial force lb.	M_z lb.in.	Axial force lb.	M_z lb.in.
0.0125	48.9	-16.445	55.51	-15.561	0.8	16.357

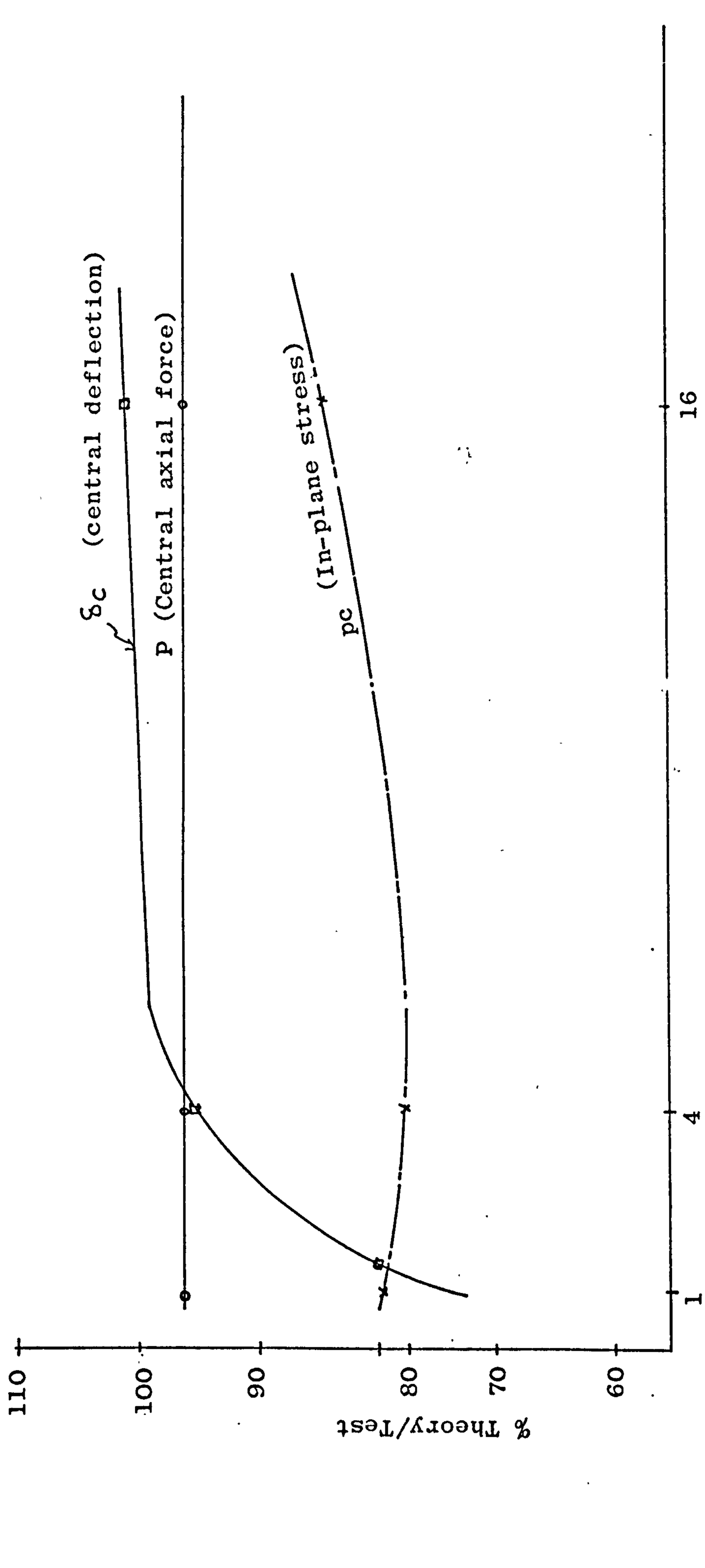

Fig. 6.1 Convergency of deflections and axial forces in Model IA (t = 0.5 in.)

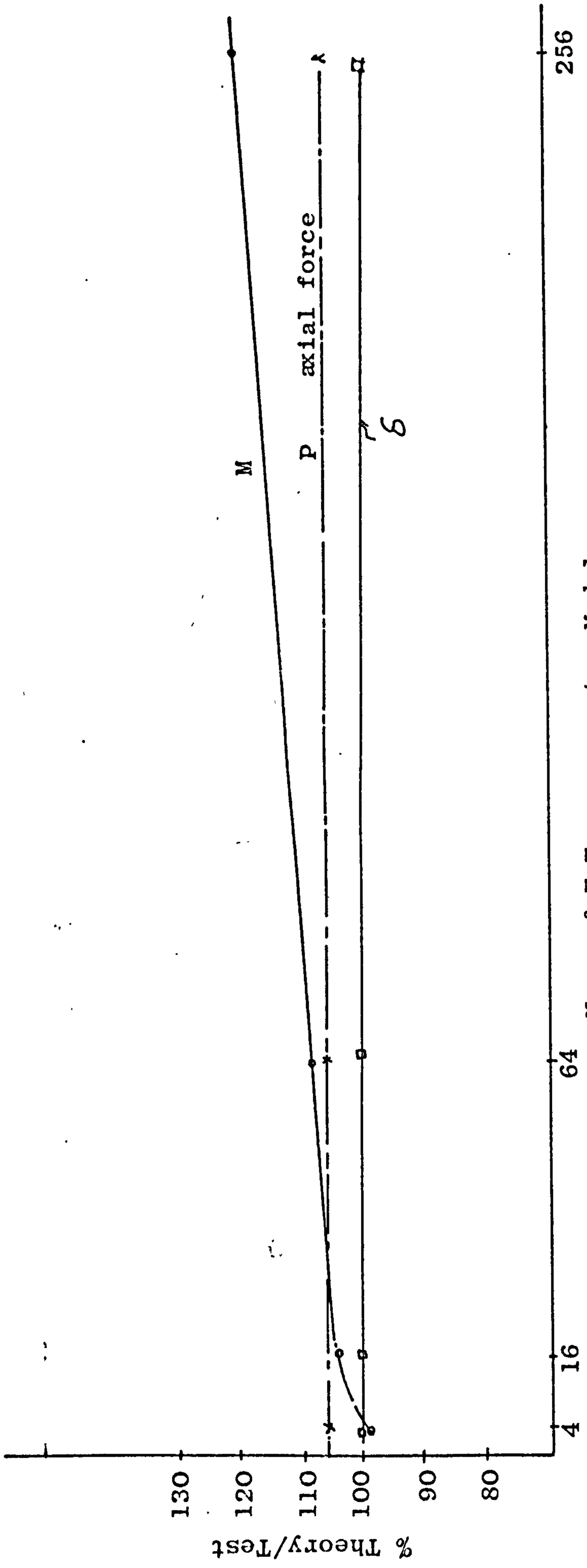

Fig. 6.2 Convergency of deflection, axial force and plate bending moments in Model II.

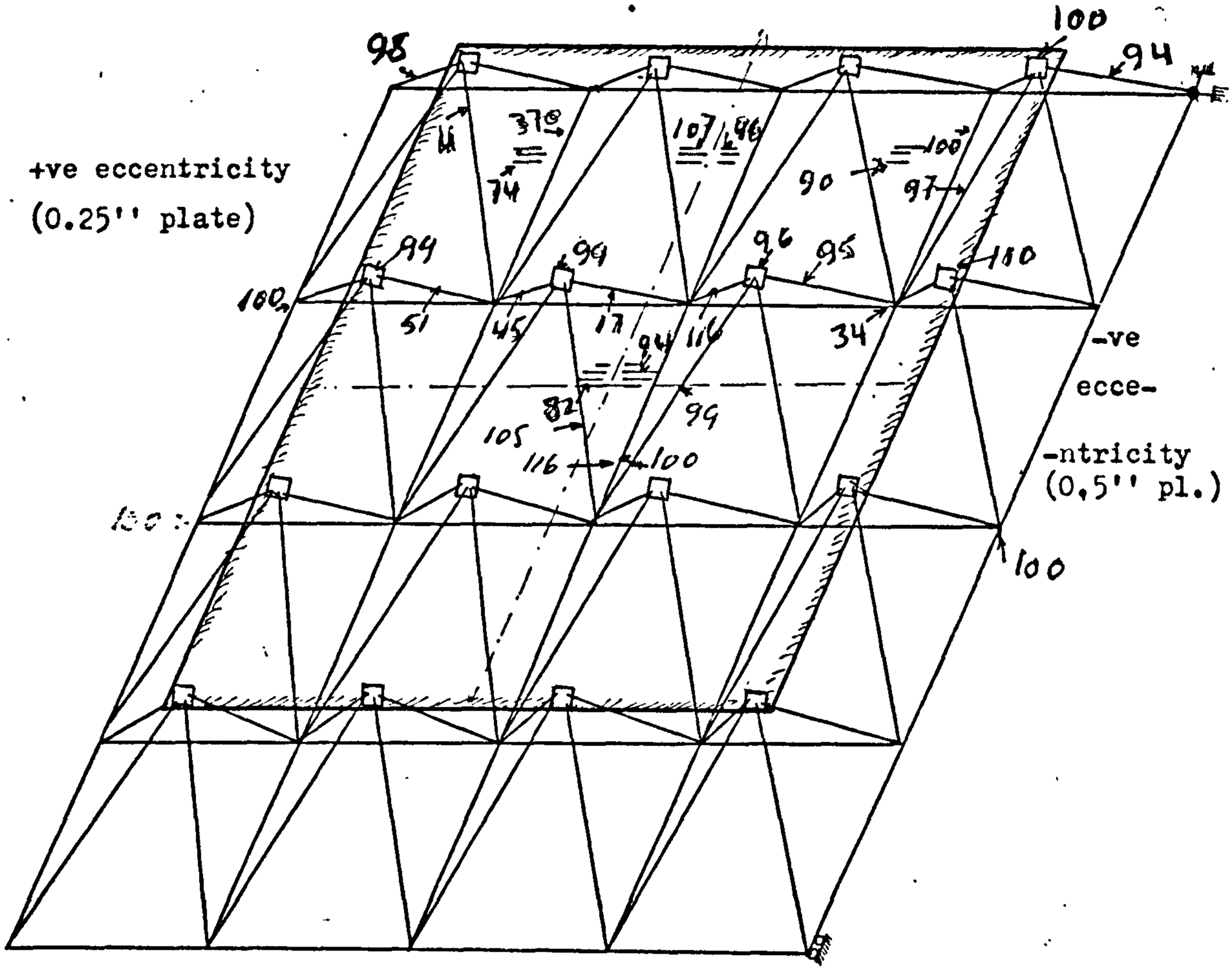

Fig. 6.3 Shows the results with eccentricity as percentages of those without eccentricity for deflections and stresses.

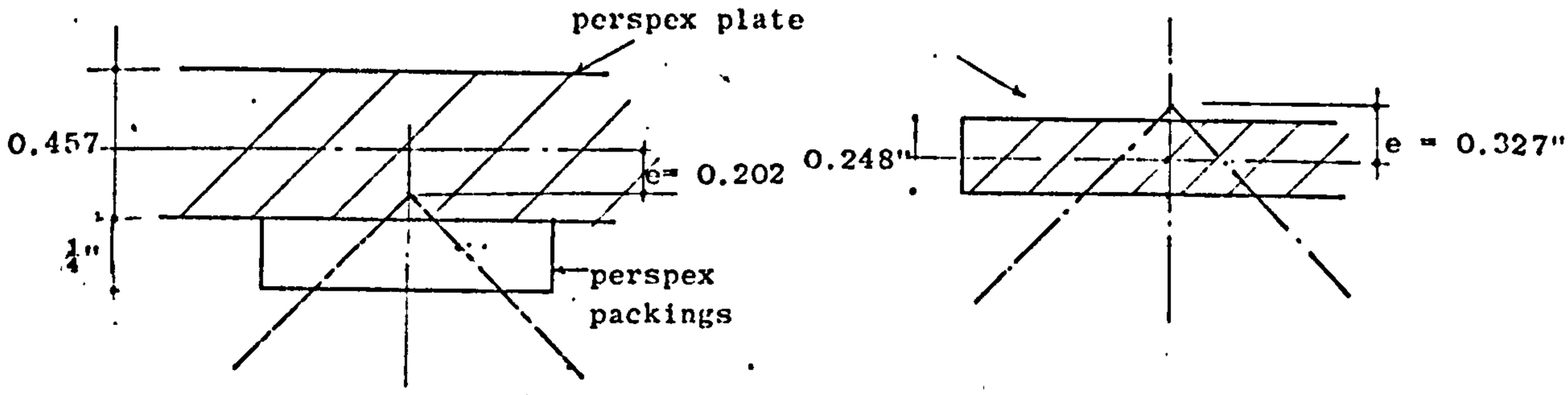

Case 1
- ve eccentricity

Case 2
+ ve eccentricity

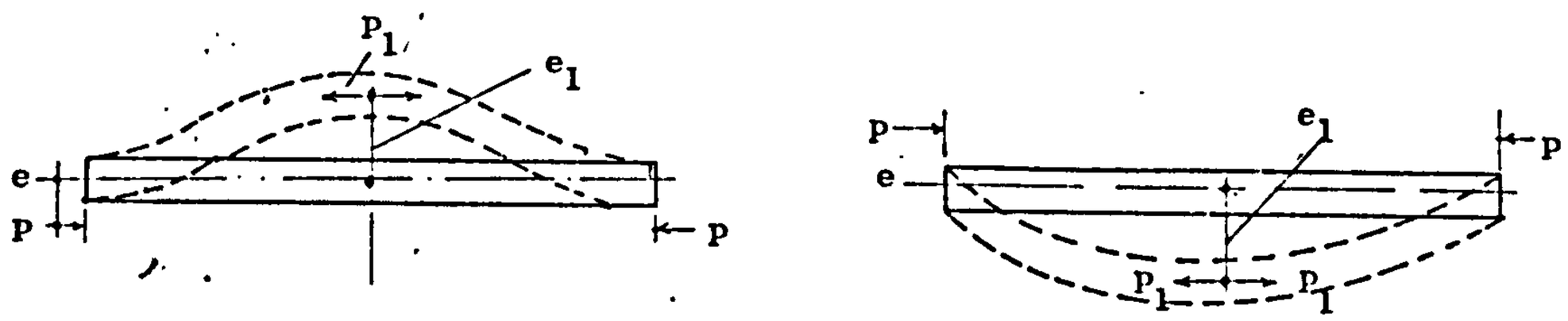

$$P \times e = P_1 \times e_1$$

if $e_1 > e$ then $P_1 < P$

and vice versa

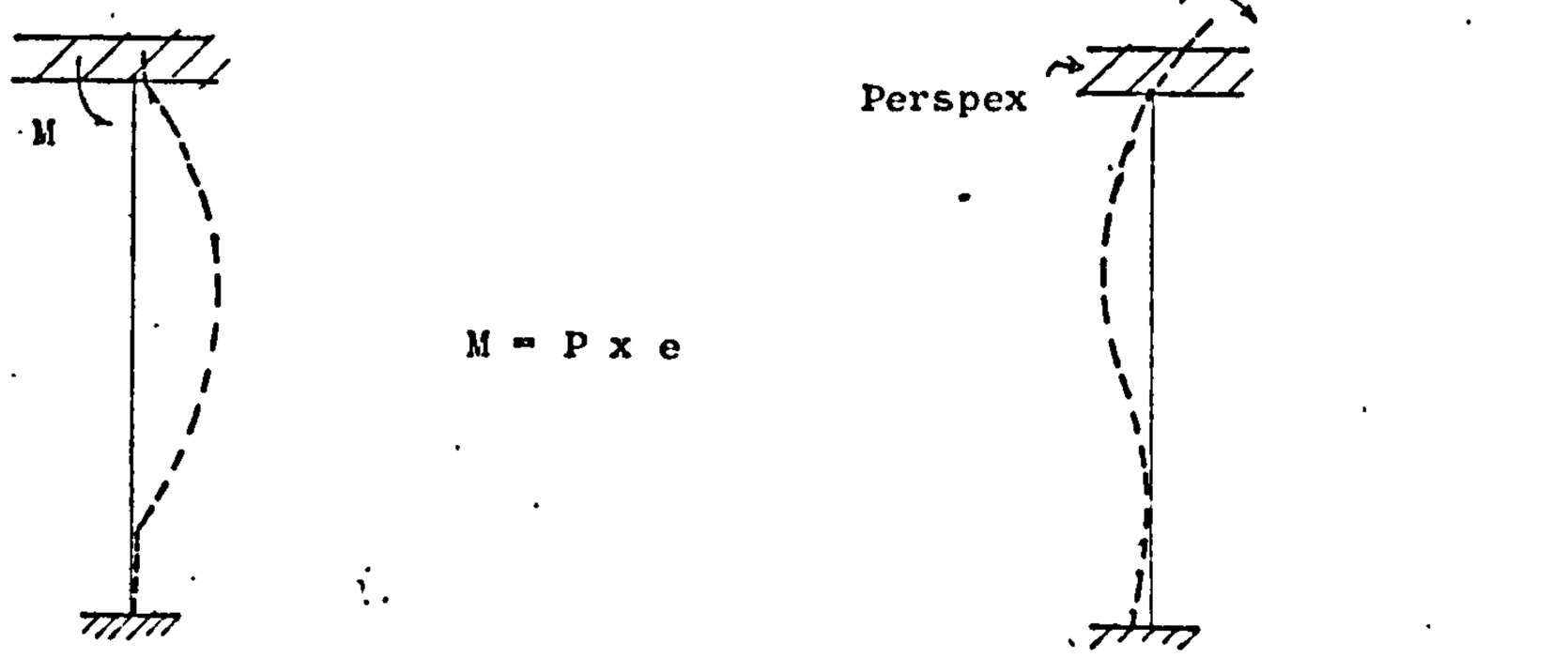

$$M = P \times e$$

Fig. 6.4 Idealization of eccentricity effects

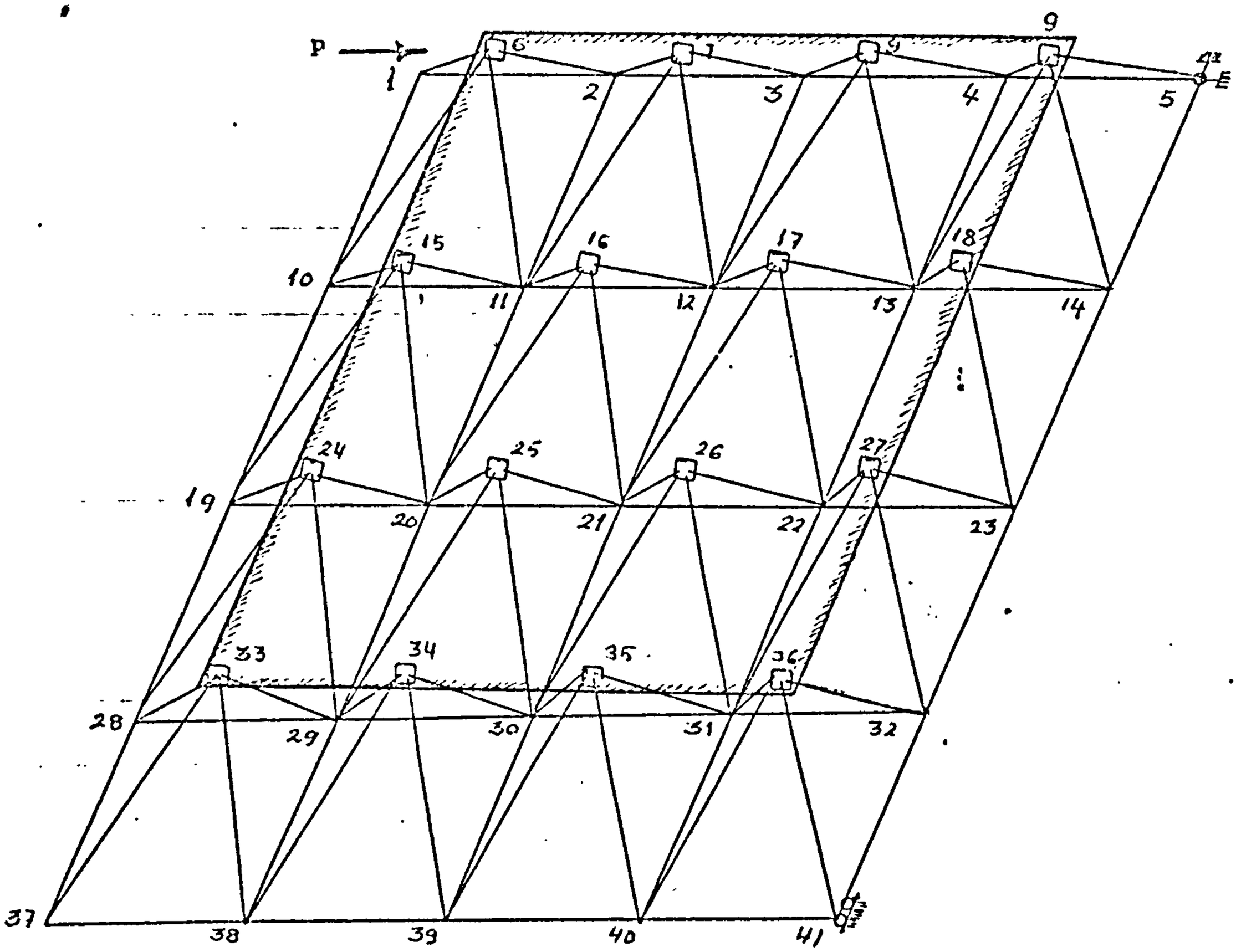

Fig. 6.5 Horizontal loading to investigate the In-plane rotation

CHAPTER 7

'THE UNIFORM MESH'

A POSSIBLE PRACTICAL STRUCTURE

7.1 Introduction

As was mentioned in the Literature Review, there are many types of double layer grids according to their basic unit configuration. Six grid types based on rectangles[24] are shown in Fig. 7.1. The most popular grids among them are the following two types.

1. Grid type 1 - which is sometimes termed 'Rectangular Parallel Mesh' (RPM) where both top and bottom grids are of rectangular patterns, but the top nodes are above the centre of the bottom rectangles, and both top and bottom sides are parallel to the boundaries. The experimental model of this research (Model I) was basically of this type.

2. Grid type 5 - which is sometimes termed 'Inclined Rectangular Mesh' (IRM) in which the bottom rectangles are offset diagonally to the top ones and also to the boundaries.

These two grids are termed 'Square Parallel Mesh' and 'Inclined Square Mesh' when their basic pattern is a square. But it is preferred to stick to 'RPM' and 'IRM' terms because the square is a special case of the rectangle.

It is noticed in the six grids shown, that bottom squares are always larger or equal to the top ones. This is because, the bottom layer is under tension while the

top layer is under compression. Since the compressive strength for tubes is less than the tensile strength because of the possibility of buckling, the top members are never made longer than the bottom members.

In the case of composite double layer grids which are made with the top layer of concrete plate and the remainder of steel tubes, the diagonal shear members will be the critical members for design and not the top plate. This is due to the high bending stiffness of the plate.

Therefore, to get an efficient structure, one should aim towards a structure with more uniform shear distribution.

7.2 The Uniform Mesh

In order to investigate the properties of composite double layer grids and to carry out parameter studies, it is necessary to simulate the relative properties of steel and concrete which would not be possible if unit dimensions were used, a structural model has to be used for such studies.

Bearing in mind that this type of structure is expected to be mostly competitive in large spans and for the reasons mentioned in para 7.1, it was decided to use a form based on Inclined Rectangular Grid, which was shown in Fig. 2.2. This was because it is more rigid and exhibits better stress distribution especially near the boundaries than the 'IRM' and the 'RPM' configurations. Also it has a more general configuration, since the IRM configuration could be a special case of it. This does not imply that it is the most efficient or economical.

This form is shown in Fig. 7.2, and will be termed 'The Uniform Mesh' because the diagonal shear members (pyramid sides) are uniformly distributed over the whole area.

It is useful to mention that the only other configuration used in what may be called composite double layer grid structures is the one used by Castillo[2] for his slab and was based on the 'RPM' configuration as was shown in Fig. 2.5.

Another comparable efficient structure could be based on the 'IRM' configuration, and will be called 'The

'IRM' composite structure", and is shown in Fig. 7.3 from which it is seen that the pyramid sides are alternatively distributed and the tube spacing in the bottom layer is double that of the Uniform Mesh. The Uniform Mesh will be particularly efficient in very large spans. For shorter spans or for less heavy loads "The 'IRM' composite structure" could be used more efficiently.

All theoretical investigations and the parameter studies in Chapter 9 will be based on the 'Uniform Mesh'.

The following are to be observed.

a) The basic pyramid unit dimensions are 120" x 120" x 42.43" as is shown in Fig. 7.4a, concrete slab thickness is 5 inches, and tubes are of 4.5 inch outside diameter and of Gauge 7, (wall thickness = 0.176 in).

b) Manufacturer properties and safe load tables were used.[20] Elastic constants are:

for steel $E_s = 30 \times 10^6$ psi, $\mu = 0.30$

for concrete $E_c = 4 \times 10^6$ psi, $\mu = 0.15$

c) A load of 100 psf was assumed to be uniformly distributed over the top layer including the self weight.

d) Four finite element subdivisions per pyramid were used. In other words a mesh of 2 x 2 finite elements.

e) The structure analysed is square in plan in order to get the largest span for a given number of joints or nodes. The structure is assumed to be simply supported along its four bottom sides, and the joints are assumed to be rigid.

f) Due to the double symmetry, one quarter of the

structure was analysed only.

g) Diagonal tubes connecting the top layer joints to the bottom layer joints (pyramid sides) are termed 'Diagonal Shear Members'.

7.3 The Variables to be Compared

In order to study the structural behaviour of the 'Uniform Mesh' and to compare it with other alternatives in Chapter 8, and also to do the parameter studies in Chapter 10, certain variables in selected members and locations are chosen to be the basis for this study and comparison.

These variables are:

1. The deflection of the joint which is located at the centre of the bottom layer when it exists, and of the node located in the centre of the top layer.

2. The axial tensile forces in the bottom layer belonging to

   a) The tube which passes (or its line of axis) through the centre point of the bottom layer, and will be called the centre tube, and its axial force will be termed 'P'.

   b) The tube with the maximum tensile force, which will be termed 'T'.

3. The axial compressive forces in the diagonal shear members which belong to:

   a) The tube which is located near the corner of the structure, which will be called the corner tube. This was particularly chosen for its high compressive force, and will be termed C_c.

   b) The tube with the maximum compressive (shear) force which will be termed 'C'.

4. The central positive moment (stress) and the

central in-plane stress which will be termed M, σ_b, σ_p respectively.

5. The maximum positive and negative moments (stresses), and maximum in-plane stresses in the concrete slab. These will be termed $+M_m$, $-M_m$, σ_{bm}, $-\sigma_{bm}$, σ_{pm} respectively.

7.4 Spans Used

In order to study the structural behaviour of the 'Uniform Mesh' and also to compare it with other alternatives, four different spans were used.

1. 40 ft. span made of four pyramid units. This case will be called DCON2.
2. 60 ft. span, made of six pyramid units. This will be called case DCON3.
3. 80 ft. span, made of eight pyramid units. This will be called case DCON4.
4. 100 ft. span, made of ten pyramid units. This will be called case DCON5.

7.5 The Stress Analysis of the Uniform Mesh

Figs. (7.5, 7.6, 7.7 and 7.8) show the axial force distribution for cases DCON2, DCON3, DCON4 and DCON5 respectively, while Figs. (7.9, 7.10, 7.11 and 7.12) show the bending moment (M_x) distribution for the slabs of these cases respectively.

Table 7.1 shows the variables mentioned in para 7.3 for cases DCON2, DCON3, DCON4 and DCON5 with the ratio of maximum in-plane stress/maximum bending stresses in concrete, and also the ratio of maximum compressive forces/ maximum tensile forces in the tubes.

Studying the above table and figures shows that:

1. When span is very short, as in case DCON2, the load is carried by combination of shear and direct compressive forces more than by bending forces. But the structure tends to behave like a slab for larger spans. This tendency is clearly seen in Table 7.6 where ratio of maximum shear force/maximum tensile force decrease with the increase of span while the ratio of maximum in-plane stress/maximum bending stress increases with the increase in span. This will be discussed further in Chapter 9.
2. Most bottom layer members are under tension, with the exception of some members near the boundaries. The maximum tensile force is not in the centre, but is always in the tube located under the third top joint counted from the top corner along the diagonal and is marked by T in the above figures. It is noticed also

that bottom layer members are more or less under comparable axial stresses, i.e. there is no vast differences in stresses between the boundary area and the centre area. This is specially clear in cases DCON4 and DCON5.

3. Most of the diagonal shear members are under compressive axial forces. The highest are in the boundary area. The difference between the maximum and corner shear forces decrease with the increase of span, until the corner force itself becomes the maximum force in case DCON5. This shows the tendency of having more or less uniform shear distribution in boundary area.

   The maximum compressive force is always less than the maximum tensile force (except in case DCON2 where shear action was dominating), but the difference is not large. This characteristic is useful in the design considerations.

4. Stresses in the slab are negligible at least for the range of loading and spans used in comparison with the allowable concrete stresses. Furthermore, in-plane stresses are negligible in comparison with the flexural stresses, as is seen in Table 7.1, although this tendency will cease for larger spans, therefore in-plane stress distributions were not shown.

   It is noticed that positive flexural stresses are higher than negative ones (except case DCON2) and the maximum bending moments are in the central area, but not at centre point, while negative ones are in the boundary area. This is because of the presence of

the internal supports, which means, having a flat slab, with rigid supports in the boundary area, hence higher -ve moments, and flexible supports especially in the central area, hence higher positive moments.

5. It is clear from above that shear members are the critical members in design consideration. For concrete slab, practical considerations might be the deciding factor.

11

TABLE 7.1

COMPARISON OF PLATE STRESSES AND TUBE'S AXIAL FORCES IN THE UNIFORM MESH

No.	Description	CASE DCON2 Span = 40 ft.	CASE DCON3 Span = 60 ft.	CASE DCON4 Span = 80 ft.	CASE DCON5 Span = 100ft
1.	Axial forces in tubes (in lbs.)				
	a) Tensile forces				
	i) Central force (P)	12452	21859	41068	62023
	ii) Maximum force (T)	13602	28214	50835	82333
	b) Compressive (shear) forces				
	i) Corner force (C_c)	-14360	-22860	-40171	-60554
	ii) Maximum force (C)	-25409	-25436	-48553	-60554
2.	Stresses in concrete plate (psi)				
	a) Bending moment				
	i) Centre point stress (σ_b)	163	183	265	349
	ii) Maximum stress (σ_{bm})	-392	367	435	520
	b) In-plane stresses				
	i) Centre point (σ_p)	-19.4	-54	-108	-177
	ii) Maximum. (σ_{pm})	-63	-68	-124	-192
3.	Ratios				
	a) σ_{pm}/σ_{bm}	0.16	0.186	0.285	0.37
	b) C/T	1.868	0.902	0.955	0.735
	c) C/C_c	1.77	1.11	1.21	1.0
	d) T/P	1.09	1.29	1.24	1.33

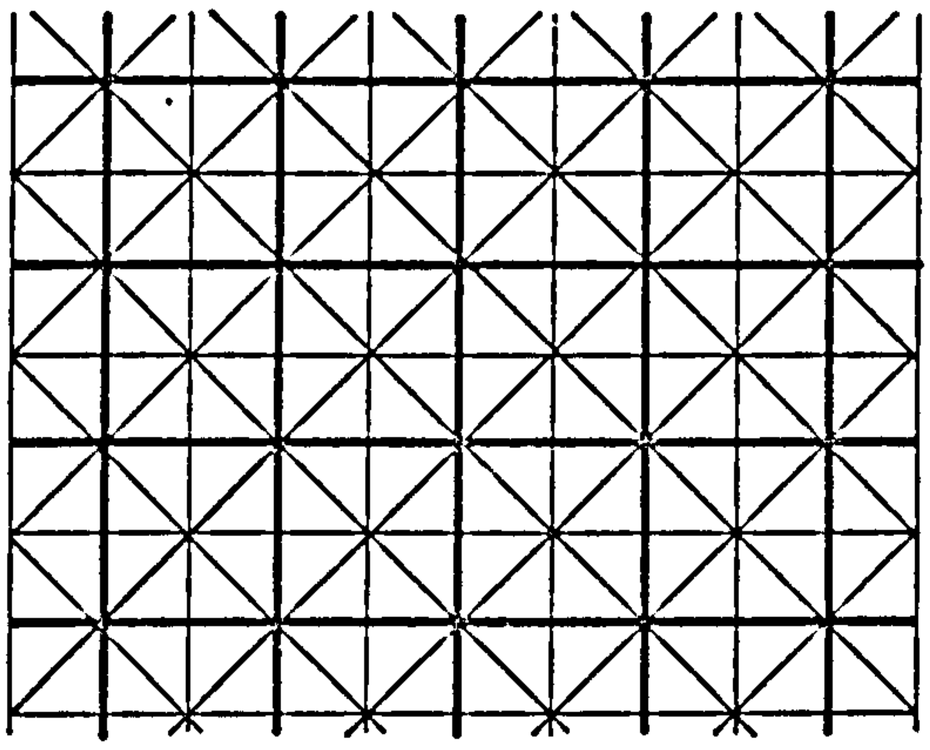

GRID TYPE 1 Square on square offset

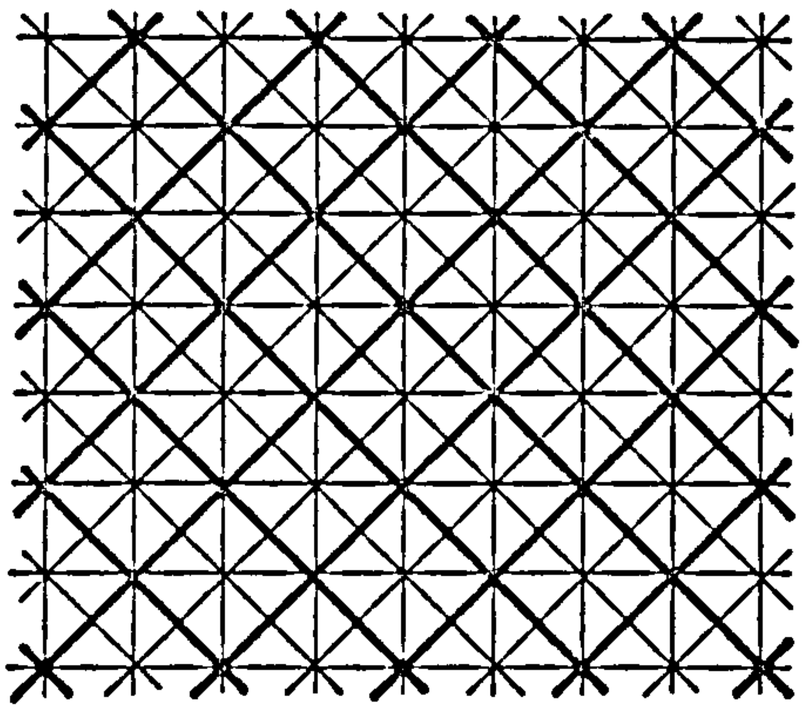

GRID TYPE 2 Square on square offset diagonally

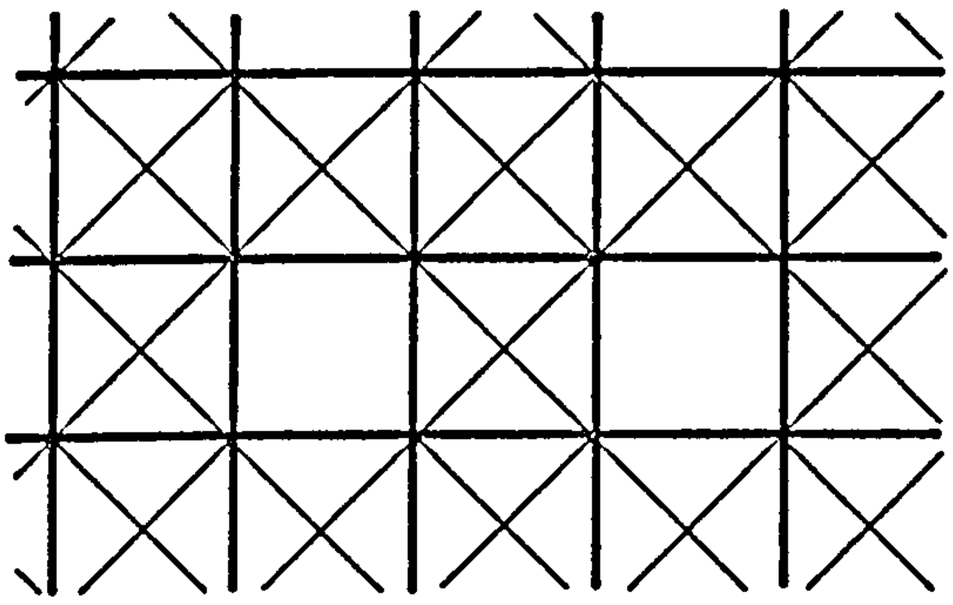

GRID TYPE 3 Square on larger square

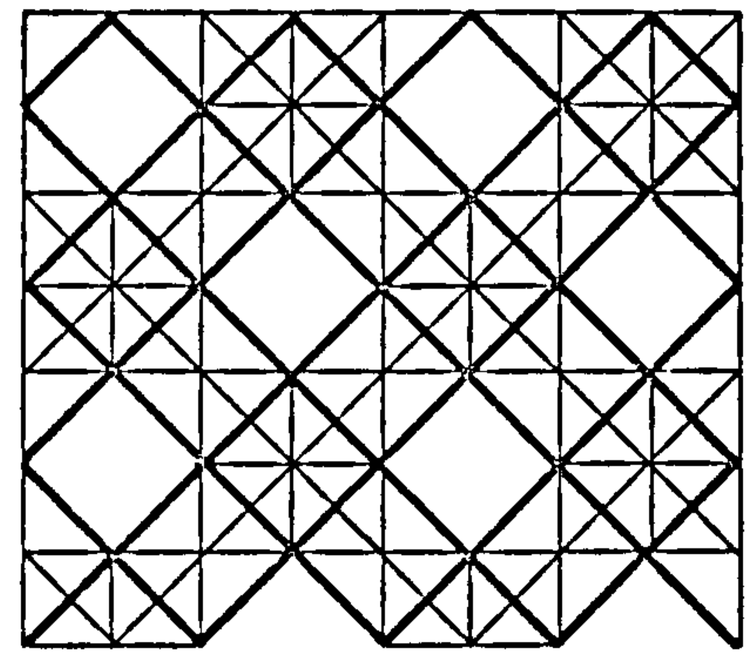

GRID TYPE 4 Square on larger square set diagonally

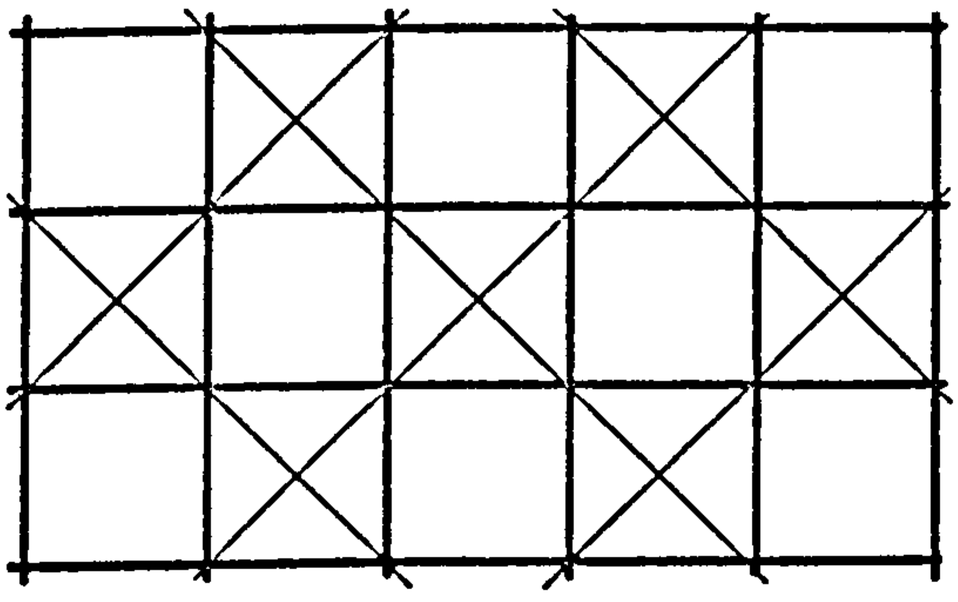

GRID TYPE 5 Square on diagonal

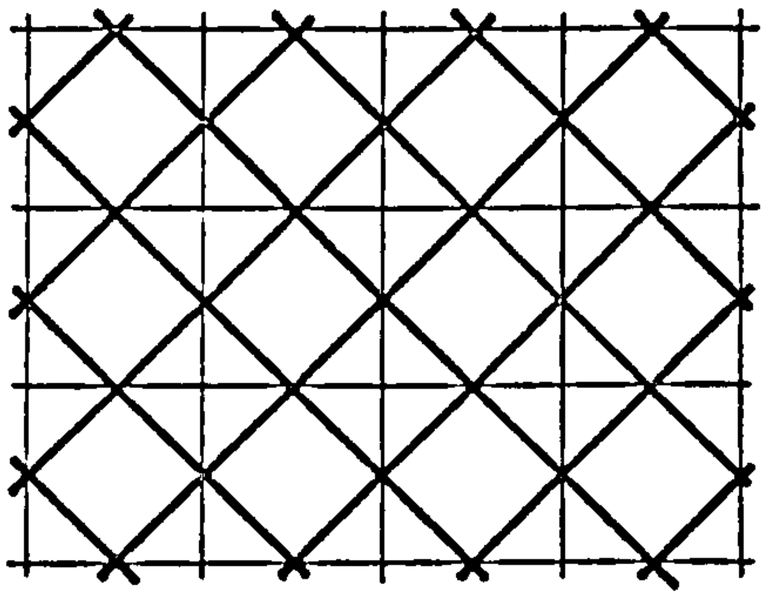

GRID TYPE 6 Diagonal on square

Fig. 7.1 Some types of square based grids.

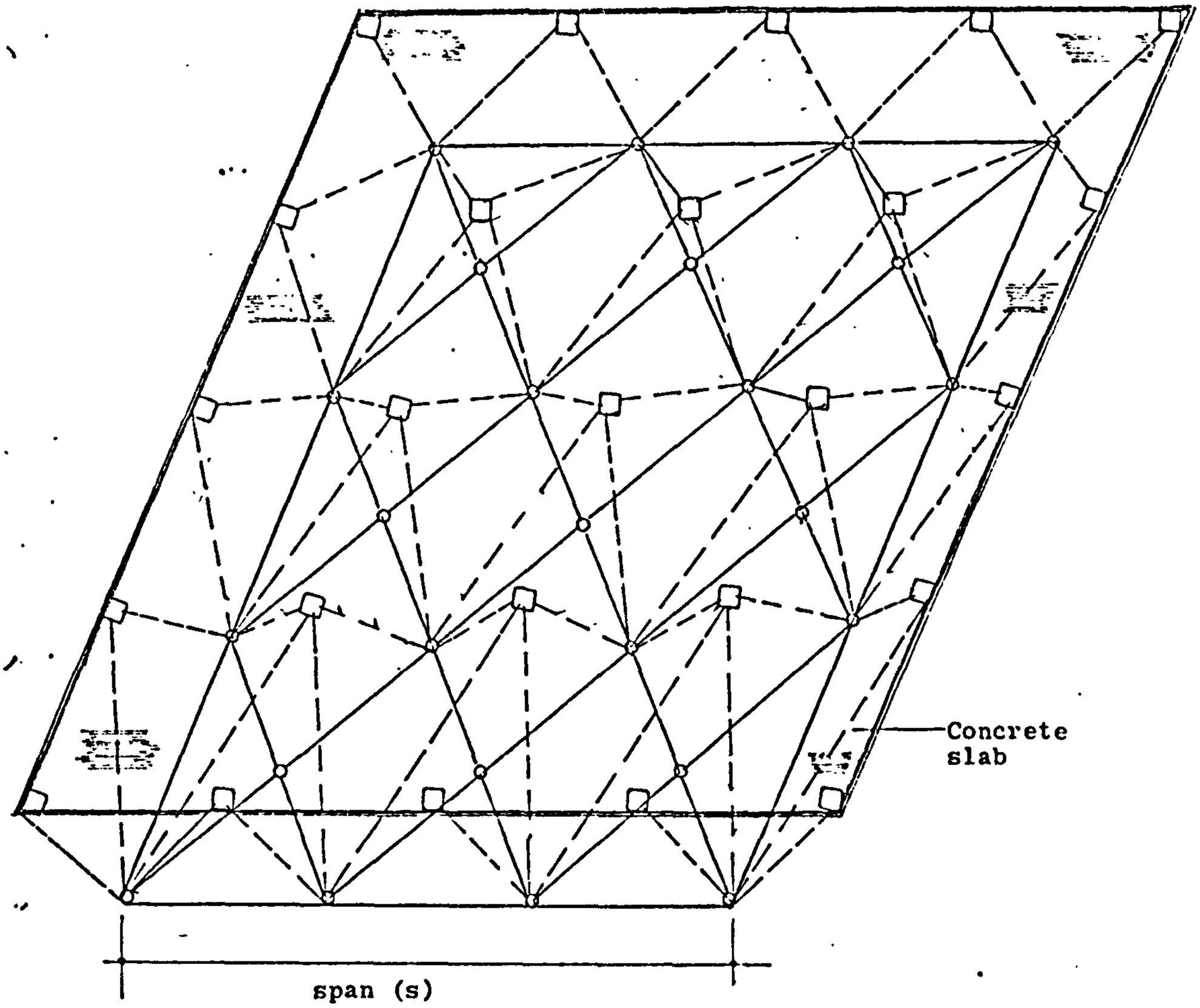

Boundary of concrete layer

Bottom layer members

Diagonal members

o Bottom layer joints

□ Top layer joints

Top concrete layer

Fig. 7,2 THE UNIFORM MESH

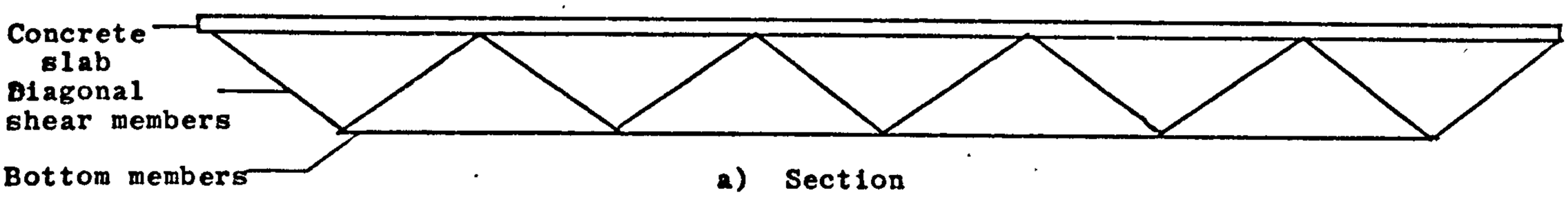

a) Section

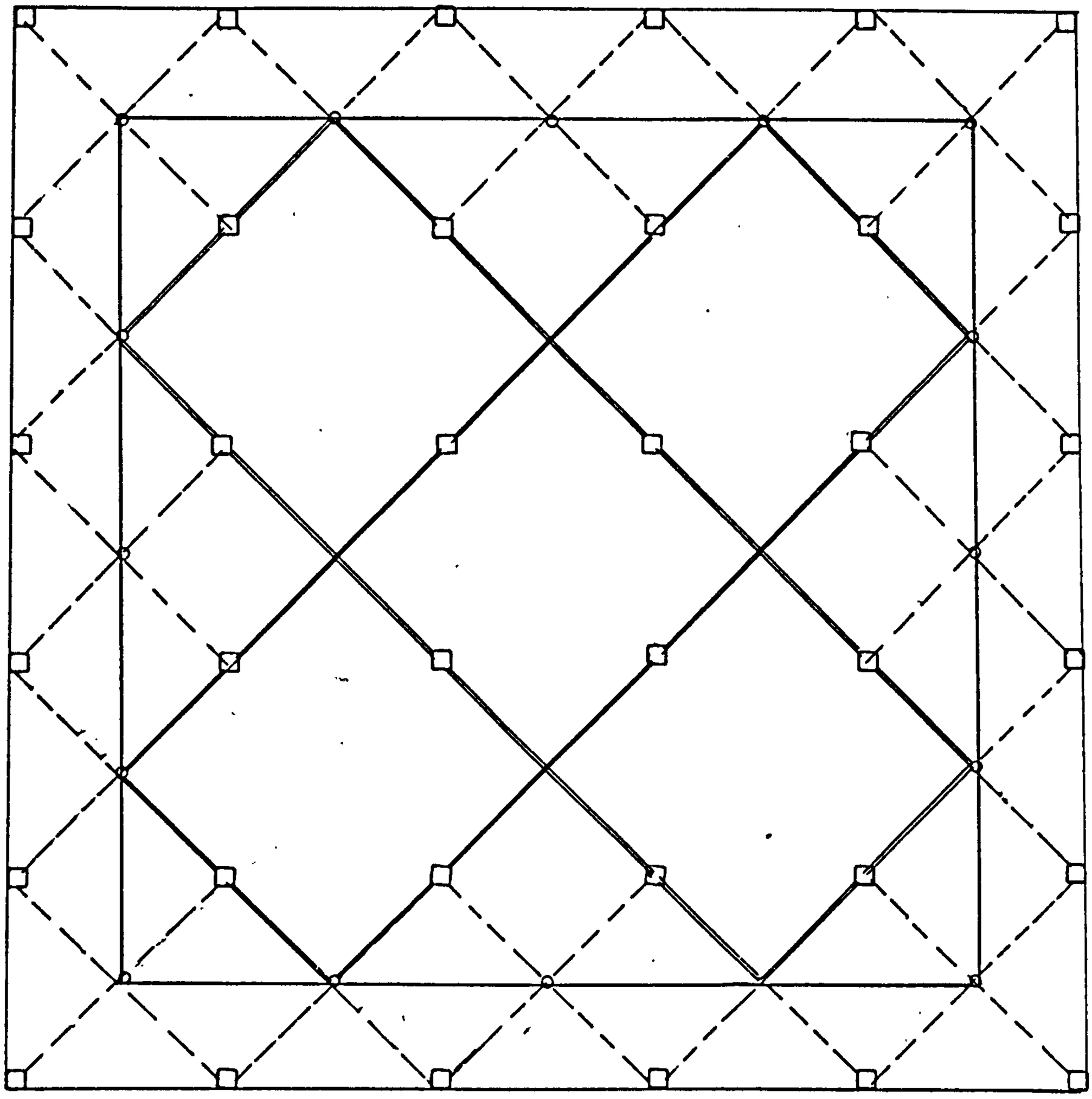

b) Plan of the IRM composite structure

Fig. 7.3

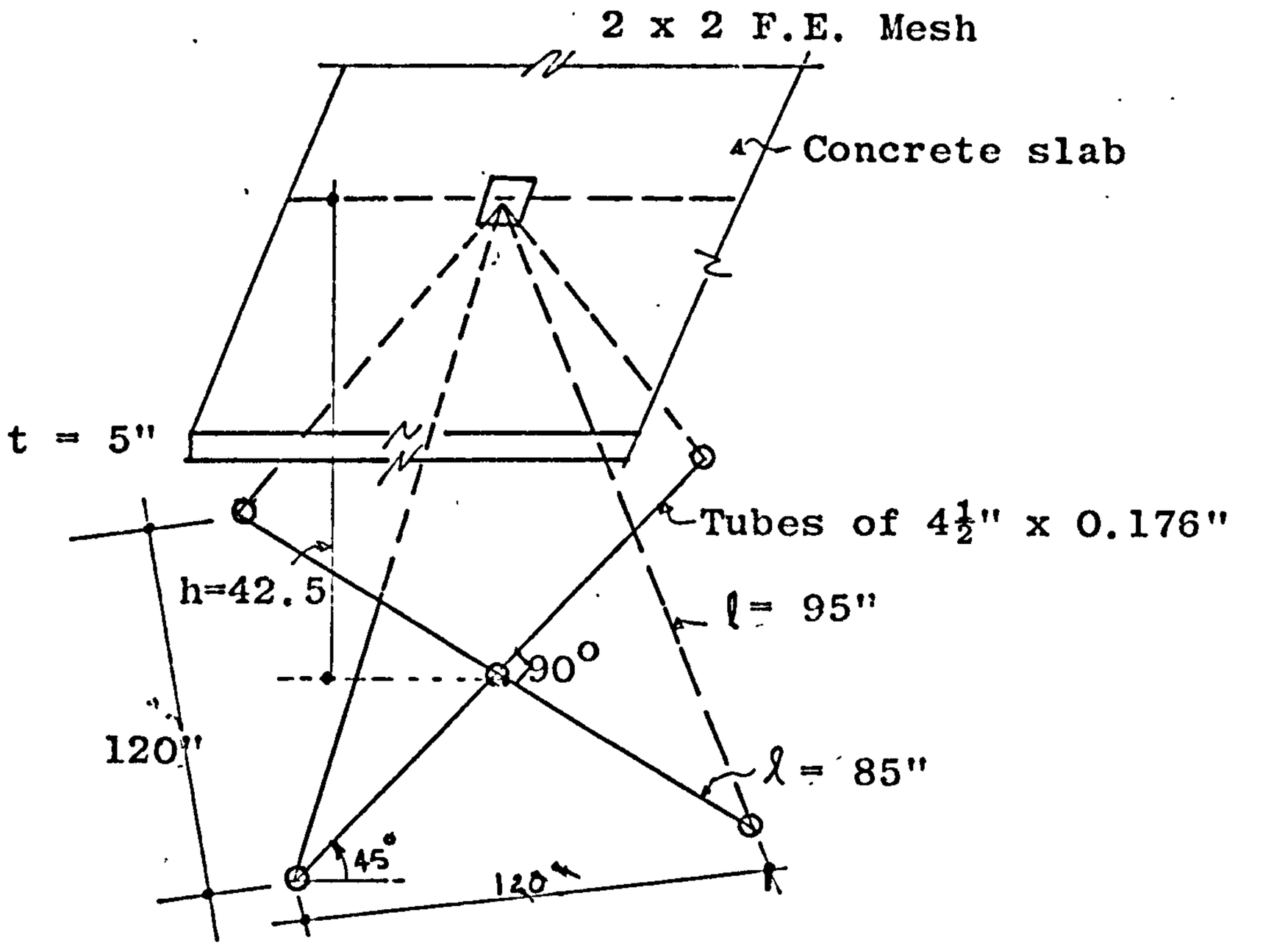

a) Basic Pyramid Unit

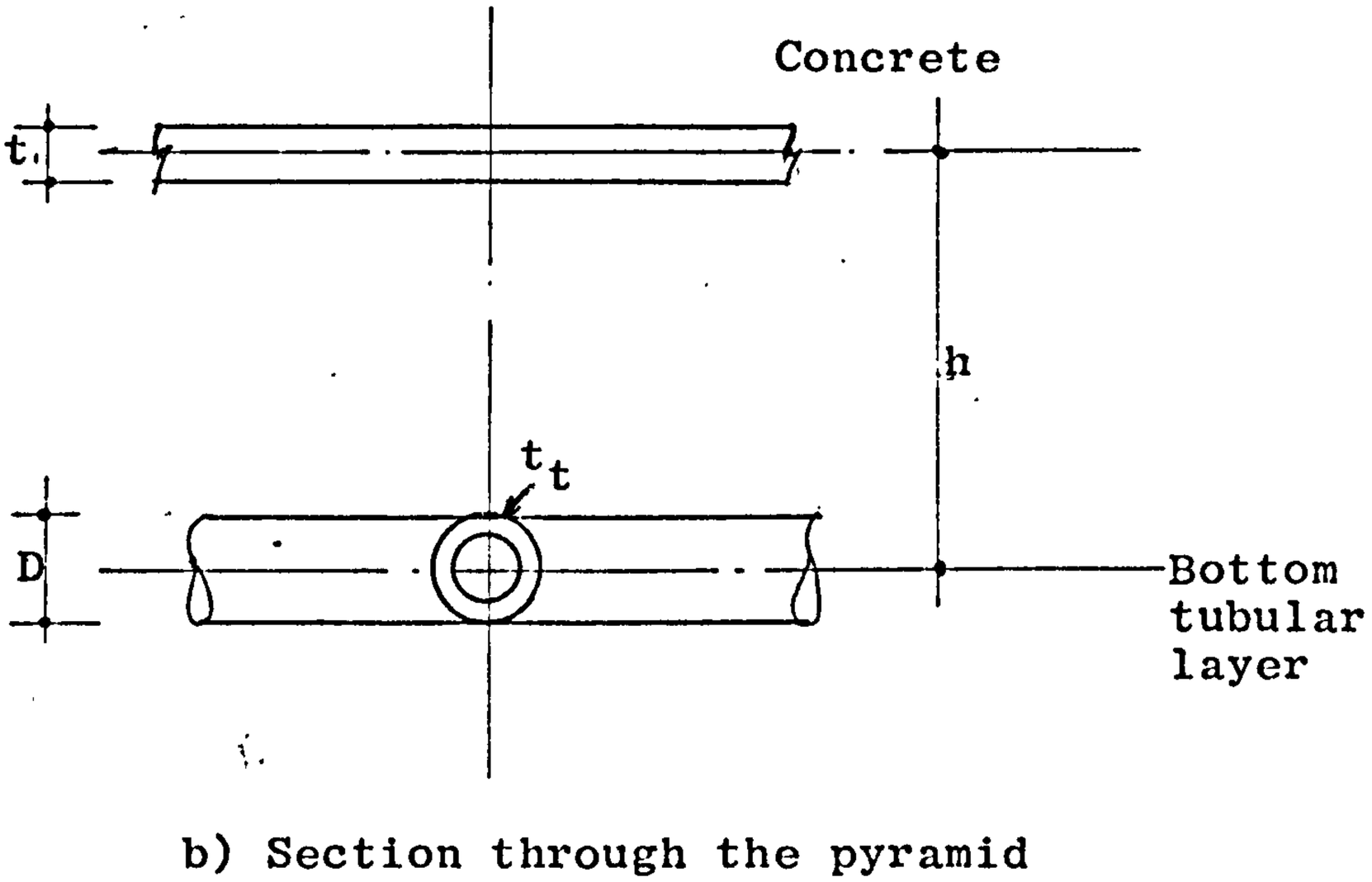

b) Section through the pyramid unit

Fig. 7.4

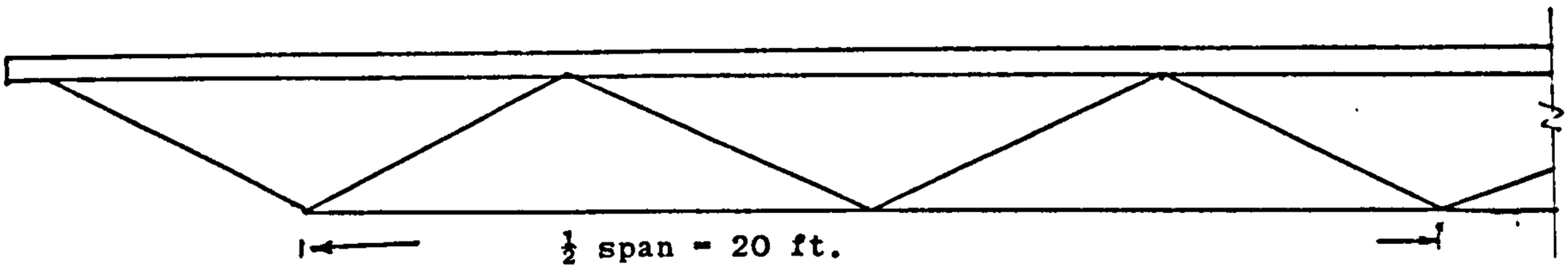

a) Section through D CON 2

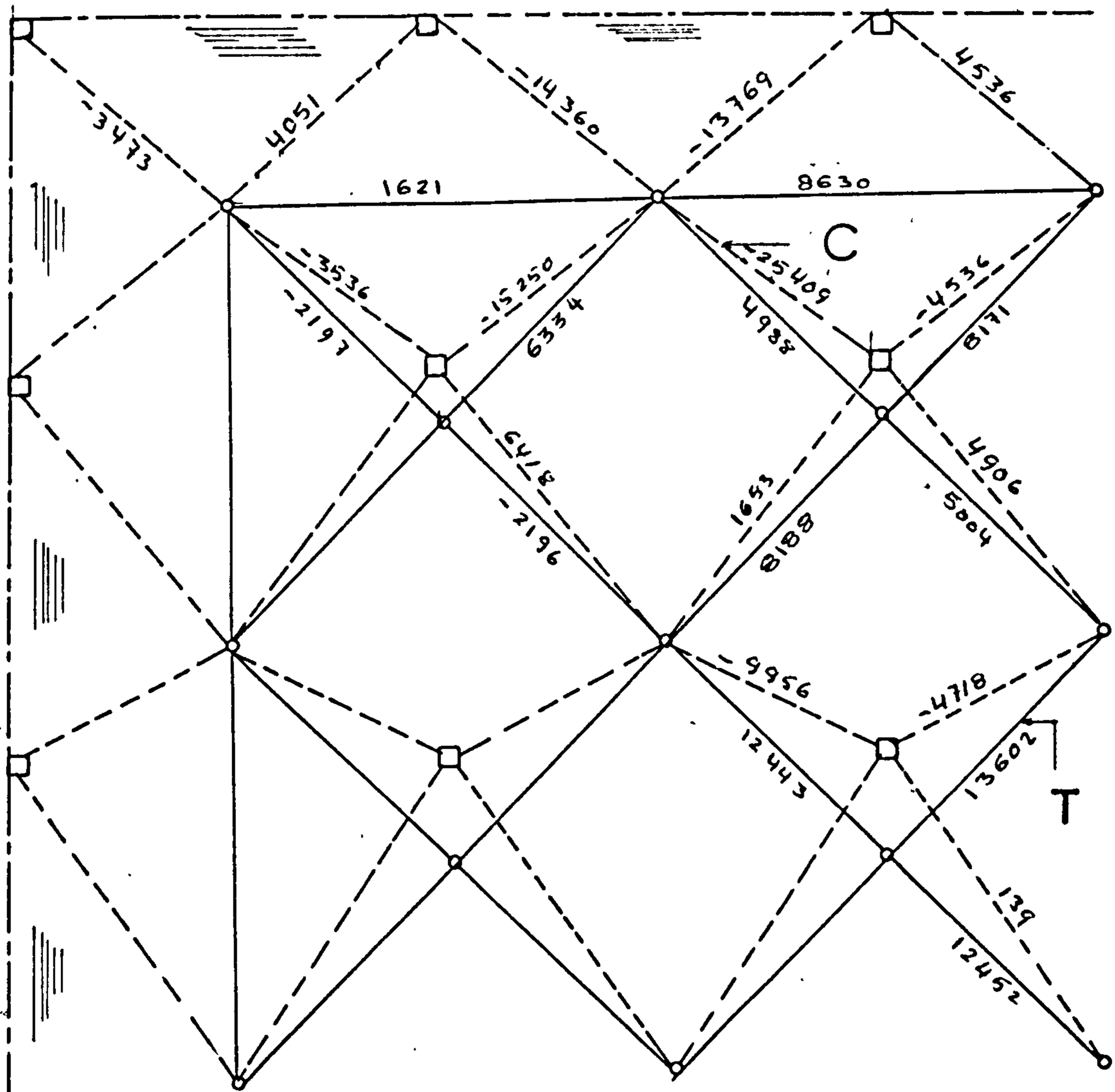

+ve: Tensile force

-ve Compressive force

Top layer concrete slab

Bottom layer tubes

Diagonal shear members

□ Top layer joints

o Bottom layer joints

C Max. compressive force

T Max. tensile force

b) Axial force distribution in a quarter of a symmetrical square 40 ft. span structure (DCON2)

Fig. 7.5

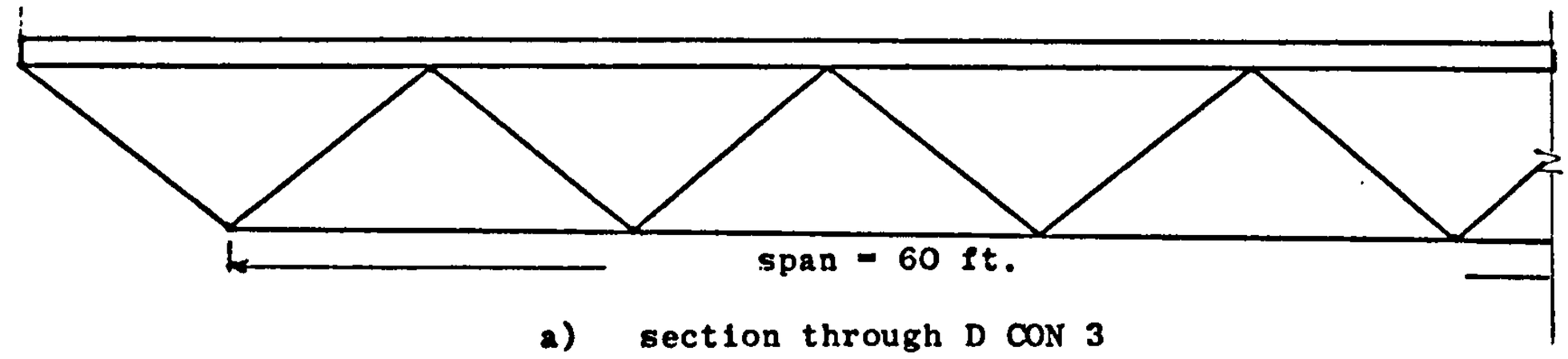

a) section through D CON 3

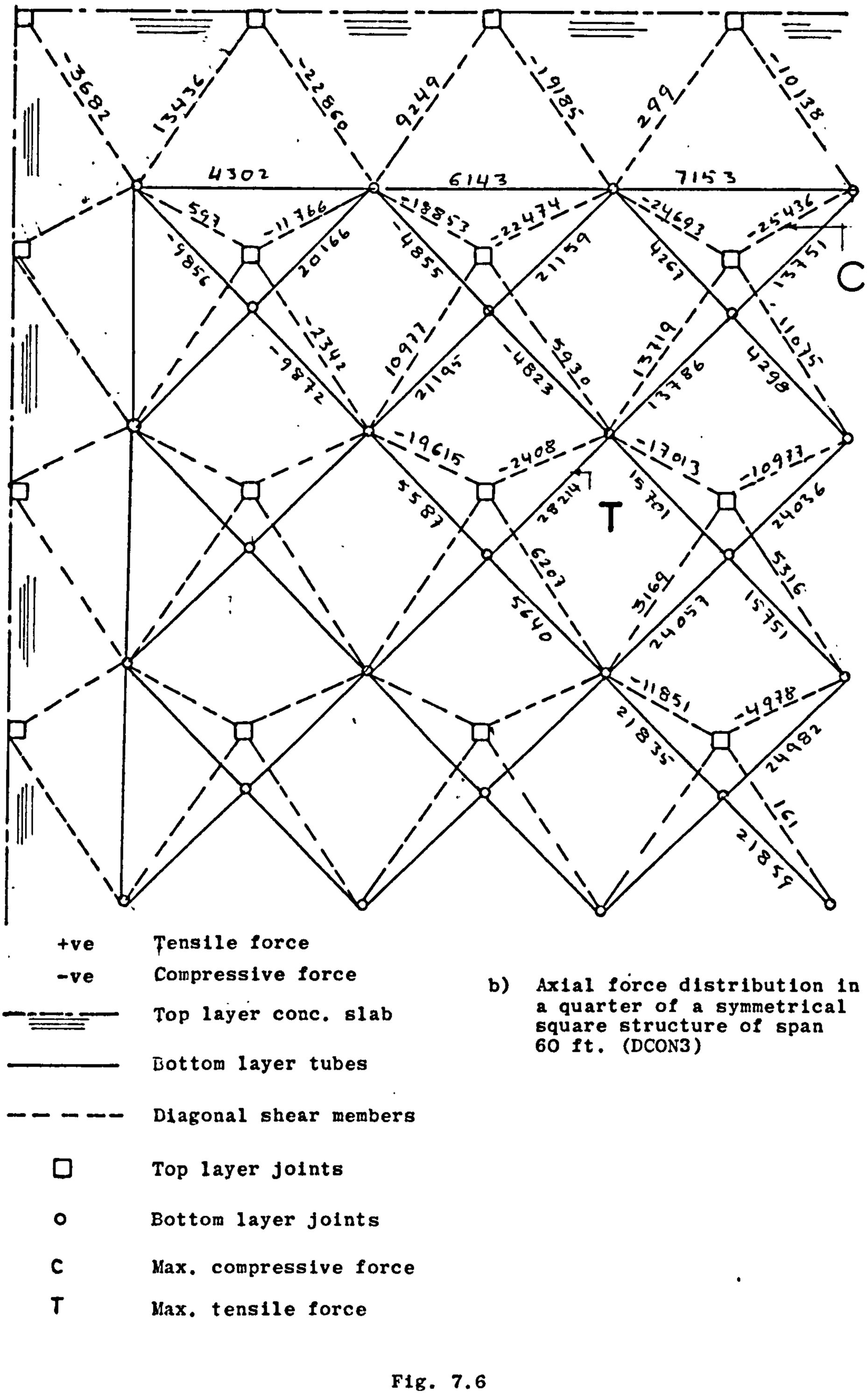

b) Axial force distribution in a quarter of a symmetrical square structure of span 60 ft. (DCON3)

+ve Tensile force

-ve Compressive force

Top layer conc. slab

Bottom layer tubes

Diagonal shear members

□ Top layer joints

o Bottom layer joints

C Max. compressive force

T Max. tensile force

Fig. 7.6

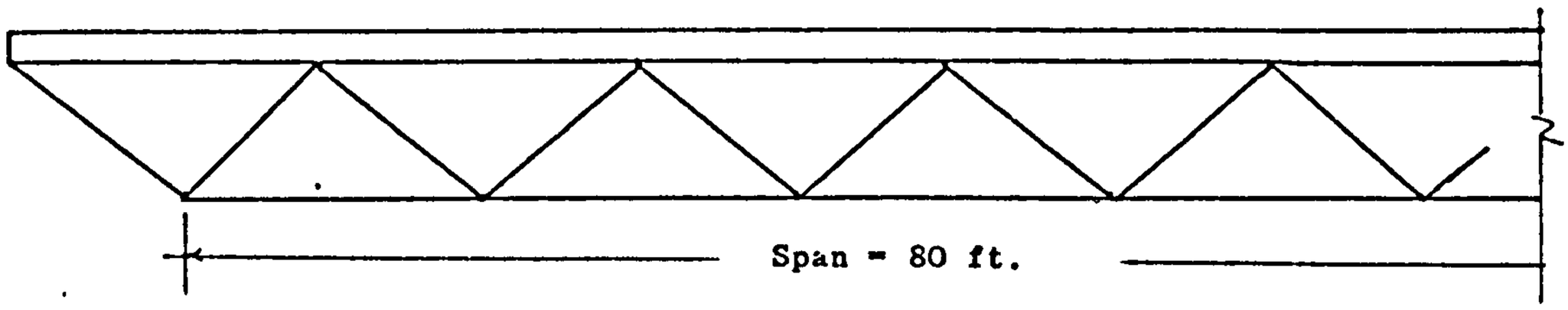

a) Section through D CON 4

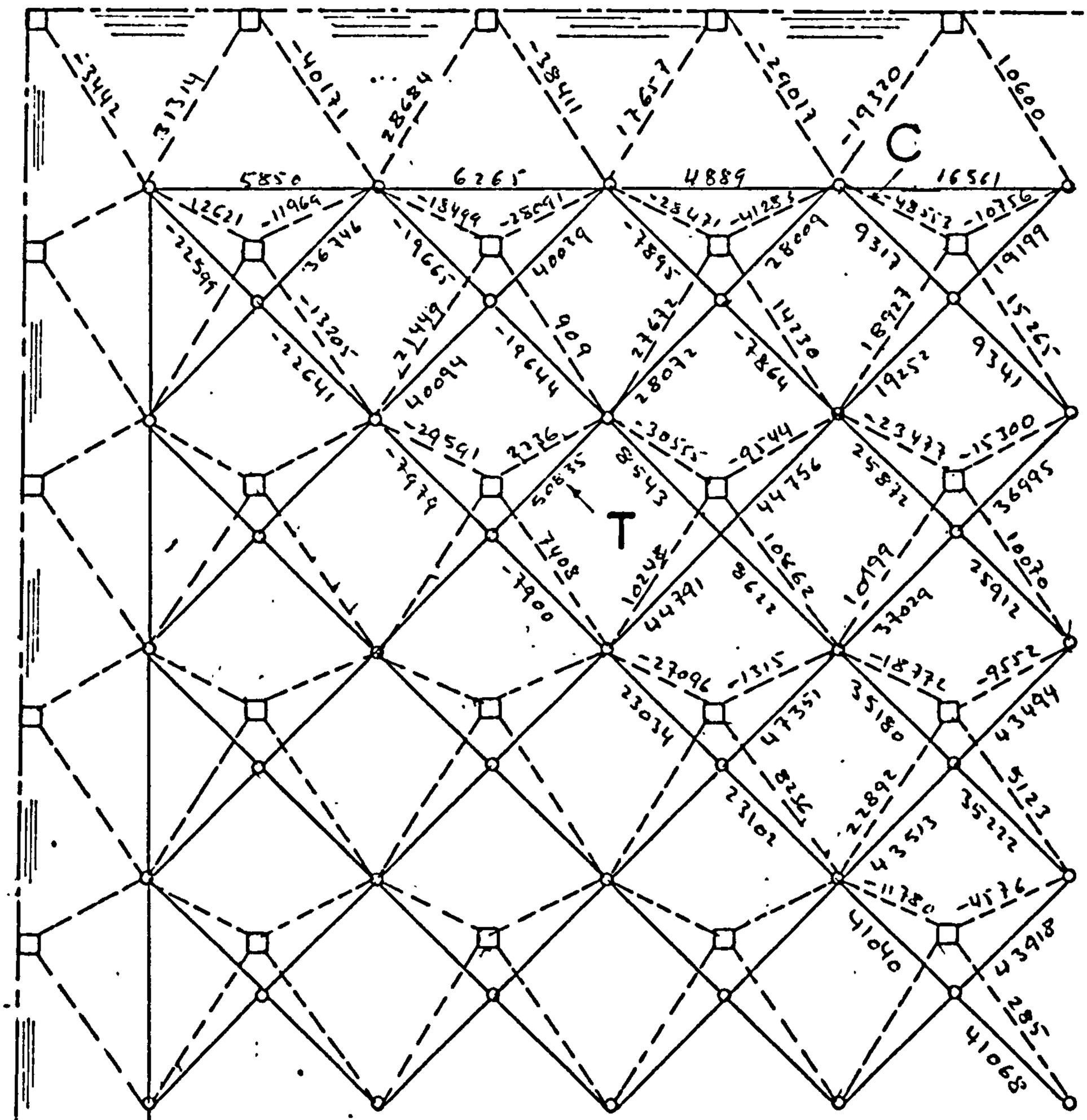

b) Axial force distribution in tubes of a quarter of a symmetrical square structure of span 80 ft. (DCON4)

+ve Tensile force

-ve Compressive force

——— Top concrete layer

——————— Tubes of bottom layer

— — — — — — — Diagonal shear tubes

□ Top layer joints

o Bottom layer joints

C Max. compression

T Max. Tension

Fig. 7.7

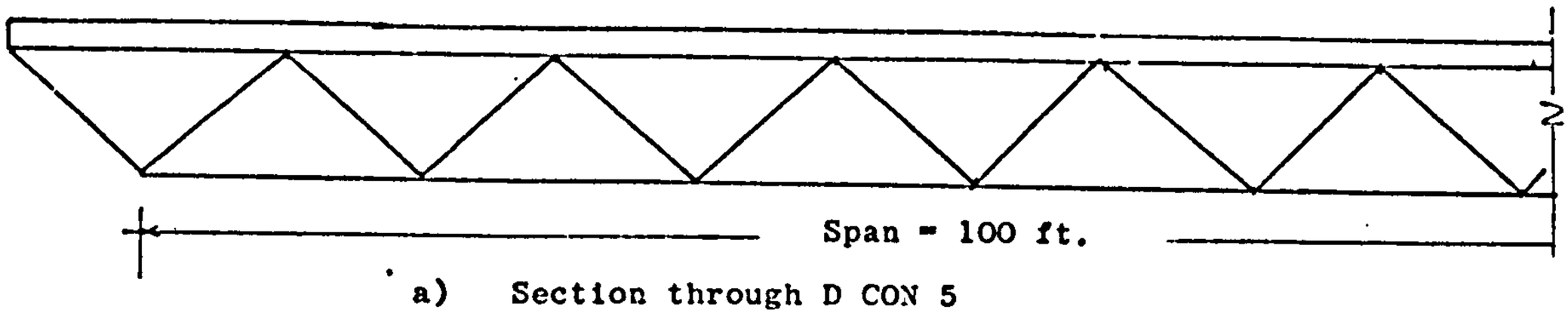

a) Section through D CON 5

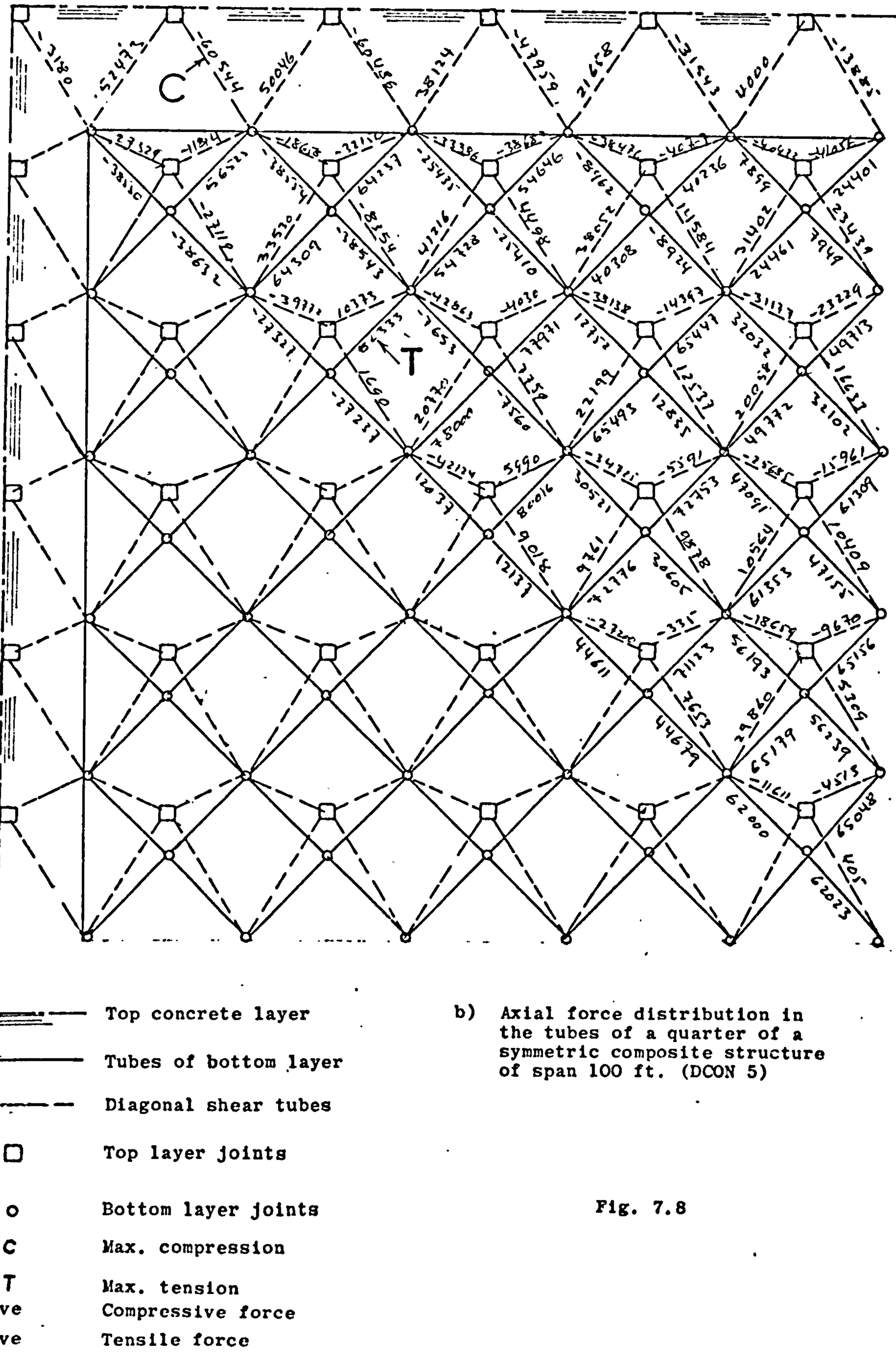

——-——	Top concrete layer
————	Tubes of bottom layer
—-—-—-	Diagonal shear tubes
□	Top layer joints
o	Bottom layer joints
C	Max. compression
T	Max. tension
-ve	Compressive force
+ve	Tensile force

b) Axial force distribution in the tubes of a quarter of a symmetric composite structure of span 100 ft. (DCON 5)

Fig. 7.8

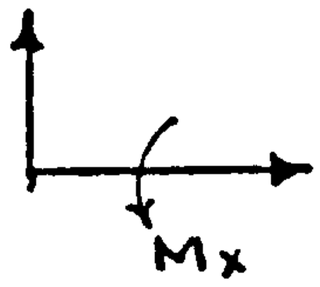

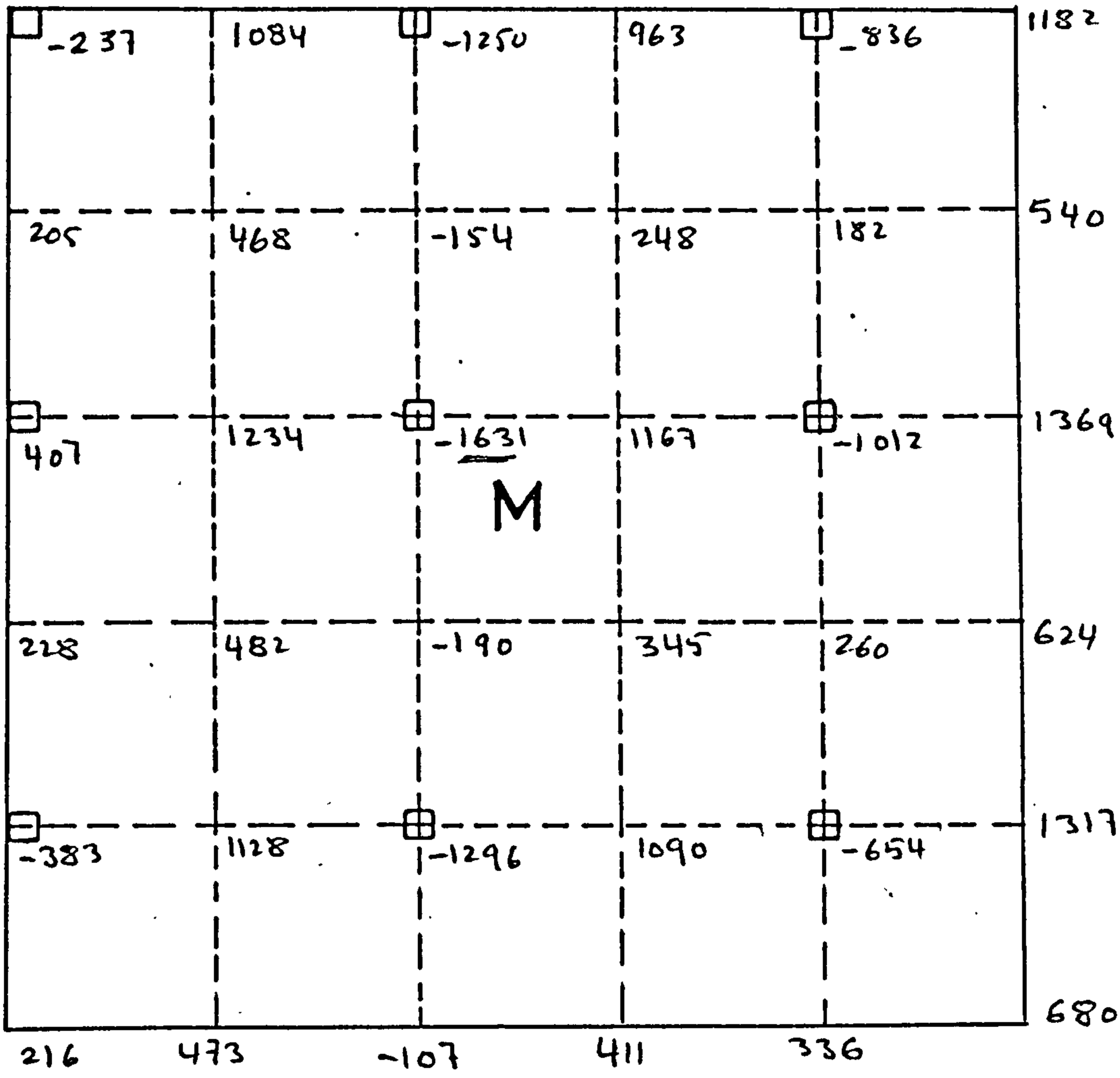

---- Finite Elements subdivision

□ Joints

M Maximum moment

Fig. 7.9 Moment distribution in concrete slab for a quarter of case D CON 2

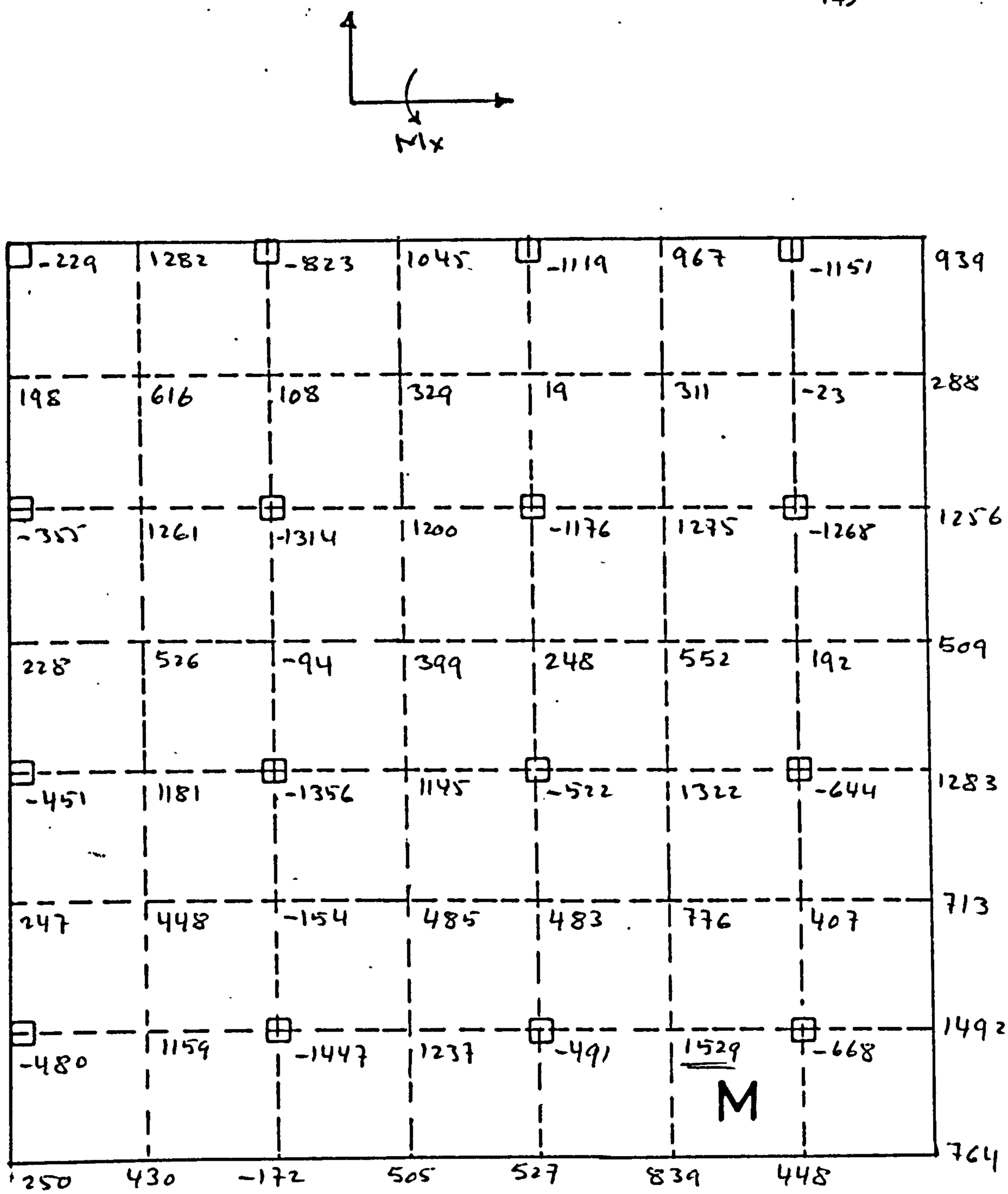

----- Finite Elements subdivisions

□ Joints

M Maximum moment

Fig. 7.10 Moment Distribution in Concrete slab for a quarter of case DCON3

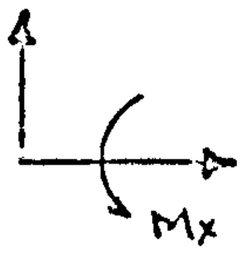

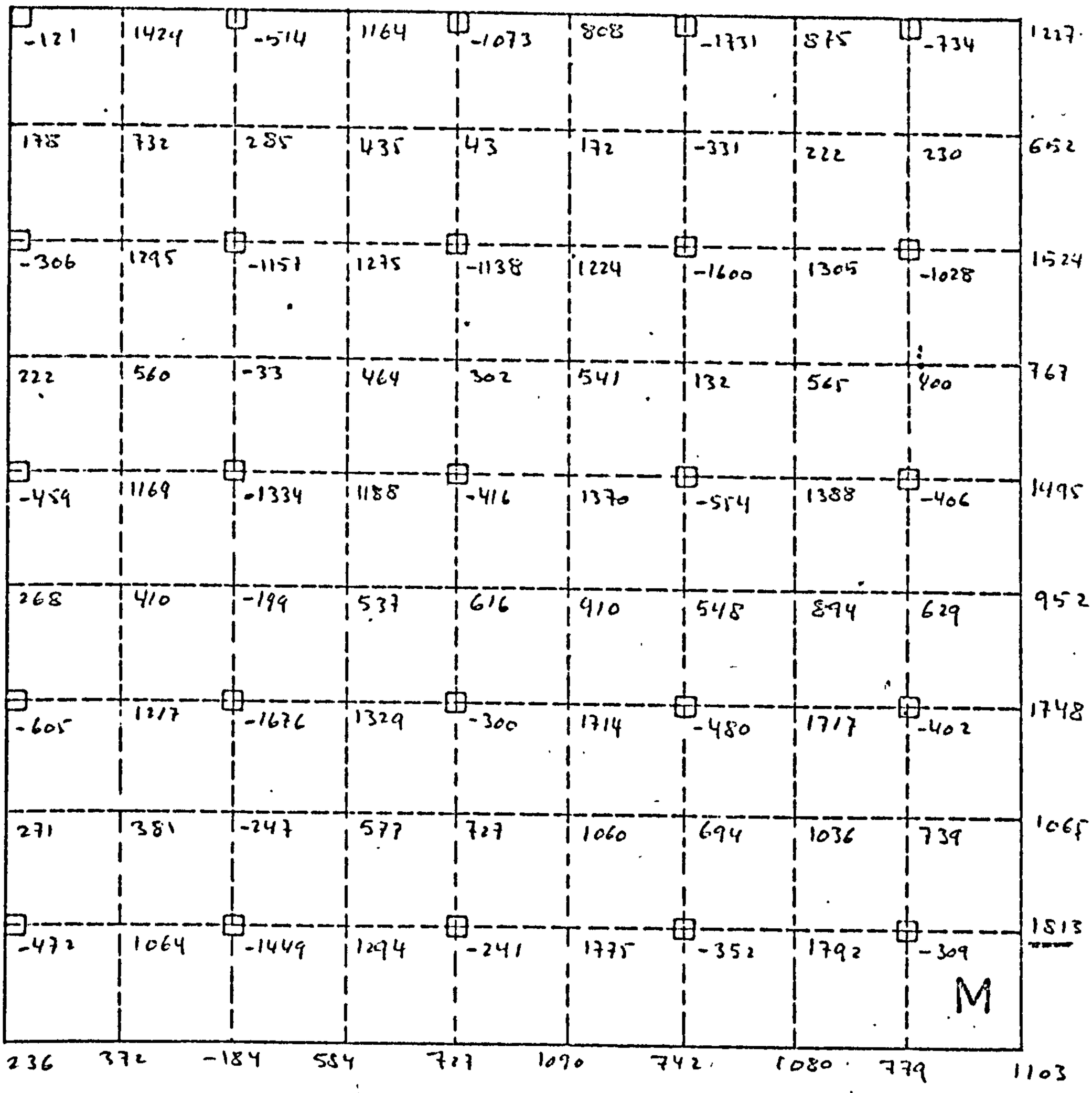

——— Finite Elements subdivisions

□ Joints

M Maximum Moment

Fig. 7.11 Moment Distribution in Concrete Slab for a quarter of DCON4

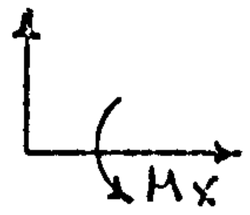

7	1600	-137	1270	-1182	954	-1192	900	-1241	880	-1252	876
153	869	491	510	24	312	-31	296	-53	287	-60	284
-242	1325	-967	1343	-1212	1366	-1289	1367	-1310	1372	-1320	1373
221	606	20	514	352	670	326	648	334	652	333	651
-508	1238	-1424	1263	-302	1499	-377	1474	-338	1474	-336	1472
268	412	-192	601	737	1059	708	1027	732	1042	732	1041
-555	1127	-1565	1370	-1391	1880	-293	1887	-250	1901	-252	1901
275	344	-247	666	911	1269	908	1249	947	1272	949	1271
-578	1102	-1600	1417	21	2025	-101	2049	-47	2070	-47	2071
278	326	-256	710	1009	1386	1037	1381	1085	1409	1089	1409
-586	1097	-1608	1448	85	2103	-21	2140	39	2165	37	2167
279	323	-256	725	1040	1423	1079	1425	1130	1454	1133	1455

M

——— F.E. sub division

□ Joints

: M Maximum moment

Fig. 7.12 Moment Distribution in Concrete Slab for a quarter of DCON5

CHAPTER 8

SOME ALTERNATIVE STRUCTURES

8.1 The Alternatives

In order to have a clearer picture of the structural characteristics of 'The Uniform Mesh' it is better to compare it with other possible alternatives.

These alternatives are

1. Double layer tubular rigid jointed structure which is basically of the same configuration as the uniform mesh is, but having a tubular top layer instead of a concrete slab.

2. As alternative 1 but with pin joints.

3. The 'IRM' composite structure as was described in para 7.2. The four spans cases for this type of structure will be termed

DCON2A, DCON3A, DCON4A and DCON5A

4. The uniform mesh structure but with pin jointed tubes.

Needless to say, that the cases to be compared have similar tubes, span and depth.

Each of the four alternatives will be dealt with briefly, the sole aim being to compare it later with 'The Uniform Mesh'.

8.2 Brief Study of the Alternatives

8.2.1 The Double Layer Grids (Alternatives 1 and 2)

Table 8.1 shows the selected axial forces and deflections in the four spans, namely 40, 60, 80 and 100 ft. respectively for alternatives 1 and 2.

Studying this table reveals

1. Both structures have almost similar behaviour and in fact the change in axial forces is negligible.

2. But there is more difference, although still small, in deflections. Alternative 2 has higher deflections which is understandable due to it being a pin jointed structure; hence of less rigidity.

3. It is further noticed that maximum and central tensile forces are of the same order, but the ratio between them increases with the increase of span.

4. There is a big difference between the maximum shear force and the corner one. The ratio between them increases with the increase of span. This shows that there are big differences in shear forces in the boundary area.

8.2.2 The 'IRM' Composite Structure

Table 8.2 shows the selected axial forces, deflections and stresses in concrete slab in the 'IRM' composite structure. It is seen from this table that

1. Shear distribution in boundary area is very good; as can be concluded from the ratio of maximum shear force/corner shear force.

2. Tensile force distribution is good too, but the ratio between the max. tensile force 'T' and the central tensile force 'P' increases with the increase of span.

3. Maximum in-plane stresses 'σ_{pm}' are much less than the maximum flexural stresses 'σ_{bm}'. But unlike the ratio 'T/p' in bottom layer the ratio $(\frac{\sigma_{bm}}{\sigma_{pm}})$ decreases with the increase of span.

It can be concluded from points 1 and 3 that this structure also tends to behave like a slab in larger spans, while it was dominated by shear action at span of 40 ft., with 4 bays only.

8.2.3 The Uniform Mesh but with Pin-jointed Tubes

Table 8.3 shows the selected deflections, axial forces and maximum stress in this structure.

It is seen from this table that both shear distribution and tensile force distribution are good, and also that the structure is dominated by shear action in very short spans and by slab action (bending action) in larger spans.

8.3 The Comparative Study

8.3.1 The dominance of axial stresses in tubes

It was found, that axial stresses are the dominant design factor in tubes in all the cases investigated. Tables 8.4a and 8.4b show examples from cases DCON4 and DCON4A which both have spans of 80 ft. to illustrate this fact.

This phenomenon is very useful and was cited in para 2.1 as being the main advantage of grid structures.

8.3.2 The Rigidity of Joints

It was found that rigidity of joints does not have overall appreciable effects on axial forces in tubes, or deflections or slab stresses.

But naturally it does have great effects on the bending stresses in tubes where it makes them the highest at the ends.

Table 8.1 which shows these forces and deflections in tubular double layer grids (alternatives 1 and 2), and Table 7.1 which shows the forces, deflections and slab stresses for the uniform mesh, and Table 8.3 which shows the forces, deflections and slab stresses for the uniform mesh but with pin jointed tubes support the above conclusions.

Therefore, it seems, that there is no significant structural advantages in having rigid joints.

8.3.3 The effects of using concrete slab

The effects could be summarized into the following:

1. Considerable structural rididity is achieved by using reinforced concrete slab instead of the top tubular grid. This is shown by a considerable reduction in deflections of up to 70% for a span of 100 ft. Table 8.5 shows the ratio of the various selected variables in the uniform mesh cases with their counterparts in Alternative 1 cases.

Fig. 8.1 shows graphically the ratios shown in Table 8.5 against the span/depth ratio.

2. It is seen from the above table and figure, that a reduction of 22% in maximum shearing force is achieved for a span of 100 ft.

3. The larger the span is, the more relative rigidity is achieved and the more reduction in forces too, in comparison with Alternative 1.

It is noticed that the corner shear force 'C_c' does not tally with this conclusion. In fact this does not effect the overall tendency but on the contrary shows the advantage of this new structure in having a more uniform shear force distribution.

8.3.4 The comparison with the IRM composite structure

Table 8.6 shows the ratios of the various selected variables in the uniform mesh as shown in Table 7.1 to their counterparts in the IRM composite structure (alternative 3) as shown in Table 8.2.

Two new variables have been introduced in Table 8.6. These were

a) The total length of all the tubes in the structure

in each case.

b) The total weighted length of all the tubes in the structure in each case. This is found as follows

If R_l is the ratio of the total length defined above for a uniform mesh case to that of the IRM composite structure case, and if R_c is the ratio of the maximum shearing forces of the same cases then

$$\text{weighted length ratio} = R_{wl} = R_l \times R_c$$

This is based on the assumption that the maximum shearing force is the deciding design factor in the two cases, and also on the fact that the maximum shear bearing members in both cases are of the same length, orientation and end support conditions, i.e. both have the same safe compressive strength.

This weighted length ratio (R_{wl}) is just a useful comparison indicator.

Fig. 8.2 shows graphically the ratios shown in Table 8.6. Studying Table 8.6 and Fig. 8.2, one may conclude the following:

1. Reduction in axial forces and deflections are achieved by the use of the Uniform Mesh. This tendency increases with the increase of span.

2. The in-plane stresses in concrete are almost the same in both structures. This is because they are mostly functions of the top layer slab cross-section and the external loading system, neither of which are changed.

3. Bending stresses in concrete have decreased showing the same tendency as other forces. This is

because bending moments in slab are a function of the external load and the vertical and rotational displacements of the joints.

4. A reduction of 45% in deflection is achieved in case DCON5 (span = 100 ft. with extra 2.6% expressed as weighted length. The prospect in this sense is even better for larger spans. This is because the ratio of length of steel tubes as shown in Table 8.6 will always be less than 2, while shear force ratio will continue to decrease with the increase of span.

TABLE 8.1

AXIAL FORCES AND DEFLECTIONS IN ALTERNATIVES 1 and 2.
(Double Layer Grids)

Case No.	Span ft.	Central bottom deflection ins.	Tension			Compression (shear)			
			Central force P lb.	Max. force T lb,	$\frac{T}{P}$	Corner forces C_c lb.	Maximum force C lb.	C/C_c	C/T
Alternative 1 - Double Layer Grid with rigid joints									
1	40	0.4095	14678	14951	1.02	-9820	-18326	1.87	1.22
2	60	1.8685	31239	34747	1.11	-10214	-35406	3.47	1.02
3	80	5.8306	56713	63869	1.13	-11475	-51235	4.46	0.8
4	100	14.2234	90255	101173	1.12	-12883	-77263	6.0	0.76
Alternative 2 - Double Layer Grid with pin joints									
1	40	0.4173	14951	15197	1.02	-9958	-18703	1.88	1.23
2	60	1.9024	31645	35253	1.11	-10298	-36033	3.50	1.02
3	80	5.9314	57426	64853	1.13	-11368	-52138	4.59	0.8
4	100	14.4613	91368	102658	1.12	-12557	-78631	6.26	0.76

TABLE 8.2

ALTERNATIVE 3 - DEFLECTIONS AND FORCES

(IRM Composite Structure)

Case No.	Span ft.	Central Top Deflection ins.	Axial Forces in Tubes							Max. stresses in Concrete		
			Tension			Compression (shear)						
			Central force P lb.	Max. force T lb.	T/P	Corner force C_c lb.	Max. force C lb.	C/C_c	C/T	Bending stress (σ_{bm}) psi	In-plane stress σ_{pm} psi	$\frac{\sigma_{bm}}{\sigma_{pm}}$
1	40	0.4006	21657	21653	1.0	-17576	-32235	1.83	1.49	367	- 57	6.44
2	60	1.1952	44429	50032	1.13	-31589	-31589	1.0	0.63	464	- 81	5.73
3	80	3.4026	80207	94271	1.18	-58402	-59006	1.01	0.63	600	-134	4.48
4	100	7.6725	123056	154989	1.26	-92314	-95760	1.04	0.62	767	-201	3.82

TABLE 8.3

ALTERNATIVE 4 - THE UNIFORM MESH BUT WITH PIN JOINTED TUBES

DEFLECTIONS, AXIAL FORCES, AND PLATE STRESSES FOR VARIOUS SPANS

Case No.	Span ft.	Central bottom deflection in.	Axial Forces in Tubes							Max. Stresses in Concrete		
			Tension			Compression (shear)						
			Central force P lb.	Max. force T lb.	T/P	Corner force C_c lb.	Max. force C lb.	C/C_c	C/T	Flexural stress (σ_{bm}) psi	In-plane stress (σ_{pm}) psi	$\frac{\sigma_{bm}}{\sigma_{pm}}$
1	40	0.2329	12578	13734	1.09	-14641	-25903	1.77	1.89	317	- 49	6.5
2	60	0.6749	21989	28379	1.29	-23134	-25913	1.12	0.91	367	- 68.3	5.4
3	80	1.9263	41276	51080	1.24	-41534	-49396	1.19	0.97	436.5	-124	3.5

TABLE 8.4

SHOWING THE MID-SECTION STRESSES IN THE SELECTED TUBES

FOR CASES DCON4 AND DCON4A WITH 80 FT. SPAN EACH

Stresses in p s i

No.	Type of Member or axial force	D CON 4						D CON 4A					
		Axial stress in psi	Shear stress Y	Shear stress Z	σ_{bx}	σ_{by}	σ_{bz}	Axial Stress	Shear stresses		Bending stresses		
									Y	Z	σ_{bx}	σ_{by}	σ_{bz}
1	Central	17,183	~0.0	- 2.22	0.0	1144	0.0	-33,558	~ 0.0	~ 0.0	~ 0	2053	0
2	Max. tensile	21,270	-16.6	- 1.87	-19.9	1548	-21.4	-39,440	~ 0.0	~ 0.0	~ 0.0	2791	16.7
3	Corner bar	16,808	20.38	40.5	132.2	-449.7	405.7	24,436	36.5	43.5	199.2	-1075.7	587.2
4	Max. Compression	20,315	-16.54	-80.4	-44.8	44.3	-88.9	24,689	-32	-75	-132.5	- 435	-369

N.B. Tubes location are identical in both cases

TABLE 8.5

RATIOS OF DEFLECTION AND TUBE'S FORCES BETWEEN THE UNIFORM MESH AND THE DOUBLE LAYER GRID (ALTERNATIVE 1) CASES

Nos.	Case	Ratios of				
		Deflection	Tension Members		Compression shear member	
			Central	Max.	Corner	Max.
1	D CON 2	0.5624	0.848	0.9098	1.462	1.386
2	D CON 3	0.3586	0.6997	0.812	2.24	0.7184
3	D CON 4	0.3297	0.7241	0.796	3.50	0.948
4	D CON 5	0.2965	0.6872	0.814	4.7	0.784

TABLE 8.6

SHOWING RATIOS OF DEFLECTION AND MAXIMUM FORCES AND TOTAL LENGTH OF TUBES USED BETWEEN THE UNIFORM MESH CASES AND THE 'IRM' COMPOSITE CASES

Span ft.	Span / Depth	Total length of tubes (ft.)		The Ratios						
					Tubes				Concrete	
		Uniform Mesh	'IRM' composite	Central Deflection	Total length Rl	Max. Tension	Max. Compression	Weighted length Rwl	Max. Bending Stress	Max. in-plane stress
40	9.66	361	255	0.688	1.416	0.63	0.79	1.116	0.895	1.103
60	14.5	702	503	0.604	1.394	0.56	0.81	1.122	0.791	0.839
80	19.3	1116	720	0.584	1.55	0.54	0.82	1.276	0.740	0.927
100	24	1763	1086	0.549	1.624	0.53	0.63	1.026	0.683	0.955

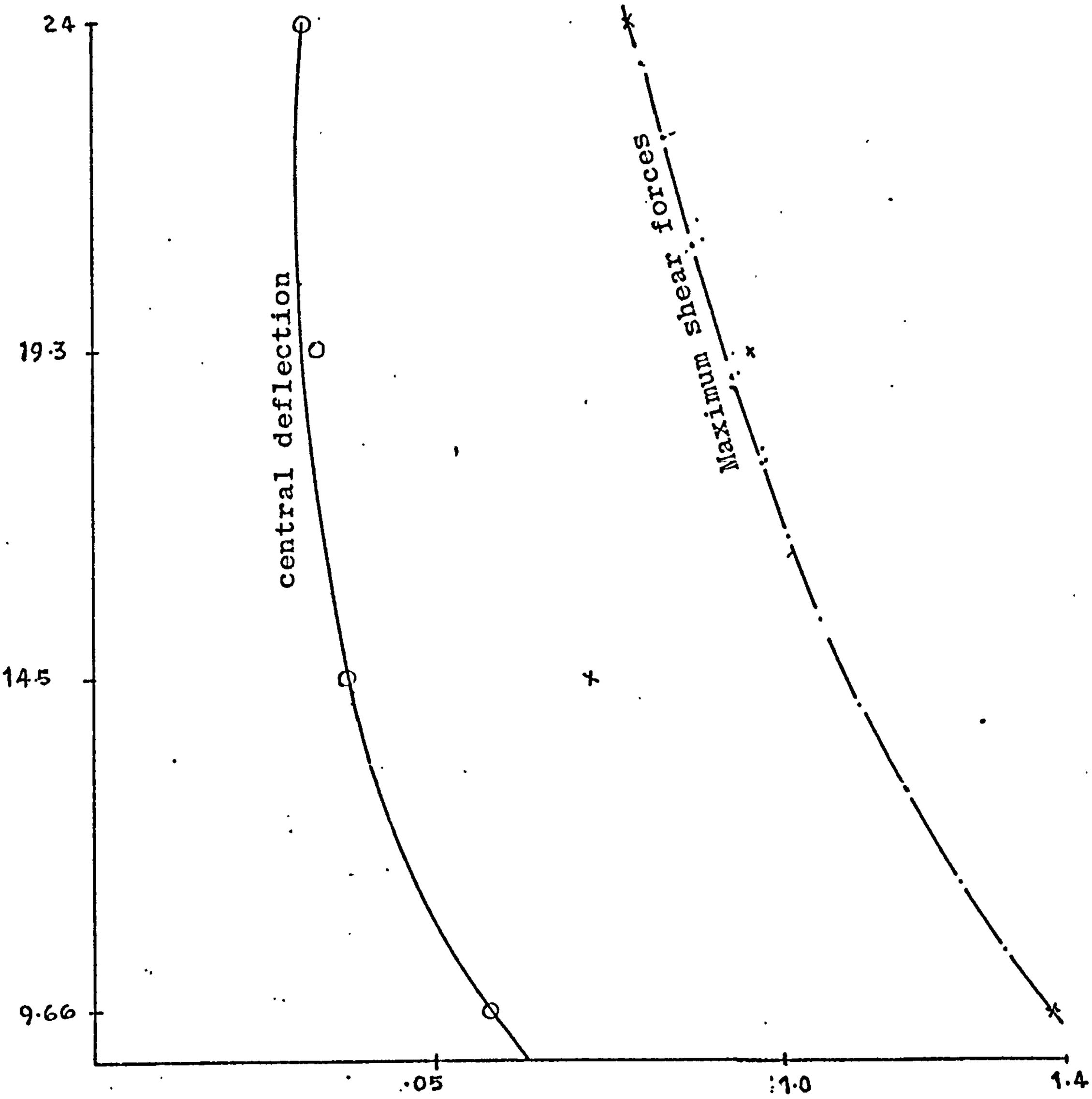

Fig. 8.1 The ratio between deflection and maximum shear force of Uniform Mesh structure and Tubular Double Layer grid structure.
(See Table 8.5)

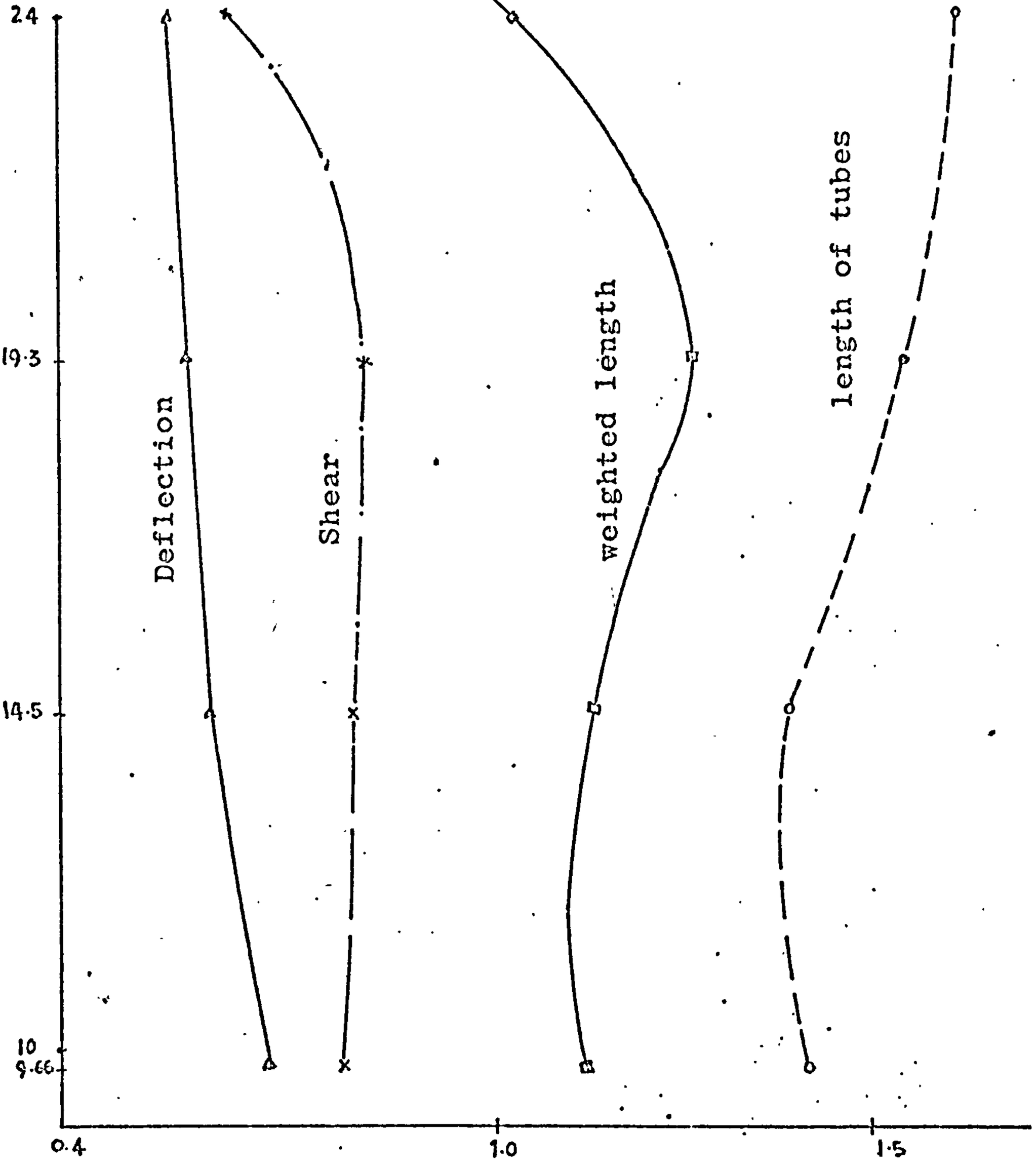

Fig. 8.2 Ratios of deflection, shear and length of tubes between the Uniform Mesh and the IRM composite structure (See Table 8.6)

→ (see ERRATA)

PAGE NUMBERING AS ORIGINAL

CHAPTER 9

THE SLAB BEHAVIOUR AND THE DETERMINATION OF SECTION PROPERTIES

9.1 The Slab Behaviour

It was mentioned in the Literature Review para 2.2 that plate analogy has been used extensively in the literature of flat grid structures. It was also mentioned that this analogy has difficulties in boundary area.

Therefore, it is only natural to expect that plate analogy will hold even more here because it is nearer to a continuum than prismatic double layer grid is.

Therefore the following is presented to explain and help in predicting the behaviour of the Composite Double layer grids.

The Composite Double Layer Grid tends to behave like a thin slab, i.e. the load is carried mostly by bending action, but when it is very rigid, then the load is carried mostly by combination of shear and direct compressive forces. Therefore slab analogy does not hold in the boundary area because of its high rigidity. Furthermore, because of the high rigidity of the boundary area, the maximum tensile force in the bottom layer is not in the centre, as is the case for a homogeneous simply supported square slab under uniformly distributed loading, but is always near the boundary area and stays there despite the increase of the span as it was found in para 7.2.

Thus it is expected that shear forces will be dominant in short spans while in larger spans, tensile

forces in the bottom layer tubes will be predominant.

Fig. 9.1a shows a sketch representing an isolated section through the composite structure, from which it is suggested that the external moment is counterbalanced by a couple of lever-arm (h), where (h) is the centre-to-centre distance between the top and bottom layers. The couple is made out of an in-plane top compressive force (C), and a bottom tensile force (T), so

$$C = T \qquad \ldots\ldots 9.1$$

and $$M = T \times h \qquad \ldots\ldots 9.2$$

hence $$T = C = \frac{M}{h}$$

or

$$\left.\begin{matrix} T \\ C \end{matrix}\right\} \propto \frac{1}{h} \qquad \ldots\ldots 9.3$$

so any increase in (h) means a decrease in both T and C.

The bending moment in the top slab has no such clear linear relationship with the depth of the structure or the external moment, because it is in fact produced by more complex factors such as

a) The superimposed load which has both local and general effects.

b) The vertical and rotational displacements of its common joints with the diagonal shear members.

c) Continuity effects.

This analogy is valid as long as the slab behaviour dominates, and the extent of this validity depends on the extent of this dominance. Therefore it is not expected to hold for short spans or for boundary areas but mainly in large spans and for central areas.

9.2 Relation between top slab thickness and stress distribution

When the composite structure behaves like a slab, then one may assume that for a section in such structure, the total contraction of the top fibres is equal to the total extension of the bottom fibres (Fig.9.1b). Hence there will be a neutral plane somewhere in the section where there will be no change in length. This location is the same location as the centre of gravity of the section, and all fibres above the neutral plane will experience compression, while those below it will experience tension.

It is clear from the above that the location of the neutral plane has no relation to the span of the structure but depends entirely on the nature of the cross-section.

Therefore an increase in the top slab thickness means raising to centre of gravity of the section towards the top layer and consequently the redistribution of the force system in the section.

Hence for any cross section, the top layer slab will have a certain depth beyond which part of it will experience tension, but since concrete is not efficient in tension, therefore it is better to have all the concrete parts of the structure under compression.

This conclusion is very important because of its expected savings in the weight of concrete and consequently on the total weight of the structure.

Of course, the same reasoning is valid with the steel tubes, which shoud not be of such a small area or a moment of inertia so as to let the centre of gravity of the section pass through the concrete layer.

9.3 Choosing an Efficient Cross-section

The following method is suggested to get an efficient cross-section.

Following the same reasoning as para 9.2, and assuming that the structure is under plate bending dominance, then it is possible to treat an isolated section of such structure as a beam section. It could be assumed that the cross-section remains plane during bending, irrespective of whether the section is made of one material or not, therefore, the strain variation is linear from top to bottom.

The location of the neutral axis is not known at first, except when the cross-section has double symmetry, then the neutral axis will be at the middle height of the section.

From the theory of pure bending of beams, the normal stress σ_x at any distance 'y' from the neutral axis is given by[25]

$$E = \frac{\sigma}{\epsilon}, \quad \sigma = E \times \epsilon = E \times k \times y \qquad \ldots\ 9.4$$

$$\therefore \quad \sigma_{xc} = k \times E_c \times y, \quad \sigma_{xs} = k \times E_s \times y \qquad \ldots\ 9.5$$

where K is the curvature of the section when under bending, E_c, σ_{xc}, E_s and σ_{xs} are modulus of elasticity and stress for concrete and steel tubes respectively.

But since the resultant axial force acting on the section is zero, therefore

$$P_c + P_s = 0 \qquad \ldots\ 9.6$$

where P_c and P_s are total concrete and steel forces respectively. Let dA denote an element of area in the cross section at a distance 'y' from the neutral axis, therefore:

$$\int \sigma_{xc}\, dA_c + \int \sigma_{xs}\, dA_s = 0$$

and from 9.5

$$kE_c \int_c y_c dA_c + kE_s \int_s y_s dA_s = 0 \qquad \ldots\ldots 9.7a$$

and

$$E_c \int_c y_c dA_c + E_s \int_c y_s dA_s = 0 \qquad \ldots\ldots 9.7b$$

where y_c and y_s are the distances of dA_c and dA_s from the neutral axis respectively.

The bending moment in the section is defined as

$$M = \int \sigma_x \times y \times dA$$

$$\therefore \quad M = \int_c \sigma_{xc} \times y_c \times dA_c + \int_s \sigma_{xs} \times y_s \times dA_s$$

and from 9.5

$$M = k E_c \int_c y^2 \times dA + k E_s \int_s y^2 \times dA$$

$$= k(E_c I_c + E_s I_s) \qquad \ldots\ldots 9.8$$

$$\text{and} \quad k = \frac{M}{E_c \times I_c + E_s \times I_s} \qquad \ldots\ldots 9.9$$

where I_c and I_s are moments of inertia of concrete and steel sections about the neutral axis respectively. The moment of inertia of the entire equivalent cross-sectional

area is I where

$$I = I_c + I_s \qquad \ldots\ 9.10$$

Using equations 9.5 and 9.9 will give the stresses in the composite section as functions of the bending moment M. Hence,

$$\sigma_{xc} = k E_c y_c = \frac{M \times E_c \times y_c}{E_c x I_c + E_s x I_s} \qquad \ldots\ 9.11a$$

$$\sigma_{xs} = k E_s y_s = \frac{M \times E_s \times y_s}{E_c x I_c + E_s x I_s} \qquad \ldots\ 9.11b$$

But since $y_c = C$ and $y_s = C_1$ according to Fig. 9.2 then,

$$\sigma_{xc} = \frac{M \times C}{IE/E_c}, \quad \sigma_{xs} = \frac{M \times C_1}{IE/E_s} \qquad \ldots\ 9.12$$

where $IE = E_c \times I_c + E_s \times I_s$

The second stage is to find the neutral axis. This will be found from Eq. 9.7b as follows

$$-E_c \times C \times A_c + E_s \times C_1 \times A_s = 0$$

$$-E_c \times C \times b \times t + E_s (h-c) A_s = 0$$

where b is the width of the concrete slab in the section

$$C = \frac{E_s \times A_s}{E_c \times b \times t + E_s \times A_s} \times h$$

or

$$C = \frac{h}{1 + \frac{E_c \times b \times t}{E_s \times A_s}} \qquad \ldots\ 9.13$$

$$\text{Let} \quad m_1 = \frac{E_c \times b \times t}{E_s \times A_s} \qquad \ldots\ 9.14$$

$$\therefore \quad c = \frac{h}{1 + m_1} \qquad \ldots\ 9.15$$

Using parallel axis theorems,[23] then

$$I_c = I_{co} + A_c \times c^2 \qquad \ldots\ 9.16$$

where I_c is the moment of inertia of the concrete slab around the section neutral axis, and I_{c_o} is the moment of inertia of the concrete section around its centre line.

$$\therefore \quad I_c = \frac{bt^3}{12} + b \times t \times c^2 \qquad \ldots\ 9.17$$

$$I_s = I_{s_o} + A_s \times c_1^2$$

From Eq. 9.15 it is possible to choose the desired section. Ideally, the most effective section is when the neutral axis is exactly in the middle height of the section, which is an I-beam or identical top and bottom layers. Also, it is ideal if permissible stresses are achieved simultaneously in both top and bottom layers.

But for the cases considered in this research it is not practical or efficient to get $c = h/2$ because the section will be very heavy due to the use of a very large steel area. In the same time if a thick concrete slab where used and a very small steel area, then there is a possibility that the neutral axis will lie through the concrete layer, which is not advisable either. This is because concrete tensile strength is negligible, therefore the concrete area below the neutral axis is not only

useless, but also unnecessary dead weight.

Hence, the following procedure will just give the section where the neutral axis will lie at the bottom fibres of the concrete slab, i.e. $c = {}^{t}/_{2}$, and this will be considered as a minimum requirement to get an efficient use of the concrete. Obviously, the choice of the exact value of c will depend afterwards on economical, architectural consideration besides the permissible stresses for steel and concrete.

So from Eq. 9.15

$$c = {}^{t}/2 = \frac{h}{1 + m_1}$$

and $$1 + m_1 = \frac{2h}{t}$$

$$\therefore m_1 = \frac{2h}{t} - 1 = \frac{2h - t}{t}$$, but according to Eq. 9.14

$$m_1 = \frac{E_c \times b \times t}{E_s \times A_s}$$

$$\therefore A_s = \frac{E_c}{E_s} \times \frac{bt^2}{(2h - t)} \quad \ldots 9.19$$

Formula 9.19 is a good guide for getting an efficient use of concrete.

It is therefore shown that stress distribution really depends on the cross-section only and its constituents. It is also noticed that the contribution from the shear members in this case is limited to providing the depth, which is naturally a very important factor in the moment of inertia, not forgetting, their basic function in transferring the shear.

The thickness of the concrete slab (t) can be found

from Eq. 9.19 in terms of steel area (A_s).

Assume $n = \frac{E_c \times b}{E_s}$, then Eq. 9.19 becomes

$$A_s = \frac{nt^2}{2h - t}$$

$$2A_s \times h - t \times A_s = nt^2$$

and

$$nt^2 + A_s \times t - 2A_s h = 0 \qquad \ldots. 9.20$$

The solution of this quadratic equation gives the thickness as

$$t = \frac{-A_s \pm \sqrt{A_s^2 + 8n \times A_s \times h}}{2n} \qquad \ldots. 9.21$$

Equations 9.12, 9.15 and 9.21 will be used later in the approximate analyses to be presented in chapter 11.

Eq. 9.19 could be used to show roughly the way in which the bottom layer steel area, and the top concrete layer thickness are related to each other. Eq. 9.19 could be expressed as

$$A_s \propto \frac{t^2}{2h - t}$$

This is because E_s, E_c and b are constants. By assuming 't' to be negligible in comparison to 2h, which it is expected to be in practice, then

$$t \propto \sqrt{2h \times A_s} \quad \text{or} \quad t \propto \sqrt{A_s} \qquad \ldots. 9.22$$

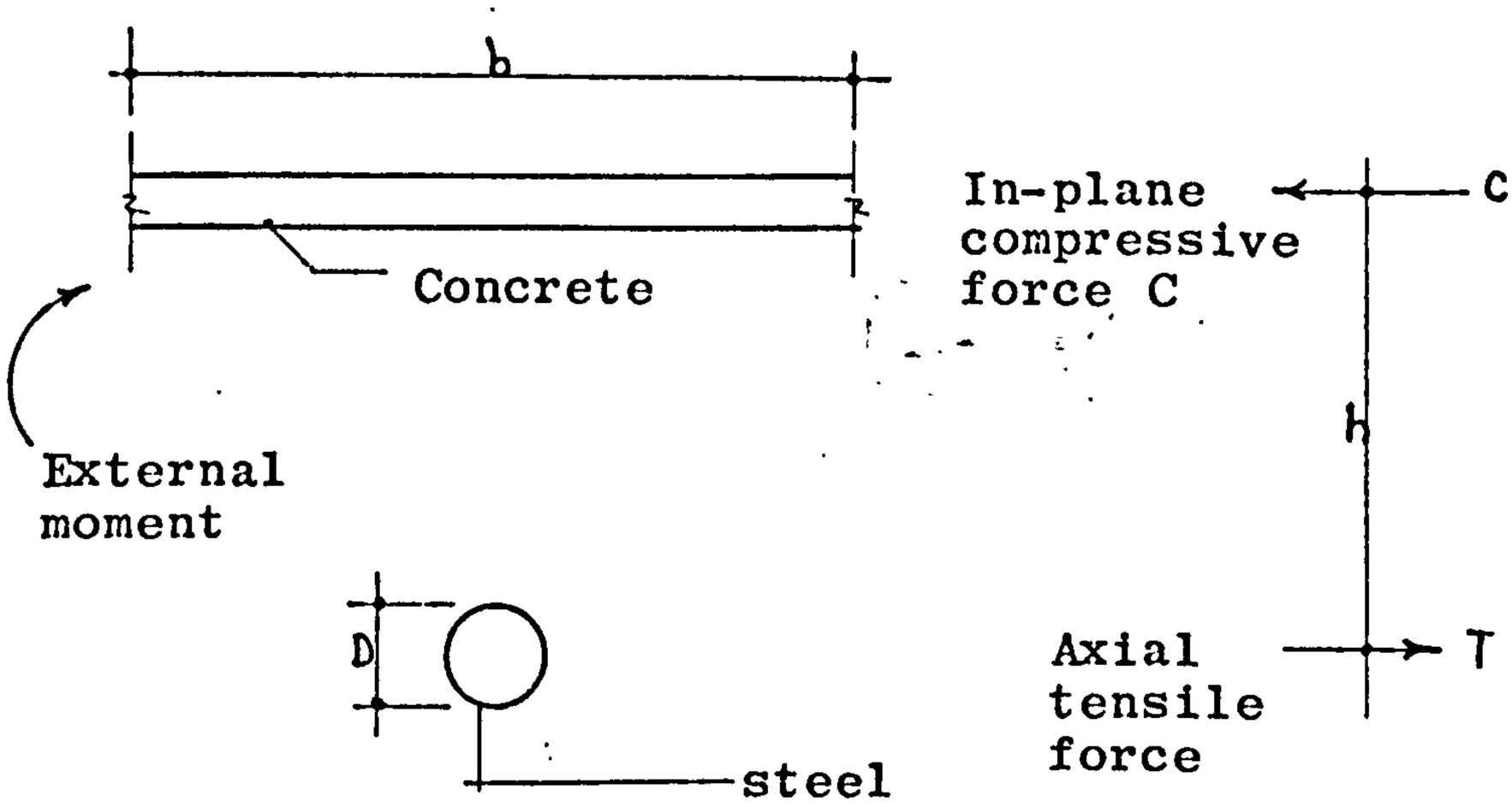

Fig. 9.1a

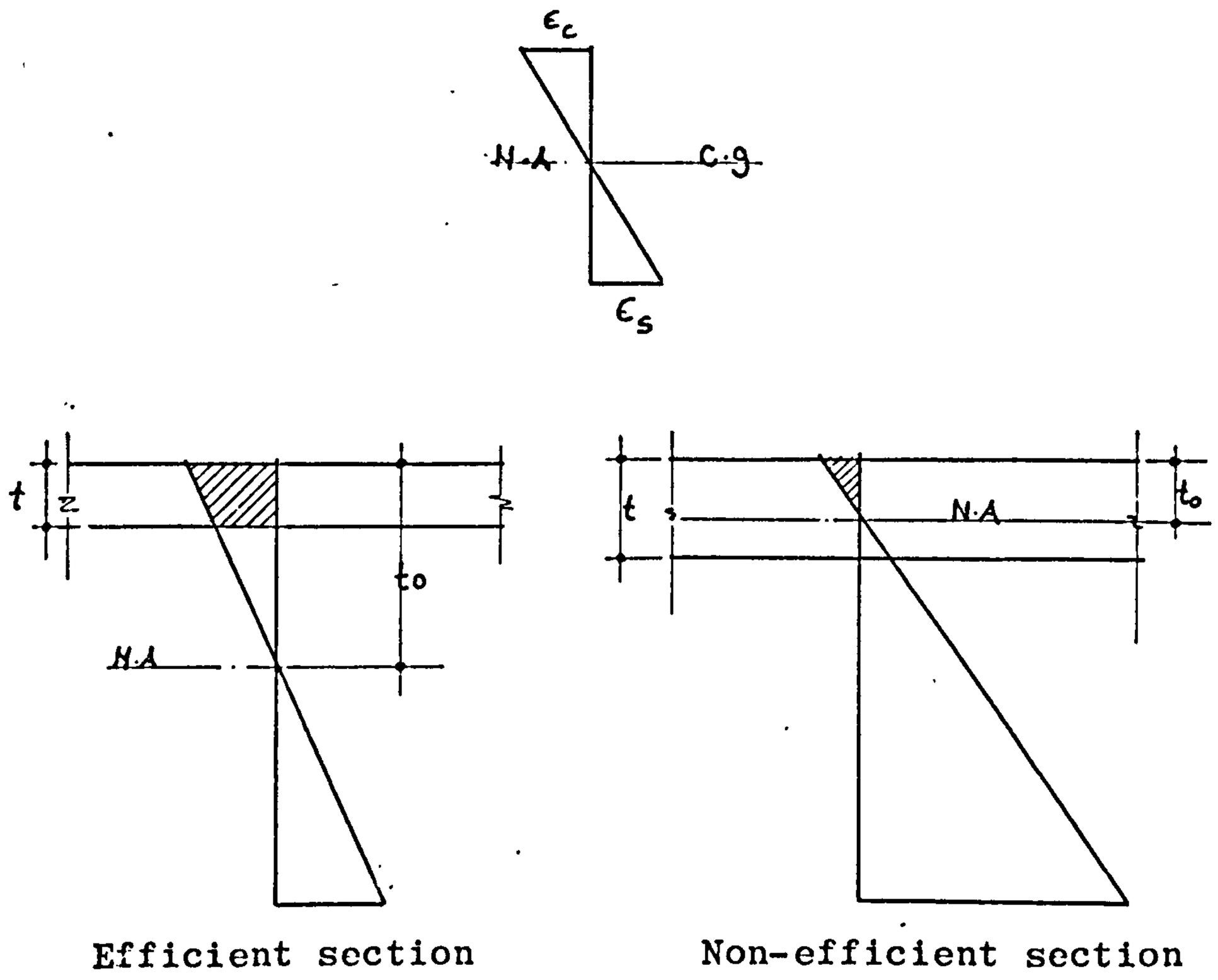

Fig. 9.1b

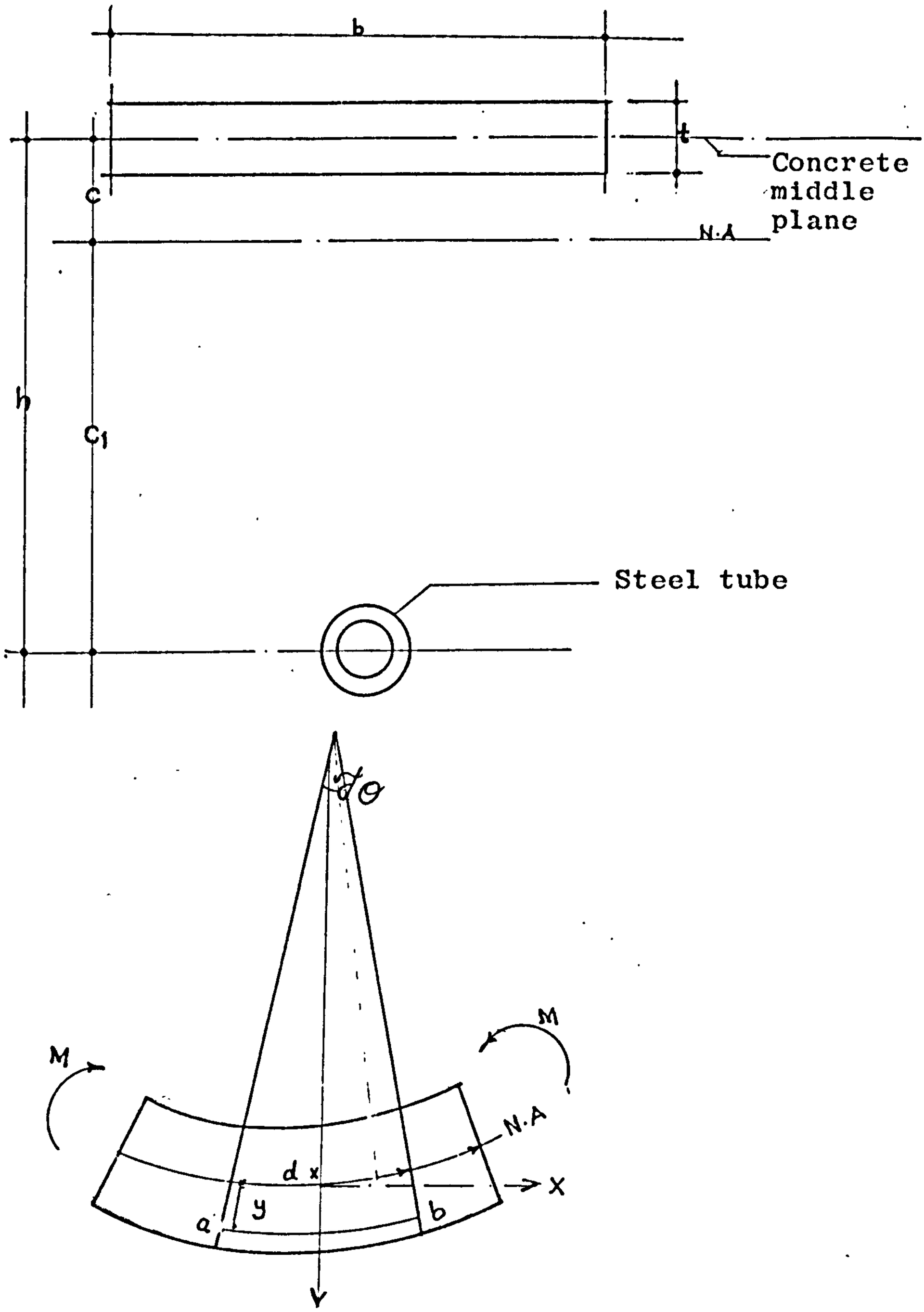

Fig. 9.2 An idealized composite beam section

CHAPTER 10

PARAMETER STUDIES

10.1 Parameters to be Studied

The parameters to be studied are defined in Fig. (7.2) and (7.4b). The four previous basic cases described in para 7.4.1 were used as a basis for parameter studies. The parameters are:

1. Span of the structure: cases DCON2, DCON3, DCON4 and DCON5 were used to study the variation of span parameter since they spanned 40 ft., 60 ft., 80 ft., and 100 ft. respectively.

DCON5 was not used any more in the other parameter studies because of its huge computer requirements.

2. Structural depth seven different depth were used

a) 30 in. The relevent cases will be called DCON2S, DCON3S and DCON4S.

b) 36.22 in. The relevant cases will be called DCON2S1, DCON3S1 and DCON4S1.

c) 42.43 in. These are the basic cases DCON2, DCON3 and DCON4.

d) 48.65 The relevant cases will be called DCON2D, DCON3D and DCON4D.

e) 54.86 in. The relevant cases will be called DCON2D1, DCON3D1 and DCON4D1

f) 84.86 The relevant cases will be called DCON2D2, DCON3D2 and DCON4D2.

This depth was chosen because, diagonal shear members make an angle of 45^{o} with the plane of the bottom tubular layer.

g) 120 in. The relevant cases will be called DCON2D3, DCON3D3 and DCON4D3.

3. <u>The concrete slab thickness (t)</u>:-

Five different thicknesses were used.

a) 2.5 in. The cases will be called DCON20, DCON30 and DCON40.

b) 5 in. which are the basic cases DCON2, DCON3 and DCON4.

c) 7.5 in. The relevant cases will be called DCON21, DCON31 and DCON41.

d) 10 in. The cases will be called DCON22, DCON32 and DCON42.

e) 12.5 in. The cases will be called DCON23, DCON33 and DCON43.

4. <u>The thickness of wall tubes</u>

The study was limited to DCON3 only, because this parameter is easier to foresee than others. The thicknesses are

a) t_t = 0.176, D = $4\frac{1}{2}$ in., which is the basic case of DCON3.

b) t_t = 0.212 in., D = $4\frac{1}{2}$ in., the case will be called DCON3M1.

c) t_t = 0.252 in., D = $4\frac{1}{2}$ in., the case will be called DCON3M2.

5. The outside diameter of tubes (D)

The study of this parameter was limited to case DCON3 also, like the wall thickness parameter and for the same reason. The wall thickness was kept constant, these diameters were

a) D = $4\frac{1}{2}$ in., G = 7 which is the basic case of DCON3.

b) D = $5\frac{1}{2}$ in., G = 7 and will be called case DCON3M3.

c) D = $6\frac{5}{8}$ in., G = 7 and will be called case DCON3M4.

10.2 Some Definitions

1. A factor 'R' will be used in tables and figures to indicate the variation of forces, stresses and deflections with various parameters. 'R' is defined as:

$$R = \frac{\text{Value of a variable at case x}}{\text{Value of the same variable at case 1}} \quad \ldots\ldots 10.1$$

In this way absolute values for the variables are obtained which make it possible to plot any combination of them using the same scale.

2. A factor of safety against over stressing will be used as a parameter. If the safe compressive force for the diagonal shear members is C_s, and C as defined before, is the maximum compressive (shear) force in the shear members, then the factor of safety here is defined as

$$F_s = \frac{C_s}{C} \quad \ldots\ldots 10.2$$

The safe compressive force (load) is found from the manufacturer's catalogue.[20] The effective length is assumed to be 0.85ℓ, where ℓ is the shear member length. This is because the shear member is effectively held in position at both ends and partially restrained in direction at both ends.

10.2.1 The Span/Depth Ratio (SDR)

A span is defined here as the shortest distance between the centres of two corner joints along one side of the bottom layer, as was shown in Fig. 7.2.

Fig. 7.4b showed a section through the structure.

It is clear that a formula has to be found to give a better expression for the span/depth ratio, because the cross-section is not a homogeneous solid slab. Therefore, to define the depth of the structure as the distance between the centre of concrete slab and the centre of steel tube is not enough because it does not take into consideration the variation of slab thickness or tube cross-section properties.

Hence, the formula below is devised to define the depth as

$$d = h + t + \frac{D}{2} \qquad \ldots. \text{ 10.3}$$

where d is the depth used in expressing the span/depth ratio (SDR) only.

h is the centre to centre distance between concrete slab layer and the bottom tubes layer.

'h' is really the z-component of the diagonal shear member length as given to the computer.

t is the thickness of the concrete slab layer, and D is the outside diameter of bottom layer tubes.

t was taken instead of $t/2$ in order to give more weight to the flexural rigidity of the slab. In effect it is assumed that tubes' centre lines meet the slab at the bottom fibres and not at the middle plane, and hence 'd' is accordingly the distance between the top fibres in the slab and the bottom fibres in the tubes, and not the centre to centre distance.

This formula was tested and found to give better correlation with force variations, than the standard

definition, in the parameter studies to be presented in Chapter 10, when there is one span but with variable section properties. But when the span varies while the section is constant, then both definitions have the same correlation with the forces.

The span over depth ratio is defined as

$$SDR = \frac{\text{span of the structure}}{\text{the depth}} = \frac{S}{d} \qquad \ldots\ldots 10.4$$

while the standard span over depth ratio will be termed

$$SHR = \frac{S}{h} \qquad \ldots\ldots 10.5$$

In order to distinguish clearly between 'd' and 'h', 'd' will be termed 'effective depth' while 'h' will be termed the 'structural depth'.

Few examples for cases with 80 ft. span only are to be given here to show that the 'effective depth' gives a better correlation with the forces than the 'structural depth' does.

Figs. 10.1 and 10.2 show clearly that maximum tensile and shear forces vary more smoothly with 'SDR' than with 'SHR' due to the change of the 'structure depth' only.

Fig. 10.3 shows the smooth variation of maximum tensile and shear forces with 'SDR' due to the change in slab thickness only, which is impossible to show in the case of 'SHR', because 'SHR' will be constant in these cases.

10.3 Variation in Span

Table 7.1 has already shown the effect of changing the span of the structure on the various forces, deflections, and stresses in the structure.

Table 10.1 shows these effects but expressed by the factor 'R' as defined in para. 10.2.

Fig. 10.4 shows these effects against the span/depth ratio 'SDR'. It is shown in this figure that all forces and stresses vary almost linearly after case DCON3 which has a span of 60 ft, (SDR = 14.5), while there is no significant difference in them between case DCON2 (span 40 ft) and case DCON3, except for the maximum tensile force 'T'.

It is seen from Fig. 10.5 which shows the rate of change of these forces 'R' with the square of the spans ($span^2$); that both the maximum tensile force 'T' and the maximum in-plane stress 'σ_{pm}' vary linearly with ($span^2$). This can be expressed as

$$M = \alpha\, q a^2 \qquad \ldots\ 10.6$$

as defined by Timoshenko[11] where M is the moment in homogeneous slab, q is the intensity of the load, a is the span of the slab, and α is a coefficient depending on the shape and the boundary conditions of the slab.

Fig. 10.6 shows the variation of the deflections with 'SDR', while Fig. 10.7 shows that the deflections vary linearly with the ($span^4$) which can be expressed as

$$w = \beta\, q\, a^4 \qquad \ldots\ 10.7$$

as defined also by Timoshenko,[11] where w is the deflection of a homogeneous slab, and q and a are as defined before, while β is a coefficient which depends on the shape and boundary conditions of the slab.

Therefore, it is clearly shown that composite double layer grids tend to behave like a slab especially in large spans as was anticipated in para 9.1.

Table 10.2 shows that the in-plane compressive forces become greater than the axial tensile forces in larger spans. This is probably due to the increase of curvature, and hence to the increase in moments in the concrete slab. Therefore, despite the fact that the in-plane and flexural stresses are uncoupled yet due to the presence of the tubes, then they will be affected by each other.

10.4 Variation in the Depth of the Structure

Tables (10.3, 10.4 and 10.5) show values of the forces and stresses in the crucial members and locations as outlined in para 7.3, at various depths together with their relative values 'R' for spans of 40, 60 and 80 ft. respectively. Table 10.6 shows comparison of in-plane and axial tensile forces.

Figs. (10.8, 10.9 and 10.10) show graphically the 'R' values for these forces and stresses against the 'R' values for 'SDR'.

Studying those tables and figures leads to the following remarks and conclusions.

1. Central tension 'P', maximum tension 'T', central plane stress 'σ_p' and maximum plane stress 'σ_{pm}' have a linear relationship with 'SDR', and in fact, their variations and that of 'SDR' are almost the same. All these forces and stresses decrease with the increase of the depth.

2. Maximum compressive forces have almost the same linear relationship with 'SDR' for the short span of 40 ft., but tends to divert from that in extreme deep conditions for larger spans, presumably due to higher rigidity.

3. Maximum bending moments does not have such linear relationship in the 40 ft. span, but tends to do so for larger spans.

4. It is noticed from table 10.6, that there is an almost exact equilibrium between the central in-plane and axial tensile forces in the 60 ft. span cases, and

tends to be so also for deeper cases of span 80 ft., and far from equilibrium in the 40 ft. span cases. This is because the 40 ft. span cases are very rigid, therefore slab analogy does not hold, while the shallow 80 ft. span cases have higher stress intensity, therefore the assumption of uniform stress distribution over the width of the section is not so valid.

5. The absolute values of neither 'SDR' nor 'SHR' as seen in the above tables are viable scales of stress conditions, in other words, an equal value of 'SDR' or 'SHR' for two different spans does not mean that the two structures under the same strain conditions qualitatively or quantitatively.

6. A corollary to that mentioned in point '1' above, is the possibility that analysis of a structure of a certain span will be enough to predict the stress conditions for the same span but with different depths. This is because

$$R = \frac{SDR}{SDR_o} = \frac{P}{P_o}$$

and $$P = R \times P_o$$

where P is a general force to be predicted for a case with span/depth ratio of 'SDR' while 'SDR_o' and P_o are the known values.

7. Fig. 10.11 shows that the rate of change of the central forces in the three spans investigated are really similar and vary linearly with 'SDR'.

10.5 Variation in the concrete slab thickness

Tables (10.7, 10.8 and 10.9) show the effects of changing slab thickness according to para 10.1 on various forces and stresses in the crucial members and locations as outlined in para 7.3, together with their relative values 'R' for the usual spans of 40, 60 and 80 ft. respectively. Table 10.10 shows the ratios of plane stress forces to the orthogonal axial forces at the centre.

It is of interest to mention that according to para. 9.3, for a section with depth (h) of 42.43 in., which is the height of all the cases to be studied in this paragraph, 5 inch is the maximum thickness for an efficient cross-section, beyond which part of the concrete will be under tension.

Studying the above tables together with their accompanying Figs. Nos. (10.12, 10.13, 10.14, 10.15, 10.16 and 10.17) leads to the following observations.

1. In regard to axial forces in the tubes

a) These forces decrease with the increase in thickness. Figs. 10.12 and 10.13 show the almost linear nature of the variation after a thickness of 7.5 inches, for the three spans and for both central and maximum shear force, and also the change in forces is very small between thicknesses of 2.5 in. and 5 in. These observations support that 5 inches is a critical thickness.

b) The rate of change of shear force is not high despite the fact that the thickness has been increased

fivefold. Knowing that shear force is really the critical factor in the design supports the need for using a thin practical slab.

2. In regard to the in-plane stress in the slab, it decreases substantially with the increase in thickness, but the rate of decrease of the in-plane force is of the same order to that of the axial force in the bottom layer tubes.

Table 10.10 shows that the ratio of $\frac{P_c}{P_x}$ (in-plane force/axial orthogonal force) is near unity in most cases and tends to be more than 1 in thin concrete slab cases of spans 60 and 80 ft. while those with span 40 ft. tend to be less than unity.

All the above observations can be clearly explained by the slab behaviour tendency as outlined in para. 9.1, and also as just explained in para. 10.5.

When increasing the slab thickness, the centre of gravity of the section moves upward towards the concrete hence the concrete slab will be taking more and more bending moments because of the increase in its rigidity For the same reason, the plane stress will be less, as well as the axial stress in the tubes.

4. The maximum negative moments show less tendency to increase with the increase in thickness as is seen in Fig. 10.17. This is because its location is always directly over the boundary supports. Therefore the variation of the thickness does not make a substantial difference, unlike the case in areas far from the supports.

10.6 Variation of the Thickness of Wall Tubes

Table 10.11 shows three cases of different wall thickness as outlined in para 10.1, which shows that both axial forces and in-plane stresses have changed with the increase of the steel area, while bending moments have decreased. This is explained because of the movement of the centre of gravity of the section towards the lower area hence the steel will take more stresses and the total in-plane stress in the slab will increase accordingly, while the slab will experience less flexural stresses.

10.7 Variation in the Outside Diameter of Tubes (D)

Table 10.12 shows three cases having tubes with different outside diameters as outlined in para 10.1.

As expected from para. 9.1, the increase in tube outside diameter meant a lowering of the centre of gravity of the section hence increasing the tensile forces in the bottom layer and also an increase in the in-plane forces in the concrete layer of almost equal rate to that of the increase in depth. At the same time there was a decrease in shearing forces at a rate equal to that of the SDR accompanied by a decrease in the flexural stresses in the slab.

10.8 An Investigation into an Economical Depth

To study the best economical depth, it is important to study among other factors, the relation between depth and maximum compressive force in the shear members, the safe compressive load, and the total amount of steel used in the structure in each case.

Table 10.13 shows the factor of safety (against overstressing) for each case, together with the total length of steel tubes.

Fig. 10.18 shows curves of factor of safety together with total length of tubes used plotted against the structural depth of the structure (h). It is clear from this figure that a depth of 84.85 in. is the best depth.

This is because, the amount of steel increases slowly and almost linearly with the increase of the depth. For a depth of 84.85 the amount of increase in steel is 18% in the three different depths, while the factor of safety increases sharply with the increase of depth up to 84.85 in. depth where it acquires an increase of about 80% for the three cases, then it starts to decrease.

This result in fact did not come as a surprise, since a depth of 84.85 in. in this particular section means that the shear diagonal members make an angle of 45^{o} with the bottom horizontal plane, which is an ideal orientation.

Finally Fig. 10.19 shows the variation of factor of safety with SDR for the three spans from which it is clearly shown that SDR does not have any structural

significance when it is treated as an absolute figure, but it does have significance when it is related to the same span.

TABLE 10.1

RATE OF CHANGE OF VARIOUS VARIABLES WITH THE CHANGE OF SPAN

(Refer to Table 7.1)

Case	Span ft.	SDR	Tubes				Factor of Safety S.F.	Bottom central deflection	Concrete	
			Tension		Compression				Max. B.M.	Max. in-plane stress
			Central P	Max. T	Corner C_c	Max. C				
D CON 2	40	9.66					1.837			
R	1	1	1	1	1	1	1	1	1	1
D CON 3	60	14.5					1.83			
R	1.5	1.5	1.75	2.07	1.59	1.0	0.99	2.91	1.12	1.02
D CON 4	80	19.3					0.96			
R	2.0	2.0	3.3	3.74	2.8	1.91	0.52	8.31	1.32	1.97
D CON 5	100	24.15					0.77			
R	2.5	2.5	4.98	6.05	4.22	2.38	0.42	18.31	1.58	3.05

TABLE 10.2

The relation between axial forces in bottom layer and in plane forces in top layer for various spans.

No.	Case	Span ft.	Central Axial Force		Concrete central in-plane stress		$\frac{P_c}{P_x}$
			P	$P_x = P/\sqrt{2}$	σ_p	$P_c = \sigma_p \times t \times b = P_{300}\,\sigma_p$	
1	D CON 2	40	12453	8804	-19.4	- 5820	0.66
2	D CON 3	60	21859	15453	- 53.5	-16050	1.04
3	D CON 4	80	41068	29035	-108.3	-32490	1.12
4	D CON 5	100	62023	43850	-177	-53100	1.21

TABLE 10.3

RELATION BETWEEN DEPTH AND FORCES FOR THE UNIFORM MESH WITH SPAN OF 40 FT.

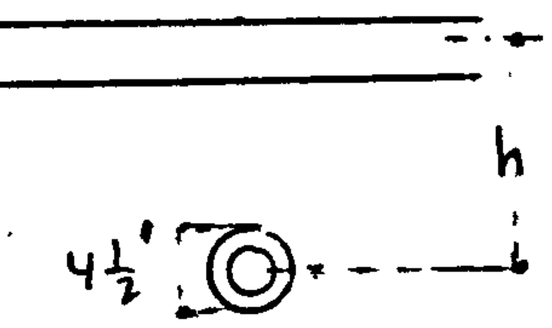

No.	Case	Structural Depth h	Tubes				Concrete			
			Tension (lbs)		Compression (lbs)		Bending Moments (lb.in.)		in-plane stress (psi)	
			Central P	Maximum T	Corner C_c	Maximum C	Central M	Maximum M_m	Central p	Maximum pm
1	DCON2S	30	16000	17594	-20024	-33373	973.3	1571	-25.3	-84.2
2	DCON2S1	36.22	13981	15332	-16769	-28766	794	1448	-22	-72
	R	1.207	0.874	0.871	0.837	0.862	0.816	0.922	0.87	0.85
3	DCON2	42.43	12452	13602	-14361	-25409	680	1369	-19.4	-63
	R	1.414	0.78	0.77	0.72	0.76	0.7	0.87	0.77	0.75
4	DCON2D	48.65	11263	12245	-12505	-22877	604	1317	-17.5	-56
	R	1.622	0.704	0.7	0.63	0.69	0.62	0.84	0.69	0.66
5	DCON2D1	54.86	10322	11162	-11042	-20931	551	1280	-16	-51
	R	1.829	0.645	0.63	0.55	0.63	0.57	0.82	0.63	0.61
6	DCON2D2	84.86	7594	7966	-6899	-15787	434	1229	-11.5	-35.4
	R	2.829	0.48	0.45	0.34	0.47	0.45	0.78	0.45	0.42
7	DCON2D3	120	5962	6038	-4766	-13430	392	1229	-8.8	-26
	R	4.0	0.37	0.34	0.24	0.4	0.4	0.78	0.35	0.3

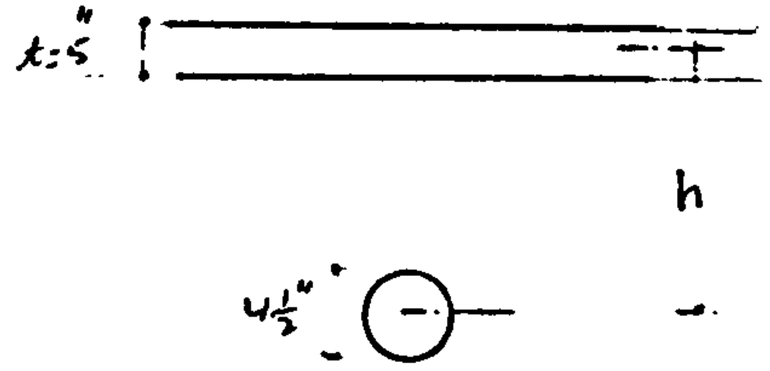

TABLE 10.4

RELATION BETWEEN DEPTH AND FORCES FOR A STRUCTURE OF SPAN 60 FT.

No.	Case	depth h	Effective depth d = h + t + D/2	SDR = Span/d	SHR = Span/h	Tubes				Concrete				
						Tension		Compression		Bending Moments		In-plane stress		
						Central force P lb.	Maximum force T lb.	Corner C_c lb.	Maximum C lb.	Centre point lb.in. M_c	Maximum M_m lb.in.	Max. σ_{pm} psi	Centre point psi σ_p	In-plane force at centre pt.
1	D CON 3S	30	37.25	19.33	24	+28833	36941	-31551	-33195	1200	1938	-92.3	-71.5	21450
2	D CON 3S1	36.22	43.47	16.56	19.88	24826	31982	-26608	-28656	929.7	1687	-78.5	-61.2	18360
	R	1.207	1.167	0.857	0.828	0.861	0.866	0.843	0.863	0.775	0.87	0.85	0.856	
3	D CON 3	42.43	49.68	14.493	16.97	21859	28214	-22860	-25436	764	1529	-68.3	-53.5	16050
	R	1.414	1.334	0.75	0.707	0.758	0.764	0.724	0.766	0.637	0.789	0.74	0.748	
4	D CON 3D	48.65	55.9	12.88	14.8	19591	25263	-19928	-23054	655.8	1425	-60	-47.6	14280
	R	1.622	1.5	0.666	0.617	0.68	0.684	0.632	0.695	0.547	0.735	0.65	0.666	
5	D CON 3D1	54.86	62.11	11.6	13.12	17818	22907	-17590	-21248	581.6	1446	-54.2	-43	12900
	R	1.829	1.667	0.6	0.547	0.618	0.62	0.558	0.64	0.485	0.746	0.587	0.601	
6	D CON 3D2	84.86	92.1	7.82	8.48	12860	15932	-10830	-16515	420.6	1192	-36.8	-29.8	8940
	R	2.829	2.47	0.404	0.353	0.446	0.43	0.343	0.496	0.351	0.615	0.4	0.417	
7	D CON 3D3	120	127.25	5.66	6	10156	11688	- 7166	-14188	363.2	1135	-27.4	-22.5	6750
	R	4	3.43	0.293	0.25	0.352	0.316	0.227	0.427	0.303	0.586	0.3	0.315	

TABLE 10.5

RELATION BETWEEN DEPTH AND FORCES IN A SPAN OF 80 FT.

(t = 5 inch, D = 4.5 inch)

No.	Case	Depth h inches	Effective depth d = $h+t+\frac{D}{2}$	SDR = $\frac{\text{Span}}{d}$	SHR = $\frac{\text{Span}}{h}$	Tubes				Concrete				
						Tension		Compression		Bending Material		In-plane stress		
						Centre force P lb.	Maximum force T lb.	Corner force C_c lb.	Maximum force C lb.	Centre point M_c lb.in.	Maximum M_m lb.in.	Maximum σ_{pm} psi	Centre point stress σ_p psi	Centre point force = xtxb lbs.
1	D CON 4S	30	37.25	25.8	32	54536	67266	-55483	-64108	1825	2513	-168.1	-146.4	-43920
2	D CON4S1	36.22	43.47	22.1	26.5	46783	57923	-46783	-55064	1377.4	2079	-142.6	-124.5	-37350
	R	1.202	1.167	0.856	0.828	0.857	0.861	0.843	0.859	0.755	0.827	0.848	0.85	
3	D CON 4	42.43	49.68	19.32	22.63	41068	50835	-40171	-48553	1103	1813	-124	-108.3	-32490
	R	1.414	1.334	0.749	0.707	0.753	0.756	0.724	0.757	0.604	0.721	0.738	0.74	
4	D CON 4D	48.65	55.90	17.2	19.73	36701	45281	-34992	-43686	927.4	1638	-109.4	- 96	28800
	R	1.622	1.5	0.667	0.617	0.673	0.673	0.631	0.681	0.505	0.652	0.651	0.656	
5	D CON4D1	54.86	62.11	15.5	17.5	33289	40834	-30861	-39971	798	1517	- 98	- 86.2	-25860
	R	1.829	1.667	0.6	0.547	0.61	0.607	0.556	0.623	0.437	0.604	0.583	0.589	
6	D CON4D2	84.86	92.1	10.4	11.3	23755	27556	-18910	-30277	525.7	1253	- 67	- 59.1	-17730
	R	2.829	2.47	0.43	0.353	0.436	0.41	0.341	0.472	0.288	0.5	0.4	0.404	
7	D CON4D3	120	127.25	7.54	8	18673	20986	-12343	-25832	427	1239	- 50	- 44.5	-13350
	R	4	3.43	0.292	0.25	0.342	0.312	0.222	0.403	0.234	0.493	0.297	0.304	

TABLE 10.6

COMPARISON OF THE CENTRAL IN-PLANE AND TENSILE FORCES
FOR VARIOUS SPANS AND DEPTHS

No.	Height h	Span 40 ft.			Span 60 ft.			Span 80 ft.		
		Axial tensile Component P_x	In-plane force P_c	$\frac{P_c}{P_x}$	Axial tensile = 0.707 P P_x	In-plane force P_c	$\frac{P_c}{P_x}$	Axial force = 0.707 P P_x	In-plane force P_c	$\frac{P_c}{P_x}$
1	30	11312	-7590	0.67	20385	-21450	1.05	38557	-43920	1.14
2	36.22	9885	-6600	0.67	17552	-18360	1.05	33076	-37350	1.13
3	42.43	8804	-5820	0.66	15453	-16050	1.04	29035	-32490	1.12
4	48.65	7963	-5250	0.66	13851	-14280	1.03	25948	-28800	1.11
5	54.85	7298	-4800	0.66	12597	-12900	1.02	23535	-25860	1.10
6	84.86	5369	-4450	0.83	9092	- 8940	0.98	16795	-17730	1.06
7	120	4215	-2640	0.63	7181	- 6750	0.94	13202	-13350	1.01

TABLE 10.7

THE EFFECT OF SLAB THICKNESS VARIATION ON FORCES IN 'THE UNIFORM MESH' SPAN = 40 ft.

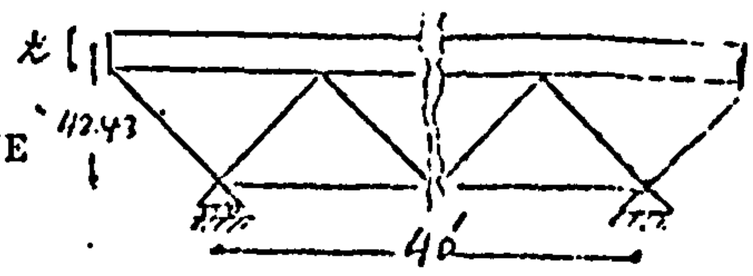

No.	Description	CASES				
		DCON20 t = 2.5 in.	DCON2 t = 5 in.	DCON21 t = 7.5 in.	DCON22 t = 10 in.	DCON23 t = 12.5 in
1	Effective depth	47.25	49.75	52.25	54.75	57.25
2	Span/depth ratio (SDR)	10.15	9.662	9.2	8.78	8.4
	$R = \frac{SDR\ (DCON2)}{SDR\ (DCON20)}$		0.952	0.906	0.865	0.827
3	Concrete plate					
a)	Moments (lb-in)					
	i) Central (M)	317	680	1446	2500	3653
	R		2.145	4.56	7.9	11.5
	ii) Max. +ve (M_m)	1187	1369	1939	2832	3848
	R		1.153	1.633	2.386	3.24
	iii) Max. -ve ($-M_m$)	-1458	-1631	-1795	-1781	-1543
	R		1.12	1.23	1.2	1.06
b)	Stresses (psi)					
	i) Central in-plane (σ_p)	-40.7	-19.4	-11.6	-7.3	-4.6
	R		0.48	0.285	0.18	0.113
	ii) Central B.M. (σ_b)	301	163	154	150	140
	R		0.54	0.51	0.493	0.46
4	Tubes					
a)	Tensile forces (lb)					
	i) Central (P)	13300	12453	11122	9496	7881
	R		0.94	0.84	0.71	0.6
	ii) Maximum (T)	14438	13602	12091	10183	8302
	R		0.963	0.856	0.721	0.59
b)	Compressive forces (lb)					
	i) Corner (C_c)	-14124	-14361	-14191	-13845	-13436
	R		1.02	1.00	0.98	0.95
	ii) Maximum (C)	-25656	-25409	-24347	-22828	-21163
	R		0.99	0.95	0.89	0.83

TABLE 10.8

THE EFFECT OF SLAB THICKNESS VARIATION ON FORCES IN
'THE UNIFORM MESH'
Span = 60 ft.

Nos.	Descriptions	CASES				
		DCON30 t=2.5in.	DCON3 t = 5 in.	DCON31 t=7.5in.	DCON32 t=10 in.	DCON33 t = 12.5 in.
1	Effective depth	47.25	49.75	52.25	54.75	57.25
2	Span/depth ratio (SDR)	15.24	14.5	13.8	13.2	12.6
	$R = \frac{SDR(X)}{SDR(DCON20)}$		0.95	0.906	0.866	0.83
3	Concrete plate					
a)	Moments (lb.in)					
	1) Central (M)	324	764	1877	3639	5696
	R		2.36	5.8	11.2	17.6
	ii) Max. +ve (M_m)	1090	1529	2559	4161	6033
	R		1.4	2.35	3.8	5.5
	iii) Max. -ve ($-M_m$)	-1373	-1447	-1519	-2115	-2702
	R		1.05	1.11	1.54	1.97
b)	Central stresses (psi)					
	i) In-plane (σ_p)	-112	-53.5	-37	-20	-12.5
	R		0.48	0.33	0.18	0.11
	ii) Flexural (σ_b)	311	183	200	218	219
	R		0.59	0.64	0.702	0.704
4	Tubes					
a)	Tensile forces (lbs)					
	i) Central (P)	22730	21859	20112	17390	14286
	R		0.96	0.885	0.765	0.63
	ii) Maximum (T)	29870	28214	25101	20996	16720
	R		0.946	0.84	0.703	0.560
b)	Compressive forces (lbs)					
	i) Corner (C_c)	-23162	-22860	-21176	-18690	-16061
	R		0.987	0.914	0.807	0.693
	ii) Maximum (C)	-25280	-25436	-25095	-24391	-23508
	R		1	0.99	0.965	0.93

TABLE 10.9

THE EFFECT OF SLAB THICKNESS VARIATION ON FORCES IN

'THE UNIFORM MESH'

Span = 80 ft.

No.	Description	Cases				
		DCON40 t=2.5in.	DCON 4 t = 5 in.	DCON41 t=7.5in.	DCON42 t = 10in.	DCON43 t=12.5in.
1	Effective depth	47.25	49.75	52.25	54.75	57.25
2	Span/depth ratio (SDR)	20.3	19.32	18.4	17.5	16.8
	$R = \frac{SDR(X)}{SDR\ (DCON20)}$		0.952	0.906	0.862	0.827
3	Concrete plate					
a)	Moments (lb.in)					
	i) Central (M)	370	1103	2887	5748	9236
	R		2.98	7.81	15.54	25
	ii) Max. +ve(M_m)	1196	1813	3544	6305	9648
	R		1.516	2.963	5.3	8.1
	iii) Max. -ve($-M_m$)	1355	1731	3060	4702	6106
	R		1.28	2.26	3.5	4.5
b)	Central stresses (psi)					
	i) In-plane (σ_p)	-224	-108	-66	-43	-28
	R		0.48	0.3	0.2	0.12
	ii) Flexural (σ_b)	355	265	308	345	355
	R		0.75	0.87	0.97	1
4	Tubes					
a)	Tensile forces (lbs)					
	i) Central (P)	42634	41068	38089	33476	27948
	R		0.963	0.89	0.78	0.66
	ii) Maximum (T)	53462	50835	45607	38545	31005
	R		0.95	0.85	0.72	0.58
b)	Compressive forces (lbs)					
	i) Corner (C_c)	-41023	-40171	-36751	-31581	-25925
	R		0.98	0.9	0.77	0.63
	ii) Maximum (C)	-48872	-48553	-47168	-45010	-42595
	R		0.99	0.96	0.92	0.87

TABLE 10.10

RATIO OF IN-PLANE STRESS TO FLEXURAL STRESSES AND IN-PLANE FORCES TO ORTHOGONAL AXIAL FORCES AT THE CENTRE

Slab Thickness ins.	Span 40 ft.						Span 60 ft.						Span 80 ft					
	Concrete				Axial force P_x lb.	$\frac{P_c}{P_x}$	Concrete				Axial force $P_x = P/\sqrt{2}$	$\frac{P_c}{P_x}$	Concrete				Axial force $P_x = P/\sqrt{2}$	$\frac{P_c}{P_x}$
	σ_p	σ_b psi	$\frac{\sigma_p}{\sigma_b}$	$P_c = \sigma_p x t x b$ lb			σ_p	σ_b	$\frac{\sigma_p}{\sigma_b}$	$P_c = \sigma_p x t x b$			σ_p	σ_b	$\frac{\sigma_p}{\sigma_b}$	$P_c = \sigma_p x t x b$		
2.5	-40.7	304	0.13	-6102	9403	0.65	-112	311	0.36	-16800	+16070	1.05	-224	355	0.63	-33600	30142	1.12
5	-19.4	163	0.12	5820	8804	0.66	-535	183.4	0.29	-16050	+15454	1.04	-108.5	265	0.40	-32520	29035	1.12
7.5	-11.6	154	0.08	5220	7863	0.66	- 37	200	0.185	-16650	14219	1.17	- 66.3	308	0.22	-29820	26929	1.11
10	- 7.3	150	0.05	4380	6714	0.65	- 20	218.3	0.09	-12000	12295	0.98	- 43	345	0.12	-25800	23668	1.09
12.5	- 4.6	140	0.03	3450	5572	0.62	-12.5	219	0.06	- 9375	10100	0.93	- 27.9	355	0.08	-20940	19759	1.06

TABLE 10.11

SHOWING THE EFFECTS OF CHANGING TUBE WALL THICKNESS

No.	Case	Tube Thickness	TUBES (axial forces)				CONCRETE SLAB								$P_x = P/\sqrt{2}$	$\frac{P_c}{P_x}$
			Tension		Compression		Flexure				In-plane stress					
							Moments		Stresses		max.	Centre point				
			Central P lb.	Maximum lb.	Corner lb.	Maximum lb.	Central lb.in	Maximum lb.in	Central psi	Maximum psi	$\sigma_{\rho m}$ psi	stress σ_ρ	force σ_ρ xt	total force P_c		
1	D CON 3	0.176	21859	28214	-22860	-25436	764	1529	183.4	367	-68.3	-53.5	-267.5	-16050	+15454	1.04
2	D CON 3M1	0.212	22024	28491	-22936	-25451	685	1450	164	348	-68.7	-53.9	-269.5	-16170	15571	1.04
	R	1.2	1.007	1.01	1.003	1.000	0.897	0.948	0.89	0.95	1.006	1.007	1.007	1.007		
3	D CON 3M2	0.252	22157	28706	-22973	-25459	626.4	1390	150.3	333.6	-69.0	-54.2	-271	-16260	15665	1.04
	R	1.43	1.014	1.017	1.005	1.000	0.82	0.909	0.82	0.909	1.006	1.007	1.01	1.01		

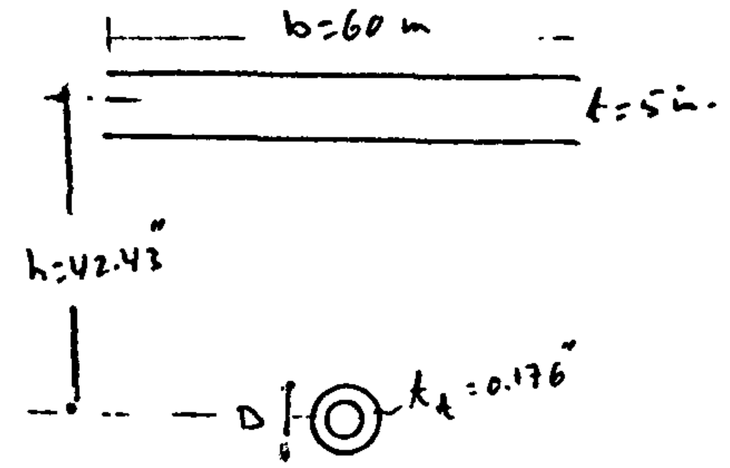

TABLE 10.12

SHOWING THE EFFECTS OF CHANGING OUTSIDE TUBE DIAMETER

No.	Case	Tubes Diam. in.	Depth $d = h+t+\frac{D}{2}$	SHR = $\frac{\text{span}}{h}$	SDR = $\frac{\text{span}}{d}$	Axial forces in Tubes				Concrete Slab							
						Tension		Compression		Flexure				In-plane stress			
										Moments		Stresses		Max.	Central		
						Central lb	Maximum lb	Corner lb	Maximum lb	Central lb.in	Max. lb.in.	Central psi	Max. psi	σ_{pm} psi	Stress σ_p	force $\sigma_p xt$	Total P $\sigma_p xtxb^c$
1	D CON 3	$4\frac{1}{2}$	49.68	17	14.5	21859	28214	-22860	-25436	764	1529	183.4	367	-68.3	-53.5	-267.5	-16050
2	D CON 3M3	$5\frac{1}{2}$	50.18	"	14.35	+21982	+28441	-22806	-25218	674	1434	162	344	-68.7	-54	-270	-16200
	R		1.01		0.99	1.006	1.008	0.498	0.99	0.88	0.94	0.88	0.94	1.006	1.009	1.00	1.00
3	D CON 3M4	$6\frac{5}{8}$	50.74	"	14.2	22055	28573	-22657	-24917	604	1358	145	326	-69	-54.4	-272	-16320
	R		1.02		0.98	1.009	1.013	0.99	0.98	0.79	0.89	0.79	0.89	1.010	1.017	1.02	1.02

TABLE 10.13

VARIATION OF FACTOR OF SAFETY IN SHEAR MEMBERS WITH STRUCTURAL DEPTH IN 'THE UNIFORM MESH'

Nos. and ratio 'R'	Structural depth inches	Safe load S_L	DCON2 Span = 40 ft.		DCON3 Span = 60 ft.		DCON4 Span = 80 ft.		Total length of tubes for spans		
			Max. = C compression in shear member	$F_s = S_{L/C}$	C	F_s	C	F_s	40 ft.	60 ft.	80 ft.
1	30	47152	33373	1.41	33195	1.42	64108	0.735	340.64	682.06	1083.5
2	36.27	46928	28766	1.63	28656	1.64	55064	0.85	345.64	691.86	1099.7
R	1.207			1.156		1.155		1.156	1.015	1.014	1.015
3	42.43	46682	25409	1.84	25436	1.83	48553	0.96	350.64	701.67	1115.7
R	1.414			1.30		1.29		1.31	1.029	1.029	1.030
4	48.65	46668	22877	2.03	23054	2.01	43686	1.06	356.89	713.91	1136.15
R	1.62			1.44		1.42		1.44	1.048	1.048	1.048
5	54.86	45942	20931	2.195	21248	2.16	39971	1.15	363.14	726.2	1156.4
R	1.83			1.56		1.52		1.56	1.066	1.065	1.067
6	84.86	40566	15787	2.57	16515	2.456	30277	1.34	403.14	804.56	1286
R	2.82			1.82		1.73		1.82	1.18	1.18	1.187
7	120	34429	13430	2.564	14188	2.430	25832	1.333	459.39	914.81	1468.25
R	4			1.82		1.71		1.81	1.35	1.34	1.36

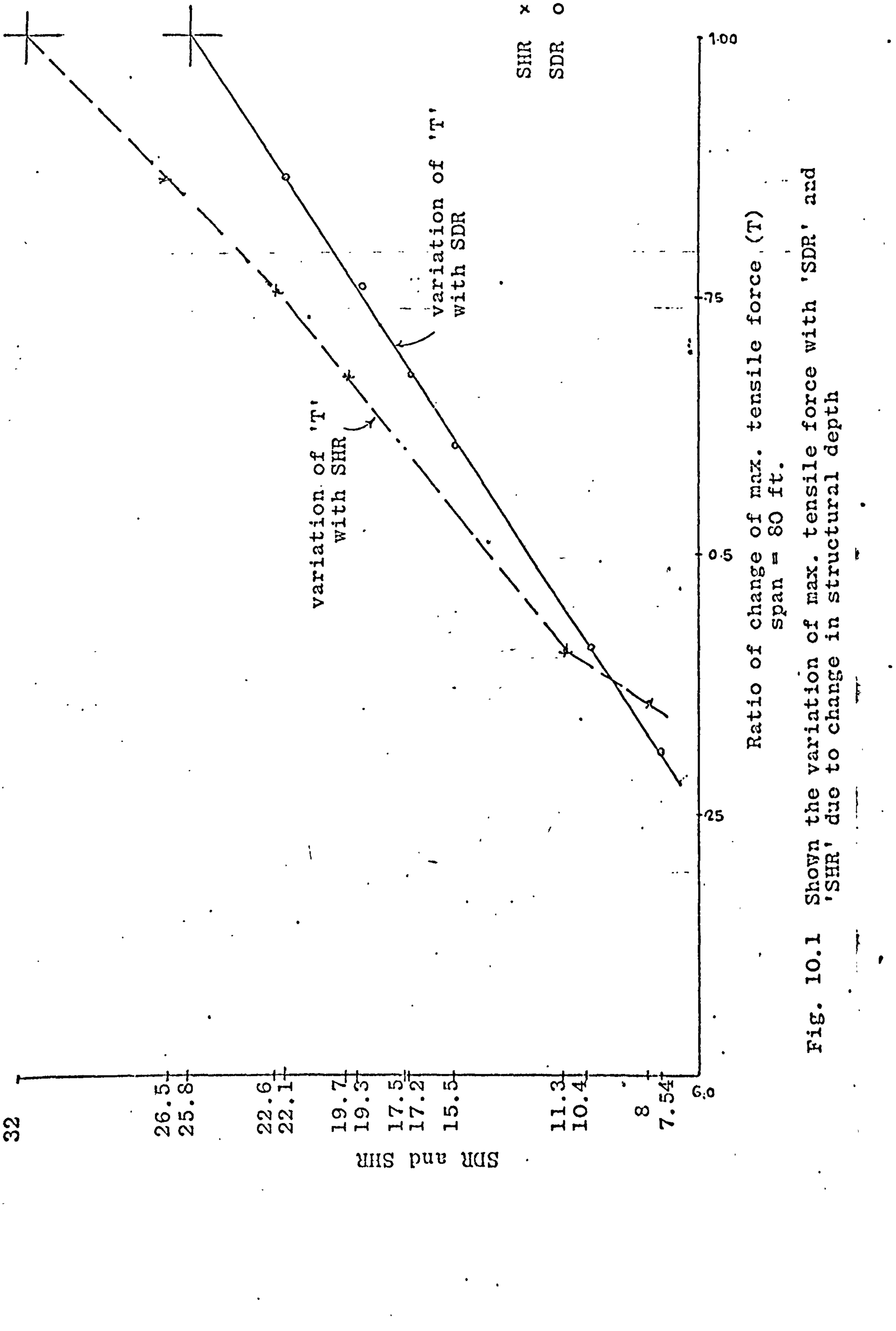

Fig. 10.1 Shown the variation of max. tensile force with 'SDR' and 'SHR' due to change in structural depth

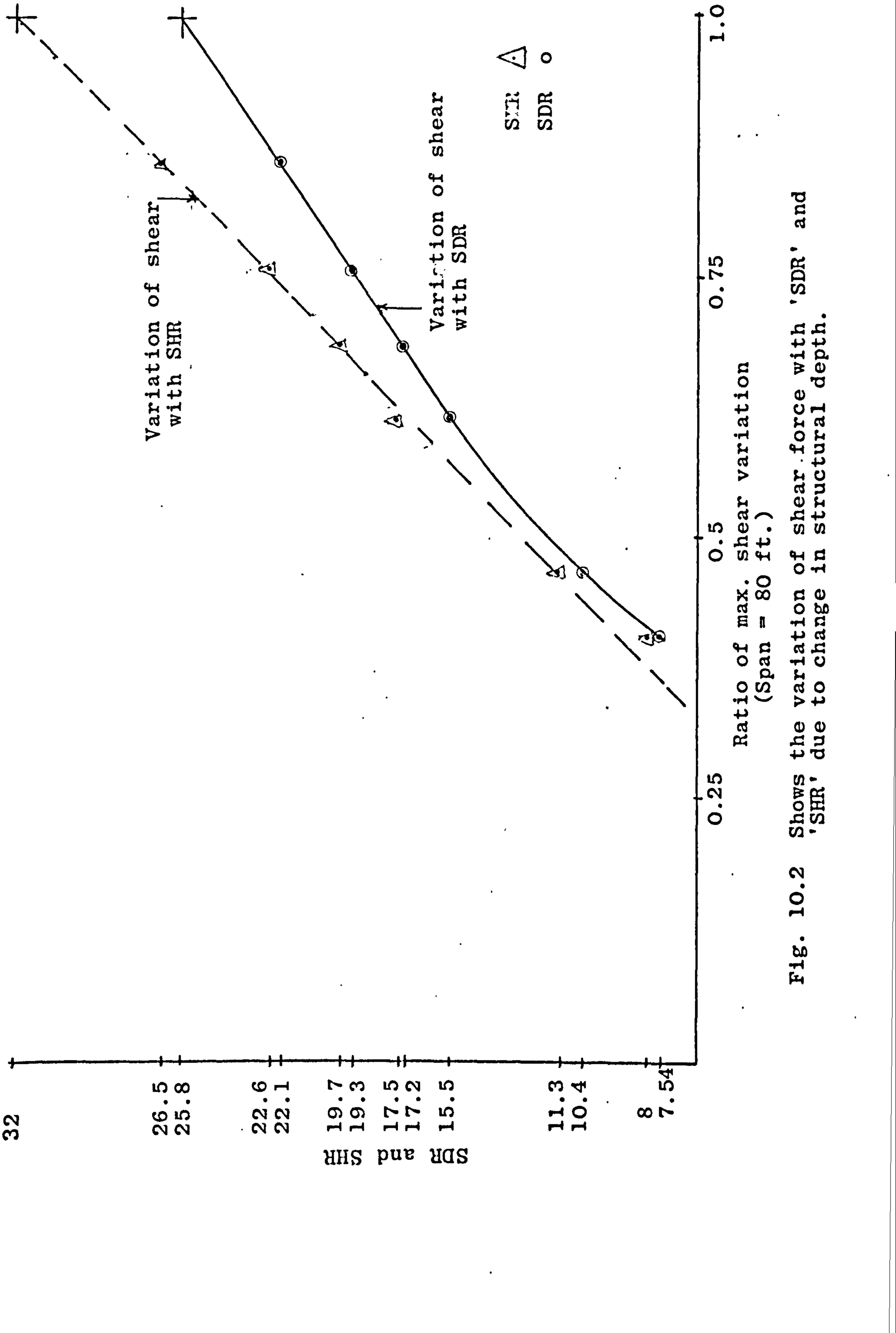

Fig. 10.2 Shows the variation of shear force with 'SDR' and 'SHR' due to change in structural depth.

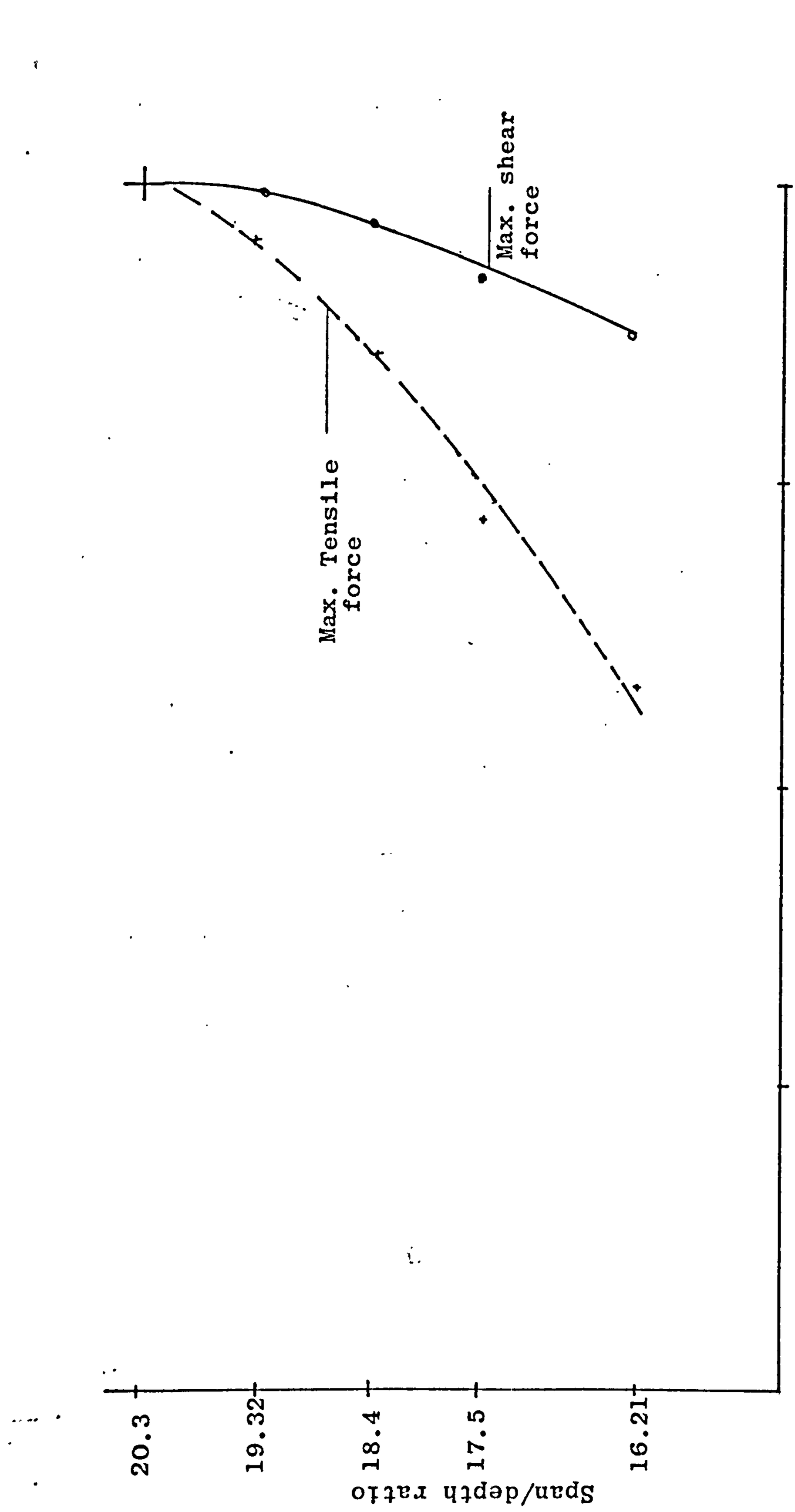

Fig. 10.3 Shows variation of forces with SDR due to the change in slab thickness only.

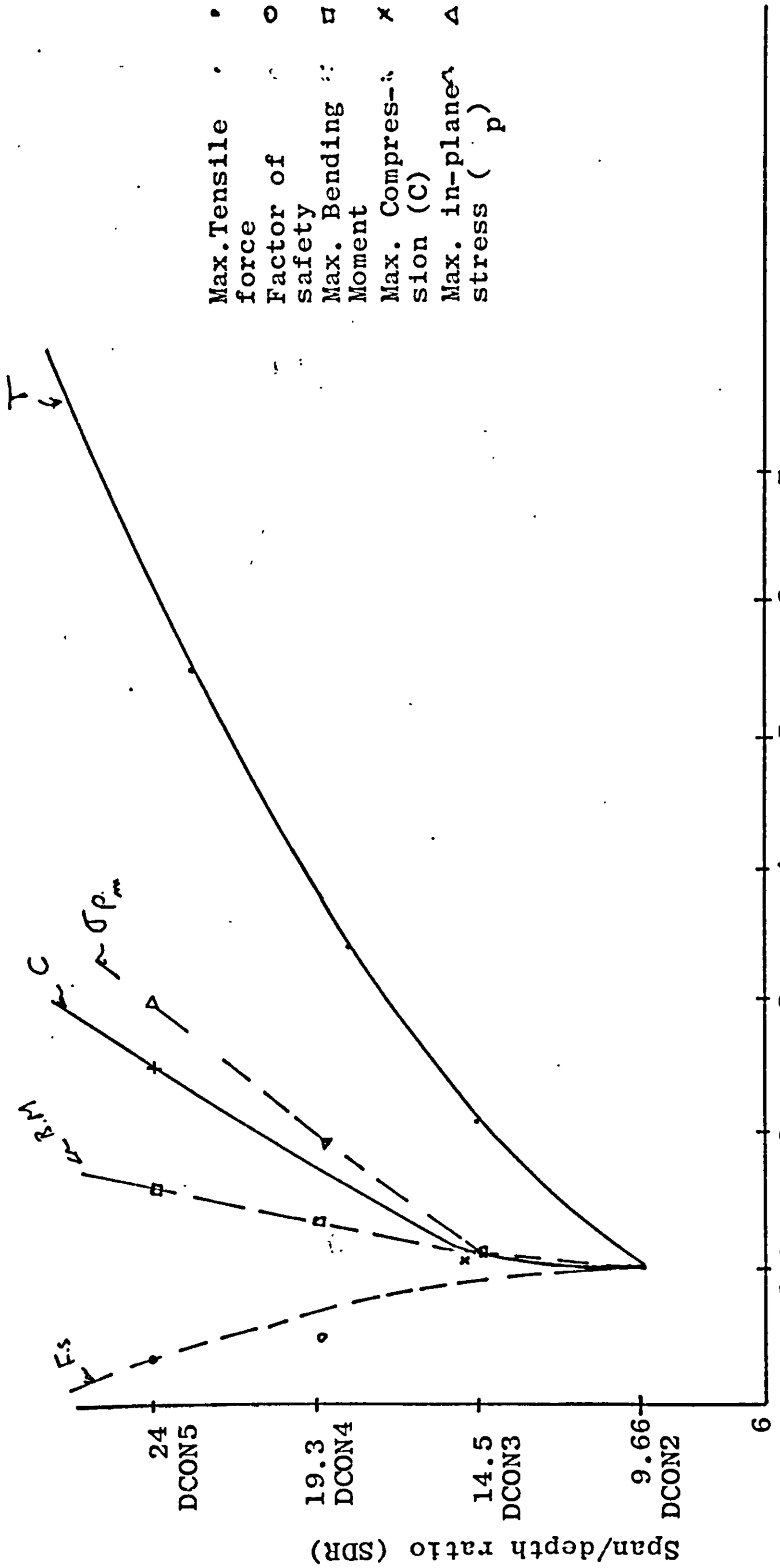

Fig. 10.4 Relation between forces and span

t = 5in

h = 42.43 in.

The ratio of all forces at a span of 40 ft. is equal to unity.

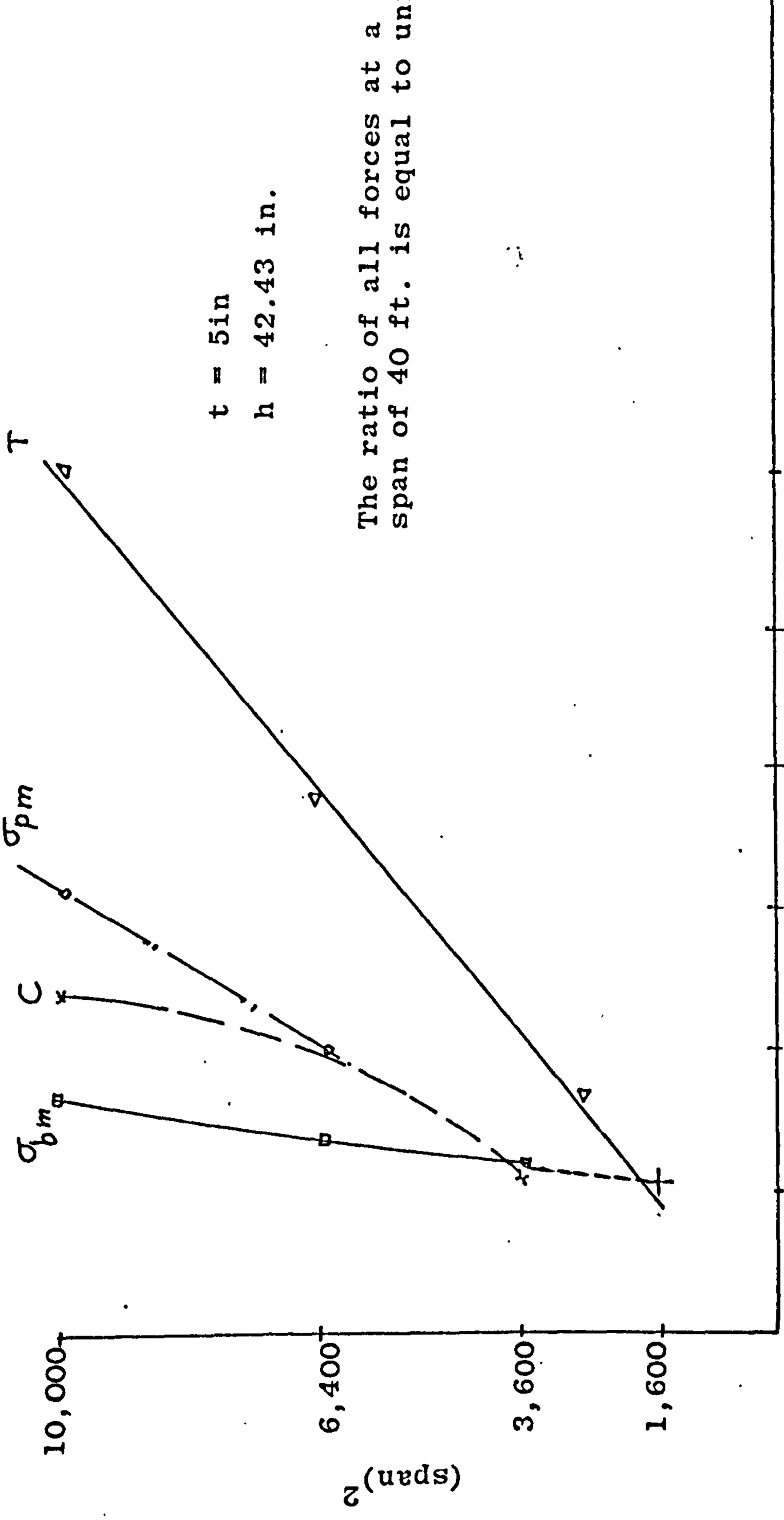

Fig. 10.5 shows the variation of forces with the $(span)^2$

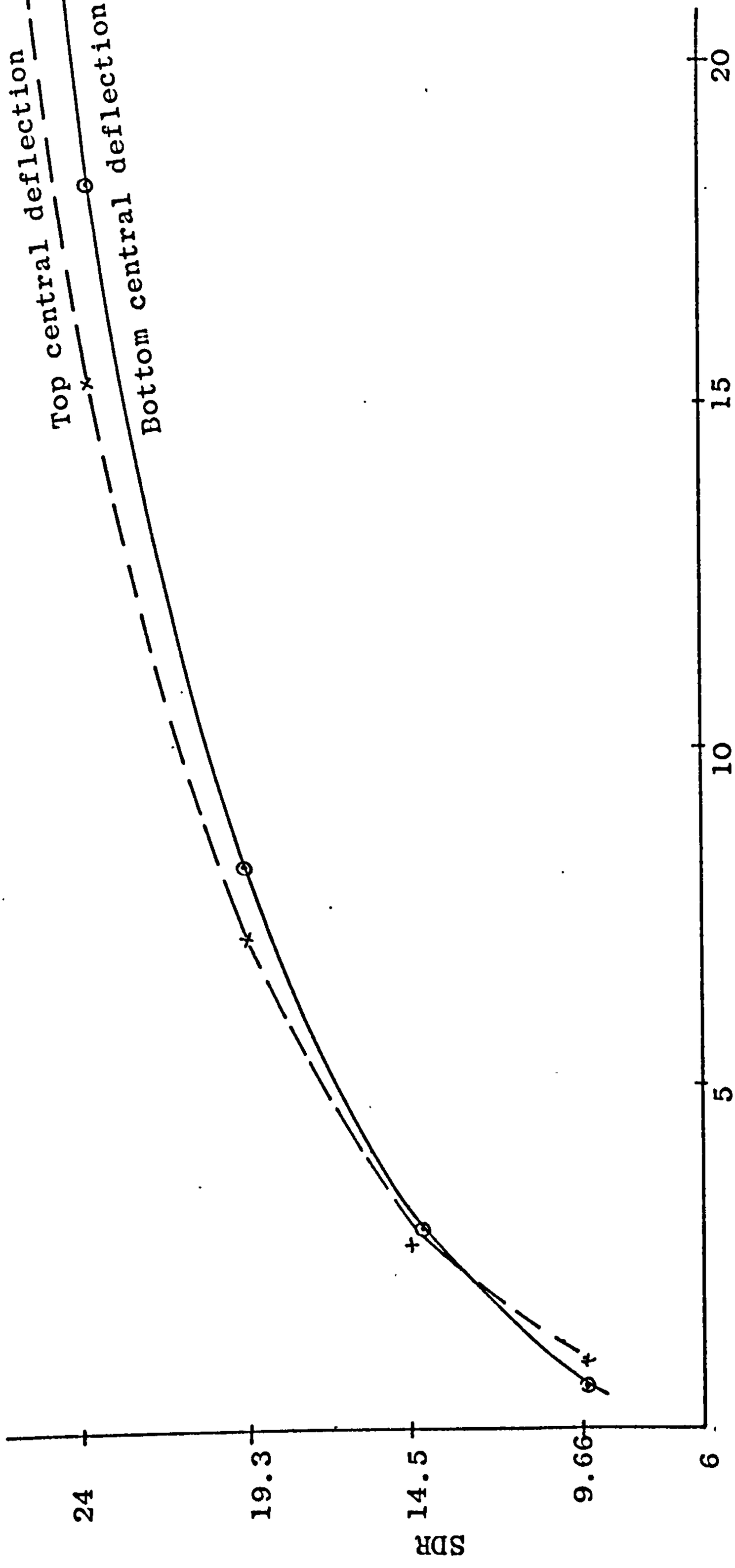
Top central deflection
Bottom central deflection
SDR
24
19.3
14.5
9.66
6
5
10
15
20
Ratio of variables
Relation between deflections and span/depth ratio
0.6
ϕ_+

Fig. 10.

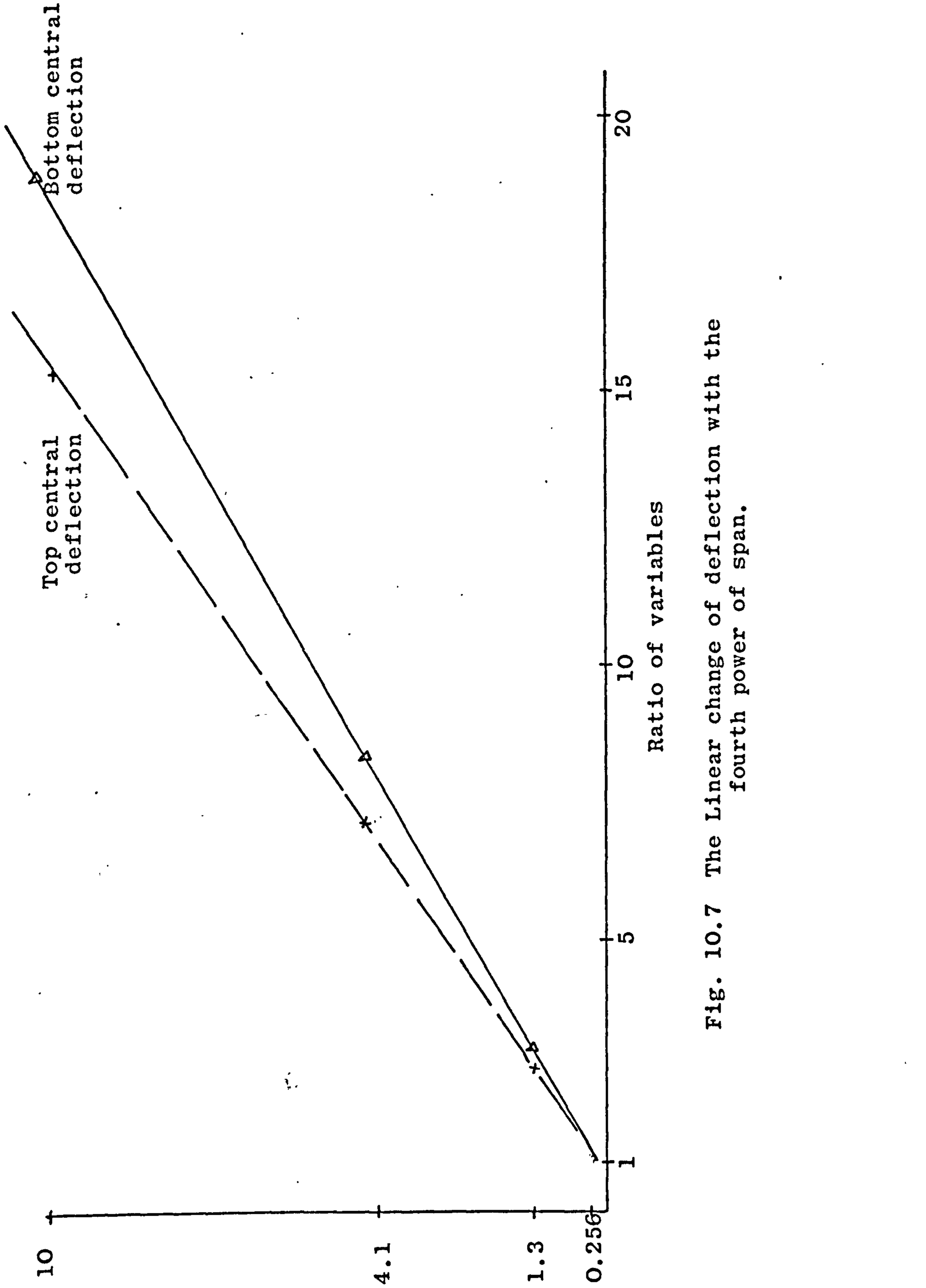

Fig. 10.7 The Linear change of deflection with the fourth power of span.

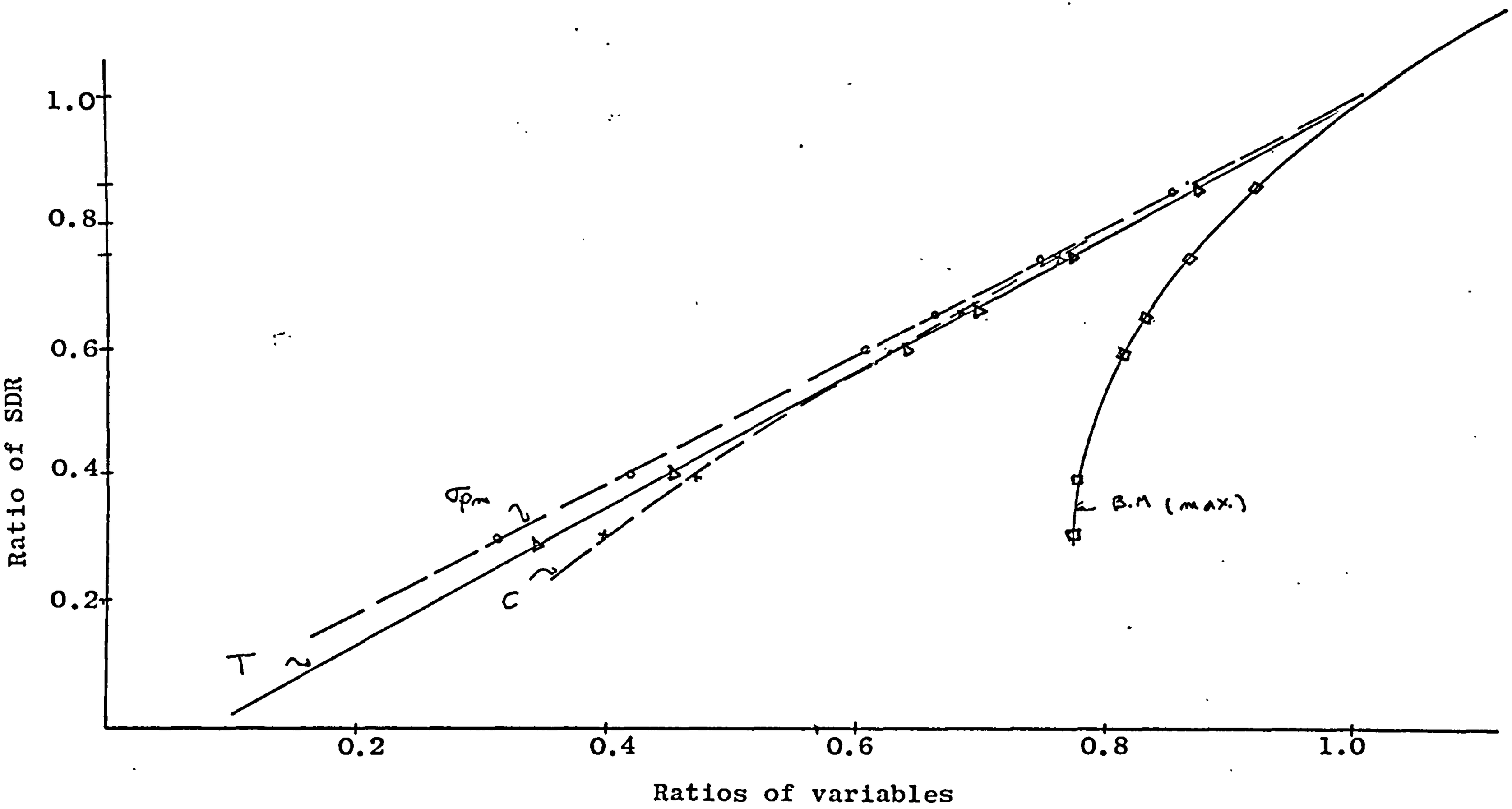

Fig. 10.8 The change of variables with SDR for span of 40 ft.

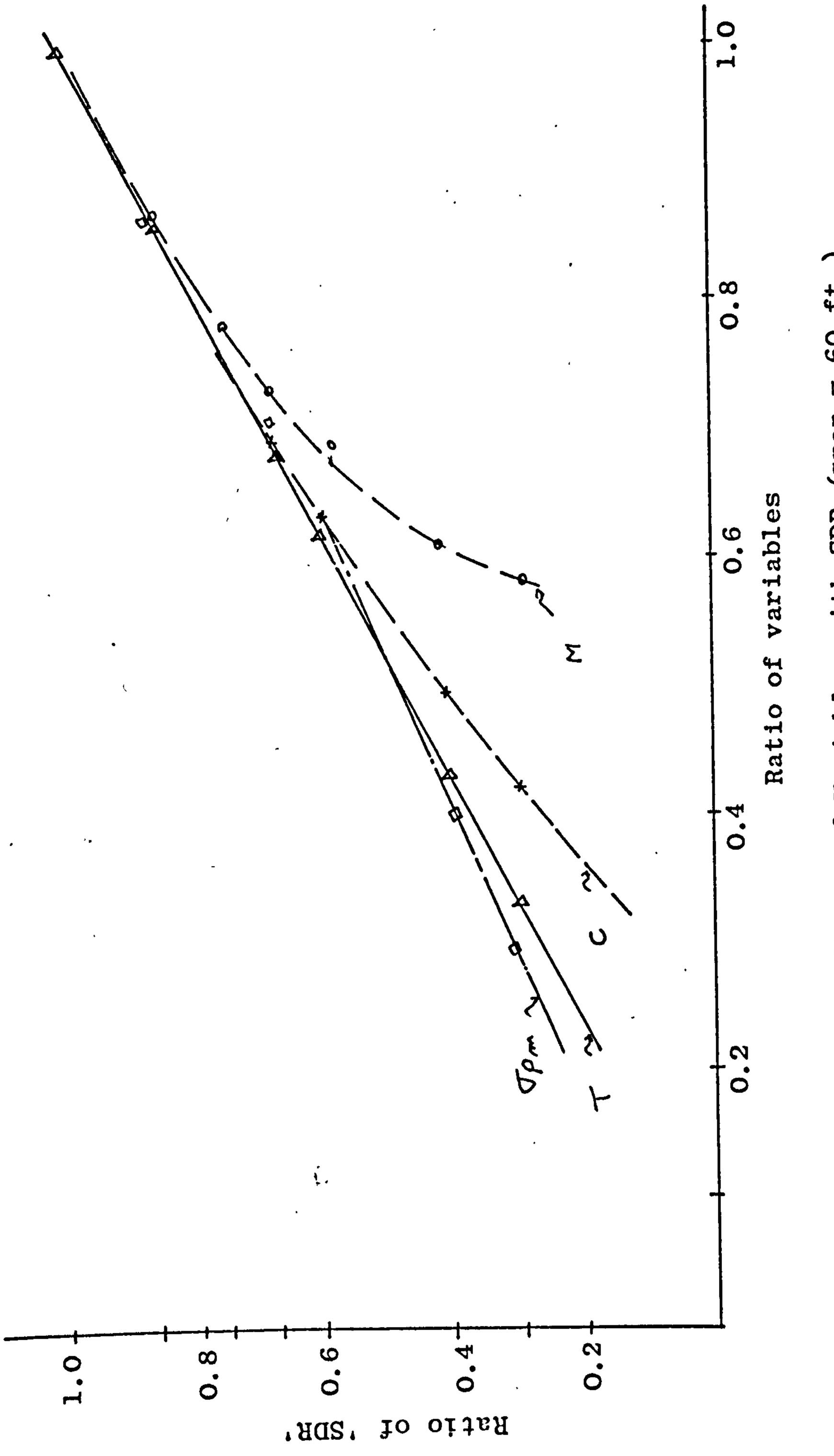
1.0
0.8
0.6
0.4
0.2
Ratio of variables
Change of Variables with SDR (span = 60 ft.)
M
C
T
C_{D_m}
Ratio of 'SDR'
1.0
0.8
0.6
0.4
0.2

Fig. 10.9

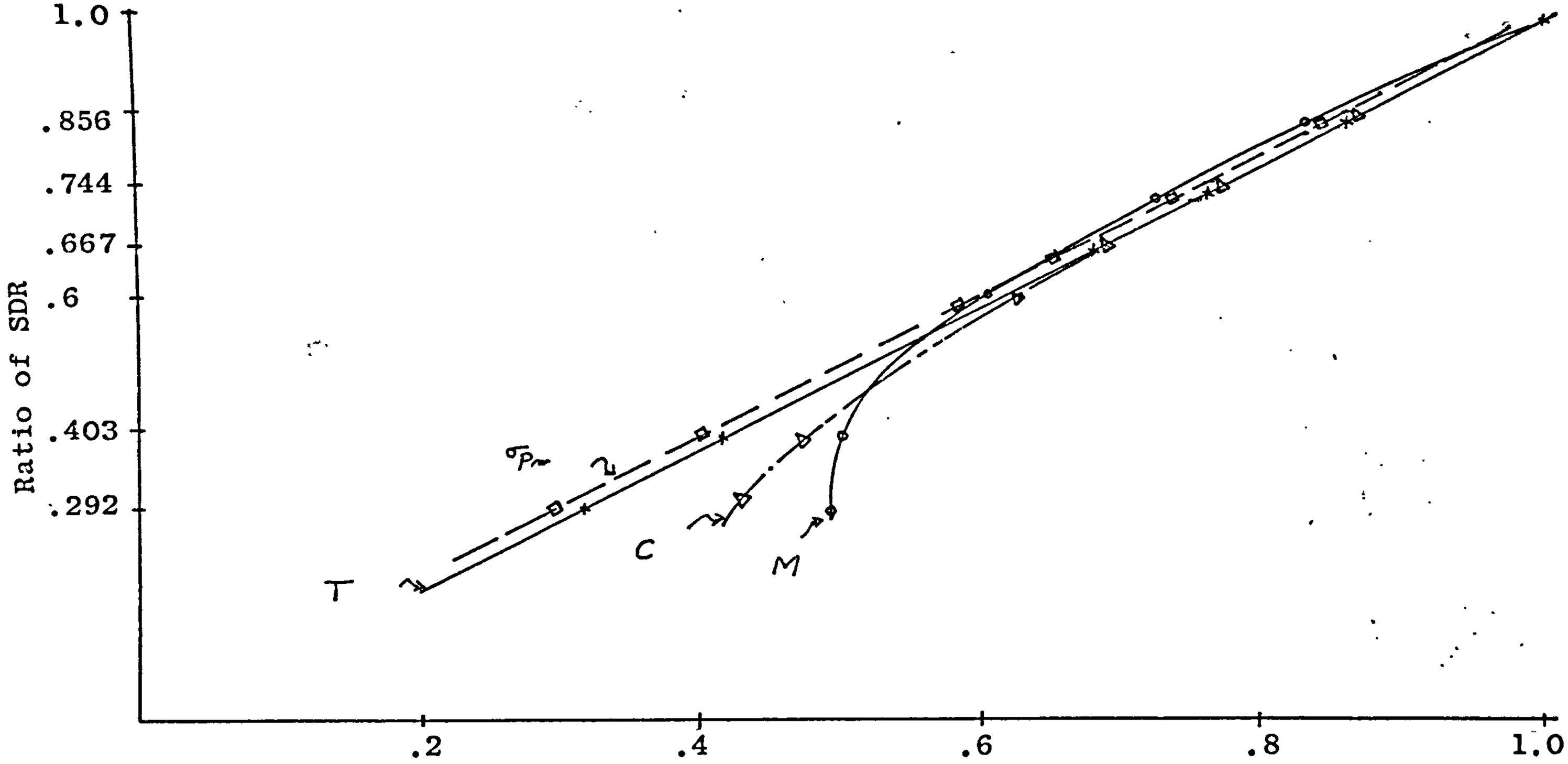

Fig. 10.10 Relation between SDR and Forces for a span of 80 ft.

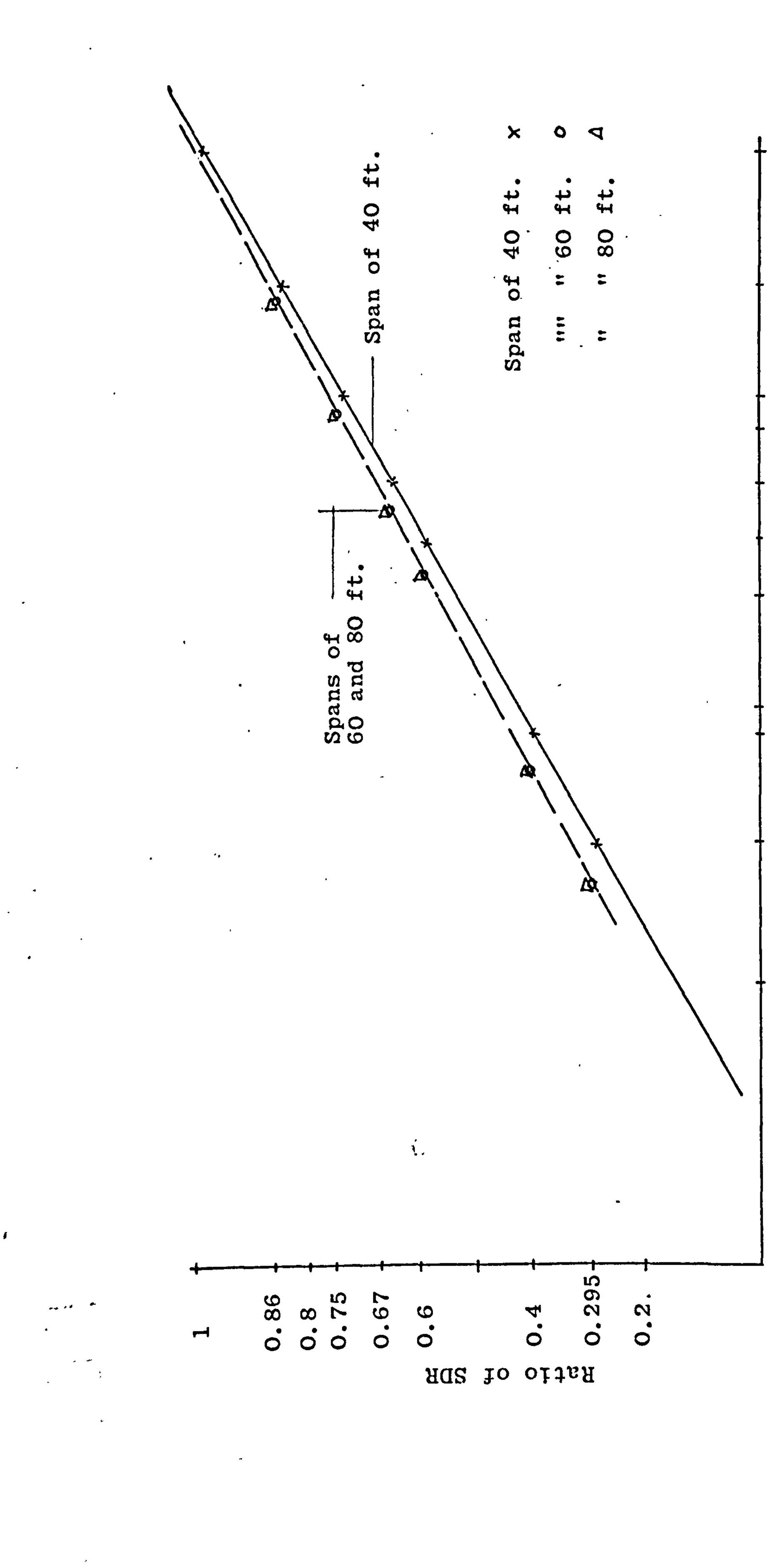

Fig. 10.11 Relation between span/depth ratio (SDR)
and the central tensile force

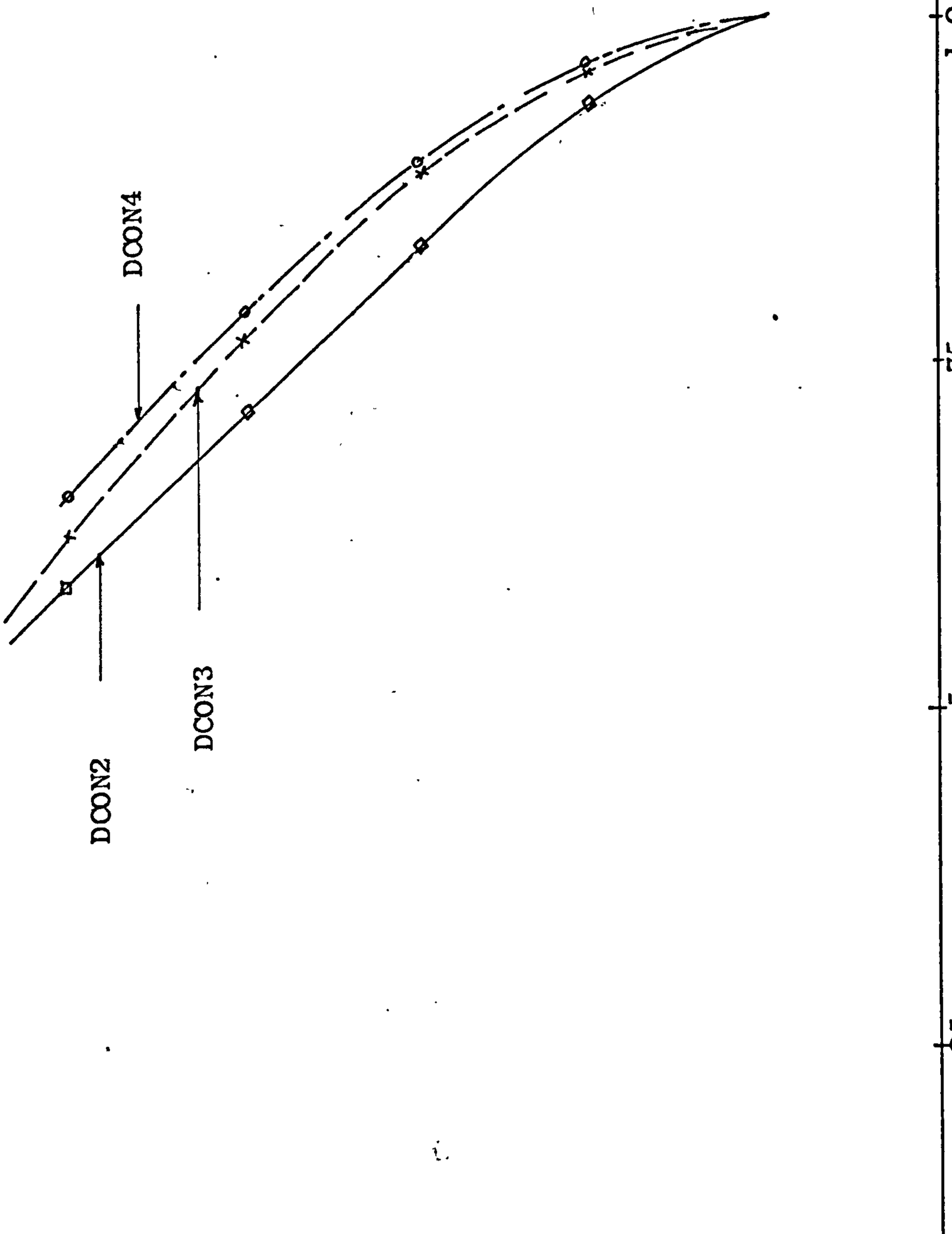
DCON4
DCON3
DCON2
1.0
.75
.5
.25
Ratio of forces at centre tube
Effect of slab thickness variation on central axial force
12.5
10
7.5
5.0
2.5
Thickness of slab in inches

Fig. 10.12

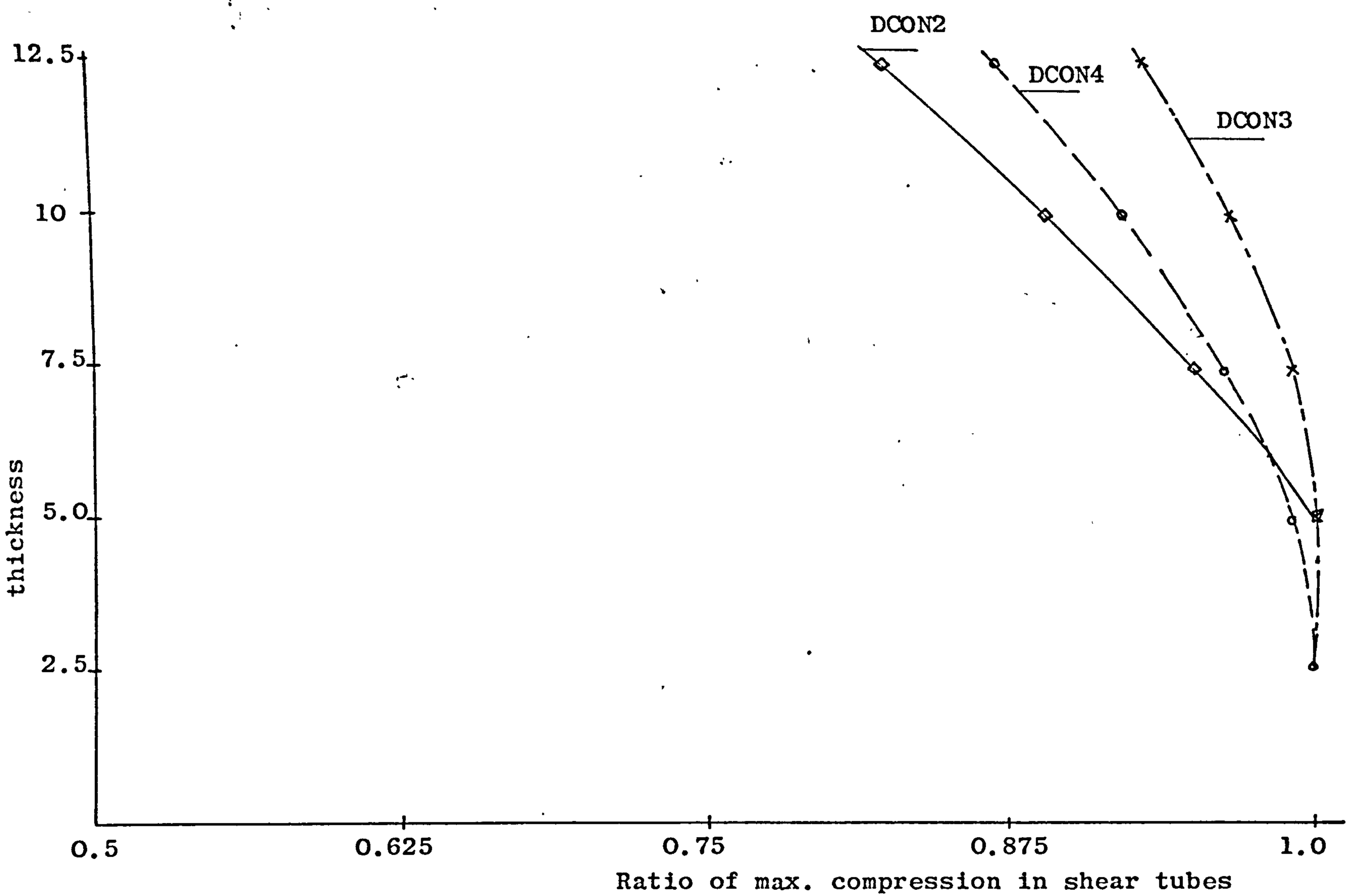

Fig. 10.13 Effects of slab thickness variation on maximum shear force

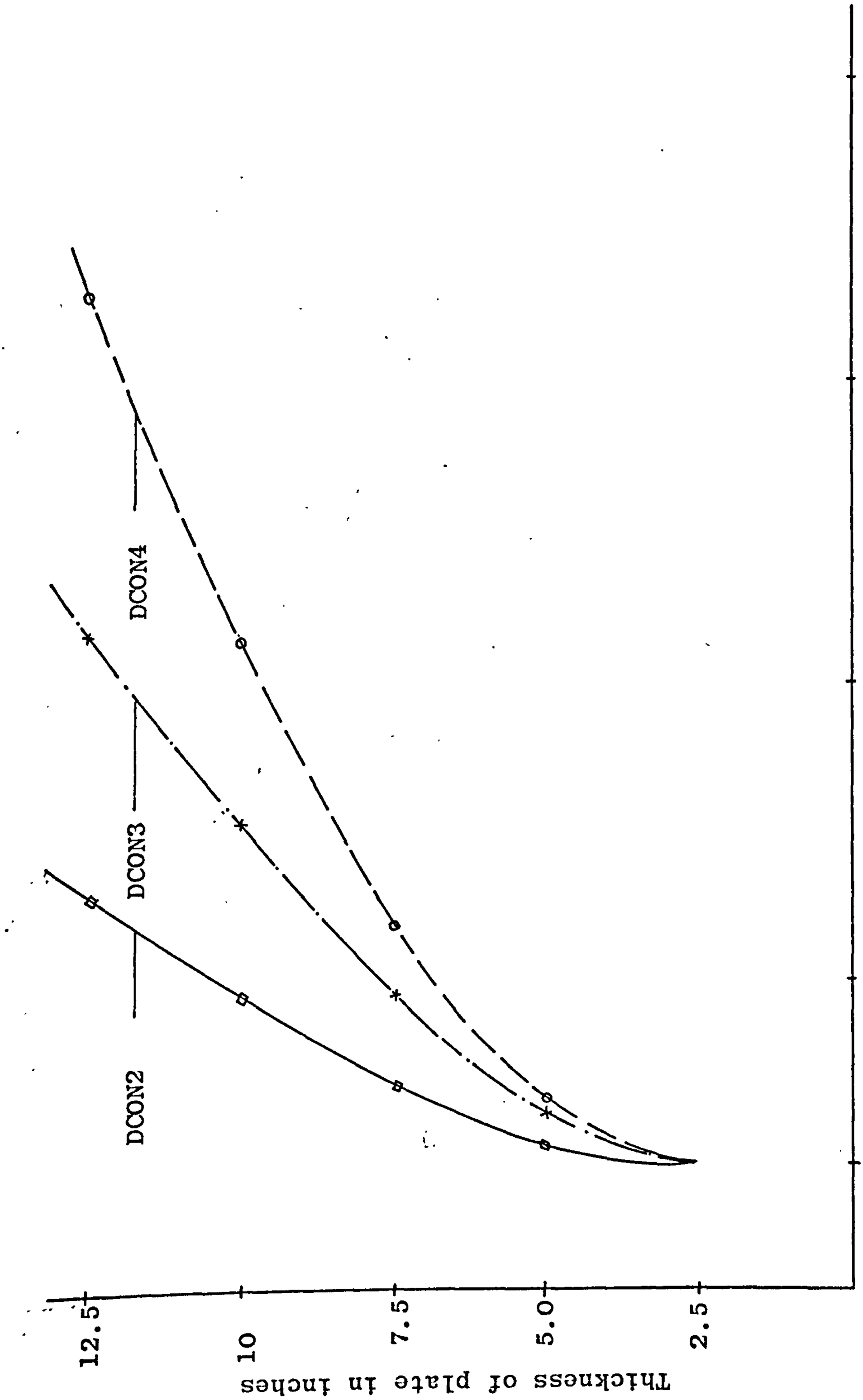

Fig. 10.14 Effect of

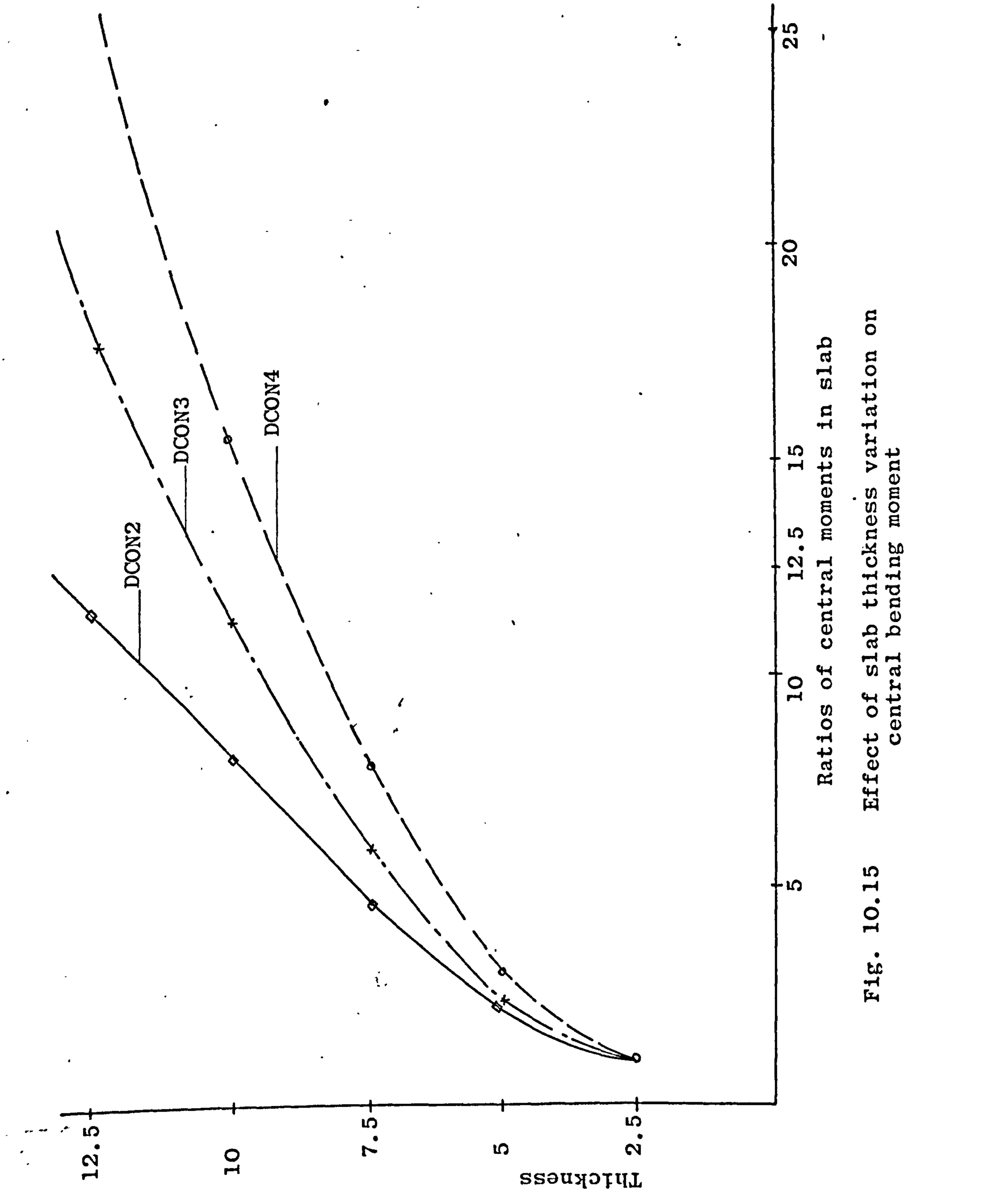
DCON2
DCON3
DCON4
25
20
15
12.5
10
5
Ratios of central moments in slab
Effect of slab thickness variation on central bending moment
12.5
10
7.5
5
2.5
Thickness

Fig. 10.15

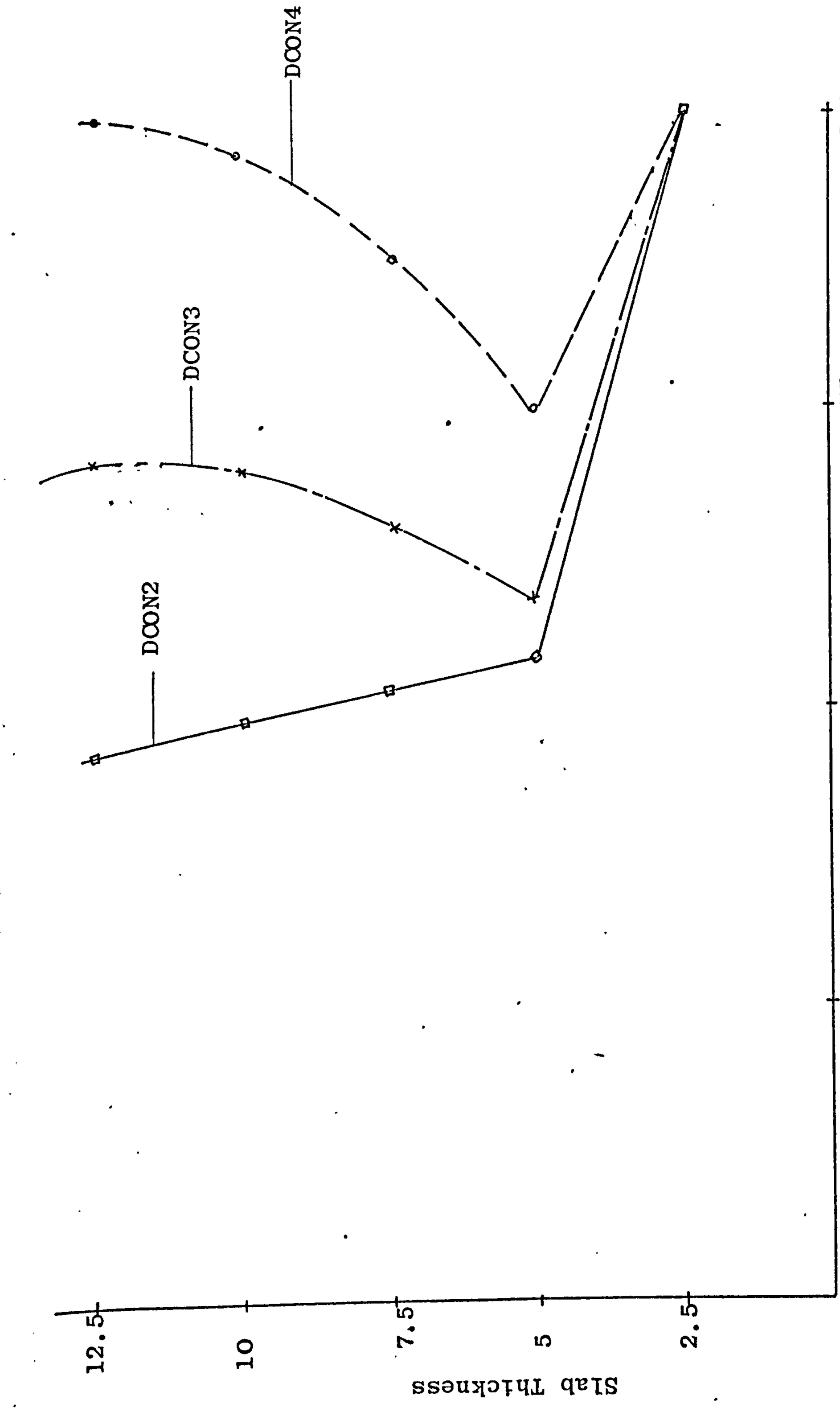
DCON4
DCON3
DCON2
1.0
0.75
0.5
0.25
Ratio of central bending stress in slab
Effect of slab thickness variation on central bending stress
12.5
10
7.5
5
2.5
Slab Thickness

Fig. 10.16

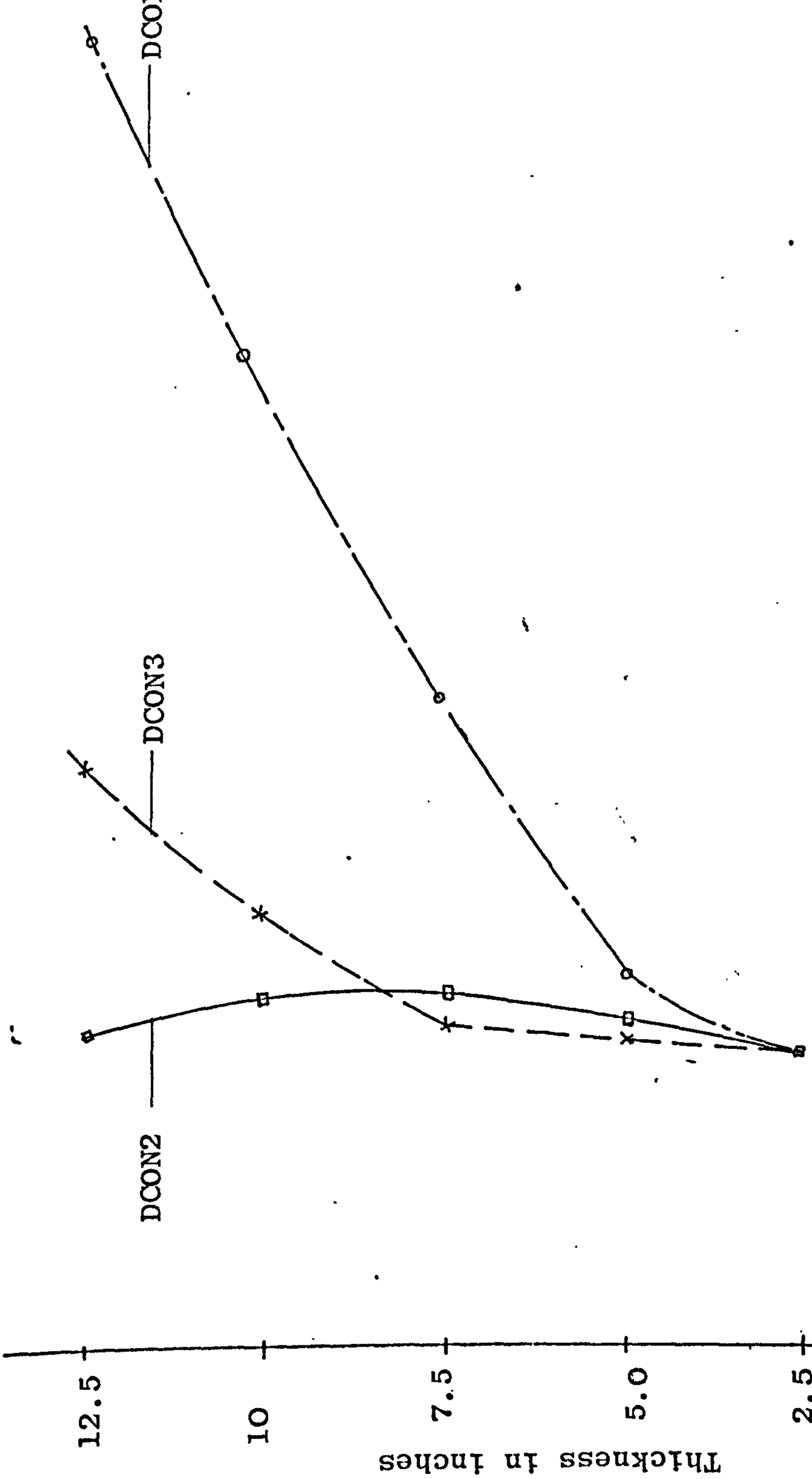
DCON4
DCON3
DCON2
5
3.75
2.5
1.25
Maximum -ve Moments
Ratio of M
12.5
10
7.5
5.0
2.5
Thickness in inches

Fig. 10.17

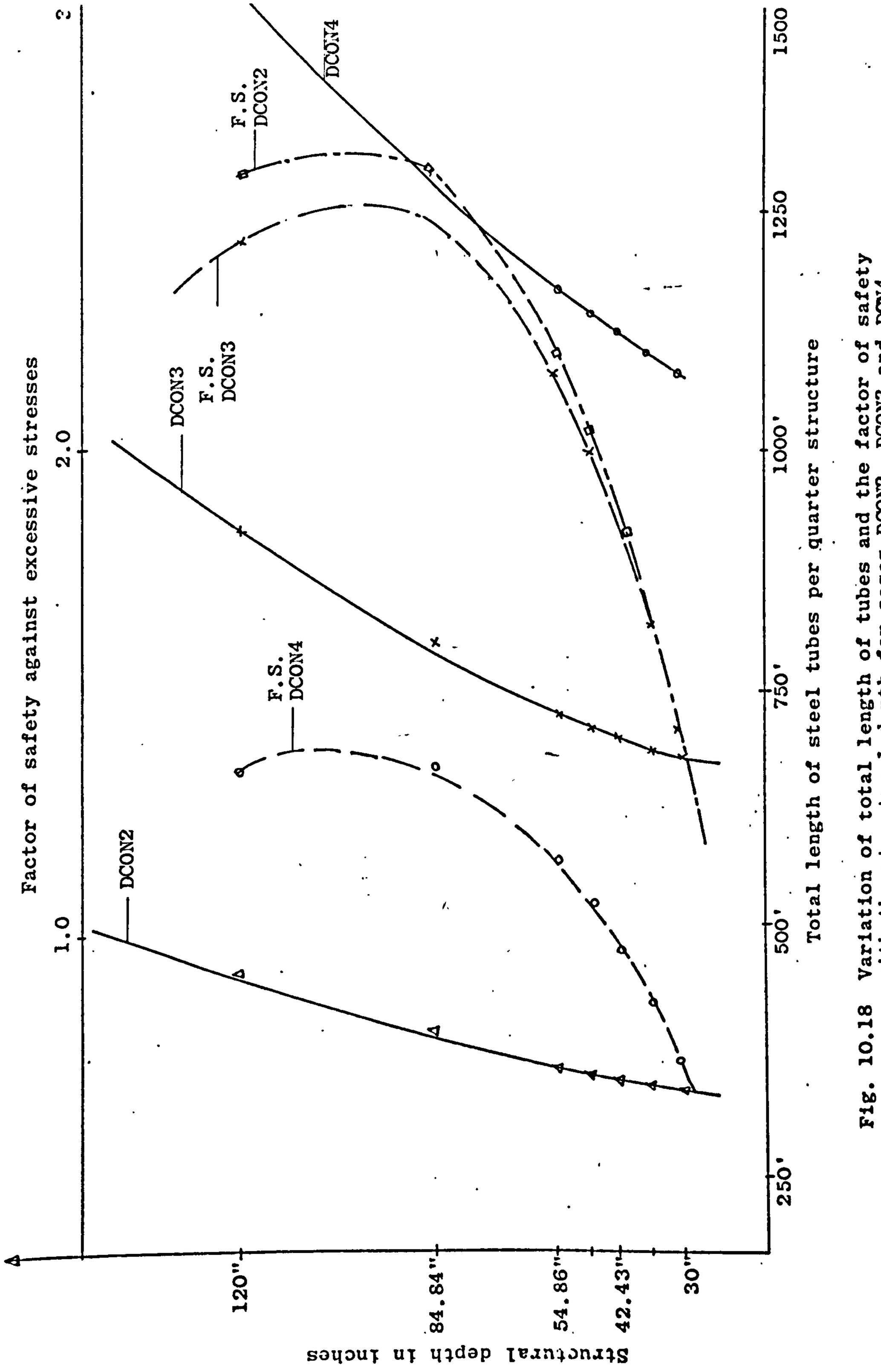

Fig. 10.18 Variation of total length of tubes and the factor of safety with the structural depth for cases DCON2, DCON3 and DCN4

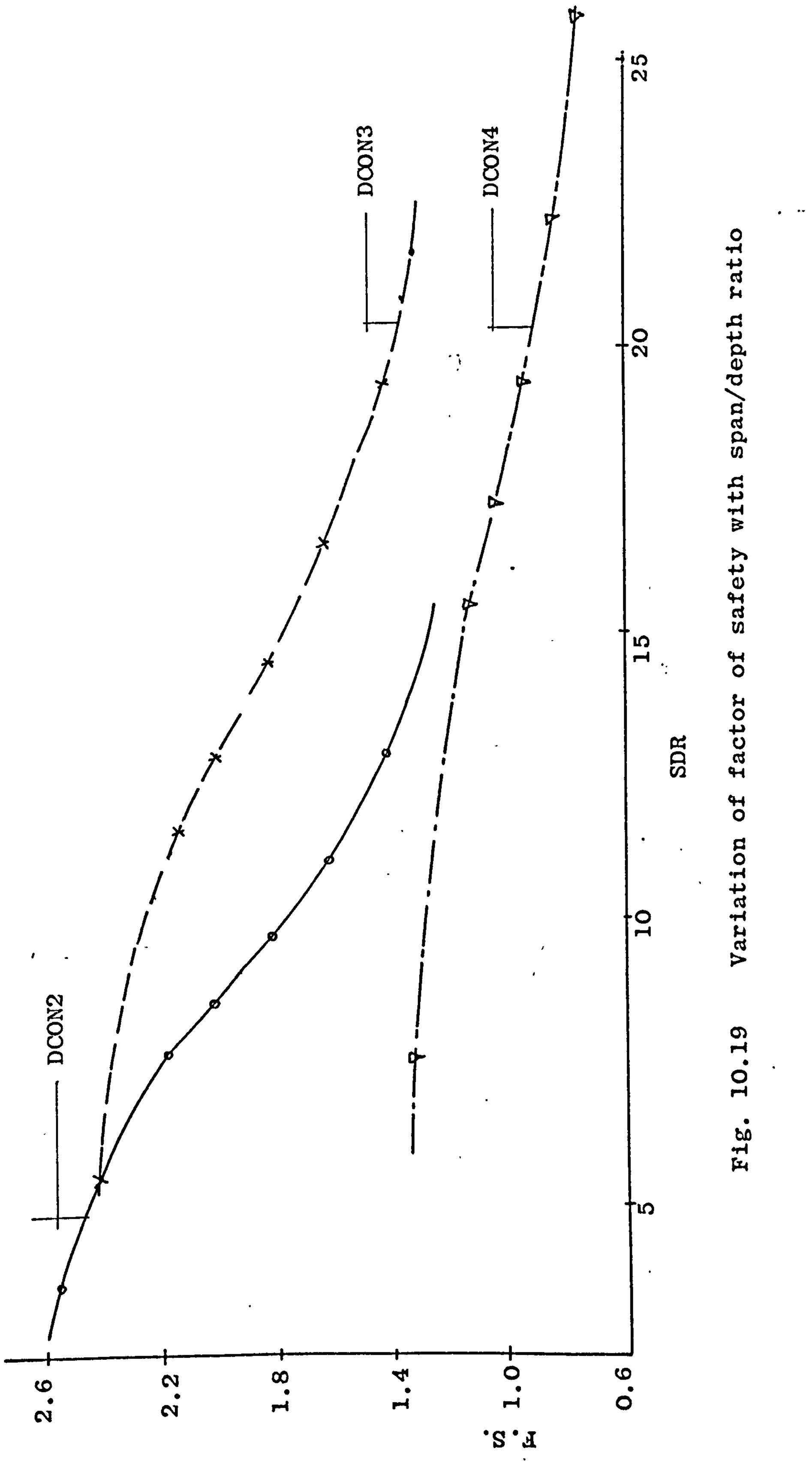

Fig. 10.19 Variation of factor of safety with span/depth ratio

CHAPTER 11

APPROXIMATE ANALYSIS

11.1 Introduction

The difficulties facing the analyst and the designer in the field of space structures was mentioned in Chapter 2 and Chapter 4 as a result of the great demands on computer time and storage. Table 11.1 shows the rate of increase in time used for the five spans studied in this work and also the computer storage used in each case together with the time and storage needed for ordinary doube layer grid of the same configuration and span. This table shows the extent of facilities required to solve problems with such short spans, where the maximum span attempted was made of 10 pyramid units (10 bays) only.

Therefore, the need for quick approximate methods is very clear, so the designer can have a fair idea about the section needed for certain span without resort to the exact analysis.

Many attempts were made during this research to find such methods. Successful attempts only are to be presented in this chapter. These attempts are classified into two categories

I. Methods using computer

II. Methods which do not need computer and based upon plate analogy.

These methods are not claimed to be alternatives to the exact method used in this thesis, but only as tools to be used in the preliminary design. They are based on the

assumptions that

a) The structure is flat and made of two parallel layers.

b) The concrete slab has a moderate thickness.

c) The structure is supported along the four sides.

d) The structure is built of identical units.

11.2 Computer Methods

It was seen in the convergency analysis in para. 6.1 and in Tables 6.1 and 6.2 that the change in axial forces in tubes was negligible during the variation of the finite element meshes. This is because the top layer slab does mainly two functions,

1. To transmit loads to the tubes.
2. To support the structure by giving planar rigidity parallel to that given by the lower tubular layer.

It seems that the use of one finite element per pyramid base (1 x 1 mesh) almost fulfilled these two functions.

These observations led to two methods (1st and 3rd)

1. Using a '1 x 1' F.E. mesh only for the composite structure.
2. Using F.E. method only for the analysis of the structure.
3. Spring analogy method.

11.2.1 Using a 1 x 1 Finite Element Mesh for the Analysis

In this method the composite structure is analysed with only one finite element per pyramid base (1 x 1 mesh). Then the top joint deflections are fed back to the slab problem as constraints. Then the slab alone is analysed using a finer mesh. The results obtained by this method (for the experimental Model I) were not promising, because the moments got were much higher than the exact results for the same mesh. This is due to the larger deflections obtained when using large mesh, as was seen in the

convergency analysis in para 6.1. This is in addition to the fact that this method still needs excessive computer requirements, while the other methods, as will be seen, yield better results with fewer requirements.

11.2.2 Using Finite Elements Only

In this method the slab alone is analysed as a homogeneous slab of thickness 't' giving it the same loading and boundary conditions of the structure as seen in Fig. 11.9b.

This new slab is then analysed using finite elements method only and as a plate bending case only. The moments found by this method are then used to find the axial stresses in the tubes and their equivalent in-plane stresses in the concrete. Any of the two plate analogy methods to be described in para 11.3 can be used for this purpose.

The results of central stresses for the uniform mesh and the 'IRM' composite mesh are shown in Tables 11.3 and 11.4, using the simple slab approach as to be outlined in para 11.4.1, which show they do compare well with the exact results.

11.2.3 Spring Analogy Method

In this method, it is assumed that the concrete slab is resting on springs as seen in Fig. 11.9c, i.e. the slab is related to the tube grid by vertical stiffnesses only.

The tube part of the structure is analysed first, giving it the same boundary and loading conditions as the

conditions are in the whole structure.

So in this case the load attributed to each joint of the tube frame is on a uniformly distribution basis. This in effect assuming as though that the slab has infinite planar and flexural rigidities. This is done by giving the top joints of the tubular frame the freedom to move in the z-direction only. Then after the analysis of the tube frame only, the load at each top joint is divided by the vertical joint displacement which gives the spring stiffness of that joint.

Afterwards, the plate alone is analysed under the same loading conditions, but adding to it structural stiffness matrix, the joint spring stiffnesses from the previous step in their proper locations.

Fig. 11.1, 11.2, 11.3 and 11.4 show the axial forces in tubes found by the use of this method for cases DCON2, DCON3, DCON4 and DCON5, expressed as percentages together with the exact answers. The results according to these figures are excellent, especially in the critical tubes.

The bending moments results found by this method and using the same Finite Element mesh i.e. 2 x 2 mesh, are shown as percentages also in Figs. 11.5, 11.6, 11.7 and 11.8 for slabs of 5 in. thickness and related to cases DCON2, DCON3, DCON4 and DCON5 respectively. The results are very good especially in the central zone which is the important part as far as positive bending moments are concerned. The negative bending moment results are not so good, but since the maximum positive moments are always

larger than the maximum negative ones (except in case DCON2 where in fact the results in both of them are excellent), then this will not affect the overall picture.

The same spring stiffnesses were added to the structural stiffness matrix of different slab thicknesses, the results were also good as long as the slabs were not very thick. But knowing that thicker slabs means less horizontal axial forces in the tubes, so a rerun of the tube frame is necessary. However this did not give the Appropriate answers. Since axial forces in tubes are not noticeably different whether joints are rigid or pin jointed as shown in Table 8.1, therefore spring analogy analysis for the tube frame alone was done on the assumption that the tubes are pin jointed.

Fig. 11.1 showed these results expressed as ratios (not percentages) of the exact results. These results are good, but the moments were not so good because vertical displacements in pin-jointed structures are more than in the rigid jointed structures, hence they have less spring stiffness, which means higher moments in the slab.

In-plane stresses in the slab can be found easily on the assumption that both axial forces and in-plane forces are equal in any section. This is based on the slab analogy assumption and justified according to what was shown to be the case in Tables 10.2, 10.6, 10.10 and 10.11.

Therefore

$$\sigma_c \times t \times b = T$$

where T is the tensile force in the tubes, and in this case let us take the maximum tensile force, t is the slab thickness, and b is the breadth of a half ($\frac{1}{2}$) pyramid base which is counterbalancing one bottom layer tube. Table 11.2 shows % results of the maximum forces, stresses and moments got by the spring analogy method which are very good, except for the in-plane stress in case DCON2 which is expected, and the maximum shear force in case DCON3 which nevertheless does not affect the overall picture as is seen in Fig. 11.2 where it is seen that there are larger shear forces with good prediction, so the max. shear force according to the spring analogy in case DCON3 is 35000 lbs. which is 120% of the maximum shear force in the exact analysis.

The springs-analogy method is very useful for the following reasons.

1. It yields very good results as was seen before.
2. It is very versatile because it can take various shapes and configurations as long as the concrete slab is of uniform and reasonable thickness, and as long as there is reasonable justification for the assumption that there are no displacements at the top joints except those in the z-direction.
3. It needs much less time and storage facilities.
4. Since the plate is analysed for bending conditions only, therefore 3 degrees of freedom are needed only.
5. A further enhancement in this sense is introduced by assuming that the tubes are pin jointed, which means

also the use of 3 degrees of freedom.

6. One-eighth ($\frac{1}{8}$) of the tubular structure only could be analysed, hence giving a greater opportunity for larger span structures.

11.3 Methods Using Plate Analogy

The basis of these methods was really established in Chapter 9 and in Tables 10.2, 10.6, 10.10 and 10.11 which showed clearly that there is a balance between top in-plane forces and bottom axial forces.

Also it was shown in para. 10.3 that there was a tendency for the structure to behave like a slab as long as the spans were not too short.

It was shown also before that the plate analogy is valid mostly in the centre area of the slab. Also it was seen in para. 7.5 that the critical members in such a structure are the diagonal shear members which are located at the supporting pyramids. It was also shown that the maximum shear force in such members is still less than the maximum tensile force (in quantity) in the bottom layer. It can be shown that the stresses in the plate are not high in comparison to the concrete compressive strength. Using the criterion suggested in para. 9.3 for choosing the efficient section and according to equation 9.21, then for the sort of tubes used in the study cases of this research namely $4\frac{1}{2}$ in. of G.7., then a 5 inch concrete slab will be the required thickness. So taking an example case DCON5 from Table 7.1, this case has a span of 100 ft. with SDR = 24 which is the longest span attempted in this research, and is under a uniformly distributed load of 100 psf, then, the max. bending stress = 520 psi, and the max. in-plane stress =-192 psi.

Then the worst case is when

stress = -520 - 192 = -712 psi which is negligible even for plain concrete compressive strength, disregarding the fact that the slab will be reinforced.

This conclusion is further enhanced by the fact that the tube section used in this case is not safe according to Table 10.1 where F.S. = 0.77. This means that in fact if a bigger tube section is to be used then the stresses will be even less.

So in conclusion, if a method is found to predict the maximum external moment acting on the cross-section of the structure, then it will be possible to find the maximum tensile force, and the maximum in-plane stress. Then if a method is found to predict also the max. bending moments in the concrete slab then it will be possible to design the structure on the assumption that the maximum shearing force is equivalent to the maximum tensile force, which is on the safe side.

11.4 Predicting Maximum and Central Tensile Forces, and Maximum and Central in-plane Stresses

Two methods were used

1) Simple slab approach
2) Slab approach, but treating the section as a beam section and finding its Moment of Inertia.

A sketch of a section through a composite uniform mesh structure is shown in Fig. 11.9a. The clear span of the section is 'a,' but because of the high rigidity of the support area it is suggested to take the span as 'a_1' by neglecting the supporting pyramids when trying to find the central tensile and in-plane stresses, while using 'a' for finding the maximum tensile and in-plane stresses. The external moment is found from text books for ordinary thin homogeneous slab of spans 'a' or a_1 as required for similar boundary and loading conditions. As for this research all cases are that of a simply supported square slab under uniformly distributed load, then the moment is[11]

$$m = .0479\, q\, a^2 \qquad \ldots\ldots 11.1$$

where q is the load intensity, and 'a' is the span of the homogeneous slab.

11.4.1 Simple Slab Approach

Referring to Fig. 9.1a and 11.9a, then

$$T = C$$

$$M = T \times h \qquad \ldots\ldots 11.2$$

$$c = \sigma_p \times t \times b \qquad \ldots\ldots 11.3$$

where

b = 60 in. in the uniform mesh configuration, whilst b = 120 in. in the IRM composite structure.

∇_p is in-plane stress

t is slab thickness, and both T and C are in the same orthogonal direction.

But the moment above is for one unit length, therefore

$$M = b \times m = T \times h$$

where m is the moment according to Eq. 11.1

$$\therefore T = \frac{b}{h} \times m \quad \ldots\ldots 11.4$$

Since b, h and m are known then T and C can be found easily.

Table 11.3 shows the results found by this method for the central tensile forces and in-plane stresses for the uniform mesh, and Table 11.4 shows the central tensile and in-plane stresses found by this method for the IRM composite structure. These results compare well with the exact solutions results.

The drawback in this method is that it does not take into consideration the properties of the section so presumably whatever the concrete slab thickness or tubes section, the results will be the same which is not really the case.

11.4.2 Slab Approach Using Sectional Moment of Inertia

This approach is more flexible because it takes into consideration the section properties.

Referring back to para. 9.3. where the procedure

for finding the moment of inertia of the section was laid out. The external moments are found as in the previous method, then the axial tensile force is found from Eq. 9.11b, as

$$P_x = \sigma_{x_s} \times A_s$$

$$P = P_x \sqrt{2}$$

In-plane stress is found from eq. 9.11a. As mentioned in sub para. 10.2.2 in defining the span/depth ratio 'SDR', the depth needs to be defined clearly, therefore two attempts were made to define the centre to centre depth of the section 'h'.

a) $h = d_1$ where d_1 is the z-coordinate of the diagonal shear member as given in the data for the exact method, or

b) $h = d_1 + t/2$ 11.5

for the same arguments used in defining 'SDR', needless to say that the depth (d) needed in 'SDR' was the total depth and not the centre to centre depth.

Definition (b) yielded better results, as is seen in Table 11.5 which shows the results for the uniform mesh by these two definitions. The results compare well with the exact ones especially for moderate concrete slab thicknesses. Hereafter, the centre to centre depth will be as defined in 'b' above.

Table 11.6 shows the results obtained for different depths of cases DCON2 and DCON3 which compare well with the exact results also.

Table 11.7 shows maximum axial tension in tubes and maximum in-plane stresses for various spans and depths of the uniform mesh. Table 11.7 also shows the results of rectangularly shaped uniform meshes which are

DCON2R which is 3 x 2 pyramids (bays)

and DCON2R1 which is 4 x 2 pyramids (bays)

Their results compare also well except the in-plane stresses as expected due to their very short span.

Table 11.8 shows the results for the 'IRM' composite mesh for the central stress of different spans, depths and slab thicknesses. The results compare well with exact ones, except for thick concrete slabs (DCON3A2, DCON3A3, and DCON3A4).

Table 11.9 shows the results for the 'IRM' composite mesh also, but for maximum stresses, for various spans. This comparison is also good.

Finally a note worth mentioning is that Table 11.7 for the uniform mesh cases and Table 11.9 for the 'IRM' composite cases show that maximum shear forces are always less than the maximum tensile forces except for cases DCON2 and DCON2A which have very short spans. This relation is expressed by $^{C}/_{T}$.

The same two tables show that the ratio '$\frac{C_c}{P}$' between the corner shear force and the central tensile force is near unity for the uniform mesh cases, but substantially less than that for the 'IRM' composite cases. Therefore the designer will have a rather fair idea about the steel part of the structure.

11.5 Predicting the Maximum Positive Bending Moment in the Concrete Slab

Fig. 11.9a shows a section through a uniform mesh. The approximate method suggested for predicting the maximum positive moment is also based on slab analogy.

Fig. 11.10a illustrates the basis of this method. According to this method it is assumed that there are roughly three independent factors contributing to positive bending moment in the concrete slab.

1. The overhang effect due to $(\frac{b}{2})$.
2. The continuity effects which is determined by both the clear span and the depth of the structure.
3. The inter joints effects which is related to the number of joint connections (i.e. pyramids). and also to where the centre of gravity of the section is.

Thus two formulas were made for two cases

a) when the slab is thick, this is determined by the use of Eq. 9.13 for finding the efficient section as described in para. 9.3.

b) when the slab is thin.

The formulae are

$$I - M = \left[\frac{b^2}{8} + \frac{0.0479\ a^2}{d} + (t-t_o)(Np - 1)\right] \quad q \qquad \ldots\ 11.6$$

used for condition (a)

$$II - \quad M = \left[\frac{b^2}{8} + \frac{0.0479\ a^2}{d} + (t - t_o)\right] \quad q \qquad \ldots\ 11.7$$

used for condition (b).

where b, a and t are as shown in Fig. 11.9a.

d is the total depth of the structure as defined in Eq. 10.3 when span/depth ratio was defined.

i.e. $$d = h + t + \frac{D}{2} \qquad \text{.... 10.3}$$

In fact the definition of 'd' does not make very much difference because its effect is small in comparison with other factors.

t_o is the efficient thickness for the steel tubes used, Eq. 11.6 is valid when $t \geqslant t_o$, while Eq. 11.7 is valid when $t \leqslant t_o$. t and t_o are as shown in Fig. 9.1b. Np is the number of pyramids along the span, and 0.0479 is a coefficient taken from Timoshenko[11] for finding central bending moments in a square simply supported slab under uniformly distributed loading. In the above two equations, the first term stands for the overhang effects, the second term for continuity effects, and the third term for the inter joints effects. The third terms were found by trial and error. t_o is found as follows.

$$C = \frac{h}{1 + \frac{E_c \times b \times t}{E_s \times A_s}} \qquad \text{.... 9.13}$$

where h is the centre to centre depth, and where C is defined in Fig. 9.2. For an efficient section C should be equal to $\frac{t_o}{2}$.

$$\therefore C = \frac{t_o}{2}$$

and the centre to centre distance will be as defined in Eq. 11.5.

$$h = d_1 + \frac{t_o}{2} \qquad \text{.... 11.5}$$

d_1 is the z-coordinate of the diagonal shear member.

Eq. 9.13 becomes

$$\frac{t_o}{2} = \frac{d_1 + \frac{t_o}{2}}{1 + \frac{E_c \times b}{E_s \times A_s} \times t_o}$$

Let $\frac{E_c \times b}{E_1 \times A_s} = k$

$$\therefore t_o^2 = \frac{2d_1}{k}$$

$$t_o = \sqrt{\frac{2}{k} \quad d_1} \qquad \ldots\ldots 11.8$$

Table 11.10 shows the results obtained by using those two formulae for cases of span 40 ft. with different slab thicknesses and structural depth. Table 11.11 shows the results for cases with span 60 ft., also with different depths and thicknesses and even with different tubes cross-sections. Table 11.12 shows the results for a span of 80 ft. also with different depths and thicknesses. Table 11.13 shows the results for a span of 100 ft. for the only two slab thicknesses analysed by the exact method (due to the excessive computer requirements).

The formulae used for the IRM composite cases are the same as for the 'Uniform Mesh', i.e. Eq. 11.6 when $t \geqslant t_o$ and when $t \leqslant t_o$ then Eq. 11.7 is valid. Table 11.14 shows the results for IRM composite structures with different spans, depths and plate thicknesses.

It is noticed from all the above tables that the approximate results compare very well with the exact ones.

11.6 Predicting Maximum Negative Bending Moment in the Concrete Slab

If the top concrete slab is considered as a flat slab resting on rigid columns (which naturally it is not), then flat slab analysis could be utilized. For a flat slab made of square panels as seen in Fig. 11.10b, assuming $a_o = b_o$ and $\frac{U}{a_o} = 0.1$ then the maximum negative moment near the columns is[11]

$$M = 0.196\ q\ a_o^2 = -1960 \text{ lb.in.}$$

where q = 100 psf, and a_o = 10 ft.

It is noticed that the moment here does not depend on the span of the structure, this is because the supports are rigid columns. Therefore this equation could be used in very short spans only where there might be some justification and where the maximum negative moment is usually larger than the maximum positive moment. Looking back to tables 10.7, 10.8 and 10.9 this formula will be useful only in cases DCON20, DCON2, DCON30 and DCON40 where the -ve moment is more than the positive one and where 1960 is larger than the four -ve moments in the mentioned cases. So the intention is to utilize this formula only when it yields larger moments (quantitatively) than the +ve max. moments found in para 11.5.

11.7 Design Procedure Using the Approximate Methods

An outline of a procedure is to be given below, utilizing the various approximate methods suggested in this chapter.

Given that the span and loading is known, and assuming the structure is simply supported along the four sides, then the section properties will be determined as follows

I. The prismatic part of the structure

1. A hypothetical equilateral pyramid is chosen, which divides the span into equal bays, and at the same time does not give a very deep or very shallow structure. This is determined by architectural, economical and practical considerations.

2. Using the approximate method suggested in para. 11.4.1, the maximum tensile force (T) can be found.

3. Assuming that the maximum shear force is equal to the maximum tensile force just found, then a section is chosen such that diagonal shear members will be under safe compressive load conditions. This section will be the typical one, if it is desired to have all tubes of the same section (A_s).

II The slab part of the structure

1. The thickness of the slab is chosen through the use of Eq. 9.21, since A_s and h are now known.

2. The maximum in-plane stress (σ_{pm}) is found by the use of Eqs. 9.11a or 11.4 assuming C = T.

3. The maximum positive bending moment ($+M_m$) is found through the use of the method in para. 11.5.

4. The maximum negative moment is found as suggested in para. 11.6.

5. The highest absolute value from steps (3) and (4) is taken as the maximum moment in the slab, and the bending stress (σ_{bm}) is found accordingly.

6. The slab flexural strength is checked for a bending stress of (σ_{bm}), and for compressive strength of (σ_{pm}).

If the stresses are found to be very low, and if practical considerations permit, then the thickness is reduced reasonably and the procedure repeated from Point II-2 above. If the stresses proved to be very high, then more reinforcement is added to the reinforced concrete slab if possible, otherwise slab thickness increased accordingly.

TABLE 11.1

TIME AND STORAGE USED FOR THE STUDY CASES

Structure	No. of Pyramids	C.D.L.G. of Uniform Mesh			D.L.G. with rigid joints			D.L.G. with pin joints		
		Band width	storage used	time used secs.	Band width	storage used	time used secs.	Band width	storage used	time used secs.
1. DCON2	4	108	36K	111	66	36K	59	33	36K	12
2. DCON3	6	144	60K	335	84	36K	83	42	36K	19
R		1.33		3.02	1.27		1.41	1.27		1.58
3. DCON4	8	180	130K	824	102	36K	180	51	36K	34
R		1.67		7.42	1.55		3.05	1.55		2.83
4. DCON5	10	216	230K	1542	120	60K	330	60	36K	55
R		2		13.9	1.82		5.59	1.82		4.58

TABLE 11.2

SPRING ANALOGY RESULTS SHOWN IN % RATIO OF EXACT RESULTS

Case	SPAN ft.	Exact Analysis				% Approximate/Exact			
		Tubes		Concrete		Tubes		Concrete	
		Max. Tensile force	Max. shear force	Max. Bending Moment	Max. in-plane stress	Max. tensile force	Max. shear force	Max. Bending Moment	Max. in-plane stress
1. DCON2	40	13602	-25409	-1631	-63 -32	100	98	100	49
2. DCON3	60	28214	-25436	1529	-68.3 -66.5	89	28*	93	97
3. DCON4	80	50835	-48553	1813	-123.8 -120	98	98	98	97
4. DCON5	100	82333	-60544	2167	-192.3 -194	96	99	97	100

* This is the only odd result but it does not make a difference to the whole picture of DCON3 because there are higher shear forces with much better results.

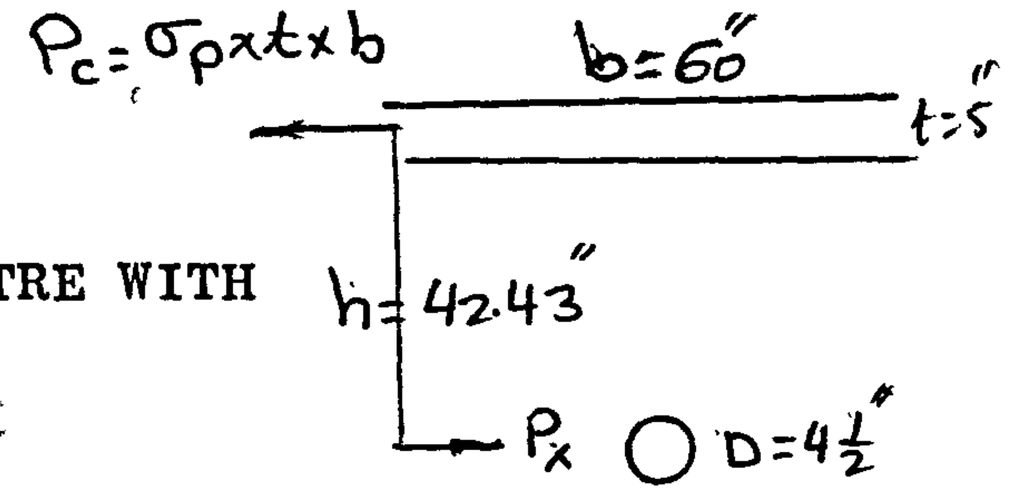

TABLE 11.3

COMPARISON OF APPROXIMATE METHODS RESULTS FOR THE CENTRE WITH THE EXACT RESULTS 'THE UNIFORM MESH'

No.	Name of case and its span in ft.	Exact results			Results of Approximate Methods							
		Steel tubes		Concrete	Plate analogy simple method			Plate alone using Finite Elements			Springs method	
		P	$P_x = P/2$	P_c	Force P_{AX}	Percentage of $\frac{P_{AX}}{P_x}$	Percentage of $\frac{P_{AX}}{P_c}$	Force P_{AX}	Percentage of $\frac{P_{AX}}{P_x}$	Percentage of $\frac{P_{AX}}{P_c}$	Tube force P_A	% $\frac{P_A}{P}$
1	DCON2 (40)	12453	8804	- 5820	6086	69	105	7706	87	132	12452	100
2	DCON3 (60)	21860	15455	-16050	16906	109	105	18164	117	113	23678	108
3	DCON4 (80)	41068	29035	-32460	33135	114	102	33444	115	103	39638	97
4	DCON5 (100)	62023	43850	-53100	54775	125	103	53550	122	100	59808	96.4

TABLE 11.4

COMPARISON OF APPROXIMATE METHOD RESULTS FOR THE CENTRE FORCES WITH THE EXACT RESULTS, THE 'IRM' COMPOSITE STRUCTURE

No.	Name of case and its span in ft.	Exact Results			Results of Approximate methods					
		Tubes		Concrete	Plate Analogy simple method			Plate alone using Finite Elements		
		P	$P_x = P/\sqrt{2}$	$P_c = \sigma_p x t x b$	Force P_{AX}	Percentage		Force P_{AX}	Percentage	
						$\frac{P_{AX}}{P_x}$	$\frac{P_{AX}}{P_c}$		$\frac{P_{AX}}{P_x}$	$\frac{P_{AX}}{P_c}$
1	DCON2A (40)	21657	15312	-11100	12172	80	110	15412	100	139
2	DCON3A (60)	44429	31411	-30360	33812	108	111	36328	116	120
3	DCON4A (80)	80207	56706	-60960	66270	117	109	66888	118	110
4	DCON5A (100)	123056	87000	99000	109550	126	111	107100	123	108

TABLE 11.5

RESULTS OF APPROXIMATE METHODS FOR CENTRAL FORCES USING PLATE ANALOGY AND SECTIONAL MOMENT OF INERTIA AND THEIR COMPARISON WITH THE EXACT RESULTS FOR DIFFERENT PLATE THICKNESSES OF 'THE UNIFORM MESH'

Nos.	Case, span and plate thickness	Exact results		Approximate external moment = $0.0479qa^2$		App. Method I (d = h = 42.43)				Method II $_t$ (d = h + $t/2$)		
		Steel	Concrete			Steel	Concrete	Percentage		Steel	Percentage	
		P_x	p	Span ft.	Moment lb.in/in.	P_{AX}	σ_c	$\frac{P_{AX}}{P_x}$	$\frac{\sigma_c}{\sigma_p}$	P_{AX}	$\frac{P_{AX}}{P_x}$	$\frac{\sigma_c}{\sigma_p}$
I	t = 5 ins.											
1	DCON2 (40 ft.)	8804	- 19.4	30	4311	5966	- 19.7	68	101	5649	64	97
2	DCON3 (60 ft.)	15455	- 53.5	50	11975	16572	- 54.6	107	102	15686	101	98
3	DCON4 (80 ft.)	29035	-108	70	23471	32481	-107	112	99	30745	106	95
4	DCON5 (100 ft.)	43850	-179	90	38799	53692	-177	122	100	50824	116	96
II	t = 7.5 ins.											
1	DCON21	7863	- 11.6			5700	- 12.7	73	109	5291	67	101
2	DCON31	14219	- 32	No change		15834	- 35.3	111	110	14698	103	102
3	DCON41	26929	- 66.3	in moments		31036	- 69	115	104	28809	107	97
4	DCON51	40918	-109.5			51304	-114.3	125	104	47622	116	97
III	t = 10 ins.											
1	DCON22	6712	- 7.3	No change		5251	- 8.7	78	120	4830	72	111
2	DCON32	12295	-20	in moments		14587	-24.3	119	121	13419	109	112
3	DCON42	23667	-43			28590	-47.6	121	111	26301	111	102
IV	t = 12.5 ins.											
1	DCON23	5572	-4.6	No change		4649	-6.2	83	135	4297	77	125
2	DCON33	10100	-12.5	in moments		12915	-17.2	128	138	11936	118	128

TABLE 11.6

APPROXIMATE CENTRAL RESULTS FOR VARIOUS DEPTHS AND SPANS OF THE 'UNIFORM MESH'

No.	Case	Structural depth in inches	Exact results		Plate analogy using method (b)					
			Steel	Concrete	Span a_1	External Moment $= 0.0479qa_1^2$	Steel	Concrete	Percentage	
			P_X	σ_p			P_{AX}	σ_c	$\frac{P_{AX}}{P_x}$	$\frac{\sigma_c}{\sigma_p}$
I	Span 40ft				30	4311				
1	DCON2S	30	11312	-23			7672	-25.5	68	110
2	DCON2D	54.86	7298	-16			4458	-15	61	93
II	Span 60ft				50	11975				
1	DCON3S	30	20385	-71.5			21311	-71	105	99
2	DCON3D	54.86	12597	-43			12383	-41	98	96

TABLE 11.7

THE MAXIMUM TENSILE AND IN-PLANE APPROXIMATE RESULTS USING PLATE ANALOGY FOR VARIOUS DEPTHS, SPANS, AND SHAPES OF THE 'UNIFORM MESH'. (plate thickness = 5 inches)

Nos.	Case	Structural depth ins.	Exact results		Approximate results using method (b)					
			Steel	Concrete	Span 'a' ft.	External Moment $0.0479qa^2$	Steel	Concrete	Percentage	
			T	σ_{pm}			T_A	σ_{cm}	$\frac{T_A}{T}$	$\frac{\sigma_{cm}}{\sigma_{pm}}$
1	DCON2	42.43	13602	- 63	40	7663	14197	-33.4	104	53
2	DCON3	"	28214	- 68.3	60	17244	31944	-75.2	113	110
3	DCON4	"	50835	-123.8	80	30656	56790	-134	112	108
4	DCON5	"	82333	-192.3	100	47900	88734	-209	107	109
5	DCON2S	30	17594	- 84.2	40	7663	19286	-45.4	110	54
6	DCON2D1	54.86	11162	- 51	"	"	11206	-26.4	100	52
7	DCON3S	30	36941	- 92.3	60	17244	43399	-102	117	111
8	DCON3D1	54.86	22907	- 54.2	"	"	25217	-59.4	110	110
9	DCON2R (3 Bays x 2 Bays)	42.43	18550	- 82.5	40	12992	17979	-25	97	30
10	DCON2R1 (4 Bays x 2 Bays)	"	22462	- 57.4	"	16272	22435	-23.4	100	41
11	DSPRING6	"	116874	-275.5	120	68975	127778	-301	109	109

N.B. The external moment for case No. 9 is $m = 0.0812\ qa^2$

The external moment for case No.10 is $m = 0.1017\ qa^2$

The exact results for case No. 11 is really by spring analogy and therefore not exact, because the problem was too big for the available computer facilities.

TABLE 11.8

THE CENTRAL APPROXIMATE RESULTS FOR THE 'IRM' COMPOSITE STRUCTURE WITH DIFFERENT SPANS, DEPTHS AND PLATE THICKNESSES USING PLATE ANALOGY AND SECTIONAL MOMENT OF INERTIA.

Nos.	Case	Thickness ins.	Span ft.	Exact results			Approximate method (b)				
				Concrete	Steel	Span ft.	External Moment lb.in/in. $m = 0.0479qa_1^2$	Concrete	Steel	Percentage	
				σ_p	P_x			σ_c	P_{xs}	$\frac{P_{xs}}{P_x}$	$\frac{\sigma_c}{\sigma_p}$
1	DCON2A	5	40	- 18.5	15311	30	4311	-19	11397	77	103
2	DCON3A	"	60	- 50.6	31411	50	11975	-52.62	31659	100	104
3	DCON4A	"	80	-101.6	56706	70	23471	-103	62051	109	102
4	DCON5A	"	100	-165	87000	90	38799	-170.5	102574	118	103
1	DCON3A1	7.5	60	- 28.1	26580	50	11975	-31.5	28397	107	112
2	DCON3A2	10	"	- 16	20605	"	"	-20.4	24448	119	128
3	DCON3A3	12.5	"	- 8.7	15232	"	"	-13.5	20282	133	155
1	DCON3AS (h = 30in)	5	60	- 65.5	40236	50	11975	-68.4	41015	102	104
2	DCON3A	"	"	- 50.6	31411	"	"	-52.62	31659	100	104
3	DCON3AD1 (h=54.86)	"	"	- 41.3	25800	"	"	-39.9	25102	97	97
1	DCON2AS	5	40	- 23	19068	30	4311	-24.6	14765	77	107
2	DCON2A	"	"	- 18.5	15311	30	4311	-19	11397	74	103
3	DCON2AD1	"	"	- 15.6	12783	"	"	-14.4	9037	71	92

TABLE 11.9

MAXIMUM APPROXIMATE RESULTS FOR THE 'IRM' COMPOSITE STRUCTURE WITH DIFFERENT SPANS

No.	Case	Exact results		Approximate results, method (b)					
		Steel	Concrete	Span a_1 ft.	External Moment = $0.0479qa_1^2$	Steel	Concrete	Percentage	
		T lbs.	σ_{pm} psi			T_A lbs.	σ_{cm} psi	$\frac{T_A}{T}$	$\frac{\sigma_{cm}}{\sigma_{pm}}$
1	DCON2A	21653	-57.1	40	7663	28650	-33.7	132	59
2	DCON3A	50032	-81.4	60	17244	64472	-76	122	93
3	DCON4A	94251	-133.6	80	30656	114618	-135	122	101
4	DCON5A	154989	-201	100	47899	179086	-211	116	105

TABLE 11.10

APPROXIMATE MAXIMUM POSITIVE BENDING MOMENTS RESULTS FOR THE 'UNIFORM MESH' WITH VARIOUS DEPTHS AND PLATE THICKNESSES BUT WITH A SPAN OF 40 FT.

No.	Case	Structural depth h	Plate thick-ness t	Total depth $d = h+t+\frac{D}{2}$	Efficient thickness t_o	Exact Max. +ve Moment M	Approximate method			% $\frac{M_A}{M}$
							$\frac{0.0479qa^2}{d}$ =76.64/d	M_A		
								Case 1 $t > t_o$	Case 2 $t < t_o$	
1	DCON20	42.43	2.5	47.18	5.03	1187	1.62		1160	98
2	DCON2	"	5.0	49.68	"	1369	1.54		1405	103
3	DCON21	"	7.5	52.18	"	1939	1.47	2138		110
4	DCON22	"	10.5	54.68	"	2832	1.40	2882		102
5	DCON23	"	12.5	57.18	"	3848	1.34	3626		94
6	DCON2S	30	5	37.25	4.23	1571	2.06	1688		108
7	DCON2S1	36.22	"	43.47	4.65	1448	1.76	1530		106
8	DCON2D	48.65	"	55.9	5.39	1317	1.37		1349	102
9	DCON2D1	54.86	"	62.11	5.72	1280	1.23		1302	102

TABLE 11.11

APPROXIMATE RESULTS FOR MAXIMUM POSITIVE BENDING MOMENTS FOR CASES WITH A SPAN OF 60 FT. OF THE 'UNIFORM MESH' TYPE WITH VARIOUS PLATE THICKNESSES, DEPTHS AND TUBES CROSS-SECTIONS

TYPE I: when $t > t_o$ then B.M. $= \left[\frac{b^2}{8} + \frac{0.0479a^2}{d} + (t - t_o)(Np-1) \right] q$

TYPE II: when $t < t_o$ then B.M. $= \left[\frac{b^2}{8} + \frac{0.0479a^2}{d} + (t - t_o) \right] q$

No.	Case	Structural depth h	Plate thickness t	Tube's outside diameter D	Effective depth d	Exact Max. Bending Moment M in lb.-in.	Efficient plate thickness t_o	$\frac{0.0479a^2}{d} = \frac{172.44}{d}$	Approximate B.M. Type I M_A	Approximate B.M. Type II M_A	% $\frac{M_A}{M}$
A	t_b=0.176										
1	DCON3	42.43	5	$4\frac{1}{2}$	49.68	1529	5.03	3.45		1593	104
2	DCON31	"	7.5	"	52.18	2559	"	3.304	2816		110
3	DCON32	"	10	"	54.68	4161	"	3.154	4050		97
4	DCON33	"	12.5	"	57.18	6033	"	3.02	5288		88
B											
5	DCON3S	30	5	"	37.25	1938	4.23	4.63	2098		108
6	DCON3S1	36.22	"	"	43.47	1687	4.65	3.97	1822		108
7	DCON3D	48.65	"	"	55.9	1425	5.39	3.08		1520	107
8	DCON3D1	54.86	"	"	62.11	1446	5.72	2.78		1456	100
9	DCON3D2	84.86	"	"	92.11	1135	7.12	1.87		1225	108
C											
10	DCON3M1 (t_b=0.212)	42.43	"	"	49.68	1450	5.51	3.45		1545	106
11	DCON3M2 (t_b=0.252)	"	"	"	"	1390	5.95	3.45		1500	108
D											
12	DCON3M3 (t_b=0.176)	"	"	$5\frac{1}{2}$	50.18	1434	5.58	3.44		1537	107
13	DCON3M4 (t_b=0.176)	"	"	$6\frac{5}{8}$	50.74	1358	6.154	3.40		1475	109

TABLE 11.12

APPROXIMATE MAXIMUM POSITIVE BENDING MOMENTS FOR THE 'UNIFORM MESH' WITH A SPAN OF 80 FT. BUT WITH DIFFERENT PLATE THICKNESSES, DEPTHS, AND STEEL TUBES CROSS SECTIONS

Nos.	Cases	Structural depth h	Plate thickness t	Effective depth d in. in.	Exact max.+ve moment M lb.in.	Efficient plate thickness t_o	Approximate B.M.			%
							$\frac{0.0479a^2}{d} = \frac{306.56}{d}$	Type I $t > t_o$ M_A lb_in	Type II $t < t_o$ M_A lb_in.	$\frac{M_A}{M}$
1	DCON4	42.43	5	49.68	1813	5.03	6.17		1865	103
2	DCON41	"	7.5	52.18	3544	"	5.88	3570		100
3	DCON42	"	10	54.68	6305	"	5.61	5290		84
4	DCON4B ($D=5\frac{1}{2}$)	"	5	50.18	1487	6.61	6.11		1700	114
5	DCON4S	30	"	37.25	2513	4.23	8.23	2612		104
6	DCON4S1	36.22	"	43.47	2079	4.65	7.05	2200		106
7	DCON4D	48.65	"	55.9	1638	5.39	5.48		1759	107
8	DCON4D1	54.86	"	62.11	1613	5.72	4.94		1672	104

N.B. All cases have D = $4\frac{1}{2}$ in., t_b = 0.176 in., steel tube area A_s = 2.39, except case No. 4 (DCON4B) which has D = $5\frac{1}{2}$ in., t_b = 0.25 in., and A_s = 4.12 in.

TABLE 11.13

APPROXIMATE MAXIMUM BENDING MOMENTS RESULTS FOR THE 'UNIFORM MESH' WITH SPAN OF 100 FT.

No.	Case	Plate thickness t	Total depth $d = h+t+\frac{D}{2}$	Effective thickness t_o	Exact Max. +ve Moment M	Approximate method			
						$\frac{0.0479qa^2}{d}$ = 479/d	M_A		% $\frac{M_A}{M}$
							Case 1 $t > t_o$	Case 2 $t < t_o$	
1	DCON5	5	49.68	5.03	2167	9.64		2212	102
2	DCON51	7.5	52.18	5.03	4657	9.18	43911		94

TABLE 11.14

'IRM' COMPOSITE STRUCTURE THE EXACT RESULTS WITH THE APPROXIMATE ONES FOR VARIOUS DEPTHS, SPANS AND PLATE THICKNESS

Nos.	Cases	Span ft.	Structural depth h	Plate thickness t	Effective depth $d = h+t+\frac{D}{2}$ in.	Exact max.+ve moment M lb.in.	Effective Plate thickness t_o	Approximate B.M. $\frac{0.0479a^2}{d}$	Approximate B.M. Type I $t > t_o$ M_A lb.in.	% $\frac{M_A}{M}$
1	DCON2A	40	42.43	5	49.68	1529	3.56	1.54	1842	120
2	DCON3A	60	"	"	"	1935	"	3.45	2325	120
3	DCON4A	80	"	"	"	2449	"	6.17	2889	118
4	DCON5A	100	"	"	"	3174	"	9.64	3528	111
5	DCON2AS	40	30	"	37.25	1881	3.34	2.06	1954	104
6	DCON2AD1	40	54.86	"	62.11	1365	4.31	1.23	1580	116
7	DCON3A1	60	42.43	7.5	52.18	3538	3.56	3.3	3550	100
8	DCON3A2	60	"	10	54.68	5688	3.56	3.15	4785	84
9	DCON3AS	60	30	5	37.25	2588	3.34	4.63	2533	98
10	DCON3AD1	60	54.86	"	62.11	1632	4.31	2.78	1873	115

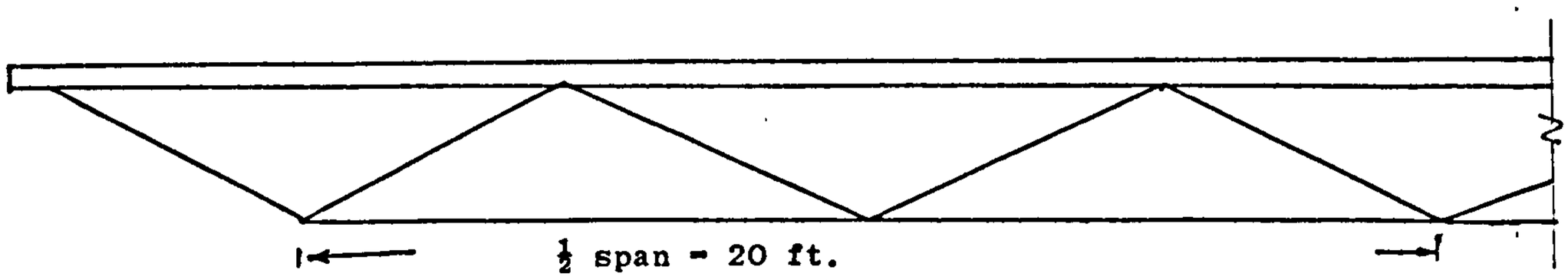

a) Section through D CON 2

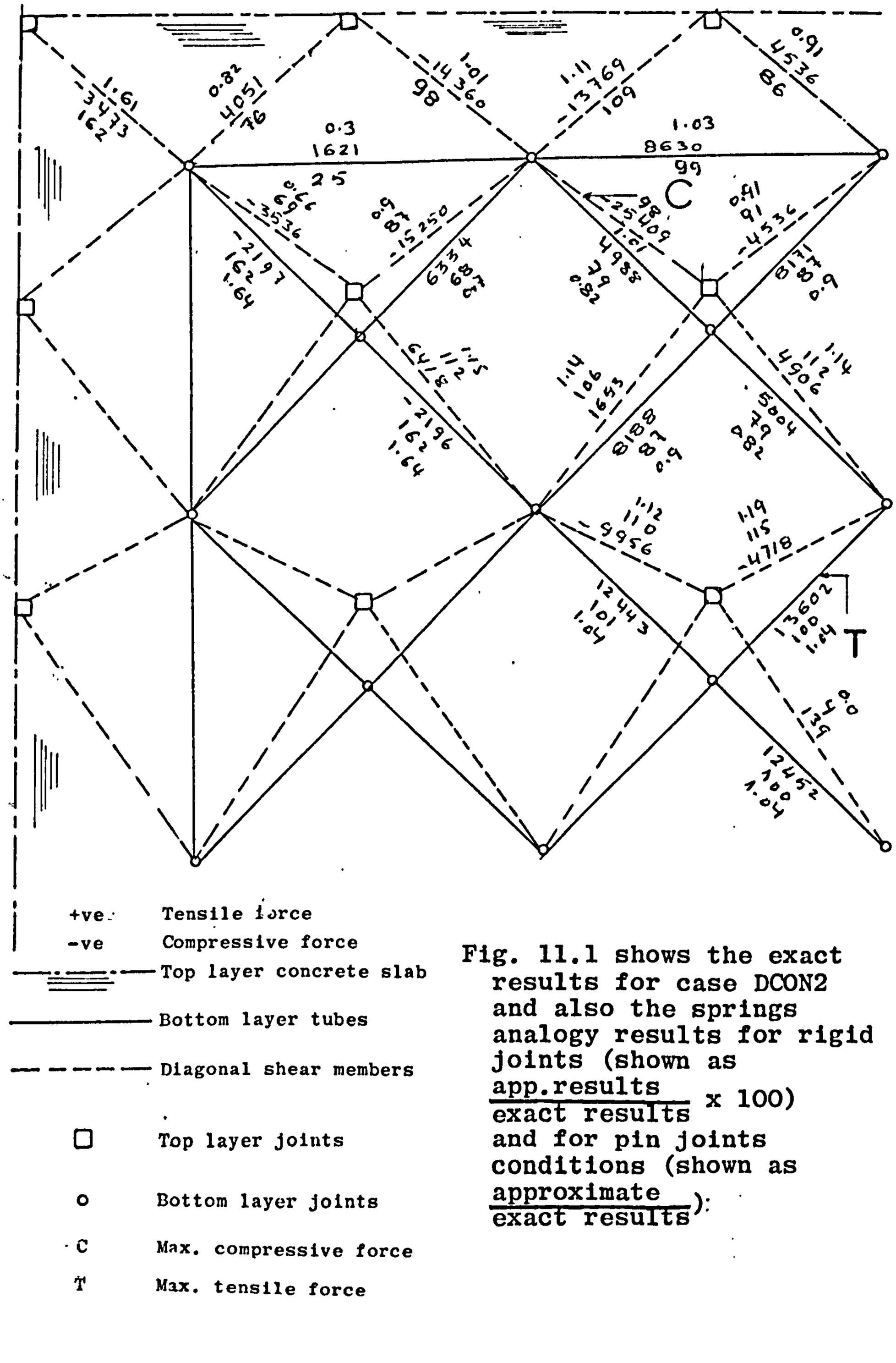

+ve Tensile force

-ve Compressive force

Top layer concrete slab

Bottom layer tubes

Diagonal shear members

Top layer joints

Bottom layer joints

C Max. compressive force

T Max. tensile force

Fig. 11.1 shows the exact results for case DCON2 and also the springs analogy results for rigid joints (shown as $\frac{\text{app.results}}{\text{exact results}} \times 100$) and for pin joints conditions (shown as $\frac{\text{approximate}}{\text{exact results}}$):

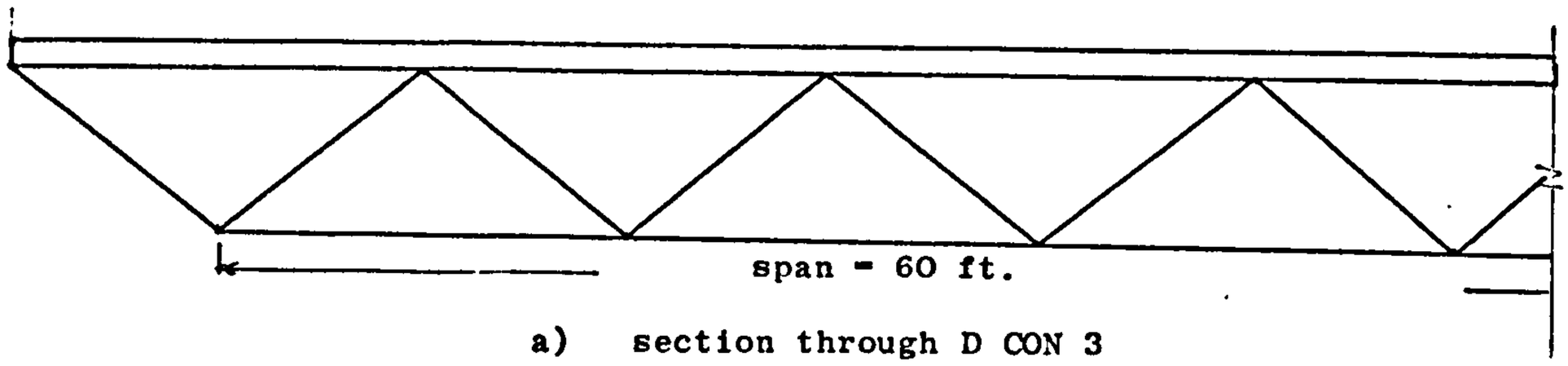

a) section through D CON 3

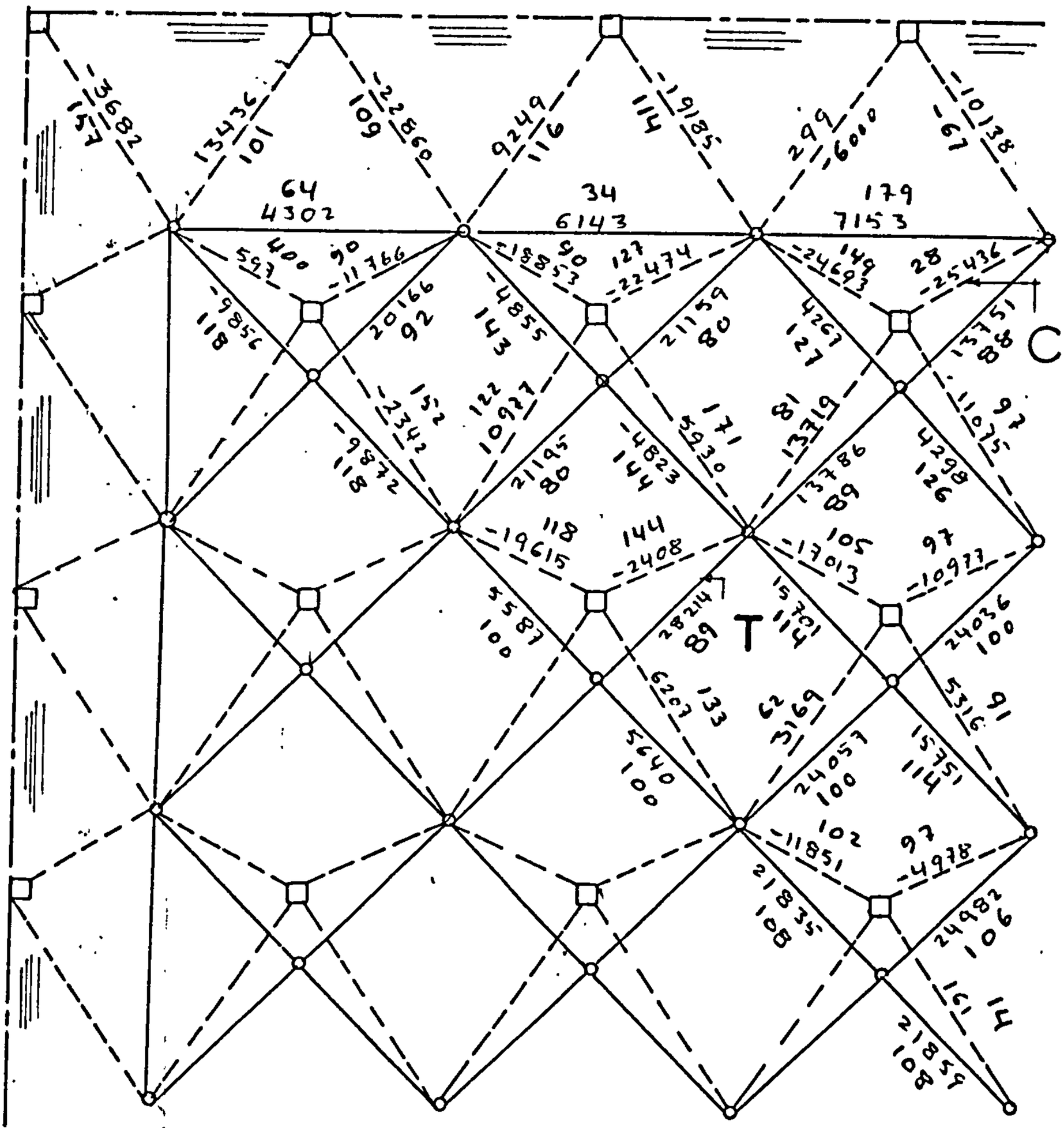

+ve Tensile force

-ve Compressive force

Top layer conc. slab

Bottom layer tubes

Diagonal shear members

Top layer joints

Bottom layer joints

C Max. compressive force

T Max. tensile force

Fig. 11.2 shows the exact results for case DCON3, and also the springs analogy results for rigid joints. Condition shown as percentages

$$\left(\frac{\text{app. results}}{\text{exact results}} \times 100\right)$$

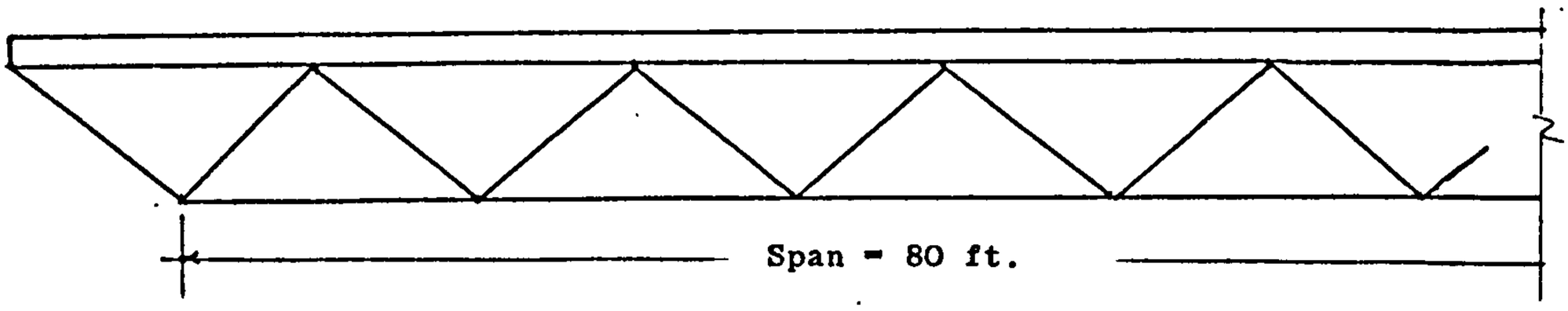

a) Section through D CON 4

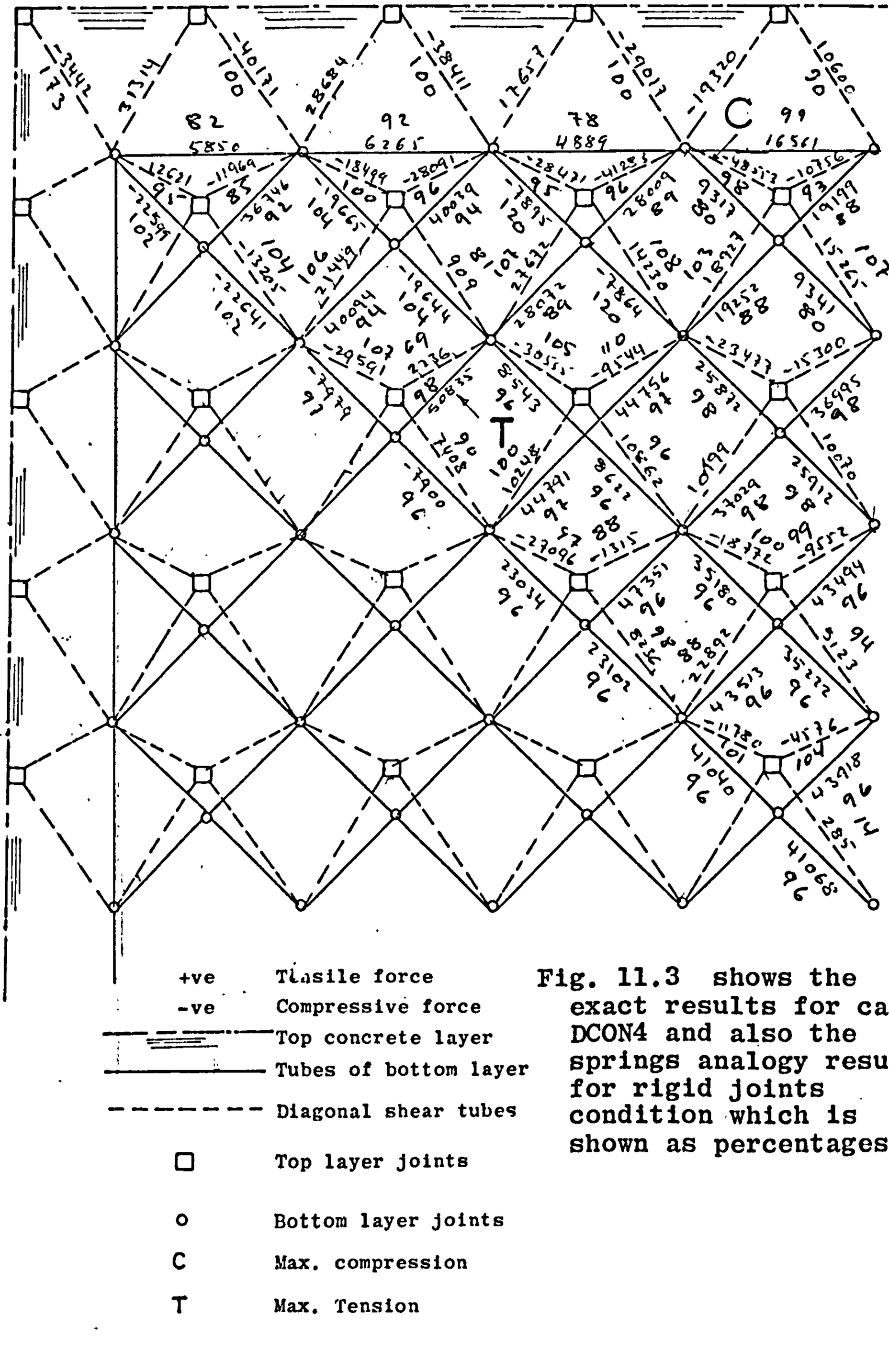

+ve Tensile force
-ve Compressive force

Top concrete layer
Tubes of bottom layer
Diagonal shear tubes

□ Top layer joints

o Bottom layer joints

C Max. compression

T Max. Tension

Fig. 11.3 shows the exact results for case DCON4 and also the springs analogy results for rigid joints condition which is shown as percentages.

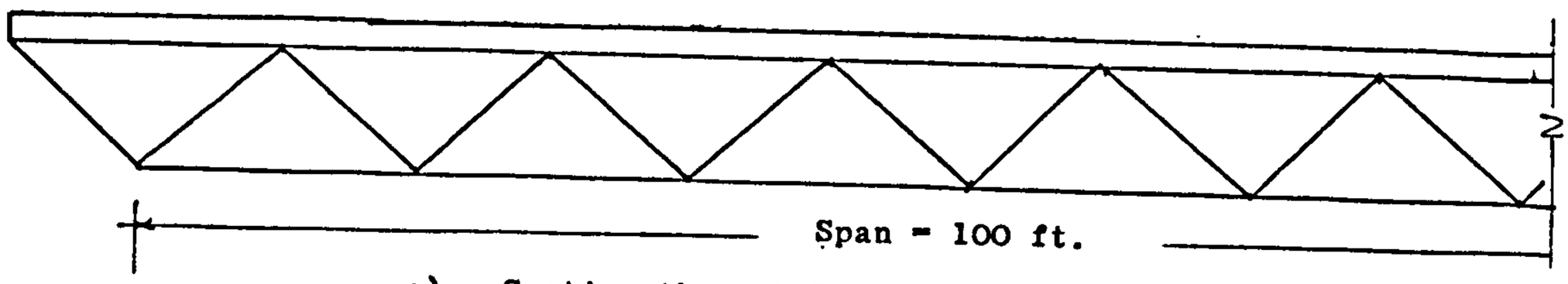

a) Section through D CON 5

Top concrete layer

Tubes of bottom layer

Diagonal shear tubes

Top layer joints

Bottom layer joints

C Max. compression

T Max. tension

-ve Compressive force

+ve Tensile force

Fig. 11.4 shows the exact results for case DCON5 and also the springs analogy results for rigid joints condition which is shown as percentages

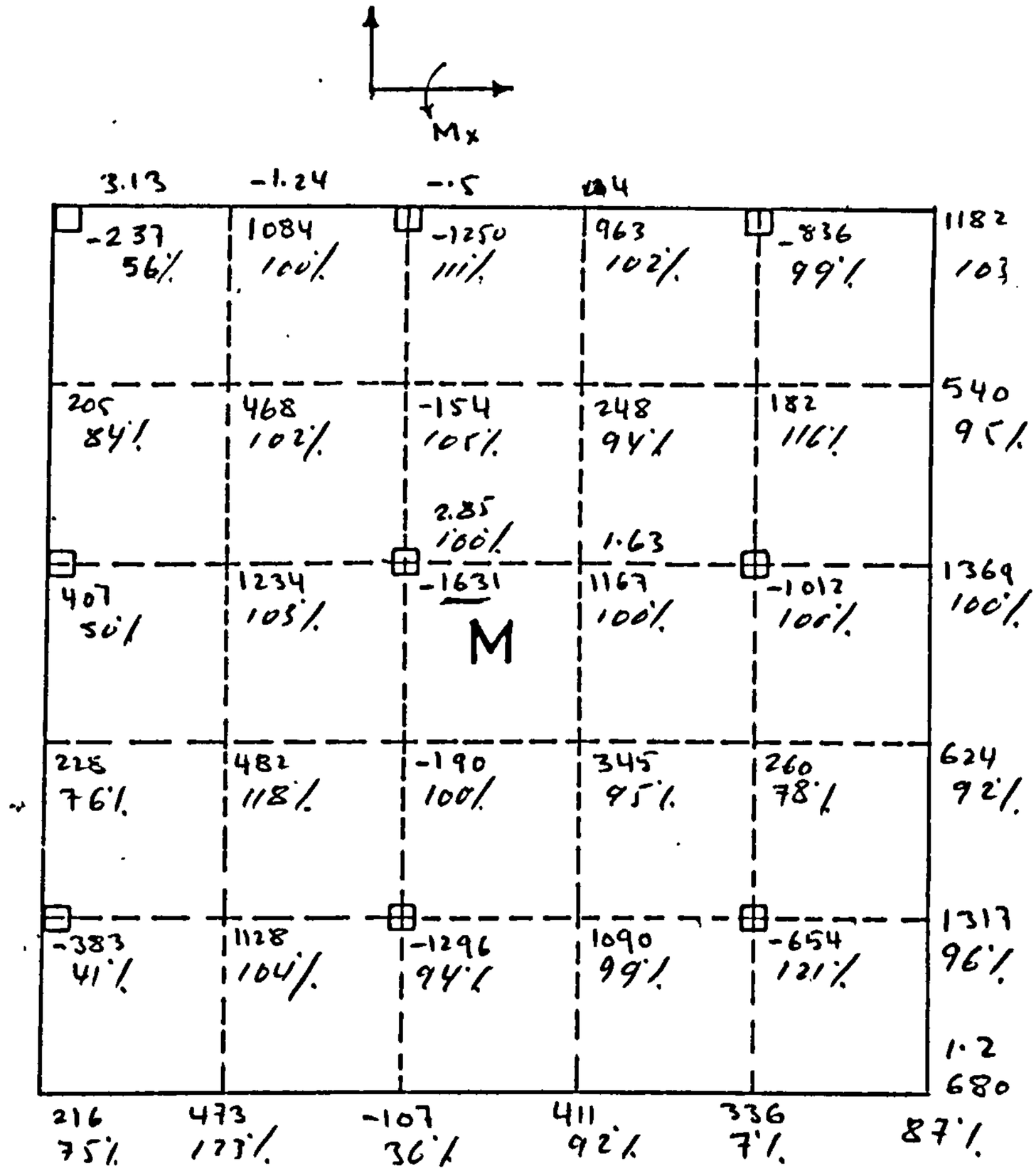

---- Finite Elements subdivision

□ Joints

M Maximum moment

Fig. 11.5 shows the exact results for bending moments in the concrete slab of case DCON2, and also the springs analogy results for rigid joints (shown as % of the exact results) and for pin joints conditions (shown only for few points as ratio of the exact one).

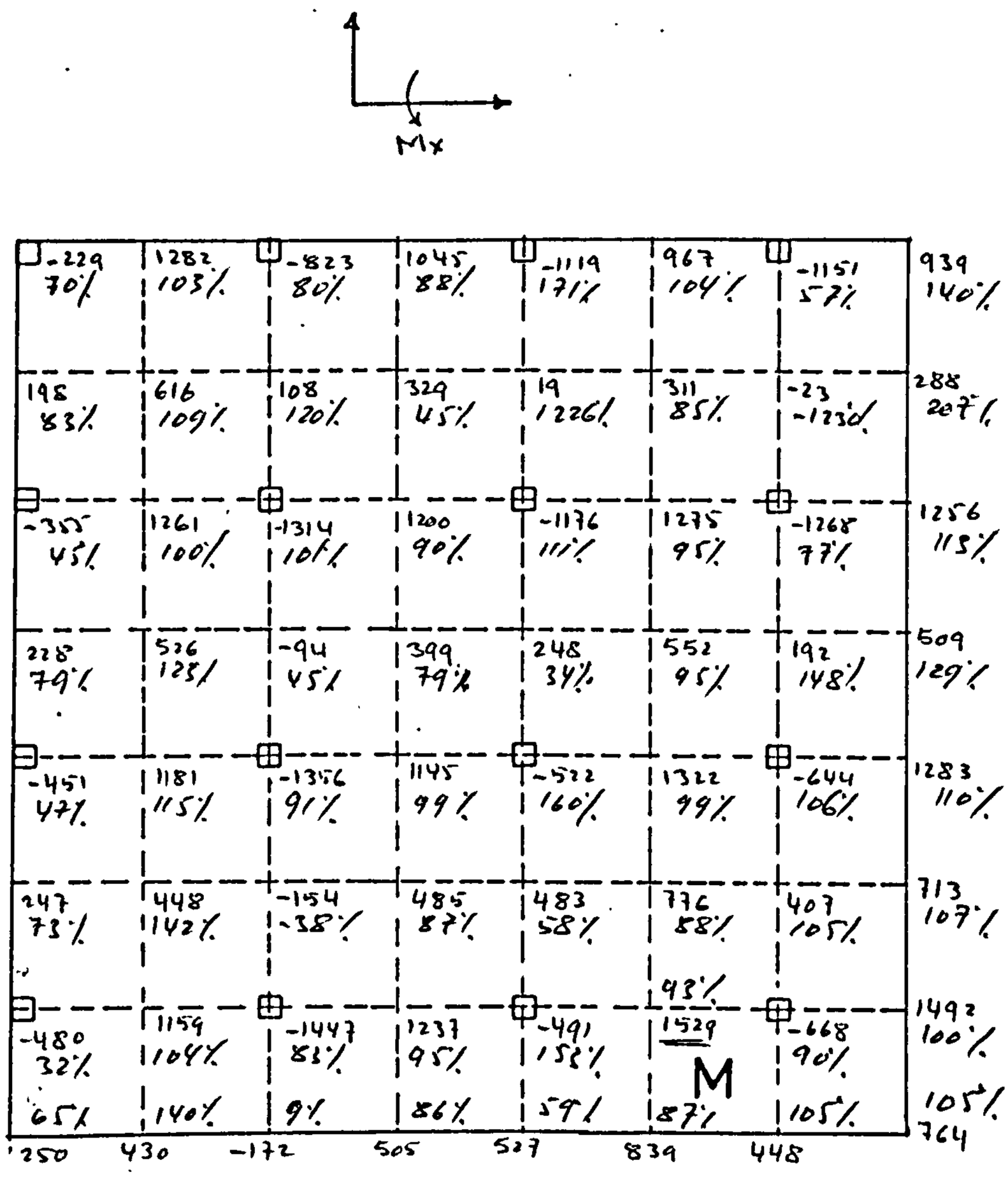

---- Finite Elements subdivisions

□ Joints

M Maximum moment

Fig. 11.6 shows the exact results for bending moments in the concrete slab of case DCON3, and also the spring analogy results for rigid joints condition as % of the exact results.

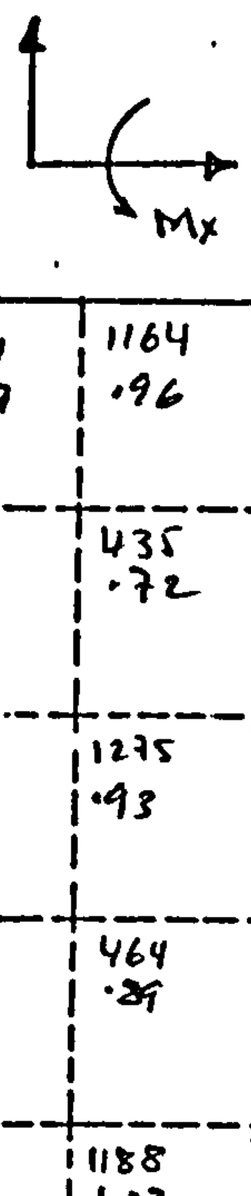

—— —— Finite Elements subdivisions

□ Joints

M Maximum Moment

Fig. 11.7 shows the exact results for bending moments in the concrete slab of case DCON4, and also the springs analogy results for rigid joints condition as ratio of the exact results

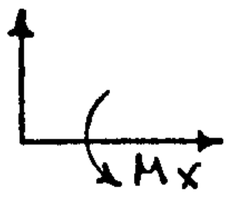

7 -18.7	1600 0.7	-137 13.5	1270 .65	-1182 1.85	954 1.07	-1192 .52	900 1.51	-1241 .36	880 1.27	-1252 1.66	876 .97
153 1.18	869 .63	491 -.08	510 .07	24 -10.7	312 0.8	-31 -8.7	296 2.09	-53 -6.3	287 1.24	-60 2.58	284 0.19
-242 0.86	1325 1.02	-967 .96	1343 .8	-1212 .94	1366 .89	-1289 081	1367 1.06	-1310 .79	1372 .96	-1320 .77	1373 .84
221 .91	606 1.27	20 1375	514 1.00	352 .59	670 .86	326 .88	648 1.04	334 .96	652 1.03	333 1.03	651 1.1
-508 .94	1238 1.14	-1424 .62	1263 1.05	-302 2.41	1499 .95	-377 1.69	1474 1.62	-338 1.76	1474 1.04	-336 1.65	1472 1.06
268 .69	412 1.76	-192 -.95	601 0.99	737 .57	1059 .77	708 .79	1027 .89	732 .86	1042 .93	732 .91	1041 .95
-555 .28	1127 1.13	-1565 .73	1370 .98	-1399 .43	1880 .86	-293 1.37	1887 .93	-250 1.3	1901 .95	-252 1.14	1901 .96
275 .59	344 1.88	-247 -.18	666 .88	911 .57	1269 .77	908 .87	1249 .91	947 .90	1272 .94	949 .93	1271 .95
-578 .25	1102 1.16	-1600 .73	1417 1.00	21 -25.	2025 .86	-101 2.5	2049 .94	-47 3.2	2070 .96	-47 2.1	2071 .97
278 .66	326 2.2	-256 -.94	716 1.02	1009 .61	1386 .78	1037 .84	1381 .91	1085 .9	1409 .94	1089 93	1409 .95
-586 .37 .75	1097 1.37 323	-1608 .47 -256	1448 1.06 725	85 -5. 1040	2103 .87 1423	-21 8.4 1079	2140 .94 1425	39 -1.8 1130	2165 .96 1454	37 -.9 1133	2167 0.97 1455
279	2.5	1.7	1.15	.65	.8	.84	.91	.9	.94	.94	.95

M

------F.E. sub division

□ Joints

M Maximum moment

Fig. 11.8 shows the exact results for bending moments in the concrete slab of case DCON5, and also the springs analogy results for rigid joints condition as ratio of the exact ones.

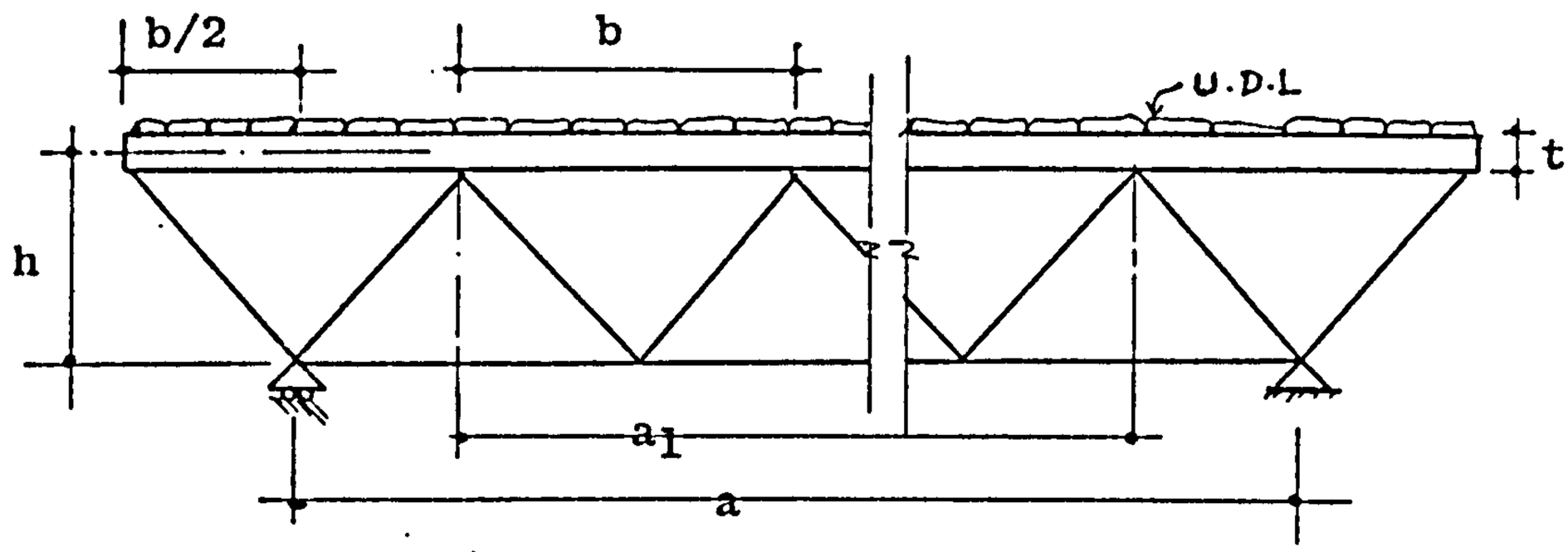

a) Section through the Uniform Mesh structure

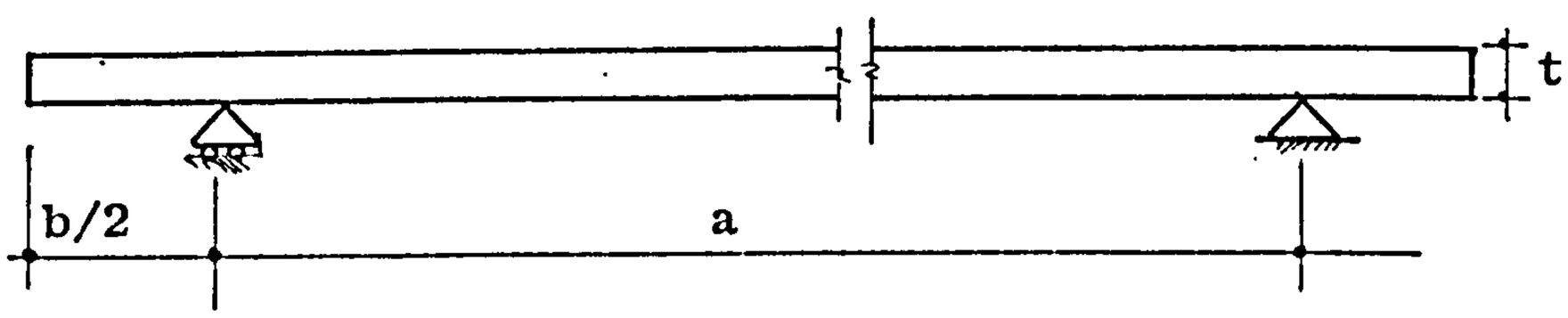

b) The homogeneous slab assumption

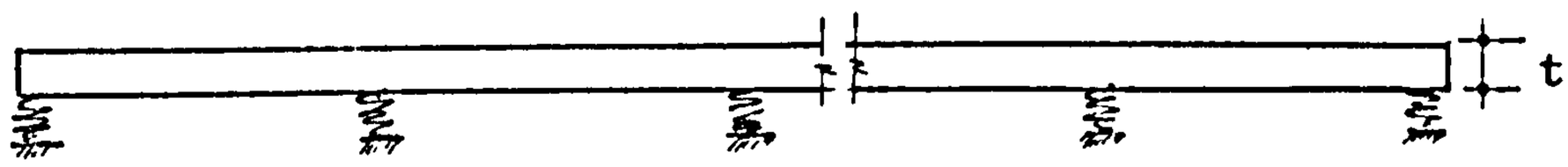

c) Slab resting on a spring mattress

Fig. 11.9

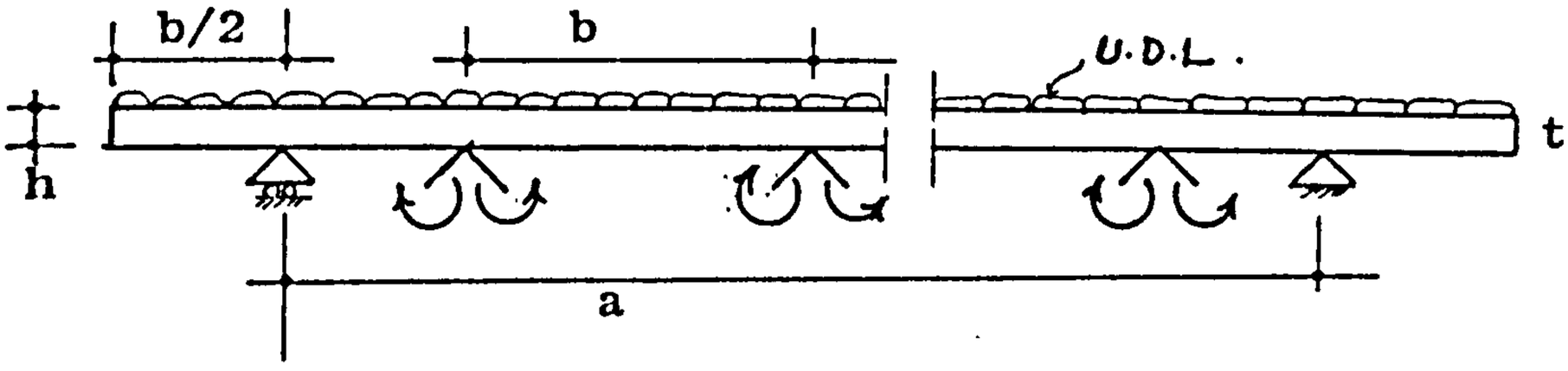

a) Assumed section for the approximate method for finding positive bending moment.

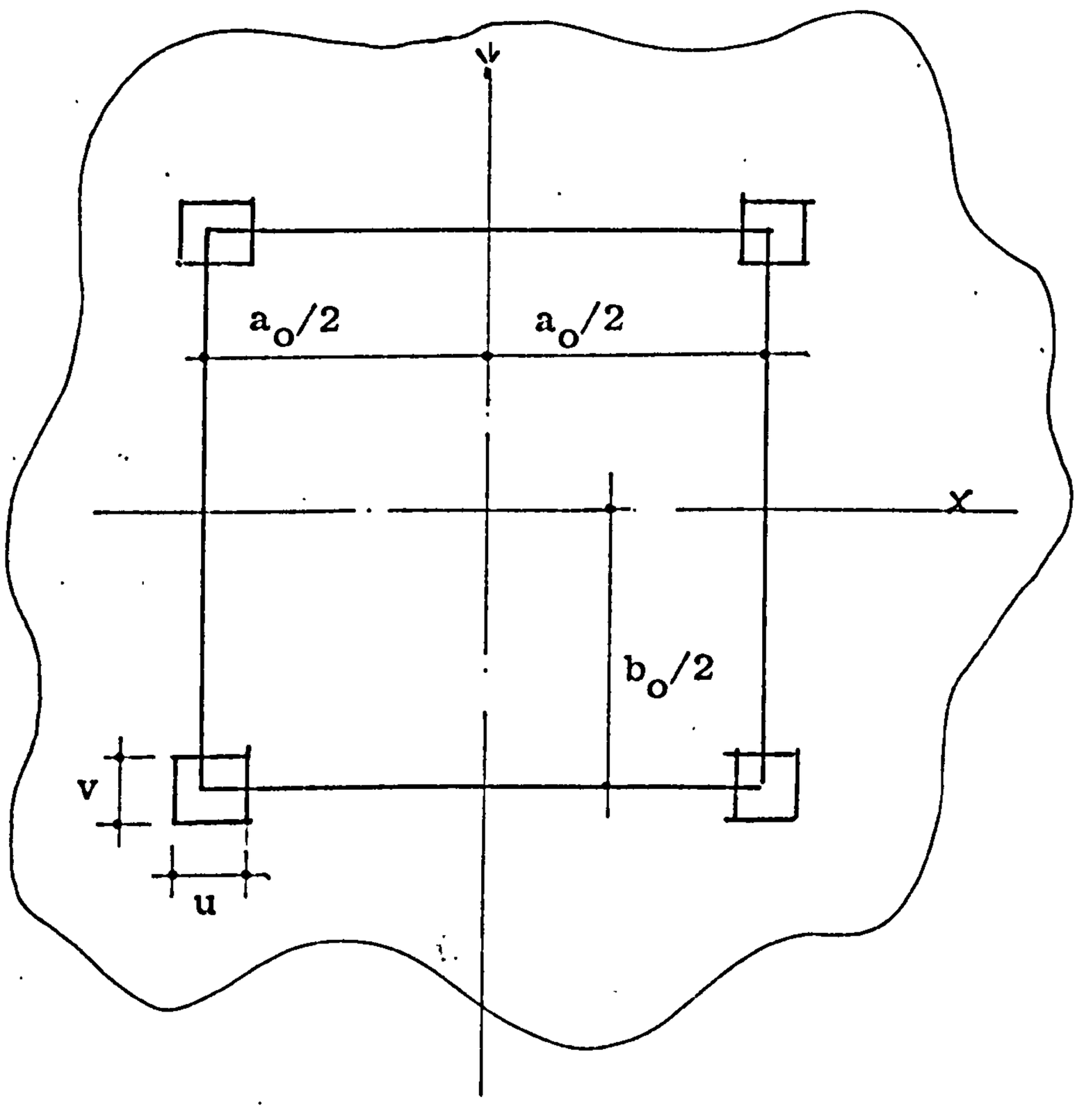

b) Flat slab panel

Fig. 11.10

CHAPTER 12

CONCLUSIONS AND FURTHER STUDIES

Composite Double Layer Grids are an evolution of the prismatic Double Layer Grids, and could have the same practical application with the added possibility of much larger spans.

In the many studies made in this research project, it was found that:

1. The composite stiffness matrix method of analysis yields reasonable and convergent results.

2. The eccentricity of top joints whether positive or negative has significant effects on both the prismatic members and the slab and is better to be avoided.

3. That the non-existence of the in-plane rotation parameter 'θ_z' in the plate analysis makes no apparent difference at least for the type of structures considered in this thesis.

4. The plate thickness has an important influence upon the strains in the tubes and naturally in the plate itself. A decrease in thickness increases the axial and bending strains in the bottom layer tubes, and also increases the in-plane and flexural strains in the plate and vice versa.

In the theoretical part of the research, the structural behaviour of the 'Uniform Mesh' and its parameter studies, together with the comparison with the tubular double layer grids of the same basic configuration, and with the 'IRM' composite structure showed that:

1. Axial strains are the dominant strains in the tubes in all cases investigated whether the tubes are pin-jointed or rigid-jointed and whether the structure is composite or not. This is a very useful phenomenon, since it means an efficient use of the prismatic members.

2. Rigidity of joints does not have an overall appreciable effect, other than decreasing the vertical displacements fractionally, and naturally introducing large bending moments at the ends of the tubes.

3. Considerable structural rigidity is achieved by using a reinforced concrete slab of practical and moderate thickness instead of the top steel tube grids. This is shown by a considerable reduction in the central deflection of up to 70% for a span of 100 ft. (10 bays) only.

4. When the span is very short, and the structure is very rigid, the external load is carried by a combination of shear and direct compressive forces rather than by bending action. The structure tends to behave like a slab in cases of larger spans, hence the load is carried mainly by bending action.

5. Most bottom layer members are under comparable tensile strains over the area of the grid.

6. Most shear members are under compressive forces, which are high at the boundary area, and are likely to be the decisive factor in the design considerations if it was intended for practical reasons to have all the tubes of identical cross-section.

7. Stresses in the slab are negligible in comparison

with the allowable concrete stresses. In-plane stresses are much less than flexural stresses, but in-plane stresses increase more rapidly than flexural stresses do in larger spans. Maximum positive bending moments are in the central area and are much higher than the maximum negative ones which are at the top joints in the boundary area. It is therefore concluded that practical consideration might be the decisive factor in choosing the slab thickness.

8. The increase in the depth of the structure reduces the stresses in the structure and vice versa.

9. The increase in the slab thickness also reduces the stresses in the structure.

10. Shear members are not as sensitive as the bottom tensile members or the top slab, to the variation in the slab thickness.

11. The span/depth ratio is a useful indicator of the size and rigidity of the structure, but it has no specific structural significance. Nevertheless, major forces in the structure vary inversely with it when the span is constant, and also major forces vary directly with it when the depth is constant.

12. As far as buckling of shear members and the total length of tubes used are concerned, an orientation of 45^{o} with the horizontal plane gives the most (economical) depth.

13. The plate analogy is a valuable asset in these structures, from which the following are obtained.

a. A method for finding the moment of inertia of the composite section which proved very useful in explaining

the composite structural behaviour and also in predicting the horizontal forces in the approximate methods.

b) The formulae introduced in Eq. 9.21 is very useful, by which an efficient thickness for the slab could be easily found, where no part of the slab will be in the tensile zone of the section. This saves money, and labour and more importantly avoids useless dead weight. This formulae was useful also in the approximate methods.

The approximate methods themselves yielded very good results especially in structures with moderate slab thickness and with not very short spans, Among the methods using a computer, the Spring Analogy Method in particular is very versatile and promising. This is because it can save a lot of computer time and storage, and at the same time gave very good results for almost all tube members and good results too for the important slab central area.

* The approximate methods which are based on the plate analogy give very good results for in-plane and axial stresses. Since the maximum shear force is always less than the maximum tensile force in the bottom layer, then any preliminary design based on the maximum tensile force will be on the safe side.

The prediction of the maximum positive bending moment gives good results also, but the drawback in it is that part of it will be based on trial and error when the slab is thicker or thinner than the efficient section. But this drawback is minimal if a moderate slab thickness is

used. The prediction of the maximum negative bending moment which is based on the flat slab analogy is very rough, but can be useful in rigid cases with very short span.

Although it is not claimed that these approximate methods are alternatives to the exact analysis, yet they can be of great help in giving a fair idea about the proper section when the envisaged span is given.

As a result of the computer limitations and the time available for this research, this thesis is somehow not as general as could be the case in some other fields of study. Therefore, the scope is quite enormous for future research in this unexplored field especially towards finding more general approximate methods, and in furthering practical applications of this type of structure.

REFERENCES

1. Makowski, Z.S. 'Steel Space Structures' London, Michael Joseph, 1965.

2. Castillo, H. 'A space frame construction with steel and reinforced concrete - the 'Tridilosa' spatial structure', Space Structures, Blackwell, Oxford, 1967.

3. Castillo, H. 'Nueva Teoria de las Estructuras'. Mexico, Ediciones Salinas, 1966.

4. Chambers, W.F., Jubb, J.E., and Levy, J.C. 'A Braced Double Skin Structure', 2nd International Conference on Space Structures, University of Surrey, 1975.

5. Bellamy, J.B. 'The Analysis, Design and Optimization of Structural Systems by a Digital Computer Programming System' Ph.D. thesis, University of Wales (Cardiff), 1969.

6. Theron, W.F.D. 'Regular Structures', B.Sc. thesis, Oxford University, 1968.

7. Livesley, R.K. 'Matrix Methods of Structural Analysis' G.B. Pergamon Press, 1964.

8. Renton, J.D. 'The Related Behaviour of Plane Grids, Space Grids and Plates', Space Structures, Blackwell, Oxford, 1967.

9. Renton, J.D. 'General Properties of Space Grids', International J. of Mechanical Science, vol. 12, pp.801-810, G.B., 1970.

10. Renton, J.D. 'The Formal Derivation of Simple Analogies for Space Frames', Proc. 1971 IASS Pacific Symposium, part II on tension structures and space frames, Tokyo and Kyoto pp.639-650, Architectural Institute of Japan, 1972.

11. Timoshenko, S. and Woinowsky-Krieger, S. 'Theory of Plates and Shells' Japan, McGraw-Hill Book Co., 1959, 2nd edition.

12. Makowski, Z.S. Free discussion on 'The Formal Derivation of Simple Analogies for Space Frames' by Renton, J.D., i.e. Ref. 10 in this list.

13. Heki, K. 'The Effect of Shear Deformation on Double Layer Lattice Plates and Shells', 2nd Int. Conf. on Space Structures, University of Surrey, 1975.

14. Hendry, A.W. 'Elements of Experimental Stress Analysis', G.B., Pergamon Press Ltd., 1964.

15. Zienkiewicz, O.C. and Cheung, Y.K. 'Finite Elements Method in Structural and Continuum Mechanics' G.B., McGraw-Hill Publishing Co. Ltd., 1967, 1st edition.

16. Zienkiewicz, O.C. 'Finite Element Method in Engineering Science, London, McGraw-Hill, 1971, 2nd edition.

17. Zienkiewicz, O.C. and Holister, G.S. 'Stress Analysis', London, John Willey & Sons Ltd., 1967.

18. Reisner, E. 'On the Derivation of Boundary Conditions for Plate Theory', Proc. Royal Soc., London, Vol. 276, 1365 (Nov. 1963), pp.178-186.

19. Nooshin, H. 'A Technique for the Analysis of Structures having Partially Constrained Joints' Civil Engineering and Public Work Review, May 1966.

20. Stewart and Lloyds Ltd. 'Structural Hollow Sections, Properties and Safe Load Tables' Nov. 1965.

21. Marshall, J. 'Aspects of Torsion of Structural Rectangular Hollow Sections' Ph.D. Thesis, University of Strathclyde, 1972.

22. Zienkiewicz, O.C. 'The Finite Element Method for Analysis of Elastic Isotropic and Orthotropic Slabs' Proc. I.C.E., August, 1964.

23. Timoshenko, S.P. and Gere, J.M. 'Mechanics of Materials' London, Van Nostrand Reinhold Co., 1972.

24. British Steel Corporation 'The Space Maker - NODUS'.